TECHNISCHE UNIVERSITÄT MÜNCHEN
TUM School of Engineering and Design

Driver's Non-Driving Postures in Automated Driving: Modeling, Assessment, and Countermeasure

Yucheng Yang M.Sc.

Vollständiger Abdruck der von der TUM School of Engineering and Design der Technischen Universität München zur Erlangung des akademischen Grades eines

Doktors der Ingenieurwissenschaften (Dr.-Ing.)

genehmigten Dissertation.

Vorsitzende:	Prof. Dr.-Ing. Katrin Wudy
Prüfer der Dissertation:	1. Prof. Dr. phil. Klaus Bengler
	2. Prof. Dr.-Ing. Frank Flemisch

Die Dissertation wurde am 25.03.2021 bei der Technischen Universität München eingereicht und durch die Fakultät für Maschinenwesen am 24.08.2021 angenommen.

Acknowledgment

Over the past few years of being a doctoral student and a research associate at the Chair of Ergonomics at the Technical University of Munich, I have been accompanied and supported by many people who made this work possible, and to whom I would express my sincere appreciation.

First of all, I would like to thank my supervisor, Professor Klaus Bengler, who gave me the chance to start my academic journey at the Chair of Ergonomics, who guided and supported me along the way to the goal. Professor Bengler has always been very generous in sharing his comprehensive knowledge and experiences. His visionary sense of perspective has inspired my research with more "bigger pictures." I am incredibly grateful for the freedom of research he granted, while facilitating sufficient resources that made this work happen.

I also wish to show my wholehearted gratitude to Professor Heiner Bubb, who always showed great interest in my research, raised conducive questions and discussions, and offered truthful advice. With his multi-field knowledge, multi-decade experience in ergonomics, and great modesty, Professor Bubb has always been an important source of inspiration and encouragement to me.

Similarly, I would like to thank Professor Katrin Wudy for accepting the chair of the examination committee, and special thanks to Professor Frank Flemisch for kindly being the second examiner and giving constructive feedback on this work.

Truthfully, I want to thank my MW3325 office colleagues Jonas Radlmayr and Anna Feldhütter for their endless support, encouragement, discussions, and most importantly, for the close friendship. Similarly, I am very grateful to my dear colleagues, Ingrid Bubb, Burak Karakaya, Lorenz Prasch, Martin Götze, and Antonia Conti, who have always been available for me whenever support of all kinds was needed. Meanwhile, many thanks to Beverley Howard for the inspiring discussions and reviews from an industrial perspective.

Besides, I would like to express my sincere appreciation to all my students for their effort in supporting me with series of experiments, especially Matthias Gerlicher, Lukas Wolf, Jan Niklas Klinkner, Guo Jun, Maurice Rang, Christoph Hera, and Christina Aures.

My deepest gratitude goes to my beloved wife, parents, and family for their unconditional, continuous, and unparalleled love, trust, understanding, and support. Most importantly, they have always been sharing my dreams and joys throughout my life. Special thanks to my two-year-old son, dear Zimo: you have been a powerful "turbo" for this work. For your information, a turbo in the good old times means an accelerator or motivator, which usually works better after a so-called turbo lag.

-Thank you very much-

Yucheng Yang (楊榆程)
31. Dec. 2020 in Eching, Germany

To My Family

Abstract

The driver being continuously in the control loop is the central premise of manually driven vehicles. The paradigm change of Level 3 automated driving (SAE J3016, 2018) allows the driver to be out of the control loop as the system fallback. The driving task is shifted from the primary task to one of the peripheral tasks (Loehmann & Hausen, 2014) within the system limit. In case of system limit, the driver in Level 3 automated driving must be available to take over the vehicle dynamic control. In this take-over process, shifting responsibility for the driving task from the automation system back to the human driver is especially safety-critical. This work addresses the effects of driver's body postures on the take-over performance in Level 3 automation and develops an active seat assist system as a countermeasure to the effect.

This dissertation consists of five experiments, including one prototype construction work. The first experiment explores the changing drivers' motivation and behavior with regard to two aspects: new non-driving related tasks (NDRTs) and associated non-driving postures (NDPs) in an automated vehicle (AV). Results show a many-to-many mapping between NDRTs and NDPs. The reclined posture is identified as a preferred NDP, which becomes the focus posture of this thesis. Focusing on the reclined and backward-shifted sitting position, the second experiment illustrates a significant influence of the torso angle, but a negligible influence of the knee angle on take-over performance. The third motion-tracking experiment offers a comprehensive insight into drivers' body motion during the take-over process. The dataset includes the trajectories, velocity, and acceleration of five body parts (wrist, breastbone, hip, knee, and ankle) in twelve initial postures. Results confirm the significant influence of the torso angle on the take-over time from a primarily motoric perspective. Drivers with large torso angles can have unstable sitting postures and more workload during the take-over process. An active seat assist prototype is developed and constructed to assist reclined and backward-shifted drivers and improve their take-over performance. The active seat assist can automatically reconfigure the seatback and longitudinal adjustment in the take-over process, and it starts simultaneously with the RtI (request to intervene). The active seat assist is integrated into the dynamic driving simulator and evaluated in the fifth experiment. Results show that the active seat assist improves reclined drivers' take-over performance (time and quality) by turning a rather sequential take-over process into what tends to be a more parallel one, thus increasing the safety of being reclined in Level 3 automation. Subjectively, the system is well accepted as useful and satisfying by offering the participants a significantly higher level of ease and comfort.

This work offers a comprehensive insight into the reclined and backward-shifted sitting position in Level 3 automated driving with empirical data. The results supplement the current research on take-over performance with the factor of body posture and enhance the understanding of the risks and challenges. The take-over motion dataset provides empirical evidence and a reference for the digital human model and vehicle interior design in the context of Level 3 automated driving. The active seat assist shows one example of the adaptive interior elements to improve take-over performance and system usability.

Zusammenfassung

Dass der Fahrer sich ständig im Regelkreis befindet, ist die zentrale Voraussetzung für manuelles Fahren. Der Paradigmenwechsel des automatisierten Fahrens nach Level 3 (SAE J3016, 2018) ermöglicht es dem Fahrer, als System-Fallback außerhalb des Regelkreises zu bleiben. Die Fahraufgabe wird von der Hauptaufgabe zu einer der peripheren Aufgaben (Loehmann & Hausen, 2014). Im Fall einer Systemgrenze muss der Fahrer bei Level-3-Automation die dynamische Steuerung des Fahrzeugs übernehmen. Bei diesem Übernahmevorgang ist die Verlagerung der Verantwortung für die Fahraufgabe vom System zurück auf den menschlichen Fahrer besonders sicherheitskritisch. Diese Arbeit befasst sich mit den Auswirkungen der Fahrerkörperhaltung auf die Übernahmeleistung in der Level-3-Automation. Zusätzlich wird ein Assistenzsystem (der „Active Seat Assist“) als Gegenmaßnahme zu diesem Effekt entwickelt.

Diese Dissertation besteht aus fünf Experimenten. Das erste Experiment untersucht neue Fahrfremdtätigkeiten und damit verbundene Körperhaltungen in einem automatisierten Fahrzeug. Die Ergebnisse zeigen eine Viele-zu-Viele-Beziehung zwischen Tätigkeiten und Sitzhaltungen. Die zurückgelehnte Sitzhaltung wird als eine der bevorzugten Körperhaltungen identifiziert, die zu dem Schwerpunkt dieser Arbeit wird. Das zweite Experiment konzentriert sich auf die zurückgelehnte und nach hinten verschobene Sitzposition und zeigt einen signifikanten Einfluss des Torsowinkels, aber einen vernachlässigbaren Einfluss des Kniewinkels auf die Übernahmeleistung. Das dritte Motion-Tracking-Experiment bietet einen umfassenden Einblick in die Körperbewegung des Fahrers während des Übernahmevorgangs. Der Datensatz enthält die Trajektorien, die Geschwindigkeit und die Beschleunigung von fünf Körperteilen (Handgelenk, Brustbein, Hüfte, Knie und Fußgelenk) in zwölf Ausgangspositionen. Die Ergebnisse bestätigen den signifikanten Einfluss des Torsowinkels auf die Übernahmezeit aus vorwiegend motorischer Sicht. Zudem haben Fahrer mit großen Torsowinkeln während des Übernahmevorgangs instabile Sitzhaltungen und mehr Arbeitsbelastung. Ein Sitzassistenzsystem wird entwickelt und konstruiert, das die Rückenlehne und die Längsverstellung während des Übernahmevorgangs automatisch zurückstellen kann, um zurückgelehnte und nach hinten verschobene Fahrer zu unterstützen und ihre Übernahmeleistung zu verbessern. Der Active Seat Assist wird in den dynamischen Fahrsimulator integriert und im fünften Versuch ausgewertet. Die Ergebnisse zeigen, dass der Active Seat Assist die Übernahmeleistung (Zeit und Qualität) der Fahrer verbessert, indem ein eher sequenzieller Übernahmevorgang tendenziell in einen paralleleren überführt wird, wodurch die Sicherheit erhöht wird. Subjektiv wird das System als nützlich und zufriedenstellend anerkannt, da es den Fahrern ein deutlich höheres Maß an Leichtigkeit und Komfort bietet.

Die Arbeit bietet umfassende empirische Daten und Analysen zur zurückgelehnten und nach hinten verschobenen Sitzposition in der Level-3-Automation. Durch den Faktor Fahrerkörperhaltung ergänzt die Arbeit die aktuelle Forschung zur Level-3-Übernahmeleistung und verbessert das Verständnis für die relevanten Risiken und Herausforderungen der zurückgelehnten Fahrerhaltungen. Der Übernahmebewegungsdatensatz liefert eine empirische Basis und Referenz für das digitale menschliche Modell und das Innenraumkonzept des automatisierten Fahrens nach Level 3. Der Active Seat Assist zeigt ein Beispiel der adaptiven Innenraumkomponenten zur Verbesserung der Übernahmeleistung und der Systemnutzbarkeit.

Acronyms

Automated driving

ACC	Active Cruise Control
ADAS	Advanced Driver Assistance System
ADS	Automation Driving System
AV	Automated Vehicle
DDT	Dynamic Driving Task
LKAS	Lane Keeping Asisstant System
NDP	Non-Driving Postures
NDRT	Non-Driving-Related Task
OEDR	Object and Event Detection and Response
ODD	Operational Design Domain
SA	Situation Awareness
SuRT	Surrogate Reference Task
SUV	Sport Utility Vehicle
TDP	Time to Driving Posture
TOT	Take-Over Time
TTC	Time to Collision
RtI	Request to Intervene

Measures

BMI	Body Mass Index [kg/m^2]
HoMT	Hand-on Motion Time [s]
HoT	Hand-on Time [s]
KSS	Karolinska Sleepiness Scale
NASA TLX	National Aeronautics and Space Administration Task Load Index
SDLP	Standard Deviation Lateral Position [m]
ST	Steering Time [s]
TT	Task Time [s]

Technical terms

AC	Alternating Current
CID	Center Information Display
DC	Direct Current
DPU	Data Processing Unit
ECU	Electronic Control Unit
EEPROM	Electrically Erasable Programmable Read-Only Memory
EMI	Electromagnetic Interference
HMI	Human Machine Interface
HTTP	Hypertext Transfer Protocol
IMU	Inertial Measurement Unit
PC	Personal Computer
PWM	Pulse Width Modulation
UI	User Interface

Seat Adjustment

SLA	Seat Longitudinal Adjustment
SHA	Seat Height Adjustment
SIA	Seat Inclination Adjustment
SBA	Seat Backrest Adjustment

Data analysis

ANOVA	Analysis of Variance
DV	Dependent Variable
FFT	Fast Fourier Transform
IV	Independent Variable
RMANOVA	Repeated Measure Analysis of Variance
RMSE	Root-Mean-Square Error

Institutions and Facilities

AAM	Alliance of Automobile Manufacturers
CES	Consumer Electronics Show
FMVSS	Federal Motor Vehicle Safety Standards
MEPS	Modular Ergonomic Mock-up
NASA	National Aeronautics and Space Administration
NHTSA	National Highway Traffic Safety Administration
SAE International	Society of Automobile Engineers International
TUM	Technical University of Munich

Contents

1 Introduction

Automated driving is currently one of the most frequently discussed innovative topics and is likely to be on the market within the next few decades (Flemisch, Kelsch, Schieben, & Schindler, 2006; Gold, 2016). Drivers already conduct non-driving-related tasks (NDRTs) in the current manual driving condition (Huemer & Vollrath, 2012), e.g., talking to the passengers and using smartphones. Drivers could spend more time on the NDRTs when they do not continuously monitor automation systems at or above Level 3 (SAE J3016, 2018). NDRTs like sending an email, eating, and making phone calls (Pfleging, Rang, & Broy, 2016) could be conducted for a longer continuous period without being interrupted by the driving task. Driver behavior influences driver posture (Jonsson, StFenlund, Svensson, & Björnstig, 2008). The conventional driving posture will no longer always be optimal for AVs' usage if drivers do not drive most of the time. Instead, drivers might use this opportunity to release themselves from the driving task and change their postures; in particular, drivers were observed reclining and adjusting the seat position to relax (Large, Burnett, Morris, Muthumani, & Matthias, 2018). Östling & Larsson (2019) identified the participants' strong interest in reclining the seat to relax in an AV in urban environments. McMurry, Poplin, Shaw, & Panzer (2018) were concerned about the safety of 'out-of-position' occupants, who are most likely rotated, seated sideways, and reclined. These drivers' non-driving postures (NDPs), which were observed in different studies, challenge the conventional interior concept and extend the possible driver states in Level 3 automated driving (Marberger et al., 2017), which should be considered in the take-over process in case of a system limit.

Current driving-task-orientated interior concepts are strictly governed by the driver's constant necessity for the dynamic control of the vehicle. It requires that the driver can reach the pedals, steering wheel, and the gear shift at all times in any sitting posture (Bubb, Grünen, & Remlinger, 2015). This premise restricts the possibilities of the interior variants (e.g., positions, types, and ranges of control elements and displays) and consequently limits drivers' behavior (e.g., postures and movements). This restricted driving behavior sets, in turn, an exact requirement for the driving-task-oriented interior concept. However, there is no single orientation or optimization goal in AVs due to the variety of NDRTs and NDPs. Diverse use cases in an AV require an interior which balances and supports the driving posture and NDPs to conduct the driving task and the NDRTs.

Different non-driving behaviors lead to different non-driving driver states (Marberger et al., 2017). These could include different cognitive, sensory, and motoric states such as mental task sets, visual behavior, and hand movements. In case of the Level 3 system limit, the system degrades to Level 2, 1, or 0. In each case, the driver has to be back in the control loop and take over the dynamic control within a minimal period (the take-over process). These non-driving driver states, including the NDPs, have to be reconfigured to individual states that are adequate to drive manually. AVs with Level 3 systems have to ensure the drivers' availability to take over and assist them with reconfiguring the driver state before the system limit is reached.

This thesis focuses on the driver's reclined and backward-shifted sitting position in Level 3 automation and addresses the two new challenges mentioned above by means of five studies.

2 Research Questions and Structure of This Thesis

This chapter poses the main research question and presents the structure of this thesis.

The paradigm shift of Level 3 automation (L. Lorenz, Kerschbaum, Hergeth, Gold, & Radlmayr, 2015) allows the driver to be out of the control loop. However, the additional driver's activities and postures should be investigated carefully due to the driver's remaining responsibility as the system fallback (SAE J3016, 2018). This thesis focuses on the driver posture in the take-over process and contributes to the current research gap (Chapter 3) with regard to take-over performance in Level 3 automated driving.

If the driver takes a reclined posture in Level 3 automation, to what extent is safety negatively affected during the take-over process, and would an active interior concept be helpful?

The answer to the main research question consists of five experiments concerning three key aspects which built upon one another: identifying driver behaviors and postures (Chapter 4), quantifying risks (Chapters 5 and 6), and developing countermeasures (Chapters 7 and 8).

1. Identifying driver behavior: what are the drivers' preferred activities and sitting postures in an AV?

   Chapter 4 summarizes the pre-publication (Yang, Klinkner, & Bengler, 2019). The users' motivation to sit differently in AVs than in conventional manually driven vehicles is confirmed. NDRTs in AVs and the associated NDPs are empirically identified. The NDP is described qualitatively and quantitatively by means of joint angles or seat adjustments. New ergonomic and functional requirements for the interior of AVs are derived.

2. Quantifying risks: if the driver does not sit in the driving position, what are the consequences regarding take-over performance?

   Chapter 5 summarizes the pre-publication (Yang, Gerlicher, & Bengler, 2018), illustrating the effect of representative NDPs on take-over performance in Level 3 automation. Chapter 6 presents the motion tracking experiment, collecting data of take-over motions from different NDPs. Trajectory, velocity, and acceleration of different body parts in different transition phases are analyzed.

3. Developing and evaluating countermeasures: how could the interior elements help reclined and backward-shifted drivers in the take-over process?

   Chapter 7 illustrates the development and construction of the active seat assist prototype, which is intended to help drivers in different take-over phases to make the take-over as quick, safe, and comfortable as possible.

   Chapter 8 evaluates the active seat assist in the dynamic driving simulator, providing empirical evidence of the efficiency, effectiveness of, and satisfaction with the active seat assist in the Level 3 take-over process.

Summarizing the structure of this thesis, Chapter 1 introduces the background. Chapter 2 raises the research questions. Chapter 3 presents the state of the art found in literature, the research gap, and clarifies the definitions applied throughout the thesis. Five experiments (Chapters 4, 5, 6, 7, and 8) are conducted to answer the main research question.

Chapter 4 and Chapter 5 are the brief summaries of two pre-publications (Yang, Gerlicher, et al., 2018; Yang et al., 2019). More detailed results can be found in the original publications.

The three studies in Chapters 6, 7, and 8 (including Appendix) are not pre-published; the procedures and results are presented and analyzed in detail in this thesis. The detailed "Discussion," "Summary," and "Limitations" of the key results are presented at the end of each corresponding Chapter 6, 7, and 8 to allow more specific content.

Chapter 9 is a general discussion, reflecting on a chicken-egg dilemma existing in the research and development of AVs, which has been pre-published previous to this work (Yang, Fleischer, & Bengler, 2020).

Chapter 10 summarizes the key findings and answers the main research question.

Chapter 11 describes the common limitations among the experiments and their limited research scopes from a critical perspective. Recommendations for future research and improvement are given.

3 State of the Art and Definitions

The literature foundation of this work, definitions, and terms are presented with regard to four aspects: the general background of automated driving and drivers' activities (Section 3.1); the driver state and various factors of take-over performance (Section 3.2); drivers' postures in vehicles (Section 3.3); the interior development of automated vehicles (Section 3.4); and the brief history of the driver seat (Section 3.5). The contribution of this dissertation to these four research fields is suggested at the end of each section.

3.1 Automation Levels and Non-Driving-Related Tasks

The SAE J3016 provides the definitions of automated driving and automation levels (SAE J3016, 2018). The six levels (Figure 3-1) range from no driving automation (Level 0) to full driving automation (Level 5), considering the different roles. The roles consist human or the automation driving system (ADS) that perform the dynamic driving task (DDT), the fallback and the operational design domain (ODD). DDT is the combination of the object and event detection and response (OEDR) plus the vehicle motion control (Figure 3-2).

The role of a human driver is highlighted within the blue block in Figure 3-1 to allow an explanation of the automation levels from a human driver's perspective:

1. In Level 0, drivers must be responsible for performing all DDTs and be the DDT fallback.
2. In Level 1 automation, drivers must supervise the sustained and ODD-specific ADS performance. Drivers must complete the OEDR and perform the other vehicle motion control (either longitudinal or lateral).
3. In Level 2 automation, drivers must supervise the sustained and ODD-specific ADS performance by completing the OEDR.
4. In Level 3 automation, drivers do not have to supervise the sustained and ODD-specific ADS performance. However, users should be DDT fallback-ready, meaning users are receptive to ADS-issued requests to intervene (RtI) or other system failures and respond appropriately.
5. In Level 4 automation, drivers do not have to supervise the sustained and ODD-specific ADS performance; users do not have to be receptive to RtI.
6. In Level 5 automation, users do not have to supervise the sustained and unconditional ADS performance; users do not have to be receptive to RtI.

Level	Name	Narrative definition	DDT		DDT fallback	ODD
			Sustained lateral and longitudinal vehicle motion control	OEDR		
Driver* performs part or all of the *DDT						
0	**No Driving Automation**	The performance by the *driver* of the entire *DDT*, even when enhanced by *active safety systems*.	*Driver*	*Driver*	*Driver*	n/a
1	**Driver Assistance**	The *sustained* and *ODD*-specific execution by a *driving automation system* of either the *lateral* or the *longitudinal vehicle motion control* subtask of the DDT (but not both simultaneously) with the expectation that the *driver* performs the remainder of the *DDT*.	*Driver* and *System*	*Driver*	*Driver*	Limited
2	**Partial Driving Automation**	The *sustained* and *ODD*-specific execution by a *driving automation system* of both the *lateral* and *longitudinal vehicle motion control* subtasks of the *DDT* with the expectation that the *driver* completes the *OEDR* subtask and *supervises* the *driving automation system*.	***System***	*Driver*	*Driver*	Limited
ADS* ("*System*") performs the entire *DDT* (while engaged*)			*System*	***System***	*Fallback-ready user (becomes the driver during fallback)*	Limited
3	**Conditional Driving Automation**	The *sustained* and *ODD*-specific performance by an *ADS* of the entire DDT with the expectation that the *DDT fallback-ready user* is *receptive* to *ADS*-issued *requests to intervene*, as well as to *DDT performance-relevant system failures* in other *vehicle* systems, and will respond appropriately.				
4	**High Driving Automation**	The *sustained* and *ODD*-specific performance by an *ADS* of the entire *DDT* and *DDT fallback* without any expectation that a *user* will respond to a *request to intervene*.	*System*	*System*	***System***	Limited
5	**Full Driving Automation**	The *sustained* and unconditional (i.e., not *ODD*-specific) performance by an *ADS* of the entire *DDT* and *DDT fallback* without any expectation that a *user* will respond to a *request to intervene*.	*System*	*System*	*System*	**Unlimited**

Figure 3-1 Summary of levels of driving automation (SAE J3016, 2018)

Figure 3-2 shows the DDT portion of the whole driving task. Drivers perform part of the DDT in Level 1–2 systems, of which the OEDR always stays a driver's task. Thus, drivers should continuously either conduct or monitor the driving task since the system limit could be reached at any time without prior warning or sign. In the Level 0 manual driving condition and Level 1–2 assisted driving conditions, driving is the primary task, consisting of three categories: navigation, guidance, and stabilization (Geiser, 1985). The secondary tasks are actions and reactions related to the driving task, such as setting the indicator, or using a high beam. The tertiary tasks have nothing to do with the driving task; they are about comfort and communication. Drivers conduct tertiary tasks in the manual driving condition, such as using the telephone, eating, or operating the infotainment system (Huemer & Vollrath, 2012). Modern advanced driver assistance systems (ADASs) in Level 1 and 2 can take over the longitudinal and/or lateral guidance (Schaller, Schiehlen, & Gradenegger, 2008). Systems like active cruise control (ACC) (Shladover, Nowakowski, Lu, & Ferlis, 2015) or the lane keeping assistant system (LKAS) (Flemisch, Kelsch, et al., 2008) are examples of Level 1 systems. The combination of active longitudinal and lateral

control systems achieves a Level 2 system, which is currently the highest automation level available in a passenger car on the market. Examples of Level 2 systems are Autopilot (Tesla), Traffic Jam Assist (Audi, Acura), Super Cruise (Cadillac), Driving Assistant Plus (BMW), and ProPilot Assist (Nissan) (Teoh, 2020).

In Level 3, 4, and 5 automation, the system takes over all the DDT. In this thesis, vehicles equipped with a Level 3, 4, or 5 system are generally labeled as automated vehicles (AVs). Automation systems at all levels do not cover the strategic parts of the driving task.

Drivers can be out of the control loop in Level 3 and Level 4 automation and even become passengers at Level 5, according to SAE J3016 (2018). In Level 3 and Level 4 automation, drivers will, by definition, eventually take over the dynamic control of the car, either as the fallback of the automation system in Level 3 scenarios or voluntarily in Level 4 scenarios. A Level 3 automation recognizes the system limit and issues a RtI (SAE J3016, 2018) or a take-over request (TOR) (Damböck, 2013) to the fallback-ready driver. The driver has to react to the RtI or TOR and take over the DDT. This transition is called the take-over process, in which the Level 3 system is degraded to Level 2, 1, or 0 systems.

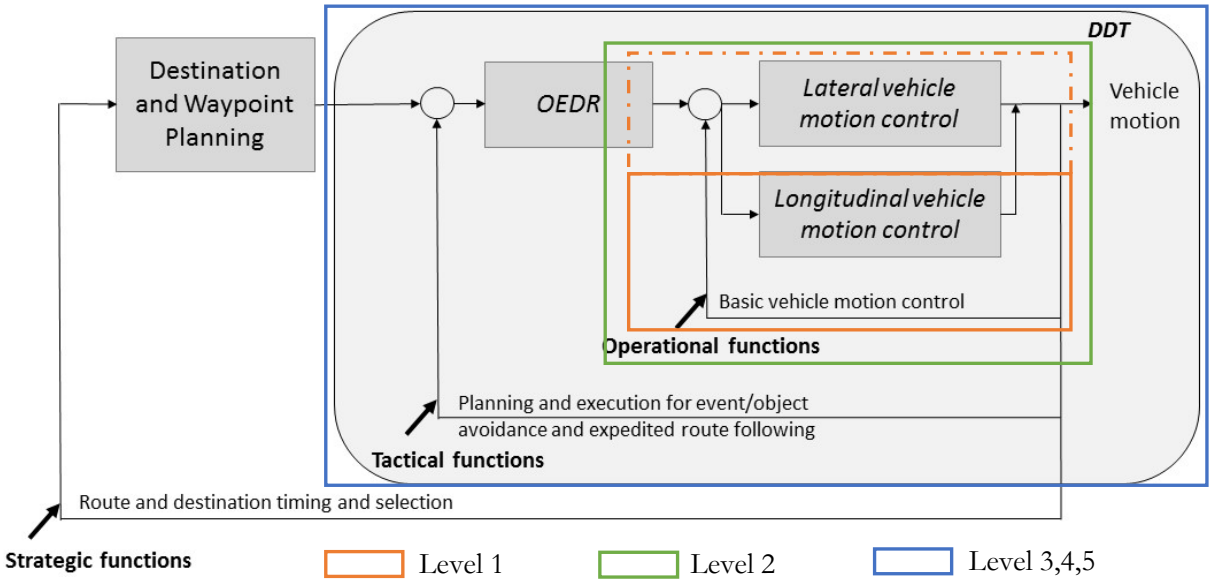

Figure 3-2 DDT portion of the driving task and the automation levels, modified from (SAE J3016, 2018)

Drivers can be out of the control loop in Level 3, 4, or 5 automated driving, so that the driving task is no longer the primary task. Thus, the term non-driving-related activities or tasks (NDRA or NDRT) is often used in the context of automated driving conditions instead of tertiary tasks in manual driving conditions. NDRTs are regarded as one of the AVs' main advantages (König & Neumayr, 2017). Drivers are expected to spend more time on NDRTs than in a manual or assisted driving condition (Jamson, Merat, Carsten, & Lai, 2013; Naujoks, Befelein, Wiedemann, & Neukum, 2018; Pfleging et al., 2016). For ergonomic research, the current difficulty is a lack of real AVs on the market to obtain a realistic understanding of AVs, limiting the participants' mental models to behave naturalistically in mockups or simulators. With this limitation, all the current empirical results show

a huge variance due to individual backgrounds and mental models. Literature offers three methods to access user behavior, activities, and postures in future AVs: observation in other means of transport such as trains, surveys or interviews in labs, and experiments in driving simulators. The transfer of those results to real AVs calls for great caution.

Naujoks et al. (2018) provide a catalog of naturalistic NDRTs. Similar results can be found in other literature, for example: eating, drinking, using a laptop, using a smartphone, doing nothing, relaxing, talking to the passenger, reading, and watching movies (Beggiato et al., 2015; Hecht, Darlagiannis, & Bengler, 2020; Hecht, Feldhütter, Draeger, & Bengler, 2020; Kyriakidis, Happee, & De Winter, 2015; Large et al., 2018; Ohmori & Harata, 2008; Pfleging et al., 2016; Russell et al., 2011; Susilo, Lyons, Jain, & Atkins, 2012). Naujoks et al. (2018) also provide a catalog of standardized NDRTs used in studies on automated driving, e.g., Surrogate Reference Task (SuRT) and n-back task. The visual-verbal 1-back task utilized in this thesis is one variant of the n-back task (Cools, 2010; Radlmayr, Gold, Lorenz, Farid, & Bengler, 2014).

There are cultural differences, but also common ground for preferred NDRTs in AVs. A Swedish study found that people in megacities may wish to work in their cars more than people in small rural communities (Jorlöv, Bohman, & Larsson, 2017), while the corresponding study in China revealed that relaxing or playing on one's phone during commuting were far more frequently mentioned than working by the megacity residents (Östling & Larsson, 2019). Participants in both studies in Sweden and China mentioned relaxing as the preferred activity on all trips generally.

This dissertation confirms most of the NDRTs that are also found in other literature. Besides, it contributes to mapping the NDRTs to the associated sitting postures in AVs with empirical data.

3.2 Driver States and Take-Over Performance

In manual or assisted driving conditions (Level 0, 1, and 2), NDRTs or tertiary tasks distract the driver's attention away from the primary driving task, which is commonly known as the "driver distraction" (Bengler et al., 2014; de Winter, Happee, Martens, & Stanton, 2014; Ferdinand & Menachemi, 2014; Foley, Young, Angell, & Domeyer, 2013; Green, 1999; NHTSA, 2014, 2016). The distraction of NDRTs at lower automation levels reduces situation awareness (de Winter et al., 2014; Dozza, 2013; Endsley, 1988; Rogers, Zhang, Kaber, Liang, & Gangakhedkar, 2011; Young, Salmon, & Cornelissen, 2013) and loss of situation awareness (Endsley, 1997), which could cause more accidents (Kaber & Endsley, 1997).

Automated driving is shifting the primary driving task from the center to the periphery of attention (Loehmann & Hausen, 2014). In SAE Level 3 automation, drivers do not have to conduct or monitor the driving task continuously (e.g., "Hands-off," "Eyes-off," and "Minds-off") and are fully enabled to engage in NDRTs (Fitzen, Amereller, & Paetzold, 2018). Drivers may conduct NDRTs and NDPs, similar to the passengers on trains (Kamp, Kilincsoy, & Vink, 2011).

While Level 3 automation allows the driver to be out of the control loop, the driver must stay ready to react appropriately to the RtI as the system fallback (SAE J3016, 2018). Marberger et al. (2017) modeled driver availability for take-over into three categories: sensory, motoric, and cognitive states.

When a take-over is required, the driver state in automation transits to a target driver state that is adequate for manual driving regarding all three states: first, reconfiguration of sensory state: e.g., redirecting the gaze from NDRTs to the relevant HMI and the driving scene (Gold, Damböck, Bengler, & Lorenz, 2013; Yang et al., 2017; Yang, Karakaya, Dominioni, Kawabe, & Bengler, 2018); second, reconfiguration of cognitive state: e.g., rebuilding the situation awareness (White et al., 2019) and reconfiguring the mental task sets or response rules (Allport, Styles, & Hsieh, 1994; Kiesel et al., 2010); third, reconfiguration of motoric state: e.g., putting hands on the steering wheel (Kerschbaum, Lorenz, & Bengler, 2015). These three states are not independent of each other and affect each other. For example, cognitive functions, such as problem-solving (Schulman & Shontz, 1971), resolving anagrams (Lipnicki & Byrne, 2005), and sensory functions, such as detection of auditory stimuli and peri-threshold odors (Lundström, Boyle, & Jones-Gotman, 2006, 2008), were improved in an upright posture compared to a supine posture. There are driver micro-motoric states such as hands off the steering (Kerschbaum et al., 2015; Naujoks, Purucker, Neukum, Wolter, & Steiger, 2015) or electronic devices in hands (Helldin, Falkman, Riveiro, & Davidsson, 2013; Naujoks et al., 2018). Besides, there are also macro-motoric states, e.g., drivers' body postures (Bohrmann & Bengler, 2020). Driver's body posture might be related to driver intent, driver affective state, and driver distraction, e.g., leaning backward might indicate relaxing, leaning forward indicates concentration (Tran & Trivedi, 2010). Similarly, Ahn, Teeters, Wang, Breazeal, & Picard (2007) found that the sitting position reflects people's affective state (e.g., slumping following a failure or sitting up proudly following a success).

Winner, Hakuli, Lotz, & Singer (2015) defined the driver state as the whole of all the driver's changing attributes of such kinds which could influence the driving task. Maurer & Stiller (2005) divided the factors into three changeable sub-categories: short-, middle-, and long-term. The short-term factors are attention, load, and emotion. The middle-term factors are fatigue, sickness, and influence of alcohol or drugs. The long-term factors are capability and personality. Drivers' non-driving behavior, i.e., the NDRTs and NDPs in AVs, are the indicators of the changing driver states during automated driving.

In Level 3 automation, the driver must be available and ready to take over the dynamic control in case of system limit. A driver is available to take over if the available time budget exceeds the predicted duration of a safe take-over process, defined by Marberger et al. (2017) from a time perspective. Although there are non-critical take-overs (Alexander Eriksson & Stanton, 2017), where the driver has more time, e.g., 30 seconds to react (Payre, Cestac, & Delhomme, 2016), the take-over process in Level 3 automation is often very time-critical and has to take place within a few seconds in most publications (Flemisch et al., 2012; Gasser & Westhoff, 2012; Gold, Damböck, Lorenz, & Bengler, 2013; Merat, Jamson, Lai, Daly, & Carsten, 2014). The time budget in Level 3 automation often ranges from 5 seconds (Feldhütter, Ruhl, Feierle, & Bengler, 2019) to 9 seconds (Körber, Prasch, & Bengler, 2017). Radlmayr & Bengler (2015) offered a detailed literature overview of the time budget in take-over experiments.

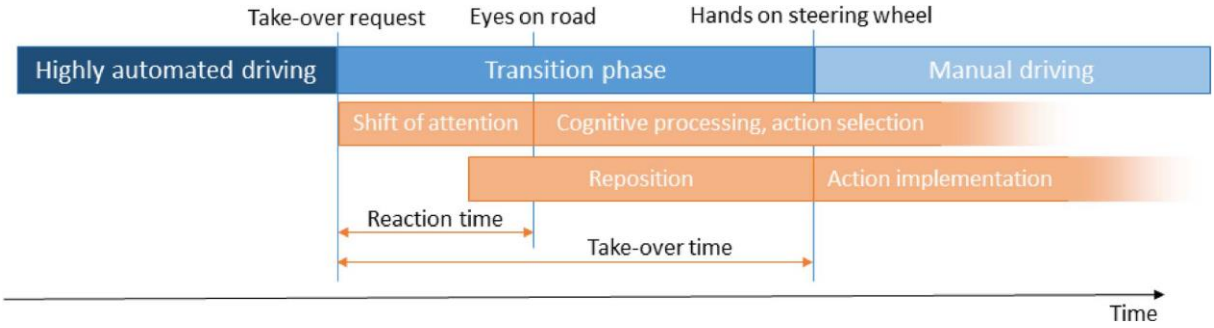

Figure 3-3 The take-over process from highly automated to manual driving (Petermeijer, De Winter, & Bengler, 2016)

In Figure 3-3, Petermeijer et al. (2016) summarized and modified the take-over process covering three works (Gold, 2016; Kerschbaum et al., 2015; Zeeb, Buchner, & Schrauf, 2015). This model also emphasizes the take-over process from three perspectives: sensory (e.g., eyes on the road), cognitive (e.g., cognitive processing), and motoric aspects (e.g., reposition), which are in conformity with the three driver states introduced by Marberger et al. (2017).

To measure the driver's performance when takeing over the dynamic control without the interference of automation systems, Damböck (2013) and Gold (2016) suggested a complete degradation of the Level 3 automation system to Level 0. Gold (2016) defined the term take-over performance based on two aspects: time (e.g., reaction time) and quality (e.g., time to collision). Common metrics concerning these two aspects are found in different experiments measuring take-over performance in Level automation (A. Eriksson, Banks, & Stanton, 2017; Feldhütter, Gold, Hüger, & Bengler, 2016; Gold, Damböck, Lorenz, et al., 2013; Gonçalves, Happee, & Bengler, 2016; Happee, Gold, Radlmayr, Hergeth, & Bengler, 2017; Hergeth, Lorenz, & Krems, 2017; Jarosch, Kuhnt, Paradies, & Bengler, 2017; Kerschbaum et al., 2015; Körber, Gold, Lechner, & Bengler, 2016; Kreuzmair, Gold, & Meyer, 2017; L. Lorenz, Kerschbaum, & Schumann, 2014; Louw et al., 2017; Naujoks, Purucker, & Neukum, 2016; Petermeijer, Bazilinskyy, Bengler, & de Winter, 2017; Vogelpohl, Kühn, Hummel, Gehlert, & Vollrath, 2018; Yang, Karakaya, et al., 2018; Zeeb et al., 2015), for example:

- Time aspects:
  Steering and braking response times i.e., take-over time (TOT) [s], eyes-on-road time [s], hands-on time [s], lane-change time [s], time on task [s], eyes-on-road time [s], steer touch [s], steer initiate [s], steer turn [s].

In this thesis, hands-on time refers to the quickest hand grabbing the steering wheel (one hand). Therefore it is called hand-on time (HoT).

- Quality aspects:
  Maximum lateral and longitudinal accelerations [m/s^2], time to collision (TTC) [s], steering wheel angle [°], standard deviation of steering wheel angle [°], absolute lateral position [m], standard deviation of lateral position (SDLP) [m], type of the first reaction, crash rate [%], checking mirrors [%].

Radlmayr et al. (2018) summarized the take-over performance metrics and proposed an integrative framework to evaluate take-over performance: The take-over performance score (TOPS) including three aspects: first, vehicle guidance parameters: crash (yes/no), time to collision, and maximal lateral and longitudinal acceleration; second, mental processing parameters: lane check (yes/no), gaze reaction time, eyes-on-road reaction time, and take-over time; third, subjective rating parameters: perceived criticality, perceived complexity of the situation, and subjective time budget.

Several external factors and driver-related factors influence take-over time and quality (Zeeb et al., 2015). Traffic situations and NDRTs influence take-over performance (de Winter et al., 2014; Happee et al., 2017; Radlmayr et al., 2014). Gold (2016) identified influencing factors of take-over performance: time budget, traffic density, NDRTs, repetition, lanes, and age. The driver state could also be an essential criterion to ensure that drivers can manage the system limits (Marberger et al., 2017). Zeeb, Buchner, & Schrauf (2016) found that a distracted drivers' take-over quality deteriorated in Level 3 automation. Similarly, Gasser et al. (2012) reported the importance of driver state, which represents the driver availability to take-over in case of system limit and eventually to be able to take over the dynamic control in Level 3 automation. Radlmayr (2020) found that driver state changes caused by prolonged periods of automation and the engagement in different NDRTs did not influence the take-over performance. A strong influence of situational factors on take-over performance was revealed, such as traffic density and take-over situation (Radlmayr, 2020). Cao, Tang, & Sun (2020) found that drivers in the rear-facing position have a longer take-over time (on average 1.5 seconds longer) than front-facing ones due to physical turning. Besides, fatigued drivers appeared to overreact to reduce the collision risk (Feldhütter, Kroll, & Bengler, 2018). Feldhütter et al. (2018) and Weinbeer et al. (2017) found no significant difference between participants' take-over time in the fatigued and alert conditions. Nevertheless, fatigued participants felt more burdened and stressed during the take-over situation. Regarding take-over quality, Feldhütter et al. (2019) revealed that fatigued drivers showed a worse take-over quality (high decelerations, inappropriate trajectories, and initial responses to the RtI, more crashes) compared to alert drivers.

This dissertation supplements the research by illustrating the effects of drivers' body postures on take-over performance in Level 3 automation. Besides, a countermeasure is developed that could compensate for the effect.

3.3 Driver Postures in the Vehicle

In the manual driving condition, the driver must be able to see the environment and the interior elements (visibility); the driver must reach the steering wheel, pedals, and the gear shift in any sitting posture at any time to exercise vehicle dynamic control (accessibility and freedom of movement) (Bubb, Grünen, et al., 2015, p. 347). These given restrictions (e.g., hands on the steering, feet on the pedals or footrest, hip points on the seat) limit the drivers' postures and movement (Bubb, Grünen, et al., 2015, p. 363). When a new car is conceived in the industry, the driver's posture is primarily determined by the steering wheel and pedals, which are already relatively fixed due to packaging concepts (Bubb, Grünen, et al., 2015, p. 355; Pischinger & Seiffert, 2016, p. 689; Schmidt, Seiberl, & Schwirtz, 2015). The seat adjustments enable a limited range of individual

sitting postures (Bubb, Grünen, et al., 2015, p. 355; Pischinger & Seiffert, 2016, p. 689). Standard SAE J1100 (2009) specifies the common vehicle dimensions (e.g., Figure 3-4).

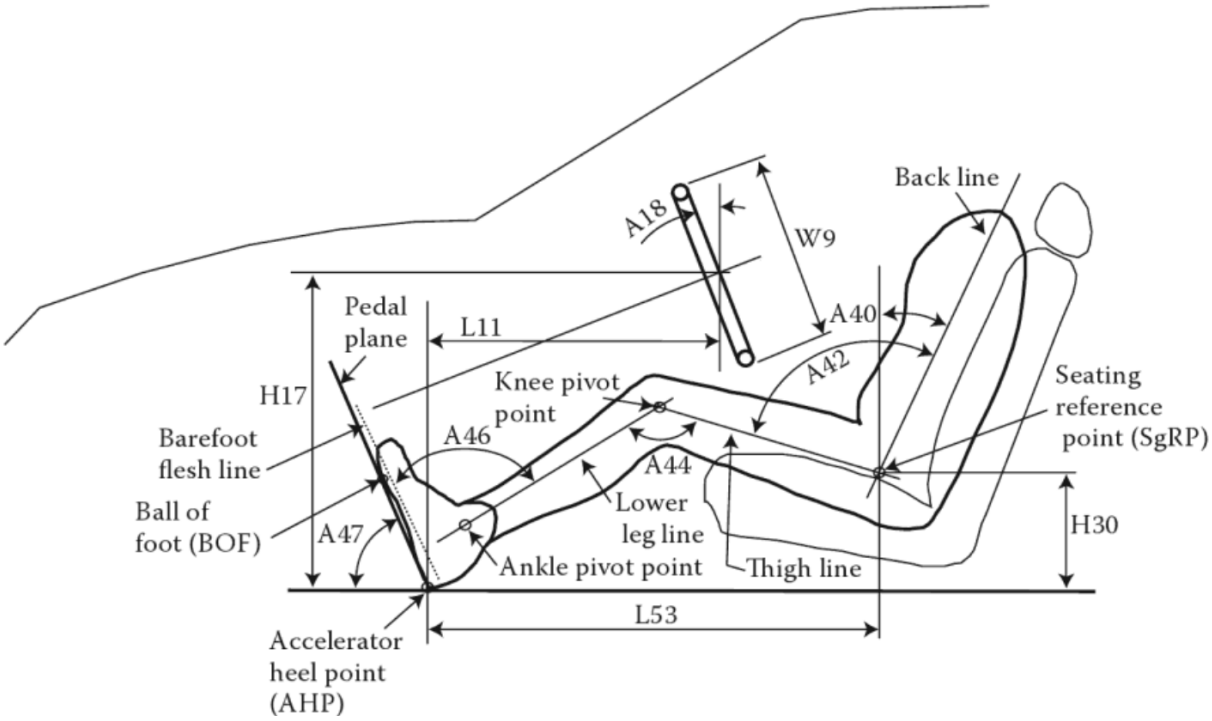

Figure 3-4 Definition of the torso angle (A40) and the knee angle (A44) (Bhise, 2016; SAE J1100, 2009)

Torso angle is labeled as A40 in SAE J1100 (Figure 3-4), the angle between the back line and the vertical. The A40 torso angle is also called the seatback angle or back angle from the perspective of automotive interior packaging (Bhise, 2016). There is no standard way to measure the torso angle due to the variable flexion of the human spine (Kolich, 2010).

Figure 3-5 shows the definitions of relevant joint angles, seat angles, and seat adjustments in this thesis. Driver postures in this thesis are defined by the joint angles in the x-z plane of the vehicle coordinate system (SAE J1100, 2009). The torso line (back line) was measured as a straight line between the shoulder and the H-point from one side of the driver (Figure 3-5, a), assuming that the driver's torso is a rigid body. In this thesis, the torso angle is the driver's actual torso angle, different from the physical seatback angle. The seatback angle is the angle between the inner surface of the seatback and the vertical (Figure 3-5, a). The seatback adjustment (SBA) (Figure 3-5, b) influences the torso angle directly when the torso has tight contact with the seatback surface.

The knee angle (Figure 3-5) is the A44 in SAE J1100 (Figure 3-4), the angle between the thigh and the lower leg. The thigh angle is defined as the angle between the thigh and the horizontal, which could also be derived by the equation *thigh angle = torso angle (A40) + 90° - hip angle (A42)*. The seat inclination adjustment (SIA) (Figure 3-5, b) influences directly the thigh angle when the thigh has tight contact with the seat surface. The angle between the seat surface and the horizontal is the seat inclination angle (Figure 3-5, a).

Instead of the virtual H-point or the seating reference point in Figure 3-4 of the H-point machine (SAE J826, 2008), the H-point (Figure 3-5, a) in this thesis means the actual hip point of the driver/participant. The H-point can be positioned by the seat height adjustment (SHA) in the z-direction and the seat longitudinal adjustment (SLA) in the x-direction (Figure 3-5, b).

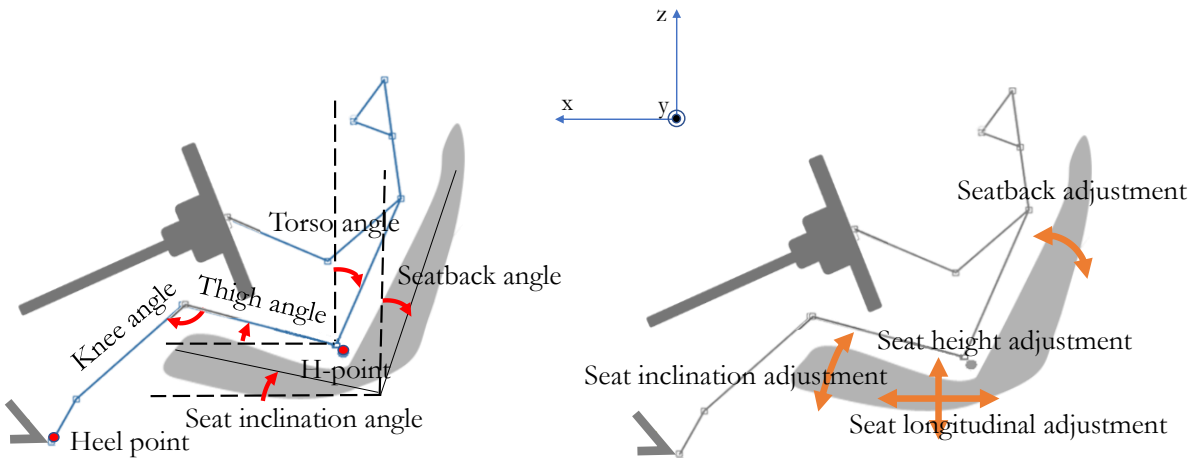

(a) Joint and seat angles

(b) Seat adjustments

Figure 3-5 Definition of joint angles, seat angles (a), and seat adjustments (b) in the vehicle coordinates' x-z plane. The directions of the red arrows in (a) indicate the positive directions of the angles.

Focusing on the driving task, the driving posture has been widely researched regarding individual preferences, sitting comfort, and safety. Damon, Stoudt, & McFarland (1966) proposed the driver's joint angles as references to vehicle concepts, torso angle: 25° ± 3°, shoulder: 39° ± 12°, elbow angle: 146° ± 17°, hip angle: 107° ± 7°, knee angle: 122° ± 8°, ankle angle: 84° ± 16°. The desired torso angle varies depending on different vehicle concepts around 25° ± 10°, the corresponding ankle angle is 87°, and the hip angle is 95° (Grabner & Nothhaft, 2002). Schmidt et al. (2015) recommended the elbow angle be between 95° and 120° for a quick and precise steering operation. With reclinable seats, most drivers prefer to sit more upright (18°–22° torso anlge) in most passenger cars, about 15° to 18° for pick-ups and SUVs, and about 10° to 15° for trucks (Bhise, 2016). Bubb, Grünen, et al. (2015, p. 363) summarized the driver's comfortable angles in different studies: the torso angle ranges from 15° to 35°; 15° to 55° for the shoulder angle; 85° to 163° for the elbow angle; 85° to 149° for the hip angle; 95° to 150° for the knee angle. Most passenger car concepts are designed with a torso angle of 22° to 25° (Grünen, Günzkofer, & Bubb, 2015, p. 191). Many headrests are designed to follow the contour of the seatback, which typically reclines at an angle of 25° from the vertical (Viano & Gargan, 1996). Andersson & Ortengren (1974) recommended a relaxed sitting position with low disc pressure with a seatback angle of 20°–30° to the vertical and a 14° seat inclination to the horizontal. The observed values vary significantly in reality, ranging from 5° to 35°, depending on the height of the seat (H30) (Grünen et al., 2015, p. 191). Federal Motor Vehicle Safety Standards (FMVSS) 202a specified that the backset (distance between the head and the headrest) should be measured with a 25° torso angle (NHTSA, 2011a), which is also the manufacturer's "design-position" in most cases. However, 80 to 85 percent of the

observed torso angles are smaller, making 21° or 22° more representative in the manual driving condition (Kolich, 2010). Park, Kim, Kim, & Lee (1998) studied the comfortable driving postures for Koreans. The trunk-thigh angle (hip angle) and the lumbar support are the most important parameters. The averaged hip angle is 117° (range: 103°–131°). The preferred seatback angle was averaged 35.5° and ranged from 25° to 45°; the participants were rather reclined when compared to other literature.

In this thesis, postures with a torso angle of less than 25° are labeled as upright postures or driving postures; postures with a torso angle of more than 25° are labeled as reclined postures (Figure 3-6).

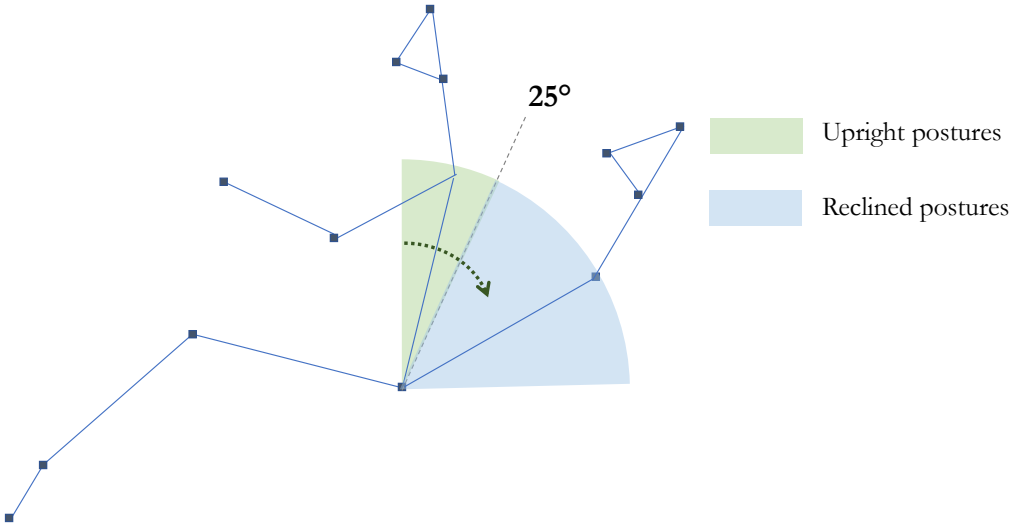

Figure 3-6 Definition of the range of upright postures and reclined postures in this thesis

Lorenz (2011) mentioned that high standard deviations apply to the data collection of comfortable angles since the preferences are individual. Jonsson et al. (2008) illustrated the intrapersonal repeatability and intraclass correlation of seat adjustment. Bubb, Grünen, et al. (2015, p. 363) explained that human bodies are so adaptive and tolerant of different postures that, apart from individual physical limitations, the discomfort is hardly noticed in the short term. Zenk (2008) and S. Lorenz (2011) showed that drivers are not able to find the optimal seat adjustment based on the perception of discomfort (Bubb, Grünen, et al., 2015, p. 374). Besides, the formation of a posture highly depends on the geometries of the interior (Reed, Manary, Flannagan, & Schneider, 2000), which vary in different laboratory settings and actual vehicles. The static postures and human movements are also inter- and intra-individually different in the experiments (Arlt, 1999).

Sitting postures are greatly influenced by drives' behavior and the adjustability of the seat and geometrical design (Jonsson et al., 2008). In Level 3 automation, the driver could be out of the control loop and conduct NDRTs. When the driver is conducting NDRTs, driver postures are labeled as non-driving postures (NDPs) in this thesis. Most drivers in an AV simulation were observed using the opportunity to change their postures and seat adjustments (Figure 3-7); they would most likely recline to relax themselves (Large et al., 2018). Kamp et al. (2011) observed different passengers' postures and activities on trains. Kilincsoy, Wagner, Bengler, Bubb, & Vink (2014) observed 12 postures on passenger back seats of a vehicle associated with eight activities:

working, eating/drinking, using a mobile device, talking/discussing, reading, watching, relaxing, and sleeping/drowsing. Zhou, Zhan, Wang, & Zhang (2017) investigated the effect of different train drivers' sitting positions on driver injury severity, indicating that those train drivers whose arms were lying on the control desk had a lower injury severity than those whose arms were dropping naturally.

McMurry et al. (2018) express their concerns that being out of position was associated with an elevated risk for serious injury. The results regarding crash safety were retrieved from the NASS-CDS database of the National Highway Traffic Safety Administration (NHTSA). Most of the out-of-position occupants were young, mostly in rotated or reclined postures, and less likely to be belted.

Figure 3-7 Examples of NDPs observed by Large et al. (2018)

Köhler, Pelzer, Seidel, & Ladwig (2019), who investigated the sitting position in higher automated driving conditions (SAE Level 4–5), attained a dataset of verified sitting postures. The automation was simulated in the passenger chamber of a compact bus, offering more degrees of freedom for seating configurations and different activities. The upper body was qualitatively described based on three aspects: lateral position, z-rotation, and sagittal position. The body parts observed were the head, shoulder, lower back, and legs. The presentation frequency of a specific posture in the different use cases was documented in percentage over time.

The Neutral Body Posture was defined by NASA (Mount, Whitmore, & Stealey, 2003), where each muscle is neither contracted nor extracted in the zero-g condition (Figure 3-8). This neutral posture is often used to reference drivers' comfort angles (Bubb, Grünen, et al., 2015, p. 363). Figure 3-8 shows that the NASA Neutral Body Posture was developed in Skylab studies (n = 12). The average hip angle is 128°, and the average knee angle is 133°. Assuming the thigh is horizontally placed on a seat surface, a 128° (± 7°) hip angle corresponds to a 38° (± 7°) torso angle, which is a rather reclined sitting posture. The relined posture in this thesis is oriented toward the average torso and knee angle of the Neutral Body Posture since the reason for being reclined is most likely to relax (Large et al., 2018; Tran & Trivedi, 2010).

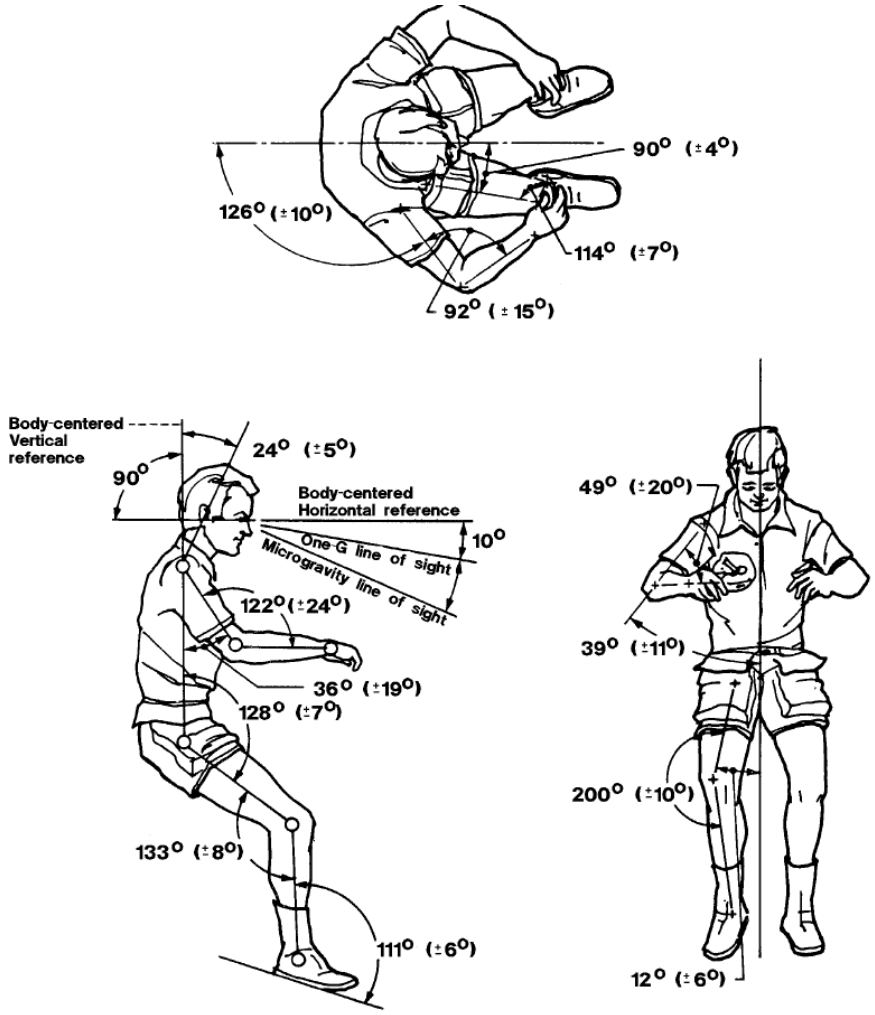

Figure 3-8 Neutral Body Posture was developed in Skylab studies by NASA, presented by mean joint angles and the standard deviations in parentheses (Mount et al., 2003)

The reclined sitting position relaxes the back muscles and leads to lower disc pressure than the upright or forward-leaning positions; the disc pressure and back muscles' electrical activity are continuously reduced when the sitting hip angle increases from 80° to 130° (Andersson & Ortengren, 1974; Grandjean & Hünting, 1977). Reclined postures may reduce the driver's secondary wake drive and cause the driver to fall asleep (Johns, 2000). Sleepiness and drowsiness can be critical in Level 3 automation, where the driver is the fallback of the system in case of system limit. Muehlhan, Marxen, Landsiedel, Malberg, & Zaunseder (2014) demonstrated the effect of body posture on cognitive performance. The sleep quality strongly affected reaction times when participants performed a working memory task in a supine posture, but this effect could not be observed in a sitting posture. Similarly, certain cognitive functions were improved in an upright posture compared to a supine posture, such as problem-solving (Schulman & Shontz, 1971), resolving anagrams (Lipnicki & Byrne, 2005), detection of auditory stimuli, and peri-threshold odors (Lundström et al., 2006, 2008).

Bohrmann & Bengler (2020) reported that reclined postures reduce motion sickness significantly. Motion sickness is an inevitable problem in AVs since the driver/occupant does not control the

motion (Diels & Bos, 2016). Rotated postures in a moving cabin could cause motion sickness since the visual input corresponds poorly with the acceleration being sensed by the vestibular system (Bubb, 2015a, p. 496). Salter, Diels, Herriotts, Kanarachos, & Thake (2019) found that rearward-facing seating orientations led to significantly more motion sickness symptoms.

Nissan Motor Corporation developed a new seat and applied the Neutral Body Posture in the studies focused on the driver's biomechanical loads. Results showed that the driver's posture remained close to the Neutral Body Posture; the physical fatigue was reduced dramatically both in the static sitting (Hirao, Kitazaki, & Yamazaki, 2006) and the dynamic driving condition (Hirao, Kato, Kitazaki, & Yamazaki, 2007).

Driver's posture is one factor that determines the all-round visibility from the driver seat, and it is highly safety-relevant (Pschenitza & Unger, 2015). The driver's eye height is one of the parameters to estimate visibility (Capaldo, 2012). The sight to the front, in turn, influences the choice of the seat adjustment, thus the driver's sitting position (D. Lorenz, 2015). SAE J941 (2010) explains the location of drivers' eyes inside a vehicle in practice.

Bubb (2015b, p. 238–253) summarized the development of the anthropometrical human models; there are physical and digital human models, including geometrical and biomechanical models. Digital human models simulate the driving postures in the early development phases, e.g., Human Builder (Dassault Systèmes), Jack (Siemens PLM), and RAMSIS (Human Solutions) (Bullinger-Hoffmann & Mühlstedt, 2016). RAMSIS is often used in the automotive field; it enables the posture model and the field-of-view model to virtually validate interior concepts at lower costs (Kremser, Lorenz, Remlinger, & Bengler, 2012). Driver's NDPs in AVs call for new digitalized simulation tools. Besides, safety assessment tools designed and valid for omnidirectional loading for NDPs in AVs are also needed (Östling & Larsson, 2019).

This dissertation contributes to associating NDPs to relevant NDRTs, modeling static NDPs with joint angles and seat adjustments, and modeling the dynamic take-over body movement. Data could support digital human modeling in autonomous driving. As the focus of the thesis, reclined postures are researched comprehensively regarding their user acceptance, the risks, the dynamic motion, and the interaction with the driver seat in the take-over process in SAE Level 3 automation.

3.4 Interior Development for Automated Vehicles

Current interior concepts applied in Level 0–2 vehicles are restricted by the driver's continuous engagement in the driving task to ensure the driver's visibility of the environment, the accessibility of the driving elements and the freedom to move (Bubb, Grünen, et al., 2015, p. 347). Bubb, Grünen, et al. (2015) offered a detailed overview of the current driving-task-centric packaging concept. NDRTs, as user scenarios in the current design process, have been considered a secondary or rather tertiary priority because of their distracting characters to the primary driving task.

The current interior concepts (e.g., the position, type, and modality of HMI) and driver behavior (e.g., movement and postures) are strictly regulated. For example, when conducting a visual-manual task (e.g., radio-tuning, navigation-setting), the Alliance of Automobile Manufacturers (AAM)

requires that: first, single glance durations should not exceed two seconds; second, task completion should require no more than 20 seconds of total glance time to task displays and controls (AAM, 2003). Similarly, NHTSA also recommends acceptance criteria to use portable and aftermarket devices during the manual driving condition. Single average glances away from the forward roadway are 2 seconds or less. The sum of the duration of all individual glances away from the forward roadway is 12 seconds or less while performing a task, such as selecting a song from a satellite radio station (NHTSA, 2016).

Driver's field of view is influenced by the eye position (SAE J941, 2010). The German StVZO § 35b and EU Guidelines RL 77/649/EWG and ECE-R 125 regulate the exact field of view of a seated driver in the manual driving condition (Lutz, Tang, & Lienkamp, 2012), which sets requirements for the dimensions of the bodywork, the interior, and the whole HMI strategy. Most importantly, drivers are expected to be seated in an upright posture to enable the necessary field of view.

The paradigm change of Level 3 automation brings new scenarios for interior design, including HMI. Drivers might conduct NDRTs as the primary task within the system limit for an extended period. On the other hand, drivers should be fallback-ready and able to take over control in case of system limit. Flemisch et al. (2011) proposed three visual elements as design guidance for HMI in AVs: first, "Automation Monitor": current automation level and its functionality; second, "Automation Scale": current automation level and available automation levels; third, "Message Field": detailed text messages and warnings. A visual warning in the traditional instrument cluster or the head-up display might not be in the driver's foveal field of view when the driver, for example, looks down and plays on his or her smartphone. A visual interface at the periphery field could convey subtle information without being annoying and disturbing the driver while performing the NDRTs and could increase the situation awareness (Yang, Karakaya, et al., 2018). Visual, auditory, tactile, and haptic stimuli are often applied to human-machine interaction (Schenk & Rigoll, 2010). Yang et al. (2017) compared five modalities (visual, auditory, haptic, thermal, and olfactory) with regard to eight aspects, including "content of information," "coverage rate," "forgiveness rate," "perceptibility" (Hoffmann & Gayko, 2012), "interpretability," "limitability," "interference potential," and "localizability." The UR:BAN project provided comprehensive HMI strategies and solutions concerning warnings, interventions, lateral and longitudinal control, as well as recommended actions for complex urban scenarios (Bengler, Drüke, Hoffmann, Manstetten, & Neukum, 2018).

Melcher, Rauh, Diederichs, Widlroither, & Bauer (2015) investigated take-over request strategies. They suggested that a basic multimodal (visual and audible) perceivable stimulus should be mandatory for RtI signals. Further enhancements (e.g., cellphone integration or break jerk) could lead to increased acceptance and perceived safety but had no effect on the response time. Bazilinskyy, Petermeijer, Petrovych, Dodou, & de Winter (2018) reviewed auditory, visual, and vibrotactile displays in various applications and suggested that multimodal warnings are the preferred option for high-urgency situations. Forster, Naujoks, Neukum, & Huestegge (2017) reported that, in addition to a generic warning tone, a semantic speech output for the

announcement of an upcoming take-over could reduce the reaction times, which reflects a reduction of the information processing time.

Hale & Stanney (2004) suggested the haptic interfaces could include tactile (e.g., the vibration of seat surfaces or the steering wheel) and kinesthetic stimulation (e.g., seat adjustment movement or steering wheel transformation). Kinesthetic devices are advantageous when tasks involve hand-eye coordination (for example, object manipulation), in which haptic sensing and feedback are crucial to performance (Hale & Stanney, 2004; Mulgund, Stokes, Turieo, & Devine, 2002). Stanley (2006) suggested that the haptic modality improved the human reaction time in response to the lane change warning compared to the auditory modality. Besides, haptic is less annoying than the auditory modality, yet the combination of haptic and auditory modalities gained more user preference for the lane departure warning.

A haptic seat might be more effective than the haptic steering wheel in AVs since haptic signals on the steering wheel might not be perceivable in hands-off situations. Petermeijer (2017) applied the haptic vibration motors underneath the surface of the seat and seatback, varying their amplitude and frequency to transfer warning or information. Results showed that multimodal take-over requests led to significantly better performance (visual, auditory, and haptic). However, the directional vibration flow as an information carrier was hard to perceive and understand.

Current seat concepts, optimized for the driving posture, might not serve out-of-the-control-loop drivers. Design and development of new seats and interior concepts are necessary (Winner & Wachenfeld, 2015). Contemporary interior and HMI concepts are developed and optimized with the driving posture models (e.g., RAMSIS). For future AVs, extended human models should be able to simulate NDPs of drivers conducting NDRTs. The absence of the driving task gives more possibility for interior concepts, especially seat configuration, e.g., adjustment range, orientation, arrangement (Tzivanopoulos, Watschke, Krasteva, & Vietor, 2015). The current driver seat concept is mostly optimized for an upright sitting posture with a "design torso angle" of about 22° to 25° (Bubb, Grünen, et al., 2015, p. 375; NHTSA, 2011a). Reclined postures might lead to discomfort and danger in the current seat concept, e.g., the headrest might not provide enough support for the head due to the displacement. A novel recliner should be offered in AVs (Östling & Larsson, 2019; Winner & Wachenfeld, 2015). As one of the first industrial applications of a recliner for the front passenger, BMW presented the ZeroG Lounger concept for the front passenger at CES 2020 (Figure 3-9). The passenger seatback is tilted back by 40° or 60° into a comfortable reclined position (BMW Group, 2020c). The First-Class rear seat in a Mercedes-Maybach S-Class (Z 223) allows rear passengers to work in an upright seatback angle of 19° and a reclined angle of 43.5° (Daimler AG, 2020b). Volvo Car Corporation published a series of patents regarding the interior systems in autonomous driving scenarios, detecting foot arrangement of the driver (Patent No. US9783206B2, 2015), adjusting interior elements once the vehicle is in an autonomous driving mode (Patent No. US9908440B2, 2016), offering a sleep mode during autonomous driving, and transiting back to the manual driving mode (Patent No. EP3000651B1, 2014).

Figure 3-9 The ZeroG Lounger concept (BMW Group, 2020c)

Similar to the theory of banked curves of train tracks, Winner & Wachenfeld (2015) proposed a concept of transversely banked chassis to compensate for the accelerations of centrifugal force in the curve and to match the banked sitting posture of drivers. This might apply to AVs and increase riding comfort in curves.

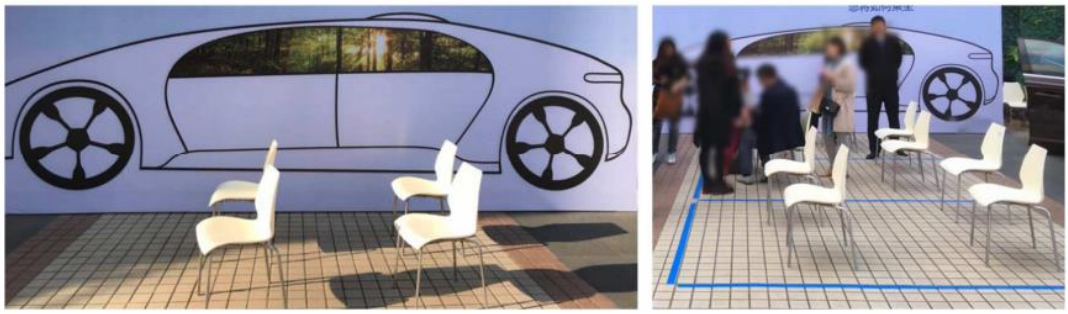

Figure 3-10 "Setting the stage": minimalist setup of a vehicle interior (Östling & Larsson, 2019)

As an adaptive interior element in AVs, Kerschbaum (2018) investigated the alternative usage of the steering wheel in automated driving, which was mainly intended for the primary driving task in the manual driving mode. Different transforming steering wheel concepts for automated cars are investigated. Results showed that the mechanical transformation of the steering wheel could lead drivers to start the transition process earlier in a take-over situation.

The "setting the stage" method allowed participants to use their imaginations to design and express their expectations for a fully automated vehicle (Figure 3-10) (Jorlöv et al., 2017; Pettersson & Karlsson, 2015). Using this method, Östling & Larsson (2019) investigated the occupant activities and sitting postures in SAE level 5 automation and found that it was important for participants in both China and Sweden to be able to recline seats, even fully horizontally. Besides, smartphones or screens on board were important. The 2015 Mercedes-Benz F 015 concept car allowed the driver

and the front passenger to rotate up to 180° to face the rear occupants (Geisler et al., 2019). A similar rear-facing driver seat concept could also be found in the MINI Urbanaut (BMW Group, 2020b). Apart from the latest research on autonomous driving, the rear-facing seat arrangement was already a topic early in the 1950s due to passive safety, before the three-point seat belt was invented. In Cornell Aeronautical Laboratory, Edward Dye suggested that good crash safety could be obtained if all seats, except the driver seat, faced the rear (Waltz & Luckett, 1950).

Since it is technically impossible to guarantee zero accidents of AVs (Shalev-Shwartz, Shammah, & Shashua, 2017), the passive safety of an AV (e.g., occupants constrain systems like a seat belt or airbags) remains essential. The validation of safety concepts is challenging due to the higher complexity and heterogeneity of AVs' uses cases and NDPs. Östling & Larsson (2019) gave an insight into the safety implications and the need for novel restraints in fully automated vehicles. The well-known "submarine effect" represents a significant cause of injuries resulting from the occurrence of frontal collisions (Otat, Otat, Tutunea, Geonea, & Marinescu, 2019). When the seatback is reclined in AVs, the "submarine effect" might become more likely to occur. The lap belt might slip over the pelvis to the abdomen as the occupant submarines into the seat and slides forward to the footwell (Östling & Sunnevång, 2017). As countermeasures, the pre-tensioning of the lap belt, combined with an inflatable seat pan structure, could help up to a 45° seatback angle (Östling & Sunnevång, 2017). The "criss-cross belt" concept with an additional shoulder belt could help to fix the occupant's upper body in a crash (Mroz, Pipkorn, Cecilia Sunnevång, Eggers, & Bråse, 2018; Östling, 2017), and could avoid the upper body sliding out when the seat is rotated (Östling & Larsson, 2019; Surya Sengottu Velavan, 2018). Current passive safety assessment tools and methods are designed for drivers in the manual driving position. For example, three dummies of the 5th percentile female, 50th percentile male, and 95th percentile male, used in crash tests, are only validated for the pure frontal or pure side impact in defined sitting postures. For other NDPs in AVs, new models and tools are needed (Östling & Larsson, 2019).

This thesis offers empirical data of static NDPs and take-over motion, which set packaging requirements of AVs. The active seat assist shows the potential of applying adaptive interior elements in AVs with good user experience.

3.5 Driver Seat History and Seats Used in This Thesis

This section provides a brief summary of the development of the automotive driver seat. The seat is one of the most important interfaces between the driver and the car to support, hold, and position the driver's body. People spend an average of 300 hours every year in the driver seat, and 25% of the body surface are in contact with the seat (Pischinger & Seiffert, 2016). Over more than 200 years, the driver seat has developed from a simple chair to a bench seat, from a bench seat to a bucket seat, from no headrest to a mandatory headrest, from no safety belt to a mandatory safety belt, from one sitting function to many comfort and safety features, from driving-task-oriented concepts to future NDRT-compatible or living-room-like concepts.

Known as the first self-propelled road vehicle, the steam-powered vehicle invented by Nicolas-Joseph Cugnot in 1769 (Figure 3-11, a) had the earliest bench seat, or rather a chair in a

vehicle (Grey, 2016). The 1886 Benz Patent Motor Car (Figure 3-11, b) had a bench seat with a leather cushion and armrests (Daimler AG, 2020a). The 1908 Ford Model T (Figure 3-11, c) integrated the bench seat, the seatback, and the armrest (Ford Motor Company, 2020). The bench seat was developed and applied widely together with the column shift, particularly in American cars, e.g., the 1959 Chevrolet Impala (Figure 3-11, d) (General Motors, 2012). In the US, the bench seat was produced until 2014 in the last generation of Chevrolet Impala (General Motors, 2012). In Europe, the bucket seat started to appear and replace the bench seat in the 1960s, e.g., the 1963-1981 Mercedes-Benz 600 (W110) had the bucket seat in the front and a functional center console (Figure 3-11, e) (Daimler AG, 2020c). Nowadays, the bucket seat dominates the global market. The front seat arrangement in most passenger cars remains similar to this example of the 1986 BMW E30 M3 (Figure 3-11, f): two bucket seats in the front with a multi-functional center console in the middle, which might be integrated with the gear shift, the hand brake, some storage compartments, or other control buttons. A special kind of seat is the racing seat (Figure 3-11, g), also known as the shell seat (RECARO Automotive, 2020), which integrates the seat with the seatback and multi-point seat belts in sports cars. Novel interior prototypes and concepts are found in the recent development of AVs, in which driver seats are not only oriented toward the driving task but also NDRTs such as relaxing and talking to the rear passengers, e.g., the 2019 Brose reclined seat (Figure 3-11, h) (Brose, 2019) and the rotating seat in the 2020 Mini Urbanaut (Figure 3-11, i) (BMW Group, 2020b).

Katz Benjamin patented the headrest, mounted or integrated on the top of the seat to restrain the rearward movement of the head in a rear impact in 1921, preventing injury to the cervical vertebrae (Patent No. US1471168A, 1921). However, driver seats in most passenger cars were not equipped with headrests until the late 1960s (examples in Figure 3-11, a, b, c, d, e). No headrest or a low headrest position may increase the whiplash effect by acting as a fulcrum, resulting in severe cervical vertebrae injury (Berton, 1968; Severy, Brink, & Baird, 1967, 1968; Viano & Gargan, 1996). Head restraints became mandatory for all cars produced after January 1, 1969, in the US. The FMVSS 202a requires head restraints to be at least 700 mm (27.5 in) above the seating reference point or limit the relative angle between the head and the torso to 45 degrees or less during a dynamic test (NHTSA, 2004). NHTSA (2011b) offers an overview of seat-relevant FMVSS regulations, the FMVSS No. 202a: Head Restraints; No. 207: Seating Systems; No. 209: Seat Belt Assemblies; No. 210: Seat Belt Assembly Anchorages.

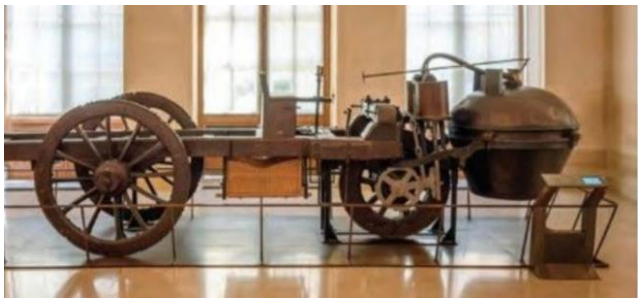

(a) The 1770 Nicolas-Joseph Cugnot's steam powered vehicle

(b) The 1886 Benz Patent Motor Car

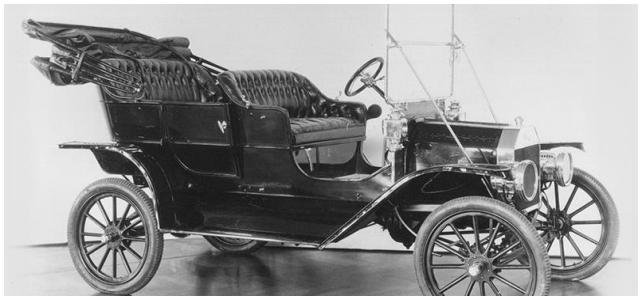

(c) The 1908 Ford Model T

(d) The 1959 Chevrolet Impala

(e) The 1963 Mercedes-Benz 600 W110

(f) The 1986 BMW E30 M3

(g) The 2020 RECARO Racing seat

(h) The 2019 Brose flexible seat system

(i) The 2020 MINI Vision Urbanaut

Figure 3-11 Examples of the development of the driver seat. Image source respectively: a (Grey, 2016), b (Daimler AG, 2020a), c (Ford Motor Company, 2020), d (General Motors, 2012), e (Daimler AG, 2020c), f (BMW Group, 2020a), g (RECARO Automotive, 2020), h (Brose, 2019), i (BMW Group, 2020b)

Primitive driver seats (Figure 3-11, a, b, c) had no other features than offering the driver a place to sit. In the 1960s and 1970s, most bench seats were not reclinable, and the seatback angle was fixed to about 24° or 25° by many manufacturers (Bhise, 2016). In 1957, the Ford Thunderbird offered

the driver a 4-way power seat (fore/aft and up/down). Its multi-level memory function could move rearward once the key turned off to allow easy exit and re-entry, and then return to the previous position once the key turned on (Mueller, 1999). Driver seats in modern vehicles can feature many comfort functions, such as 30-way power seat adjustment (e.g., the 2017 Lincoln Continental), heating, ventilation, massage, and outward-swiveling functions (Wysocky, 2016). Besides, there are passive safety features in modern car seats, such as the seat-mounted thoracic side airbags, providing a protective cushion between the occupant and the intruding door (Gaylor, Junge, & Abanteriba, 2017). Regarding active safety, Mercedes introduced the PRE-SAFE® occupant protection system in 2002, which prepares the driver for the potential collision by preventive tensioning of the front seat belts and repositioning of the front-passenger seat (Daimler AG, 2002).

Bohlin from Volvo AB invented the first three-point seat belt system comprising two lower and one upper anchoring device in 1959 (Patent No. US3043625A, 1959). The 1959 Volvo PV544 was built as the world's first car with standard-fit three-point safety belts (Volvo Car, 2009). The three-point belt proved, by a statistical analysis of more than 28,000 accident cases, to be fully effective against ejection out of the car (Bohlin, 1967). The mandatory seat belt laws were introduced in Europe and Australia in the 1970s and New York in 1984 (A. Cohen & Einav, 2003). Mercedes-Benz first introduced the airbag and belt tensioner on the 1981 S-Class W126 (Daimler AG, 2006). In 1972, Donald Lewis invented the inflatable seatbelt, also known as the seatbelt airbag, to increase the seat belt area and distribute the force (Patent No. US3841654A, 1972).

(a) Seat in Chapters 4 & 6 (b) Seat in Chapter 5 (c) Seat in Chapters 7 & 8

Figure 3-12 The conventional seats used in the five experiments of this thesis

In the five studies of this thesis, the three seats (Figure 3-12) used are conventional driver seats taken from the current series products, which are neither optimized nor built for unconventional sitting positions in AVs, e.g., the reclined posture. The first seat (Figure 3-12, a) was installed in the Modular Ergonomic Mock-up (MEPS) for the experiment in Chapter 4 and installed in the Motion Laboratory for the experiment in Chapter 6. The second seat (Figure 3-12, b) was installed in the

driving simulator for the experiment in Chapter 5. The third seat (Figure 3-12, c) was taken from the MEPS and modified in Chapter 7. It was equipped with the active seat assist system, installed in the dynamic driving simulator for the experiment in Chapter 8. All of these are the facilities of the Chair of Ergonomics at the Technical University of Munich.

The research into automobile seats is often found in the fields of automobile packaging, considering anthropometric and biomechanical aspects (Park et al., 1998), comfort (Heckler, Wohlpart, & Bengler, 2019; Kolich & Taboun, 2004), discomfort (Ulherr, 2019), and safety (Kang & Chun, 2000). This dissertation contributes to illustrating the mismatch between the current seat concept and the NDPs in AVs, setting new requirements, and introducing the active seat assist as a new effective feature in the take-over situation for Level 3 automobiles.

4 Exploration and Identification: User Behavior

AV users would conduct more NDRTs and stay in different NDPs, which can differ from, and have wider ranges than, the current driving posture.

This chapter describes the first experiment of this thesis, focusing on exploring and identifying the users' needs regarding NDRTs and the associated NDPs. This study, consisting of an online questionnaire and a laboratory experiment, has been pre-published with the title: "How will the driver sit in an automated vehicle? – The qualitative and quantitative descriptions of non-driving postures (NDPs) when non-driving-related tasks (NDRTs) are conducted" (Yang et al., 2019) in Proceedings of the 20th Congress of the International Ergonomics Association (IEA 2018). This chapter provides the most important findings and discussions. More details can be found in the original publication. This experiment was conducted with the assistance of Jan Niklas Klinkner as part of his semester thesis (Klinkner, 2017).

To explore the user behavior and avoid restrictions of the participants' minds, participants in the questionnaires and the experiment were not instructed with regard to a specific level of automation. Only the generic "automated driving" was mentioned.

The online study ($n = 122$) identifies 13 NDRTs that would be conducted by significantly ($\alpha = 0.05$) more drivers in automated driving than in conventional manual vehicles. They are: telephoning with/without a hands-free system; doing nothing, day-dreaming or relaxing; using an infotainment and navigation system; using a smartphone; using a tablet or a laptop; reading newspapers, books; working and studying; watching movies; taking care of children; playing video games; sleeping; body care (e.g., make-up) (Yang et al., 2019). The identified activities present the delta between activities in conventional vehicles and AVs. Some of those activities are already conducted in conventional vehicles but would be more frequently carried out in AVs and have different user expectations.

The four most frequently mentioned postures: seated facing/against the driving direction, seated facing the front-seat passenger, and reclined facing the driving direction are mapped to the activities (Figure 4-1). It is a many-to-many relationship, which means an NDRT can be matched to more than one posture, and each posture can also fit more than one NDRT (Yang et al., 2019). This finding could explain the context of the posture and predict the posture range of one activity with various probabilities.

Overall, the conventional upright "seated facing the driving direction" is still the most popular sitting posture (71.41%), followed by the "reclined facing the driving direction" (10.29%), "seated against the driving direction" (7.90%) and "seated facing the front-seat passenger" (7.54%) positions. The reclined posture is the preferred posture among all the non-conventional sitting postures, especially when drivers are "sleeping" (71%), or "doing nothing, day-dreaming, or relaxing" (29%) (Yang et al., 2019). Furthermore, most of the current interior dimensions are adequate regarding the geometrical requirement, while the space between the seatback and the

steering wheel could be expanded. Drivers intend to be backward-shifted during automated driving (Yang et al., 2019). This expansion could be realized by the steering wheel longitudinal adjustment, SLA, and SBA.

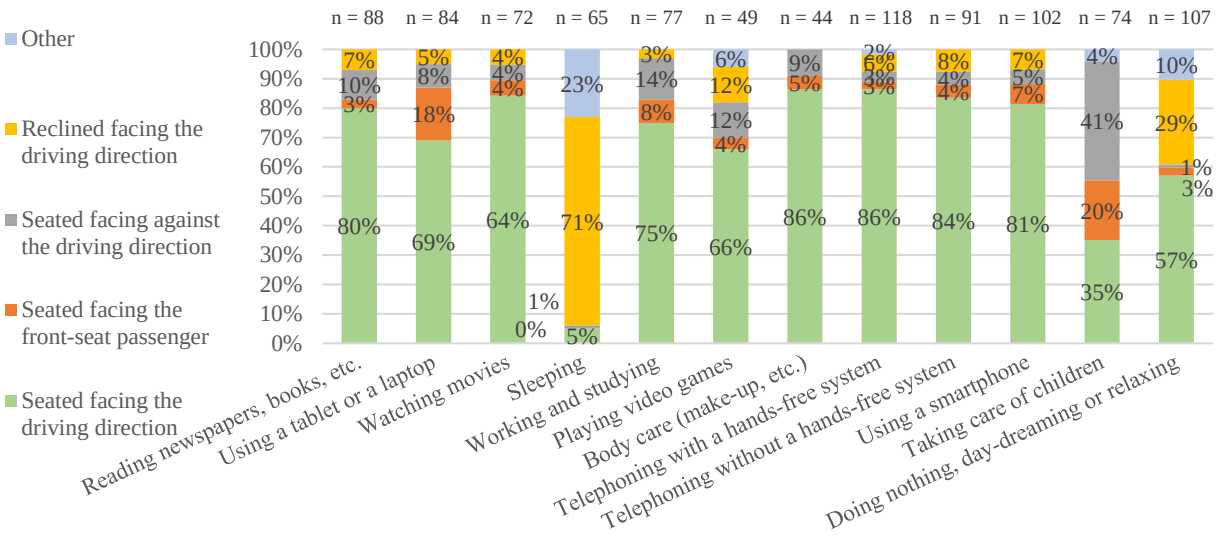

Figure 4-1 The many-to-many relationship between NDRTs and NDPs (Yang et al., 2019)

Based on the online study, a follow-up laboratory experiment (n = 16) was conducted in the Modular Ergonomic Mock-up (MEPS) of the Chair of Ergonomics at TUM. Figure 4-2 shows the experimental setup and some examples of participants conducting instructed NDRTs. The seat applied was a conventional driver seat taken from the current product (Figure 3-12, a). The results of Yang, Klinkner, et al. (2019) illustrate a significantly more extensive range of all NDPs: torso angle: -19° to 74°, thigh angle: -7° to 66°, knee angle: 63° to 180° than the typical driving posture (Damon et al., 1966): torso angle: 25° ± 3°; hip angle: 107° ± 7°; knee angle: 122° ± 8°. Figure 4-3 presents the distributions of joint angles and the seatback angle of each NDRT. Data could be applied to a digital human model to predict the sitting position given a certain NDRT in AVs. The reclined and backward-shifted sitting position, prominently presented in both the questionnaire and the laboratory experiment, became the focus of further experiments in the next chapters.

Though the joint angles of NDPs are distributed widely, their medians were very close to those of the standard RAMSIS driving posture (S. Lorenz, 2011). The transitions among the NDPs are comfort-relevant within the automation system limit. In contrast, the transitions from NDPs to driving posture and the transition from NDRTs to the driving task in case of system limit would be very urgent and safety-critical.

Moreover, fifteen requirements of the driver seat regarding the structure, positioning, adjustment, and material; four package requirements of space; three requirements of storage and eleven other requirements concerning infotainment and lighting system were derived and listed in the original publication (Yang et al., 2019).

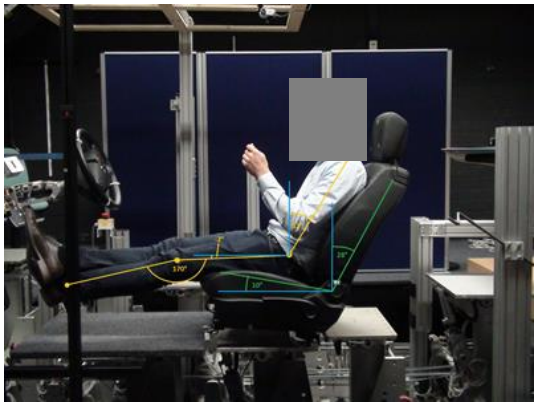

(a) Reading

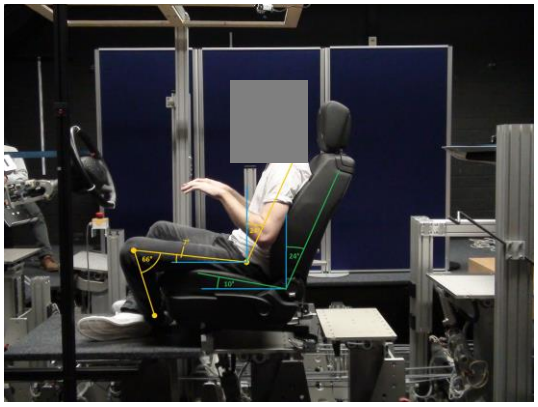

(b) Using tablet or laptop

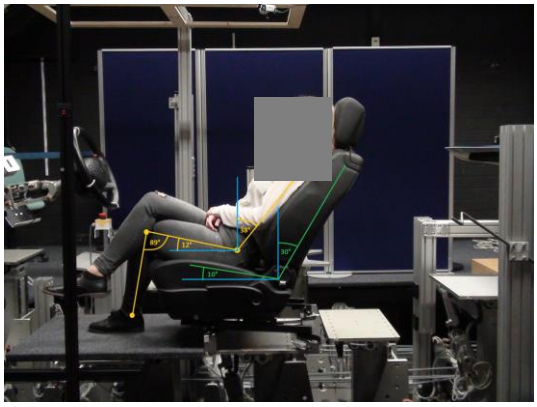

(c) Watching movies

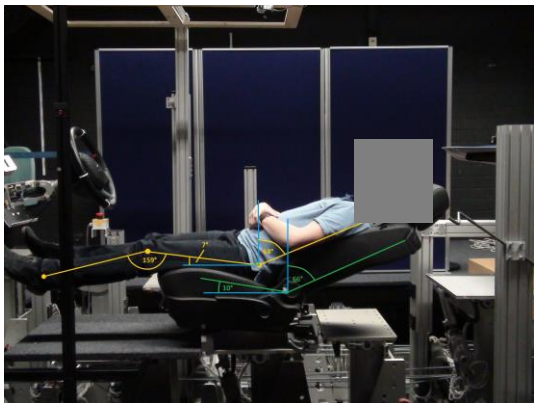

(d) Sleeping

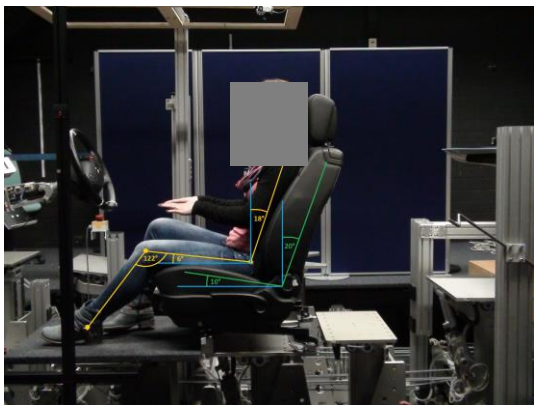

(e) Working and studying

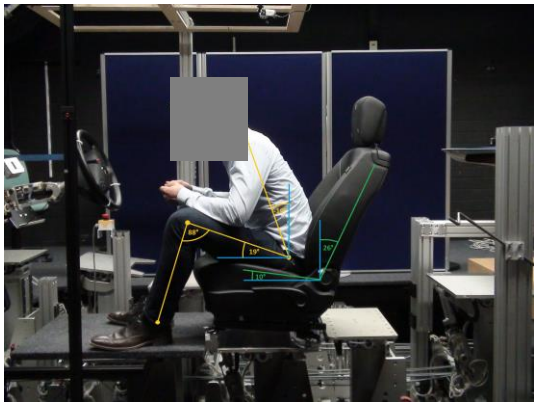

(f) Playing PC games

Figure 4-2 Examples of postures for different NDRTs. Images with kind permission of Jan Niklas Klinkner

NDP results in this experiment were collected in the laboratory with a driving-posture-oriented seat concept (e.g., Figure 4-2, Figure 4-3), which is not compatible with most NDPs. This might explain the fact that the medians of the joint angles of all collected NDPs are very close to those of the RAMSIS driving posture. Applying these results to digital human models or transferring them to other interior setups should be questioned and calls for great caution. The human body is adaptive and would typically adopt a particular posture given a particular seat (Jonsson et al., 2008). NDPs might vary a lot if the physical conditions change. Ideally, driving-task and driving-posture-

oriented interior concepts should be adjusted to fit NDRTs and NDPs concerning functionality and ergonomics before valid NDPs are exercised and observed. These changes in goals and contexts will lead to fundamental changes in the whole interior development and testing, which are, in turn, dependent on NDPs. There is a relatively uninform standard driving posture due to the restricted driving task, but the distribution of NDPs is extensive and dynamic. An accurate presentation and evaluation of realistic NDPs might only be found iteratively in more specified use cases and through long-term observations in the real AVs. The results of this study should be interpreted as the pure user wishes based on the current mental models without real experience of AVs. This dilemma and an iterative approach to obtain the changing human behavior and opinions are discussed in Chapter 9.

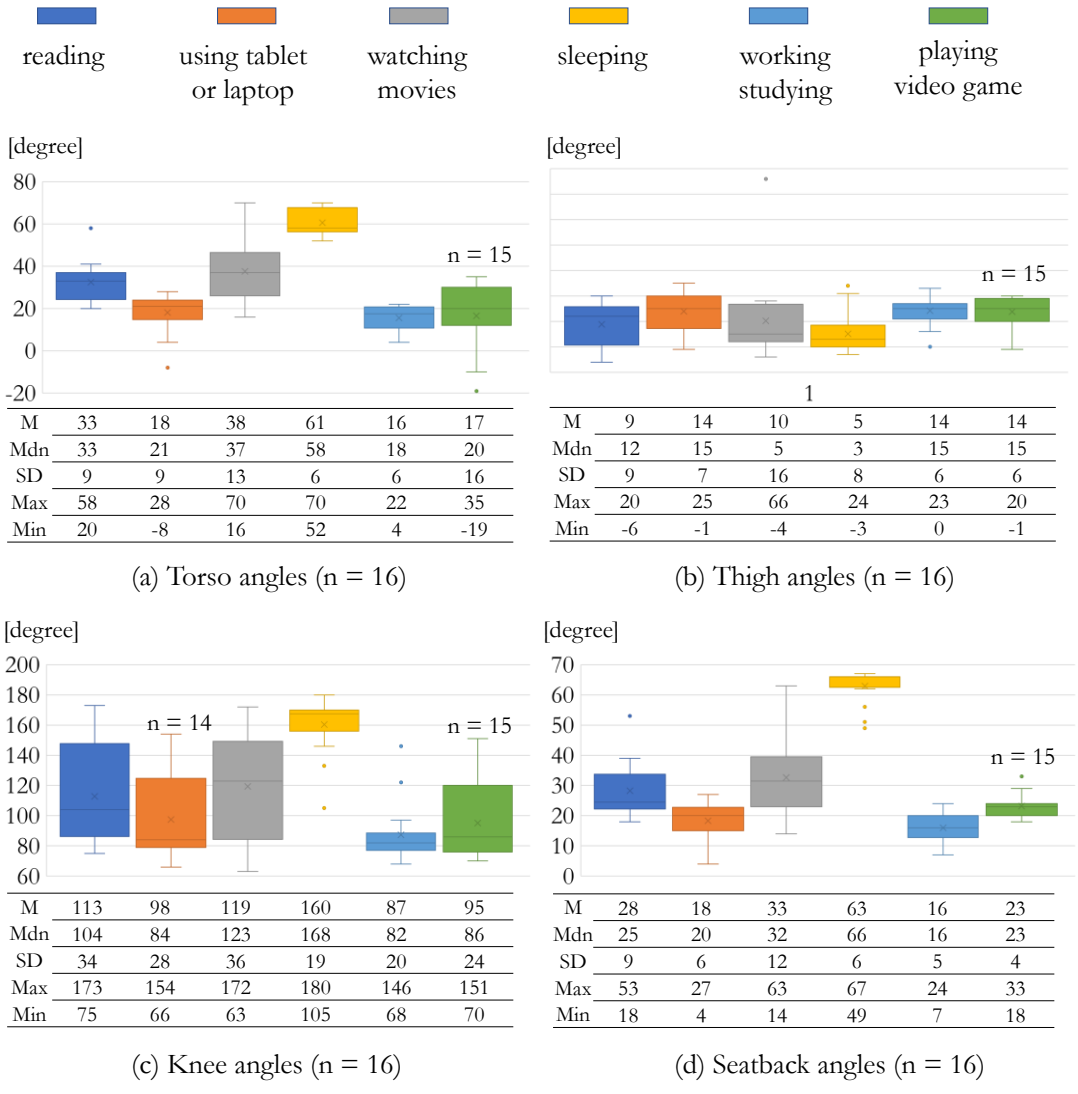

	reading	using tablet or laptop	watching movies	sleeping	working studying	playing video game
M	33	18	38	61	16	17
Mdn	33	21	37	58	18	20
SD	9	9	13	6	6	16
Max	58	28	70	70	22	35
Min	20	-8	16	52	4	-19

(a) Torso angles (n = 16)

	reading	using tablet or laptop	watching movies	sleeping	working studying	playing video game
M	9	14	10	5	14	14
Mdn	12	15	5	3	15	15
SD	9	7	16	8	6	6
Max	20	25	66	24	23	20
Min	-6	-1	-4	-3	0	-1

(b) Thigh angles (n = 16)

	reading	using tablet or laptop	watching movies	sleeping	working studying	playing video game
M	113	98	119	160	87	95
Mdn	104	84	123	168	82	86
SD	34	28	36	19	20	24
Max	173	154	172	180	146	151
Min	75	66	63	105	68	70

(c) Knee angles (n = 16)

	reading	using tablet or laptop	watching movies	sleeping	working studying	playing video game
M	28	18	33	63	16	23
Mdn	25	20	32	66	16	23
SD	9	6	12	6	5	4
Max	53	27	63	67	24	33
Min	18	4	14	49	7	18

(d) Seatback angles (n = 16)

Figure 4-3 Joint angles and seatback adjustments of NDPs in different NDRTs, modified from (Yang et al., 2019)

5 Assessment: Take-Over in Non-Driving Posture

Torso angle is identified as a significant influencing factor of the take-over performance: 38° reclined drivers have worse takes over performance, whereas a larger 133° relaxed knee angle does not affect the take-over performance if the reachability of pedals is ensured.

This chapter describes the second experiment of this thesis, focusing on the effects of the reclined posture on take-over performance. This work has been pre-published with the title: "How does relaxing posture influence take-over performance in an automated vehicle?" (Yang, Gerlicher, et al., 2018) in the Proceedings of the Human Factors and Ergonomics Society Annual Meeting 2018. This chapter provides the most important findings and discussions. The experiment was conducted with the assistance of Matthias Gerlicher as part of his semester thesis (Gerlicher, 2017). The experiment was carried out in the driving simulator of the Chair of Ergonomics at TUM. The seat used was a conventional driver seat taken from a current product (Figure 3-12, b)

The relaxed torso angle (38°) and knee angle (133°) in this experiment are oriented toward the Neutral Body Posture defined by NASA (Mount et al., 2003). The upright posture was oriented toward the experiment in Chapter 4, the mean values of the seatback angle (24°) and the knee angle (114°) in the position "seated facing the driving direction", which are in the range of the comfort angles of a a driving posture according to Bubb (2015b, p. 240) and S. Lorenz (2011). In this experiment, the torso angle was directly manipulated by the seat adjustments SBA (Figure 5-1), assuming that the torso angle equals the seatback angle when the participants lean on the seatback closely. The fixed heel method was applied to ensure the pedals' reachability, while adjusting SLA for a relaxed knee angle of 133°. The heel was only fixed to the accelerator heel point when adjusting SLA, while the participants' feet were free to move during automated driving. As a result, different participants' leg length had different SLA (Figure 5-1), while having the same knee angle.

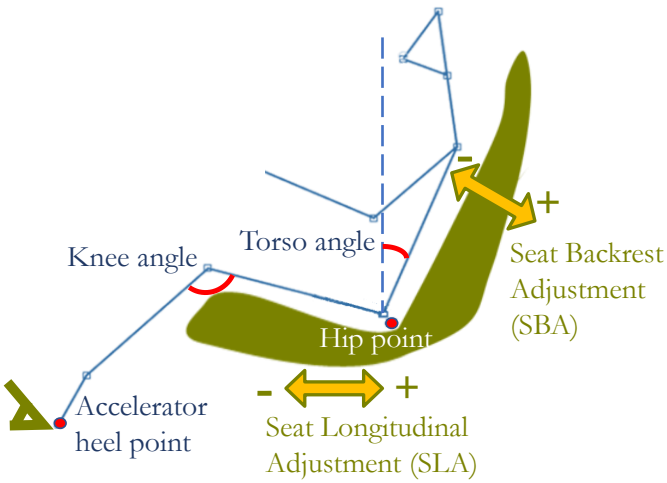

Figure 5-1 Using SBA to adjust the torso angle and SLA to adjust the knee angle, and the heel fixed at accelerator heel point (Yang, Gerlicher, et al., 2018)

In this two-by-two within-subjects-design experiment (n = 32) in the driving simulator, participants experienced a 40-minute Level 3 automation in four different postures (Figure 5-2). Participants had to take over the dynamic control of the vehicle once in each sitting posture. The take-over performance (hand-on time, take-over time, maximum longitudinal deceleration, maximum absolute lateral acceleration, time to collision, and standard deviation of lateral position) of each posture was measured and evaluated.

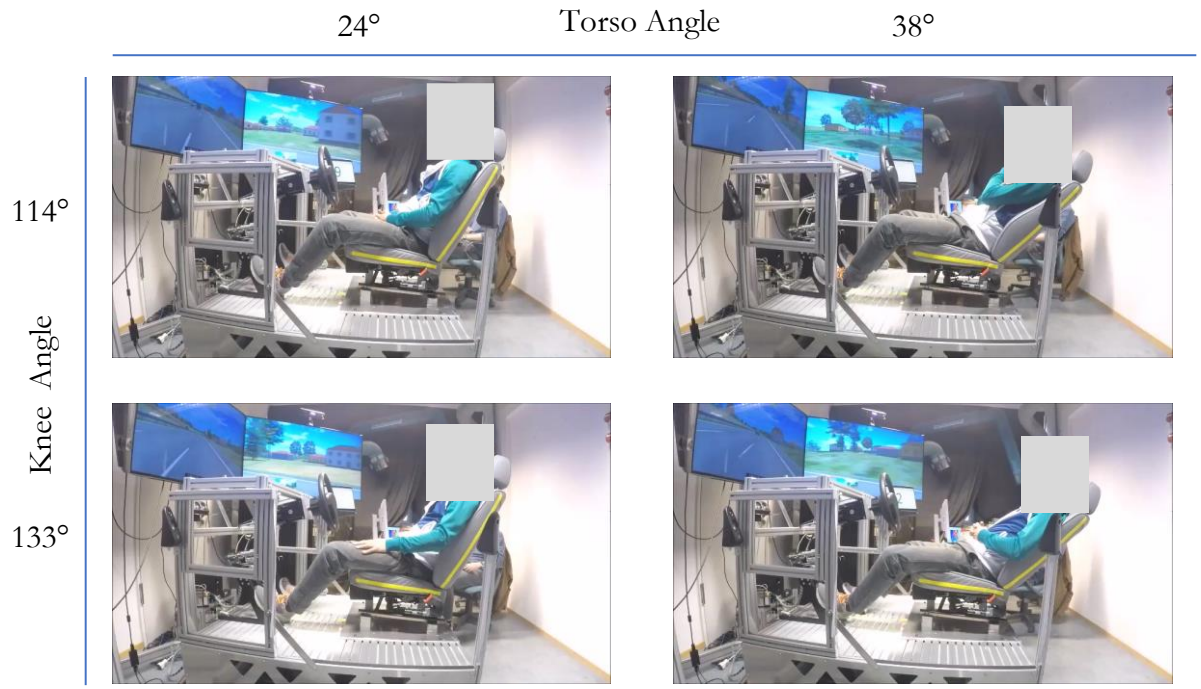

Figure 5-2 The two-by-two within-subjects-design experiment in the driving simulator and four postures of different torso angles and knee angles (Yang, Gerlicher, et al., 2018)

Results show that drivers with a 38° torso angle have a significantly longer hand-on time (M = 1.68 s, SD = 0.55 s) than drivers with a 24° torso angle (M = 1.53 s, SD = 0.56 s). Drivers with a 38° torso angle brake excessively harder, with a higher longitudinal acceleration (M = -5.08 m/s^2, SD = 3.34 m/s^2) than drivers with a 24° torso angle (M = -3.89 m/s^2, SD = 2.85 m/s^2). Excessively hard braking in this simple take-over scenario indicates a bad perception or understanding of the scenario–a scarcity of situation awareness (SA)–and is regarded as a bad take-over performance (Yang, Gerlicher, et al., 2018). There is no significant difference found in different knee angles. Sixty-six percent of participants found it was very hard to take over in the reclined and backward-shifted position. Sixty-three percent agreed that a seat that can automatically move back to an upright driving position would help the take-over (Yang, Gerlicher, et al., 2018).

Concluding, the torso angle is identified as a significant influencing factor of take-over performance. Reclined drivers with a 38° torso angle have a worse take-over performance, whereas a larger relaxed knee angle does not affect take-over performance due to the heel-fixed method (Yang, Gerlicher, et al., 2018). In other words, adjusting the SBA to a reclined posture with more than around 38° should not be recommended for drivers at Level 3 automation since it impairs take-over performance even in simple take-over scenarios, even though reclined drivers managed to

take over without a crash in this experiment. However, adjusting the SLA to a relaxed 133° knee angle is unproblematic for take-over performance, as long as the pedals' reachability is ensured.

Suppose the scenario is more complex or critical, e.g., higher traffic density or a smaller time budget for taking over, participants with large torso angles may not be able to handle the situation. Furthermore, as a side effect, reclined postures may make drivers fall asleep more easily (Johns, 2000). This side effect would be much more likely to happen in reality than in the laboratory, where participants were kept vigilant by the intensive n-back task. A limit of the SBA during Level 3 automated driving smaller than 38° should be considered. The exact appropriate threshold for a reclining angle needs to be further investigated with extended ranges of postures, demographic characters, traffic scenarios, vehicle types, and passive safety concepts.

There was only one RtI in the familiarizing trial before the experiment, which seemed insufficient to compensate for the learning effect. The results show that the participants reacted significantly more slowly (longer hand-on time) in the first take-over than the other three take-overs, independent of sitting posture. Even though this was compensated partly by counterbalancing the sequence, the sequence effect still generated outliers and distorts the distribution. Two RtIs in the familiarizing trial would have been enough to dim this learning effect of the take-over process to a stable level. This fact shows that experiencing the take-over situation is an influencing factor on take-over performance. Experience, useful tutorials, introductions, and training on the new automation functions and their system limits could be beneficial and necessary. Especially in take-over experiments, it is recommended to have at least two take-over trials before the experiment starts. However, more than two take-over trials might "over-train" the participant to automatically react to the RtI with an established pattern. Based on these lessons learned, there were two take-over trials before the experiment started in the experiment of Chapter 8. The results in Section 8.3.1 confirmed the well-counterbalanced sequence effect.

Subjectively, reclined and backward-shifted drivers had an unsafe feeling of being further away from the control elements. This unusual feeling preloaded drivers with a certain tension, prioritizing the motoric movement as a first reaction above the observation task when the RtI occurred. Drivers would react quickly, lacking adequate awareness, by, for example, braking inappropriately and unnecessarily hard. Reclined drivers wished to be assisted both physically and cognitively in take-over situations. Interior elements and HMIs might help drivers to resume the driving posture and reconfigure the driver state, e.g., the active seat assist (Chapters 7 and 8).

In this experiment, the conventional driver seat was not optimized for a reclined posture, which caused discomfort. Future seat configurations for AVs may have more degrees of freedom, fit relaxing postures and other NDPs. The simulator in this experiment was static; more dynamics in the real vehicle will influence the stability and the acceptance of reclined postures. The simulator had a limited fidelity of the driving environment: three displays for the outside view and no interior panels or doors, offering unrealistically good visibility of the driving scene for reclined postures. In actual vehicles, reclined drivers' visibility might be significantly constrained by the interior trim panels. A worse take-over performance is expected due to the decreased visibility in reality.

6 Modeling: Take-Over Motion

Reclined drivers accelerate harder leaning forward to compensate during a take-over process. However, larger torso angles still result in unstable body postures and longer take-over time. Evidence supports a critical torso-angle threshold between 30° and 50°.

This chapter describes the third experiment of this thesis, a motion tracking experiment.

Chapter 4 found that the reclined posture is an appealing NDP for AV drivers (Yang et al., 2019). However, Chapter 5 demonstrated that the take-over performance of reclined drivers (38° torso angle) was significantly worse than that of ones seated upright (24° torso angle) (Yang, Gerlicher, et al., 2018). This chapter focuses on tracking the driver's body movement during the take-over process in a strictly controlled environment to investigate reclined drivers' take-over from a primarily motoric perspective.

In this motion tracking experiment, a mock-up including a steering wheel, three paddles, and a car seat (H30 = 30 cm) was built (Figure 6-1). The steering wheel was fixed on an office table (height = 72 cm), and the pedals were fixed on the ground. The seat used was the one from Chapter 4 (Figure 3-12, a). The seat was mounted on two long aluminum rails to prevent it from tipping over and to enlarge the longitudinal adjustment to the original seat rail. A laptop was placed on the table in front of the steering wheel to trigger the artificial RtI. The reflective parts, mainly metal parts in the laboratory, were covered by blankets and tapes to avoid interfering reflections of the emitted infrared light from Vicon cameras.

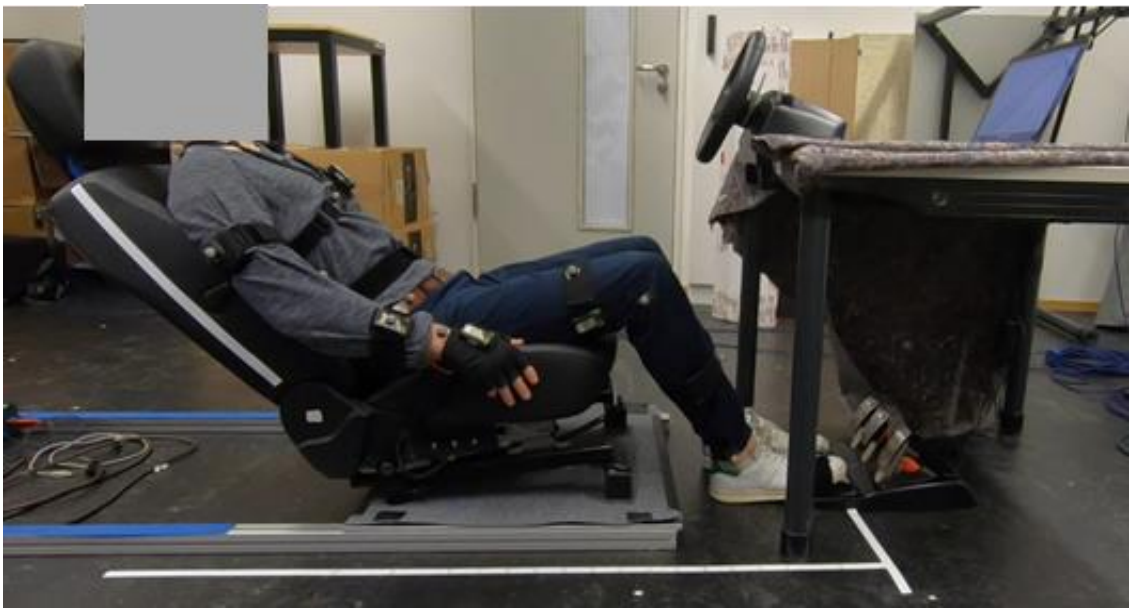

Figure 6-1 The minimalist driving mock-up

The experiment took place in the Motion Laboratory of the Chair of Ergonomics at TUM. It was conducted with Maurice Rang's and Jun Guo's assistance as part of their master's theses (Guo, 2019; Rang, 2018).

6.1 Objectives and Hypotheses

The objective of this experiment was to reproduce the reclined drivers' disadvantages in the take-over situation from a primarily motoric perspective and to quantify its geometrical and temporal consequences.

Two steps were taken: collecting the take-over motion data of different postures and then analyzing the data. The take-over motion (trajectory, velocity, and acceleration of the body segments) is the focus. Other factors, such as the cognitive state, sensory state, NDRT) should be minimized or controlled in this experiment.

The analysis of the trajectories was explorative. No specific hypothesis was made for the geometrical consequences of reclined postures.

The hand movement and hand-on time are essential elements of take-over quality (Gold, 2016; Kerschbaum, 2018). Two hypotheses similar to those in Chapter 5 were made regarding the influence of the torso and knee angles on hand-on time.

- H_{11}: Torso angle affects hand-on time.
- H_{12}: Knee angle affects hand-on time.

Subjectively, more than 80% of participants found it hard or very hard to take over from the reclined and backward-shifted position described in Chapter 5 (Yang, Gerlicher, et al., 2018). Participants in this chapter could evaluate the reclined postures from a primarily physical perspective. One hypothesis for subjective perception was made.

- H_{13}: Drivers need make different levels of effort to take over in reclined postures.

6.2 Method

The within-subjective design was chosen, allowing a direct comparison of different postures within one anthropometrical and demographical character.

6.2.1 Controlled Take-Over Process

The focus is on the take-over motion of different initial sitting postures. Other influential factors of take-over performance (e.g., driver cognitive and sensor states, traffic situation, time budget, fatigue, NDRTs) are minimized or controlled by the following experimental setups:

- No traffic scenario
- No driving tasks
- No NDRT

- Standardized artificial take-over task: in case of an RtI signal, participants should put their hands back to the 9 and 3 o'clock points of the steering wheel, steering 90° to the left, and braking hard simultaneously. The take-over task should be performed as quickly as possible.
- Strictly controlled sitting positions (Section 6.2.2).
- Transparent experiment procedure: participants knew exactly what was going to happen.
- Expectable RtI: the "pre-RtI" notification pre-warned and prepared the participant focusing on the coming RtI.
- Unplannable RtI: the "pre-RtI" notification was given randomly 10 – 15 seconds before the real RtI to avoid the participant counting down for the RtI.
- Salient multimodal RtI warning signal with a red full screen and a sharp beep tone.

The pre-RtI was an oral notification to prepare the participant for the coming RtI. On the one hand, this made it possible to control the participants' cognitive status to a similar level by pointing out the task shortly before the RtI happened. On the other hand, the randomly varied time delay between the pre-RtI and the real RtI allowed participants to react to the RtI signal instead of planning it.

6.2.2 Independent Variables

Two independent variables (IVs) are the torso angle (four variants) and the knee angle (three variants). Figure 6-2 shows twelve different postures formed by four torso angles (10°, 30°, 50°, 70°) and two knee angles (105°, 130°), and one variant of the 90° knee angle with crossed legs.

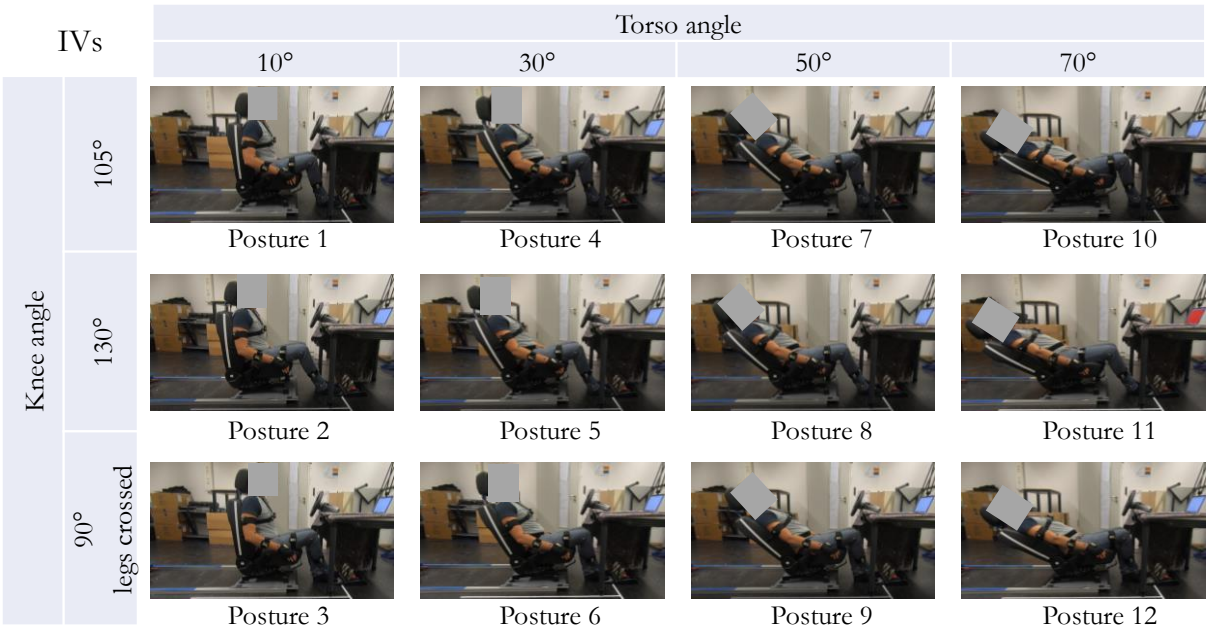

Figure 6-2 Twelve postures defined by torso angle and knee angle variants

As in Chapter 5, the torso angle in this experiment was directly manipulated by SBA, assuming the torso angle equals the seatback angle (the white line on the side of the seatback). The precondition was that the participant's back had full contact with the seatback. Unlike the "fixed-heel" method in Chapter 5, when adjusting SLA to manipulate the knee angle, in this experiment, the "fixed-toe" method was applied (Figure 6-3). The fixed point was still the accelerator heel point. When adjusting the SLA, the toes (or toes boxes of shoes) were to be at the fixpoint and were not to move until the target knee angle was reached. Unlike in Chapter 5, the fixed-toe posture was to be kept until the RtI. The "fixed-toe" method enabled the participant's feet to rest completely on the floor without tension, which is relevant in the AV scenarios where drivers do not have to drive and conduct NDRTs, e.g., when they relax. Despite the slightly longer distance to the pedals, participants could still reach the pedals in case of a RtI. However, it may make the sitting postures less stable in the take-over process when drivers try to stretch out the whole leg to brake hard.

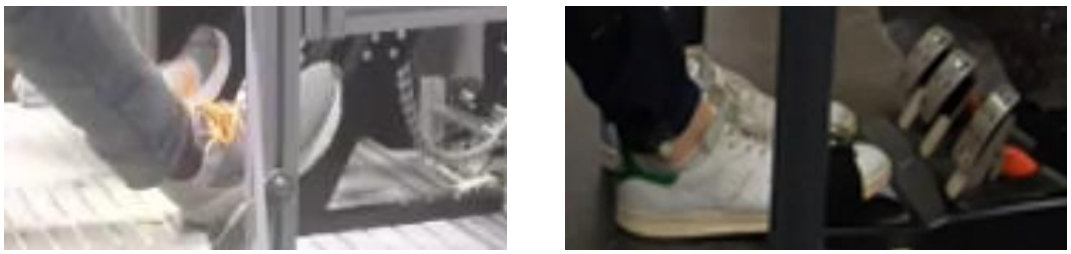

(a) Fixed heel (b) Fixed toe

Figure 6-3 Comparison of the fixed-heel and fixed-toe methods

In all 12 postures, participants were asked to let both hands hang down naturally beside the thighs and on the upper edges of the seat (Figure 6-2).

Due to the limited number of participants, a complete counterbalance was not possible. Only the factor knee angle was counterbalanced, meaning participants had different sequences of knee angles with increasing torso angle conditions.

6.2.3 Dependent Variables

Table 6-1 shows three objective measurement categories, consisting of twelve dependent variables (DVs) over different measurement periods and data sources. The raw data of the applied motion tracking system Vicon was the marker positions (x, y, z coordinates) attached on the right-hand side of the body with a 100 Hz frequency. Trajectories of wrist, breastbone, H-point, knee, and ankle were directly measured, while the velocity and acceleration were derived. The trigonometric functions are applied for the angle calculation under the assumption that body segments are rigid bodies. The take-over process is considered starting from the RtI to the end of the take-over task. Since the motion tracking system captured only the right half of the driver's body (except the chest), all the objective DVs are limited to represent the movement of the right half of the driver's body (except the chest).

Table 6-1 Definitions of different dependent variables

Categories	Body parts	Measurement period	Data source	DVs
Movement range	1. Wrist 2. Breastbone 3. H-point 4. Knee 5. Ankle	1. First reaction to RtI to hand-on 2. Hand-on to the end of the left steering	Vicon motion	1. Trajectory
				2. x-, y-, and z-displacement [m]: d_x = |max (x) - min (x) | d_y = |max (y) - min (y)| d_z = |max (z) - min (z)|
				3. Fitted planes and curves
Movement speed & acceleration	Torso (Breastbone and H-point)	1. First reaction to RtI to hand-on 2. Hand-on to the end of the left steering	Vicon motion	4. Maximum angular speed [°/s]
				5. Maximum angular acceleration [°/s^2]
		The time point of hand-on	Vicon motion	6. Hand-on torso angular speed [°/s]
				7. Hand-on torso angular acceleration [°/s^2]
Time metrics of the hand	1. Hand (Video) 2. Wrist (Vicon Motion)	1. RtI to hand-on 2. Hand-on to the end of the left steering	1. Video 2. Vicon motion	8. Hand-on motion time (HoMT) [s]
				9. Hand-on time (HoT) [s]
				10. Steering time (ST) [s]
				11. Task time (TT) [s]
Subjective evaluation	All	Torso angle: 10° 30° 50° 70°	Questio-nnaire	12. Task load

The first category, "movement range," illustrates the body parts' trajectories during the take-over process and the changing geometrical requirement when drivers recline to different torso angles, especially the spaces needed for the movement of the hand. The x-, y-, and z- displacements indicate the required free space of one specific trajectory in each direction. The displacement distribution represents the possible movement ranges of different drivers and from different sitting positions. The fitted planes and curves show the movement pattern of the hand.

The maximum torso angular speed and acceleration represent how fast and quickly drivers would lean forward to take over and how much effort they would put into it in different postures. The hand-on torso angular speed and acceleration illustrate the torso movement status at the moment when the driver's hands are just on the steering wheel and about to steer.

The take-over time was investigated separately in different phases from the RtI to the end of the standard take-over task using the driver's right hand as a reference. Four temporal periods in the whole take-over process were defined in Figure 6-4: hand-on motion time (HoMT), hand-on time (HoT), steering time (ST), and task time (TT). The reaction time, HoMT, and ST are independent of each other, while the HoT consists of the reaction time and the HoMT, and the TT is the whole take-over task time. HoMT was directly calculated using Vicon tracking data, starting when any

body part started to move as the initial motoric reaction to the RtI. HoT, ST, and TT were collected using GoPro videos.

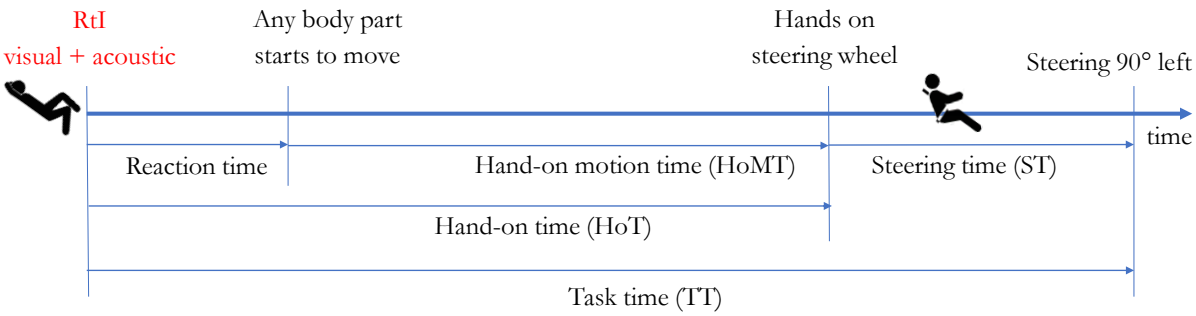

Figure 6-4 Definitions of four time metrics during the take-over process

For the subjective evaluation, the NASA TLX (Hart & Staveland, 1988) questionnaire was applied in the experiment after each torso condition. The weights of items are eliminated, which is a common modification (Hart, 2006). Items are analyzed individually.

6.2.4 Motion Tracking Setups

The Captiv motion and the Vicon camera system were redundantly applied for motion tracking. The two types of systems had the same measurement scope to test different tracking systems' suitability in take-over experiments. A field-view GoPro camera was placed on the right side of the driver. Due to the limited number of sensors, only the right half of the body was tracked, except for the chest.

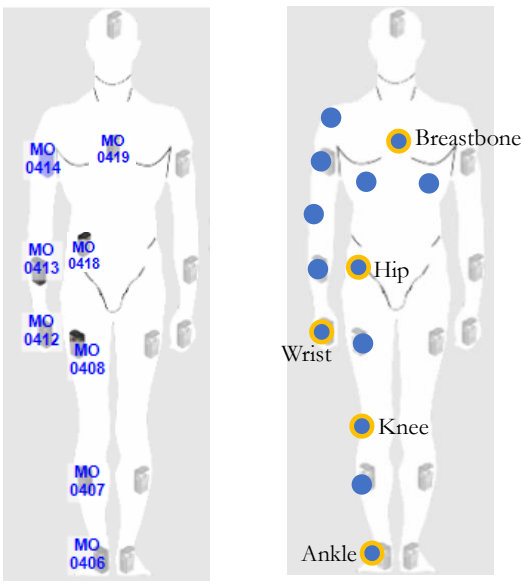

(a) Captiv (b) Vicon

Figure 6-5 Distribution of the Captiv and Vicon sensors

Eight Captiv inertial measurement units (IMU) were fixed onto the chest (middle), right upper arm, right lower arm, right hand, hip, right thigh, right lower leg, and right foot of each participant (Figure 6-5, a).

Thirteen reflective Vicon markers were attached on the participant's chest (left, middle, and right), right shoulder, right upper arm, right elbow, right lower arm, right wrist, hip, right leg, right knee and right lower leg, as well as on the right ankle (Figure 6-5, b). Among these 13 markers, the breastbone, the hip, the wrist, the knee, and the ankle were five focus tracking points (emphasized by orange circles in Figure 6-5, b), whose raw data were exported and analyzed. The Vicon marker on the right wrist represents the driver's right hand. No other hand motion, e.g., finger movement or hand joint rotation, was tracked. For the chest movement, one marker was attached to the middle of the breastbone. No marker was mounted on the feet, because they might not have been visible to the tracking cameras. The ankle point was the closest point to represent the braking behavior of the right foot.

Figure 6-6 shows the right half of the tracked driver's body in both systems. Captiv, as an "Inside-In System" (Menache, 2011), did not need an external camera and had thus no reference to the external environment (Figure 6-6, a). The body segments in the Captiv model were relative to each other. In contrast, Vicon is an "Outside-In System" (Menache, 2011). The capture sources (cameras) are outside the driver's body, while the markers are placed on the driver's body. Seven Vicon cameras were built around the driver's right side (Figure 6-6, b). The body segments in the Vicon model were relative to the camera positions, providing the system references to the environment and the absolute position of markers in the coordinates. Vicon could thus position the track body into a coordinate system, corresponding to the real world.

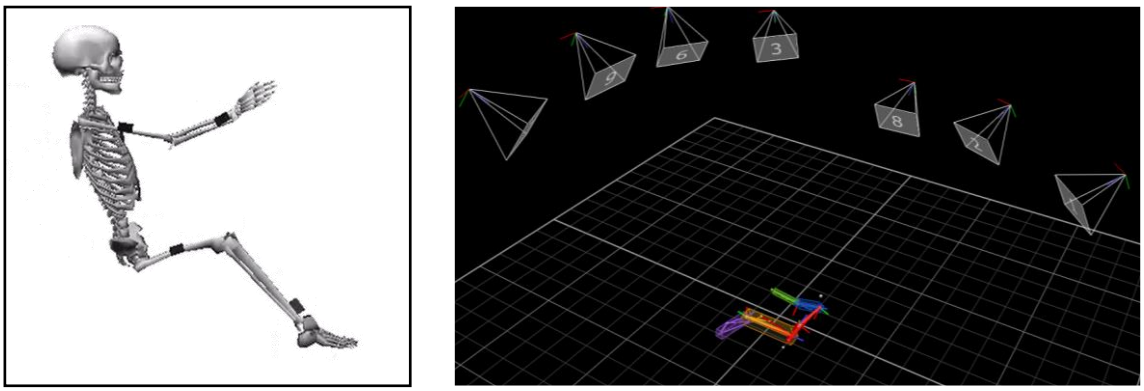

(a) Captiv (b) Vicon

Figure 6-6 Manikins of both tracking systems

The 0-0-0 origin point of the coordinator system of the Vicon in this experiment was located on the floor and the driver's right-hand side (Figure 6-7). In the negative y-direction, a GoPro scene camera was placed for monitoring the experiment and the analysis of the movement.

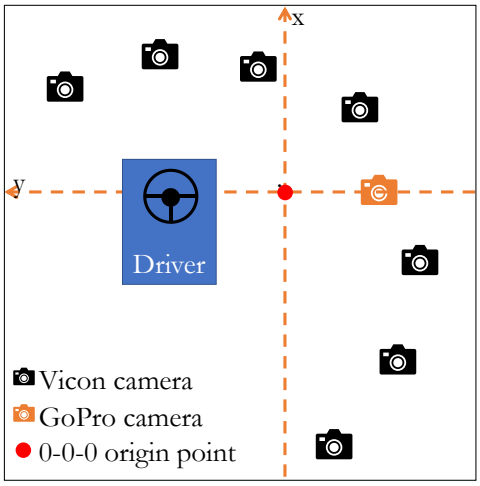

(a) Cameras and driver positions from the top-view

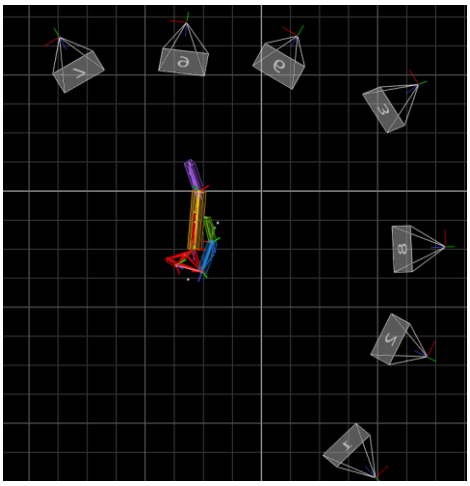

(b) Same perspective as (a) in Vicon environment

Figure 6-7 Camera arrangement around the driver and the model view in the Vicon software[1]

6.2.5 Experimental Procedure

Participants were welcomed and informed about the procedure of the experiment, the demographic data were collected, and the anthropometric data were measured. Participants were instructed about the experimental procedure, the seat positions, the take-over task, and the take-over signal (RtI). Tracking sensors were then placed (Figure 6-5) on the participant's body. Participants were to exercise and familiarize themselves with the take-over task while wearing all the sensors. Both Captiv and Vicon systems must be calibrated before every measurement. After ensuring that the participant's motion was tracked by two systems and recorded by the GoPro camera, measurements could be started.

The experimenter adjusted the SBA and SLA to 12 defined postures in a counterbalanced sequence. An angle ruler was used for measuring the joint angles, and the "toe-fixed" method was applied. After the target posture was taken, the experimenter gave a verbal "pre-RtI" signal. The participant waited for 10 to 15 seconds until the real RtI was triggered. The RtI signal was a red screen on the laptop in front of the participant and a loud double-beep tone. The participant then performed the defined take-over task (Section 6.2.1) as quickly as possible. Afterward, the experimenter adjusted the next posture and repeated all the procedures above until the twelve postures had been conducted, and twelve take-over processes had been recorded.

Participants filled out the NASA TLX questionnaire four times, i.e. after three take-overs in each torso angle condition (10°, 30°, 50°, 70°). The participants were not instructed that the

[1] The Vicon x-y-z directions shown here and described in the rest of the thesis are corrected according to the automotive convention (SAE J1100, 2009). The original raw Vicon data in this experiment had a different x-y-z definition. The transitions are as follows: $X = -Y_{\text{Vicon Raw Data}}$; $Y = X_{\text{Vicon Raw Data}}$; $Z = Z_{\text{Vicon Raw Data}}$. The origin 0-0-0 point stays the same.

questionnaire was explicitly about comparing the torso angle, rather generically about three previous take-overs, to avoid bias.

6.2.6 Participants Sample

Twenty-eight participants took part in this experiment. There are n = 27 complete datasets. Participants were between 21 and 53 years old (M = 26.70 years, SD = 5.70 years). The participants' body height was distributed between 166 cm and 198 cm (M = 179.30 cm, SD = 9.45 cm). The self-reported weight ranged between 54 kg and 100 kg (M = 74.44 kg, SD = 12.91 kg). Three participants' body size groups were built according to their body height (Figure 6-8). They were noted according to the convention of the clothing industry. The small-sized are noted as the "S" (< 175cm), "M" for the middle group, 175cm–185cm, "L" for the large group (> 185cm).

Participants had been holding a driving license for 4 to 27 years (M = 9.00 years, SD = 4.15 years). 26% of the participants drive less than 1,000 km per year, 30% between 1,000 to 5,000 km, 30% between 5,000 to 10,000 km, 15% more than 10,000 km every year.

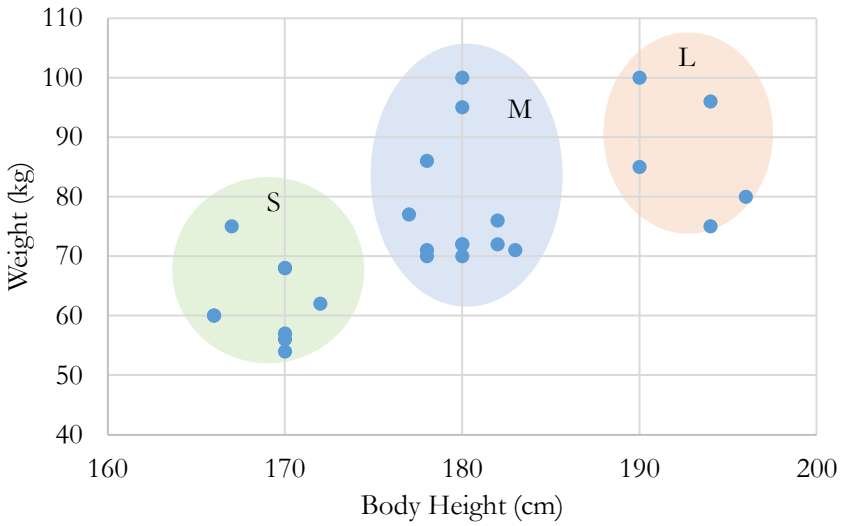

Figure 6-8 The three groups of small (S), medium-sized (M), and large (L) participants

6.2.7 Data Pre-Processing

The tracking data quality of both redundant systems was checked after the experiment. The Captiv data were discarded due to widely distributed interference and a lack of post-processing possibility. Details can be found in Appendix A.

The Vicon system offered different tools to manually repair some data frame by frame after the measurement, e.g., manual labeling, gap filling. The raw data could be exported to be processed in external programs.

The main problem of Vicon data was undetected markers. Markers were sometimes covered by the table, the steering wheel, or the participant's body. Small gaps of recognition could be filled by applying the "pattern filling" function. Large gaps, undetected markers at the beginning of or at

the end of one continuous movement path could not be filled. The second problem was the wrong labeling of the marker, which could be solved by manual labeling as long as markers were tracked. The Vicon data were partially repaired. Out of 12 * 27 = 324 take-overs, 224 datasets are available, having no loss of data in any body part in the x-, y-, and z-direction. Additionally, fifteen cases had to be discarded for specific body parts (details and reasoning in Table B-1 in Appendix B). Four discarded cases concerning trajectory data affect the whole Section 6.3. Eleven discarded cases affect Sections 6.3.3.3, 6.3.3.4, and 6.3.4.1 due to the hand-on phases cutting criterion. There are n = 222 datasets for the hip analysis, n = 223 for the breastbone, n = 223 for the knee, n = 221 for the torso angular speed/acceleration, n = 213 for the HoMT, and n = 210 for the hand-on torso angular speed/acceleration. The "n" here means the number of available take-over measurements, not the number of participants.

A further problem was the sensor noise. Some markers were placed on the surfaces of different everyday clothes of participants. Some were attached to the IMU Captiv sensors. Local displacements of sensors could not be avoided due to the elasticity and movement of the textile. The frequency components of human motion typically range from 0 to 10 Hz; Shah, Falco, Saveriano, & Lee (2016) found empirically that the frequency threshold = 5 Hz guarantees the same performance as 10 Hz, even for quick human action like a cartwheel. A first-order Butterworth low-pass filter was applied to the trajectory data to filter out such high-frequent movement. The frequency threshold was set to 5 Hz. Figure B-1 in Appendix B illustrates the frequency spectrum of the filtered results of all the motion data (x-y-z positions of all participants' breastbones, hips, wrists, knees, and ankles) by fast Fourier transformation (FFT). The primary frequency components of the take-over motion in this experiment are less than 3 Hz.

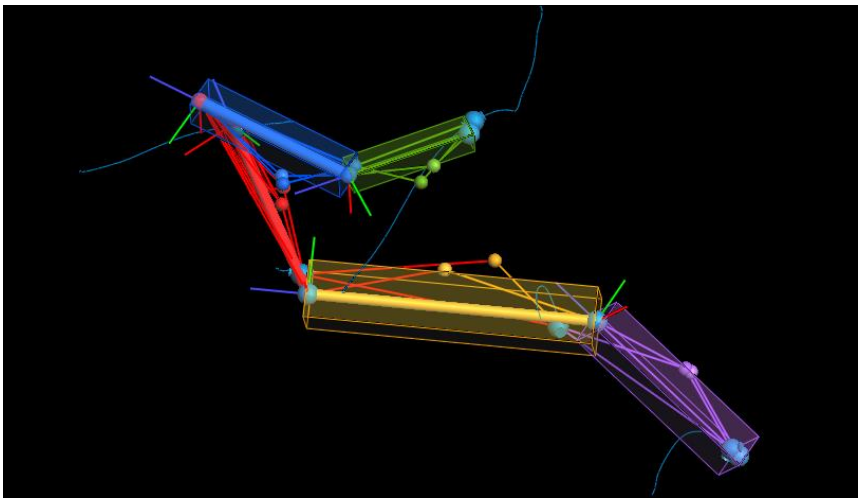

Figure 6-9 An example of Vicon tracking data with body segments, joint points, and their trajectories

Figure 6-9 visualizes an example. Differently colored blocks represent different body segments. Each segment is considered a rigid body: the green part represents the lower arm; the blue part is the upper arm; the red part is the torso; the yellow part is the thigh; the purple part is the lower leg. This screenshot was taken in the middle of a take-over process from a 50° reclined sitting posture. The blue curves are the trajectories of the breastbone, the wrist, the H-point, the knee, and the

ankle. The trajectories started from the driver's first reaction to the RtI to the end of the take-over task, including leaning forward, hand-on, steering, and braking.

6.3 Results

The Vicon raw data of the five focus points (breastbone, hip, wrist, knee, and ankle) were exported and processed manually by the external programs Excel, R, and Matlab. A presentation of all trajectories can be found in Appendix C. The "toe-fix" method controlled and limited the movement of legs and feet. The knee and ankle results are presented in Appendix C and D. Results in different knee angle conditions are presented in Appendix E. This section focuses on the upper body (breastbone, hip) and the hand (wrist) in different torso angle conditions.

Trajectories of the wrist, the breastbone, and the H-point are analyzed in Section 6.3.1. The wrist trajectories are regressed in planes and curves in Section 6.3.2. Torso angle speed and acceleration are analyzed in Section 6.3.3. Time metrics of the hand are analyzed in different take-over phases, postures, and demographic characteristics in Section 6.3.4. Subjective evaluation is illustrated in Section 6.3.5.

Boxplots are used to demonstrate the distribution of the data. Outliers in all boxplots are values that are more than 1.5 times the interquartile range away from the bottom or top of the box, labeled with red '+' markers in the boxplots. These outliers are included in the statistics. Excluded outliers are due to technical errors and are mentioned explicitly in each specific case. Statistical significance is labeled with "*" in the boxplots, following the convention: * for $p < 0.05$, ** for $p < 0.01$, *** for $p < 0.001$.

6.3.1 Trajectory and Displacements

The take-over process starts from the driver's first reaction to the RtI and ends with the take-over task, ranging from about 70 to 250 data frames. The cutting criterion of the start point of the take-over motion is when any body segments start to move after the RtI signal. Participants initialize their take-over motion with different body parts, sometimes with the upper arm, sometimes with the thigh. Most of them start with the thigh, followed quickly by other body parts. Any initial movement is defined as a sign of the start of the reaction to the RtI. To avoid false positives, the first three non-zero records in succession indicate the beginning point. When the steering wheel is turned left for 90 degrees (maximum of the wrist z-position), the trajectory ends. The take-over motion includes two phases. First, the hand-on phase: the driver reacts to the RtI signal, changes his or her posture from NDP to driving posture, i.e., leaning forward, sitting up, putting their hands on the steering wheel and their foot on the brake pedal. Secondly, the steering phase: the driver conducts the defined take-over task, i.e., steering 90° to the left and braking hard.

Figure 6-10 shows an example of take-over trajectories from a reclined posture (torso 70°, knee 105°) in a 3D view. Two phases from the perspective of a hand are marked in different colors for all the trajectories: the hand-on phase (blue trajectories) and the steering phase (green trajectories). Despite a different 0-0-0 point, the x-, y-, and z-directions correspond to the vehicle coordinates convention (SAE International, 2009). The 2D views of this example can be found in Figure C-1.

As an overview, the 2D views of all 224 take-over motion are presented in Figure C-2, Figure C-3, and Figure C-4.

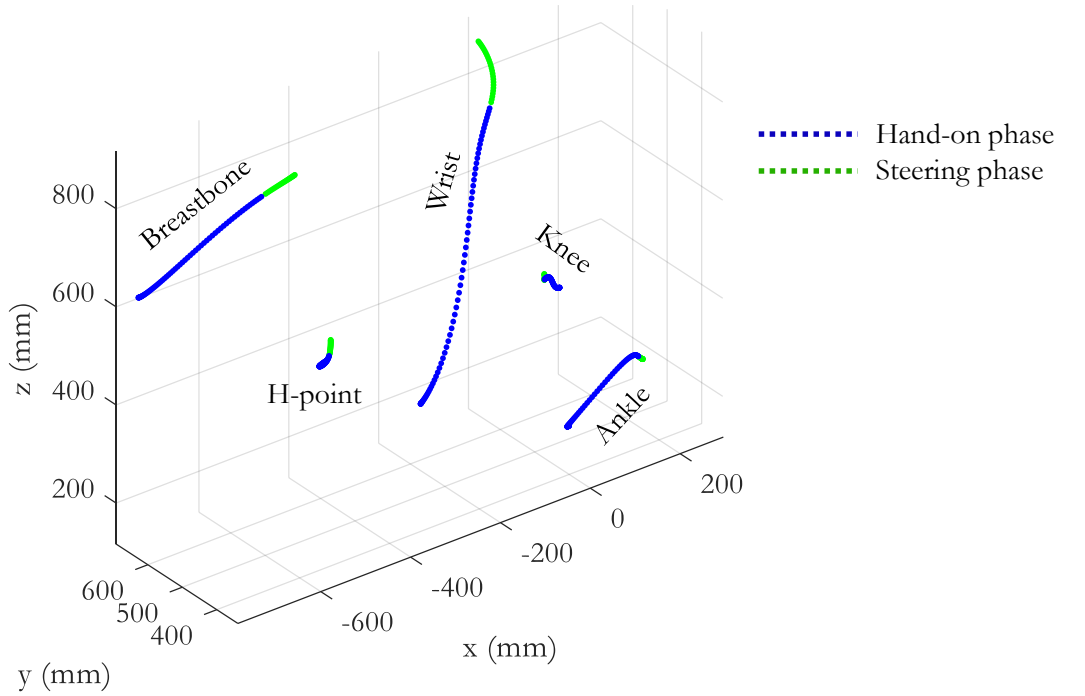

Figure 6-10 An example of trajectories of take-over motion from a reclined posture (torso 70°, knee 105°)

Figure 6-11 visualizes the definition of the DV "displacements," taking the wrist as an example. The x-, y-, and z-displacements represent the geometrical requirement of the specific trajectory in each x-, y-, and z-direction.

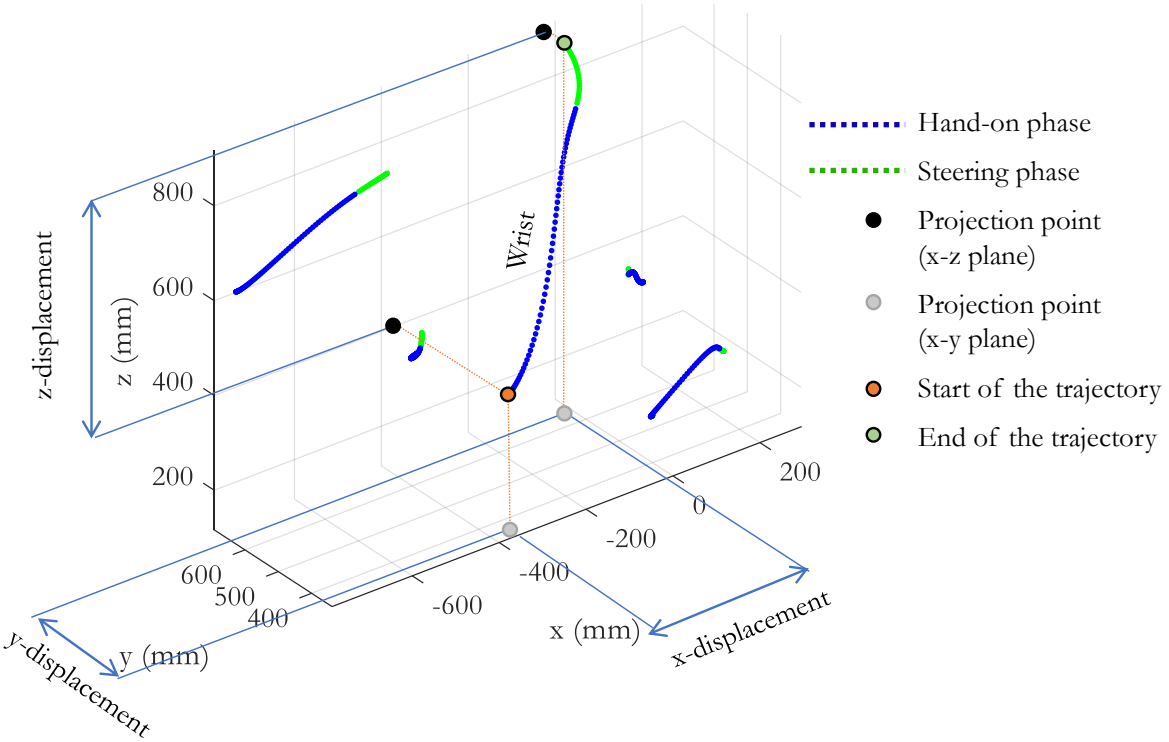

Figure 6-11 Definition of the x-, y-, and z-displacement of one specific trajectory

In the following sections, the x-, y-, and z-displacements of the wrist, the breastbone, and the H-point during the take-over process in different torso angle conditions are presented. The influence of knee angles on the x-, y-, and z-displacements is relatively small due to the "toe-fix" method (see Section 6.2.2). The trajectories of knee and ankle are presented in Appendix Figure C-5, Figure C-6 , Figure D-1, Table D-10, Table D-11, Table D-12, Figure D-2, Table D-13, Table D-14, Table D-15. The results in different knee angle conditions are presented in Appendix E.

6.3.1.1 Wrist

Figure 6-12 shows all 224 trajectories of the wrist in the take-over process, including the hand-on phase (blue) and the steering phase (green). The trajectories start from the right side of each individual's thigh, move toward the steering wheel, and end with turning the 3 o'clock point of the steering wheel 90° to the left. Different starting points of the trajectories represent different sitting postures with individual anthropometric characteristics. A detailed investigation of the wrist movements pattern can be found in Section 6.3.2.

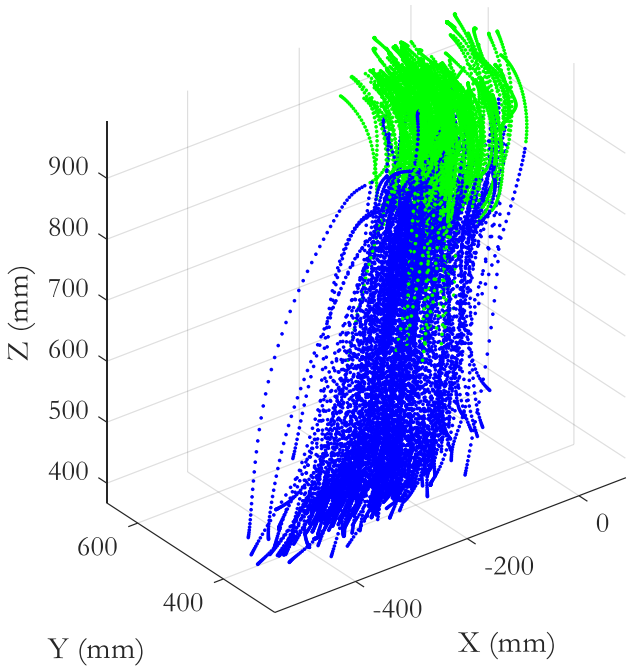

Figure 6-12 Trajectories of the wrist in take-over processes

The boxplots in Figure 6-13 show the distributions of the x-, y-, and z-displacements of the right wrist in 224 take-over processes. The corresponding descriptive statistics are shown in Appendix D in Table D-1, Table D-2, and Table D-3. The displacements are grouped by different torso angles (the knee-angle grouped diagrams in Appendix E, Figure E-1).

All torso angle conditions taken together, the z-displacements of the wrist are on average (M_{M_z} = 487 mm) greater than the x-displacements (M_{M_x} = 267 mm) and the y-displacements (M_{M_y} = 229 mm). The x-displacements are more heterogeneous (M_{SD_x} = 75 mm) than the y-displacements (M_{SD_y} = 50 mm) and the z-displacements (M_{SD_z} = 33 mm). The torso angle affects

the x-displacements (Δ_{M_x} = 94 mm) significantly more than the y-displacements (Δ_{M_y} = 31 mm) and the z-displacements (Δ_{M_z} = 13 mm).

The x-displacements distribute widely from 61 mm to 501 mm. The mean value increases consistently from 225 mm to 318 mm as the torso angle increases. The SD remains similar above 70 mm. The y-displacements range from 105 mm to 348 mm. Except for the torso 10° condition, the mean y-displacements decrease slightly from 242 mm to 211 mm as the torso angle increases, while the SD stays similar around 50 mm. The z-displacements range from 389 mm to 572 mm. The mean z-displacements increase slightly from 479 mm to 492 mm as the torso angle increases, while the SD stays around 35 mm.

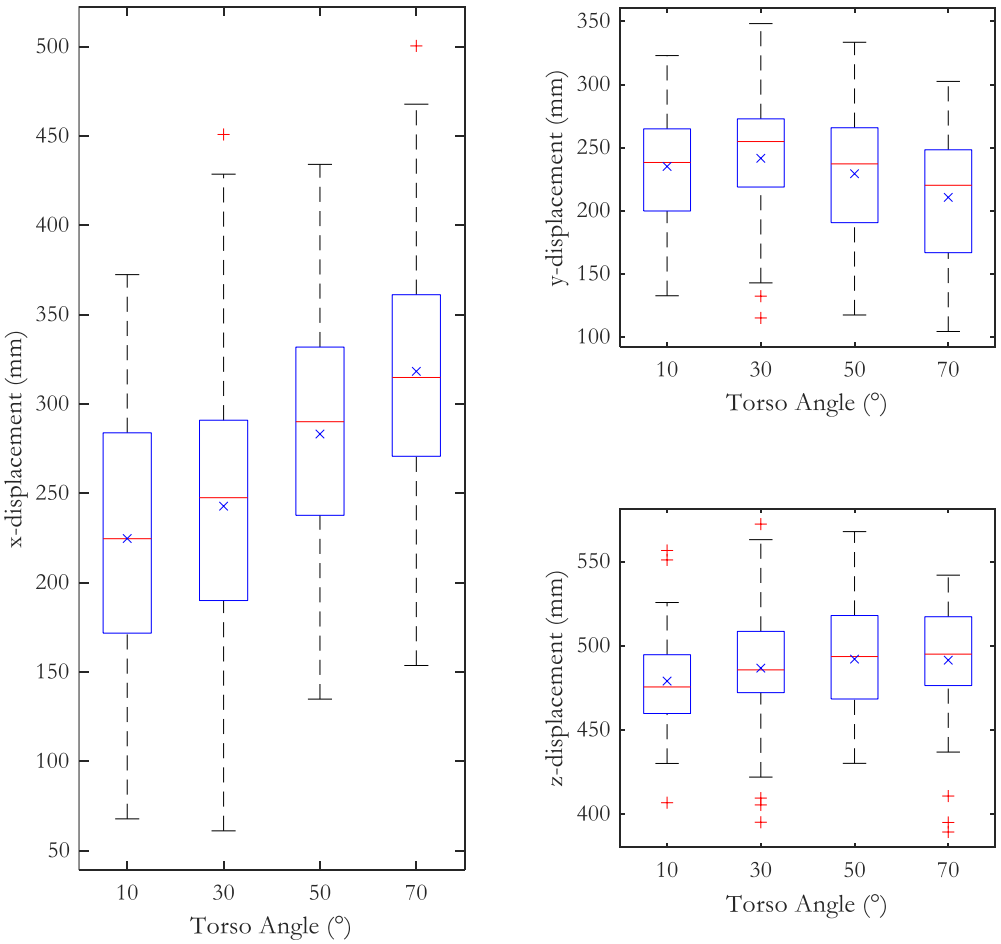

Figure 6-13 The x-, y-, and z-displacements of the wrist in different torso angle conditions

6.3.1.2 Breastbone

The breastbone represented the movement of the upper body and is one of the torso angle calculation points (the hip-point is another one). One outlier is excluded (details and reasoning in Table B-1 in Appendix B). Figure 6-14 shows all 223 trajectories of the breastbone in the take-over process, including the hand-on phase (blue) and the steering phase (green). Different starting points of the trajectories represent different sitting postures with individual anthropometric characteristics. The green parts of the trajectories indicate that participants were still moving their upper bodies during steering action. The longer arciform trajectories are from the 50° or 70° torso

conditions where the upper body needs to lean forward first. The short trajectories are from the 10° or 30° torso conditions. In the 10° torso condition, drivers did not have to lean their torsos during the take-over process. In this case, the movement of the torso represents the instability of the upper body during hand-on, steering, and braking actions.

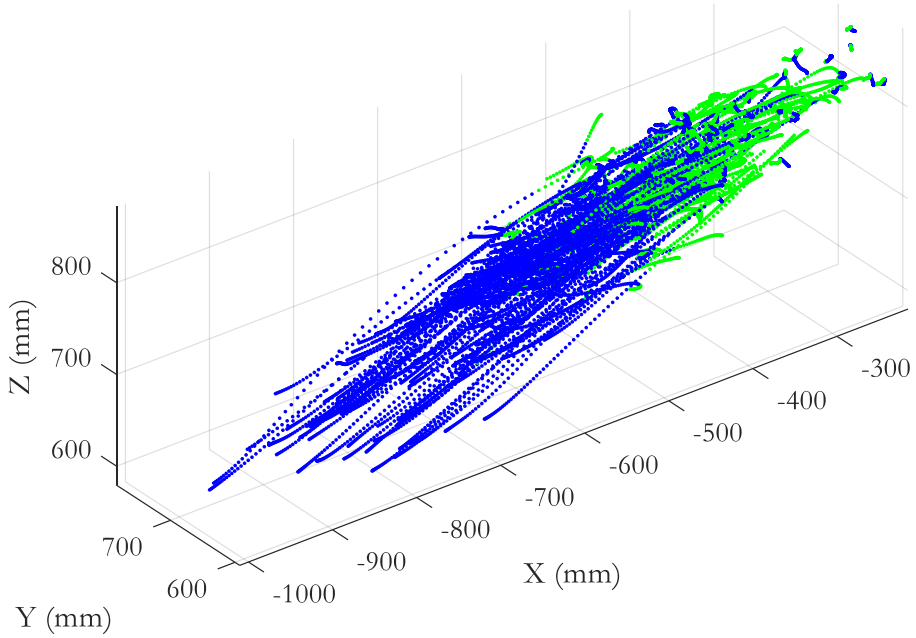

Figure 6-14 Trajectories of the breastbone in the take-over processes

The boxplots in Figure 6-15 show the distributions of the x-, y- and z-displacements of the breastbone in 223 take-over processes. The corresponding descriptive statistics are presented in Appendix D in Table D-4, Table D-5, and Table D-6. The displacements are grouped by different torso angles (the knee-angle grouped diagrams in Appendix E, Figure E-2).

The breastbone and the H-point directly define the torso angle. The initial torso thus directly influences the displacement of the breastbone. The larger the torso angle is, the longer the distance the breastbone moves in the x-direction (Δ_{M_x} = 404 mm) and the z-direction (Δ_{M_z} = 94 mm). The effect of the increasing torso angle on the y-direction (Δ_{M_y} = 28 mm) is also shown, but it is smaller.

In the 10° torso condition, drivers did not have to lean their torsos forward to steer and brake. The x-, y-, z-displacements of the breastbone are similar around 10 mm, representing the stability of the upper body.

In the 30°, 50°, and 70° conditions, the x-displacements are more widely distributed from 4 mm to 611 mm than the y-displacements (2–121 mm) and the z-displacements (1–183 mm). The mean x-displacements increase consistently from 109 mm to 415 mm as the torso angle increases, while the SD remains large, around 100 mm. The mean y-displacements increase consistently from 28 mm to 42 mm as the torso angle increases, while the SD stays around 26 mm. The mean z-displacements increase consistently from 16 mm to 105 mm as the torso angle increases, and the SD increases from 11 mm to 36 mm.

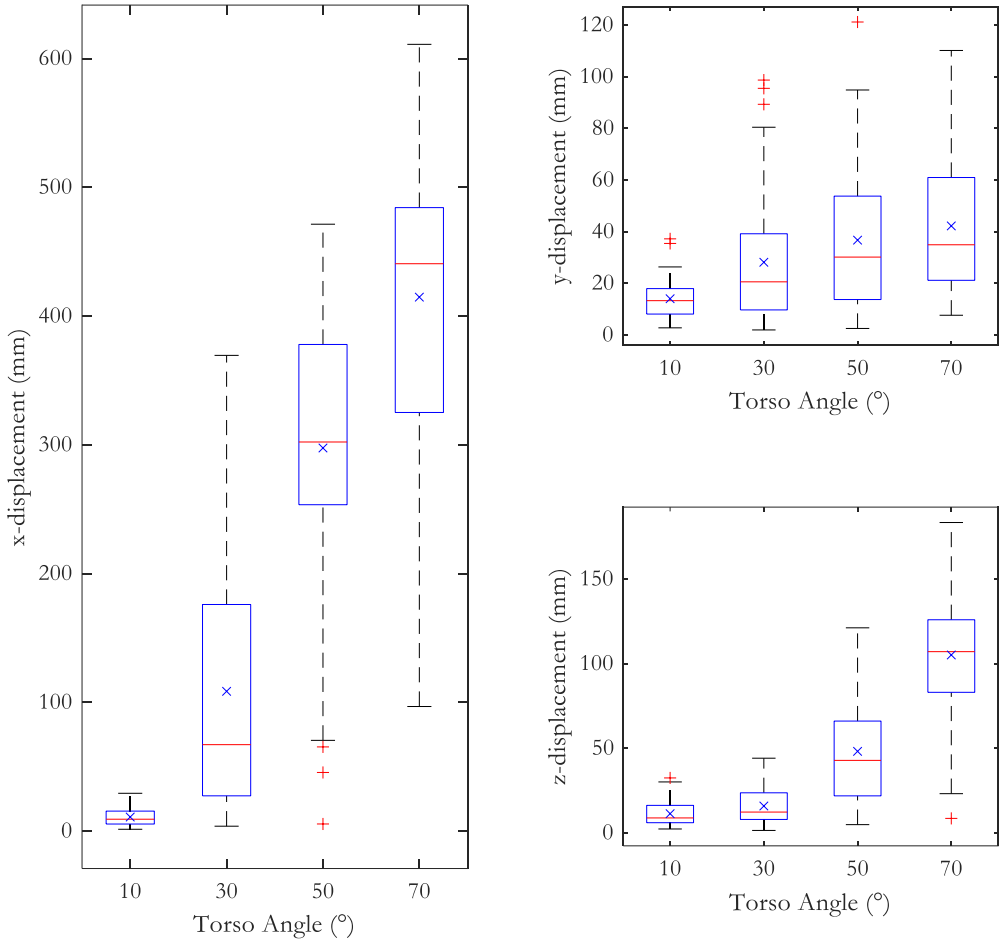

Figure 6-15 The x-, y-, and z-displacements of the breastbone in different torso angle conditions

6.3.1.3 H-point

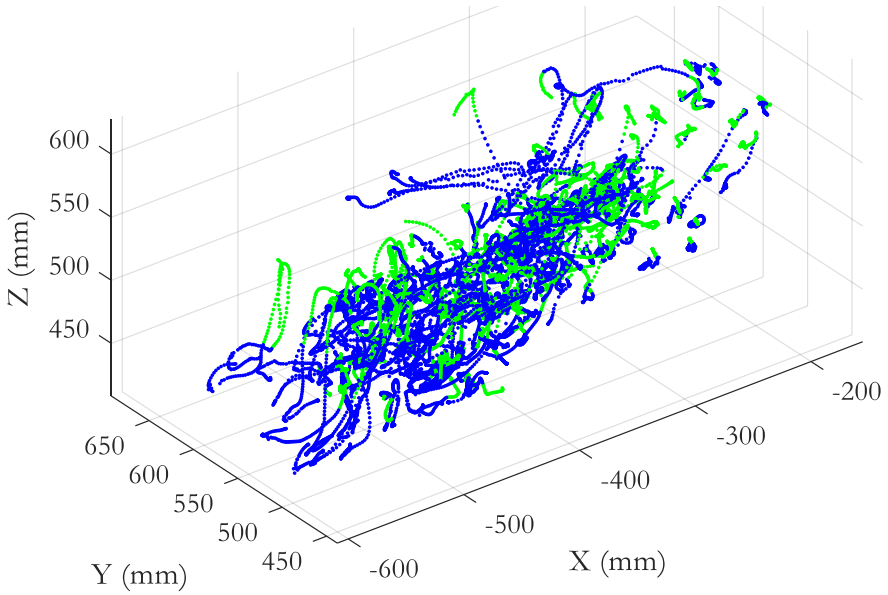

Figure 6-16 Trajectories of the H-point in the take-over processes

The H-point represents the sitting position and its stability. Together with the breastbone point, the torso angle is calculated. Two outliers are excluded for the H-point analysis (details and reasoning in Table B-1 in Appendix B). Figure 6-16 shows all 222 trajectories of the H-point in the take-over process, including the hand-on phase (blue) and the steering phase (green). Different starting points of the trajectories represent different sitting positions with individual anthropometric characteristics. The movement of the H-point indicates the stability of a sitting position during the take-over process.

The boxplots in Figure 6-17 show the distributions of the x-, y- and z-displacements of the H-point in 222 take-over processes. The corresponding descriptive statistics can be found in Appendix D in Table D-7, Table D-8, and Table D-9. The displacements are grouped by different torso angles (the knee-angle grouped diagrams are shown in Appendix E Figure E-3).

Results show that in both the x-direction (Δ_{M_x} = 61mm) and the y-direction (Δ_{M_x} = 20 mm), the larger the torso angle is, the bigger the average displacement of the H-point, and the less stable the sitting posture. The H-point in the z-direction (Δ_{M_x} = 6 mm) stays rather uninfluenced by the increasing torso angle.

The x-displacements are more widely distributed from 2 mm to 206 mm than the y-displacements (3–169 mm) and the z-displacements (6–82 mm). The mean x-displacements increase consistently from 20 mm to 81 mm as the torso angle increases, especially when the torso angle is greater than 30°. The red dashed line in Figure 6-17 (a) between the 30° and 50° schematically symbolizes a torso-angle threshold concerning the x-displacement. The x-displacement starts to increase more quickly when the torso angle is higher than the threshold, as discussed in Section 6.4.4. The SD increases in a similar pattern from 16 mm to 48 mm. The mean y-displacements increase consistently from 13 mm to 33 mm as the torso angle increases, while the SD increases and stays around 20 mm. The mean z-displacements remain between 25 mm and 31 mm as the torso angle increases, and the SD also stays around 16 mm.

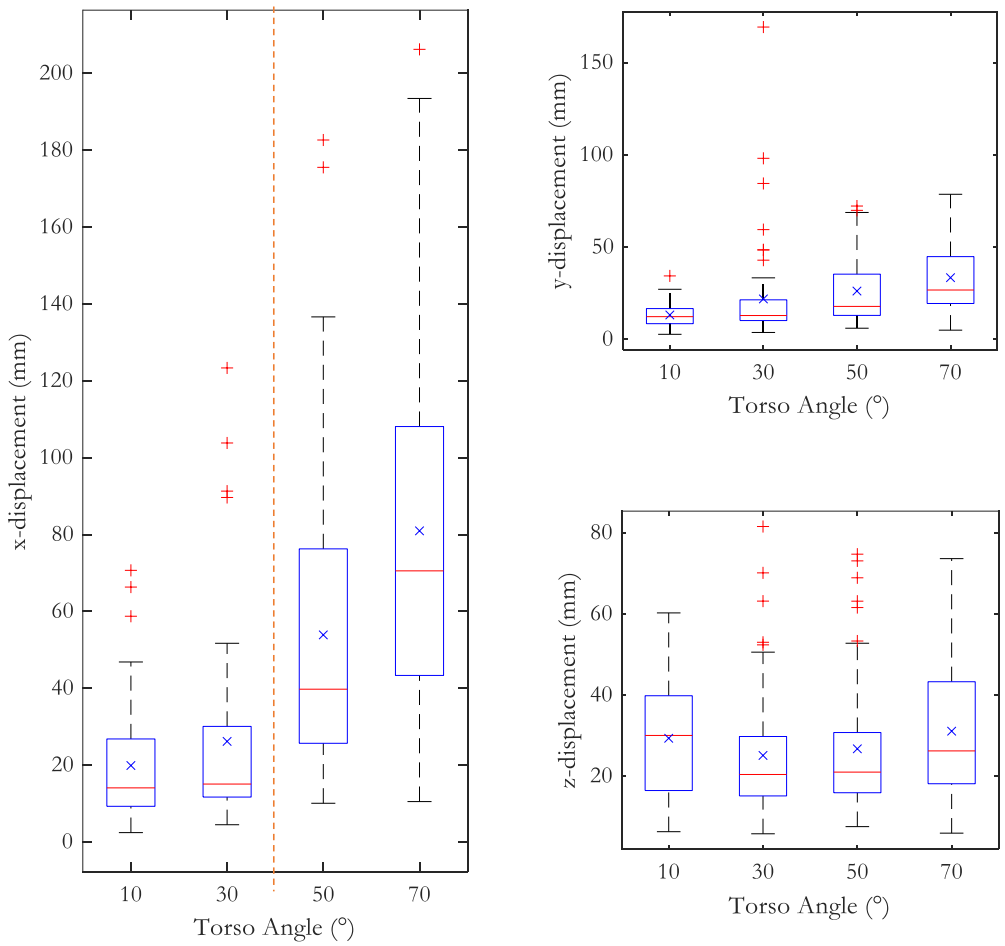

Figure 6-17 The x-, y-, and z-displacements of the H-point in different torso angle conditions

6.3.2 Regression of Hand Trajectories

In this section, the hand movement pattern, represented by the wrist movement in this experiment, is investigated. Wrist trajectories are regressed in different polynomials (planes or curves). The goal is to model the hand movement in the take-over process, taking all 12 different sitting postures of 27 participants into account. The regressed trajectories include both the hand-on phase and the steering phase of the take-over process.

6.3.2.1 The 3D Fitted Planes

Figure 6-18 (a) shows 224 take-over trajectories of the wrist in x-y-z coordinates. The blue points are the individual measurements recorded in 100 Hz.

There was no obstacle between the hand and steering wheel; drivers were able put their right hand straight onto the steering wheel (the 3 o'clock position) and steer to the left. Each wrist movement can be regressed to a plane with a very high adjusted R square (> 0.9). The average of 224 adjusted R square values is 0.98.

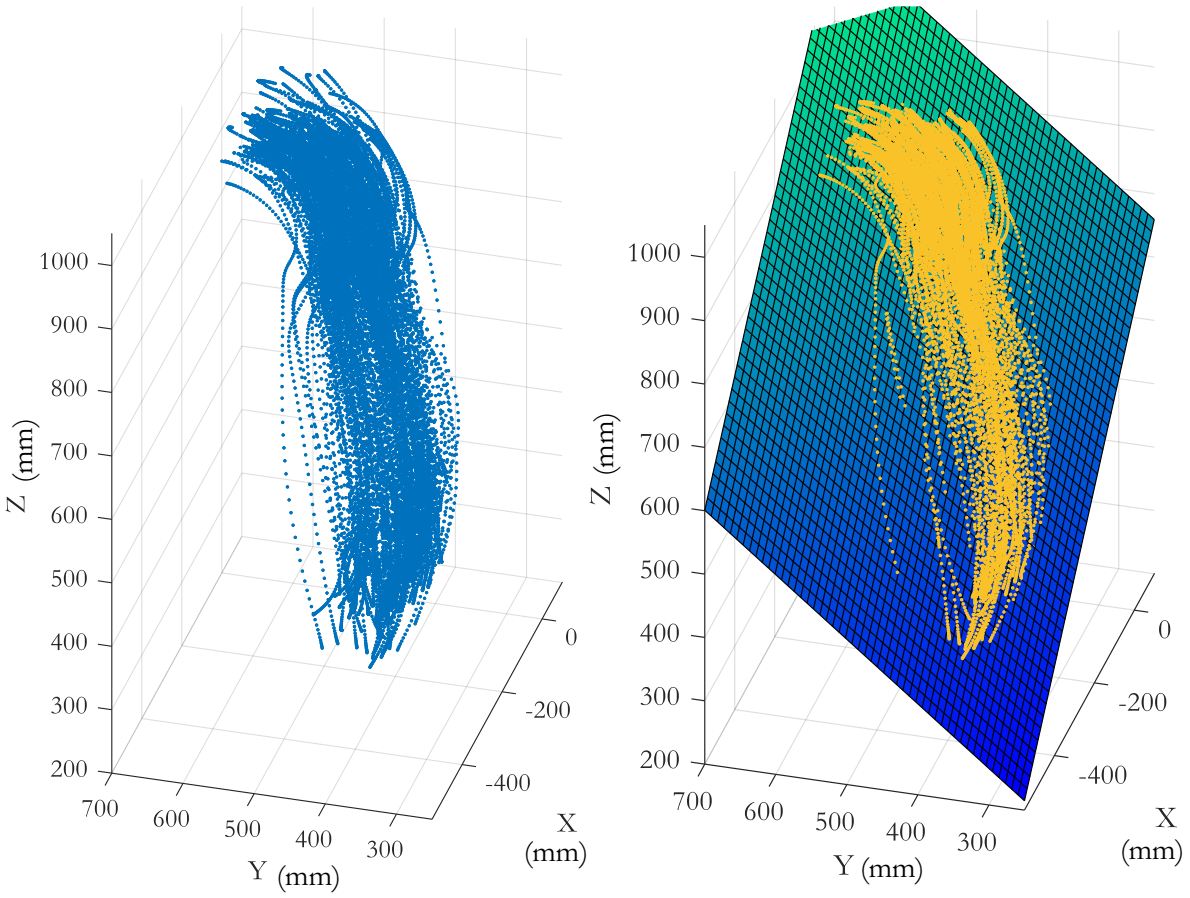

(a) Hands' trajectories (b) Hands' trajectories and the fitted plane

Figure 6-18 Trajectories of the wrist in 224 take-overs from 12 sitting postures (a) and the fitted plane (b)

Additionally, all 224 take-over trajectories of the wrist could also be regressed on one single plane (Figure 6-18, b). The regression results in Table 6-2 indicate a good fitting quality. The adjusted R square is 0.85, and the root-mean-square error (RMSE) is 67.71 mm.

Table 6-2 Regression coefficients and the fitting quality of the wrist trajectories

Fitted surface					
	All 224 take-over				
	$z = p_{00} + p_{10}*x + p_{01}*y$				
Coefficients (with 95% confidence bounds)	p_{00}	461 (451.4, 470.6)	Quality	R^2 adj.	0.85
	p_{10}	0.8377 (0.8256, 0.8498)		RMSE	67.71
	p_{01}	0.8580 (0.8407, 0.8752)			

Subgroups are built to investigate the anthropometrical (body height and weight) and the postural (torso angle and knee angle) influence on the plane of this wrist movement. The fitted planes (Figure 6-19) of the subgroups are slightly shifted and rotated from the original plane (Figure 6-18, b).

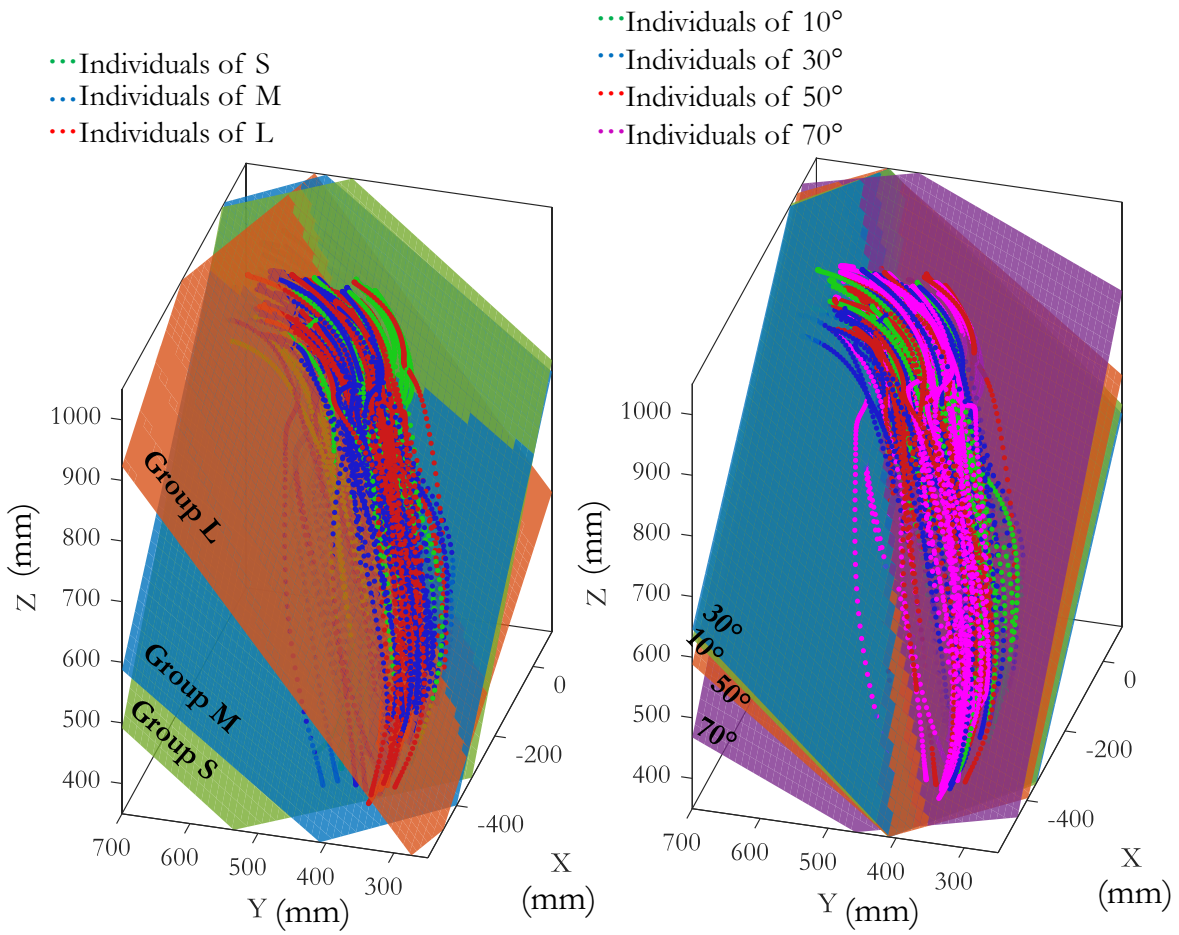

(a) Fitted planes grouped by body size (b) Fitted planes grouped by torso angle

Figure 6-19 Various fitted planes grouped by body size (a) and initial torso angle(b)

Figure 6-19 (a) shows the fitted planes of the wrist of three body-size subgroups (S, M, L), defined in Section 6.2.6. For the group "L," the red trajectories are regressed on the orange plane; for the group "M," the blue trajectories are regressed on the blue plane; for the group "S," the green trajectories are regressed on the green plane. The shifting and rotating directions of the planes accord with the decreasing body sizes. The rotating pattern is visualized in the Discussion section 6.4.1. The parameters and the fitting quality are shown in Table F-1 in Appendix F.

Figure 6-19 (b) shows the fitted planes of the wrist of four torso-angle subgroups (10°, 30°, 50°, 70°). For the 10° torso angle group, the green trajectories are regressed on the green plane; for the 30° torso angle group, the blue trajectories are regressed on the blue plane; for the 50° torso angle group, the red trajectories are regressed on the orange plane; for the 70° torso angle group, the magenta trajectories are regressed on the violet plane. The shifting and rotating directions of the planes accord with the increasing torso angles, except for the 10° subgroup. The rotating pattern is visualized in the Discussion section 6.4.1. The parameters and the fitting quality are shown in Table F-2 in Appendix F.

The minor influence of the knee angle on the hand-on movement can be found in Figure F-1 and Table F-3 in Appendix F.

6.3.2.2 The 2D Fitted Curve

The 2D regression in this section provides a more detailed view of the patterns in each x-, y-, and z-direction.

Figure 6-20 shows the 224 wrist trajectories in the x-y, x-z, and y-z plane. The blue points are the individual measurements recorded in 100 Hz. The black lines are the linear fitted lines in each plane. The regressions with higher orders improve the goodness of fit only very marginally.

Table G-1 in Appendix G shows the parameters and the goodness of fit of each fitted curve.

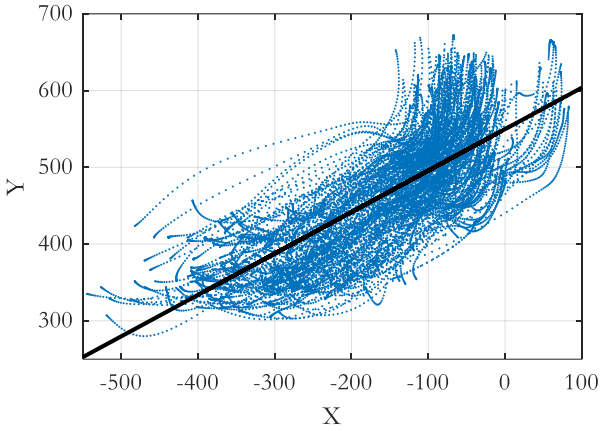

(a) Hands' trajectories and the fitted line, x-y plane

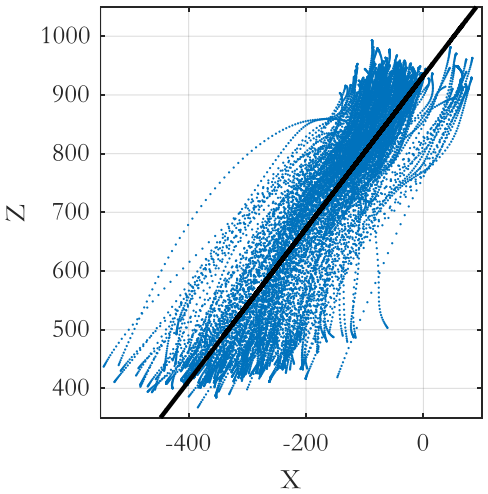

(b) Hands' trajectories and the fitted line, x-z plane

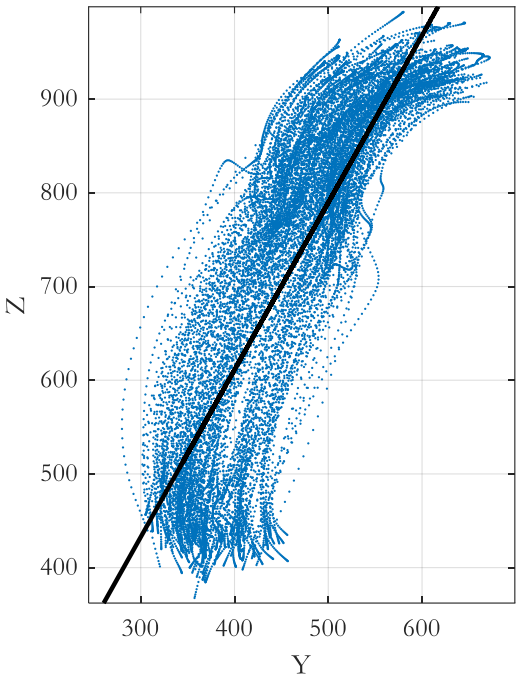

(c) Hands' trajectories and the fitted line, y-z plane

Figure 6-20 The wrist trajectories in 224 take-overs and their fitted curves in x-y, x-z, and y-z planes

The adjusted R-squared of the regression in the x-y plane is 0.60; it is 0.72 in the x-y plane; it is 0.78 in the x-z plane. In the x-y plane (the top view), the movement is very individually different (Figure 6-20, a). Drivers' wrists made a concave-like, convex-like, or a mixed curve to reach the steering wheel. The adjusted R-squared is higher in the x-z plane (the side view, Figure 6-20, b) and the y-z plane (the front view, Figure 6-20, c), which both include the z-direction. The distance between the upper edge of the seat to the steering wheel in the z-direction stays constant,

independent of the sitting positions. The highest adjusted R-squared in the x-z plane benefits from the fact that the steering action is close and parallel to the extension of the fitted line.

Curve fittings of different subgroups are presented in Appendix G (body-size subgroups: Figure G-1, Table G-2, Table G-3, and Table G-4; torso-angle subgroups: Figure G-2, Table G-5, Table G-6, and Table G-7; knee-angle subgroups: Figure G-3, Table G-8, Table G-9, and Table G-10).

6.3.3 Torso Speed and Acceleration

The line between the driver's breastbone and the H-point represents the driver's upper body, assuming it is rigid. The flexion and the extension within the torso are ignored. The angle between the upper body and the vertical is the torso angle. According to the convention in the literature (Section 3.3), the positive direction of the torso angle is toward the seatback, illustrated by the black positive sign and arrow in Figure 6-21. The larger the torso angle is, the more reclined the driver is.

In this thesis, the torso angle is the projection of the actual torso angle in the x-z plane (Figure 6-21). The raw Vicon data are x-y-z positions of each marker. The calculation of the torso angle is based on the x-z positions of the breastbone and the H-point, using the inverse trigonometric function: $torso\ angle = arctangent\ ((x_{hip} - x_{brestbone})/(z_{brestbone} - z_{hip}))$.

The driver leans forward, reducing the torso angle to sit straight. The driver may end up with a small or even negative torso angle reaching the steering wheel. Some drivers may then readjust the torso angle during steering by shifting the H-point forward or leaning back again, which increases the torso angle.

Drivers with an initial torso angle of 10° and 30° might not need to lean forward much to take over, while drivers with an initial torso angle of 50° and 70° might have to. However, this behavior is individually different.

In the following three sections, the backward readjustment of the torso angle is not considered; only the forward-leaning movement is considered, during which the torso angle decreases. Reduction of the torso angle results in negative angular speed and acceleration values. The highest speed and acceleration are the minima of negative values. However, the negative signs are eliminated for ease of reading and understanding. The torso angular speed and acceleration are positive values in a forward-leaning movement, illustrated by the orange positive sign and arrow in Figure 6-21. The higher the torso angular speed/acceleration is, the faster/more quickly the driver leans forward.

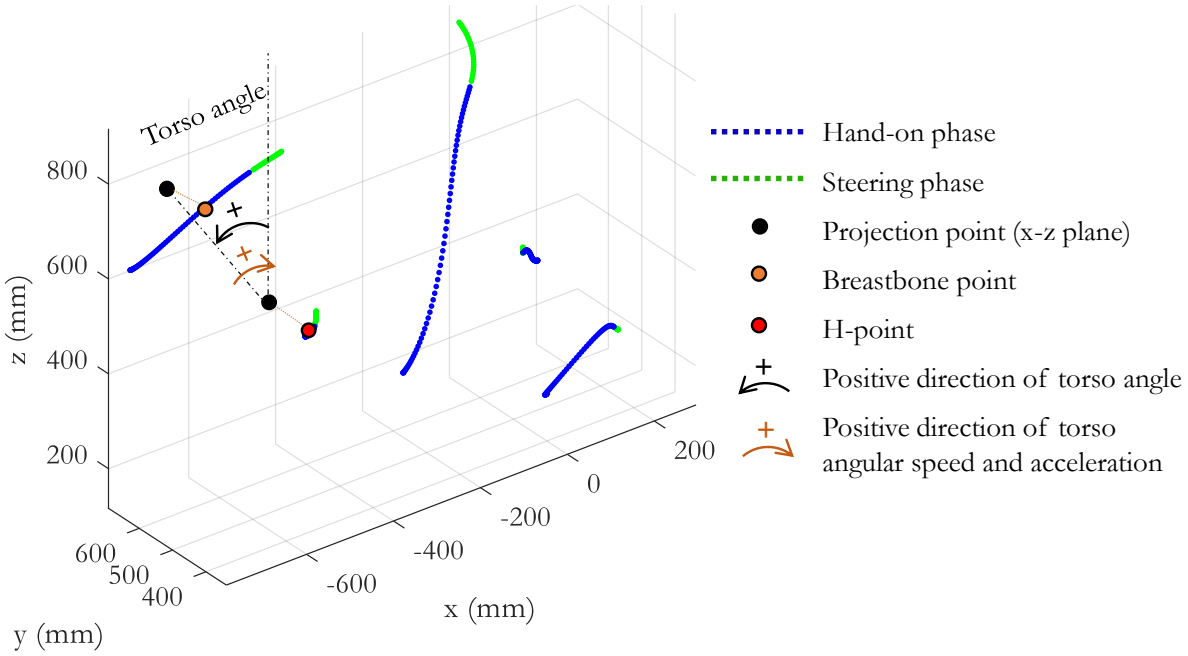

Figure 6-21 Definition of the simplified torso angle in the x-z plane

The torso angular speed and acceleration are the first and second derivatives of the torso angle with respect to time. A small fluctuation in original high-frequency position data (100 Hz) results in enormous values in its first and second derivatives, which is not the goal of this calculation. Shah et al. (2016) suggested that no significant frequency component of human motion is greater than 10 Hz. The torso angle data is thus downsampled to a frequency of 10 Hz to calculate the angular speed and acceleration.

The maximum torso angle speed (Section 6.3.3.1) and acceleration (Section 6.3.3.2) concern the whole take-over process, consisting of the hand-on phase and the steering phase. The hand-on torso angular speed and acceleration (Section 6.3.3.3 and Section 6.3.3.4) concern the last data frame of the hand-on phase. Descriptive statistics and their trends are reported. The repeated measure ANOVA analysis is impossible due to a lack of complete datasets, similar to HoMT in Section 6.3.4.1.

6.3.3.1 Maximum Torso Angular Speed

The maximum torso angular speed is the highest torso angular speed one participant reached during the forward-leaning movement in one take-over process (the hand-on and the steering phases). Three outliers are excluded (detail and reasoning in Table B-1 in Appendix B). The distribution of the maximum angular speed (n=221) in different initial torso angle conditions is presented in Figure 6-22; the descriptive statistics are reported in Table 6-3. The minor influence of the initial knee angle on the torso angular speed is presented in Figure H-1 and Table H-1 in Appendix H.

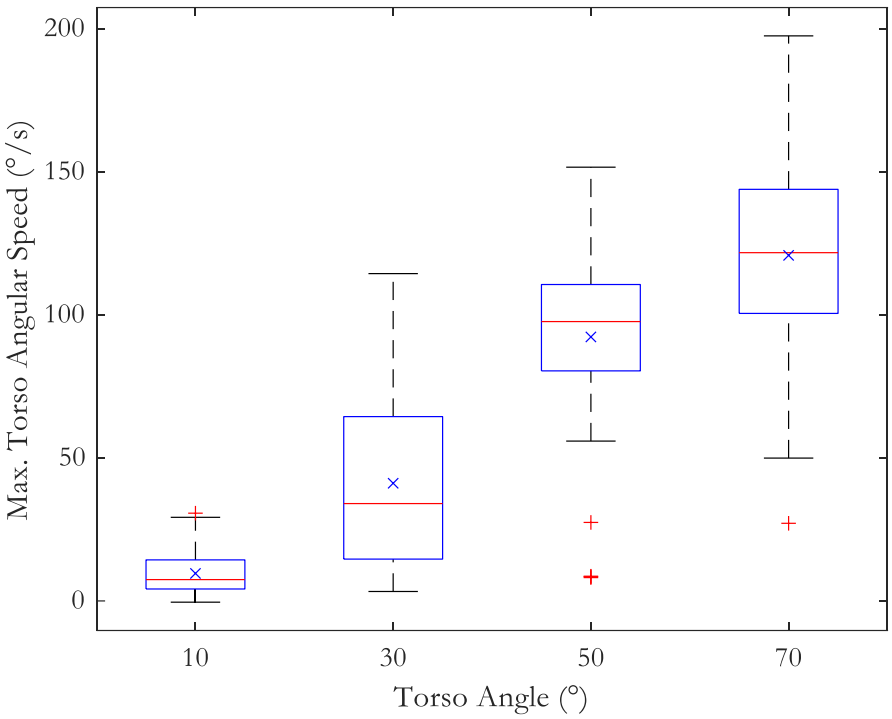

Figure 6-22 The maximum torso angular speed during the take-over process in different torso angle conditions

Figure 6-22 shows that drivers reach, on average, a higher maximum torso angular speed as the initial torso angle increases. The average of the maximum angular speed increases consistently from 10 °/s to 121 °/s (Table 6-3).

Table 6-3 Descriptive statistics of the maximum torso angular speed in different torso angle conditions

Descriptive Statistics

	Max torso angle speed (°/s)			
	Torso 10°	Torso 30°	Torso 50°	Torso 70°
Valid n	46	57	61	57
Mean	9.61	41.13	92.27	120.77
Median	7.46	34.03	97.64	121.72
Std. deviation	7.40	29.67	28.38	31.71
Minimum	-0.43	3.30	8.16	27.13
Maximum	30.67	114.40	151.60	197.49

Assuming that a human torso length is r = 0.45 m (from the hip to the breastbone), as an example, the medians of the maximum torso angular speed correspond to a breastbone speed of 0.05 m/s for torso condition 10°; 0.27 m/s for torso condition 30°; 0.77 m/s for torso condition 50°; 0.96 m/s for torso condition 70°. The arc length formula $s = 2\pi r(\theta/360°)$ is applied in this calculation.

6.3.3.2 Maximum Torso Angular Acceleration

The maximum torso angular acceleration is the highest torso angular acceleration the participant reached during the forward-leaning movement in one take-over process (the hand-on and the steering phases). Three outliers are excluded (detail and reasoning in Table B-1 in Appendix B). The distribution of the maximum angular acceleration (n=221) in different initial torso angle

conditions is presented in Figure 6-23; the descriptive statistics are reported in Table 6-4. The minor influence of the initial knee angle on the torso angular speed is presented in Figure H-2 and Table H-2 in Appendix H.

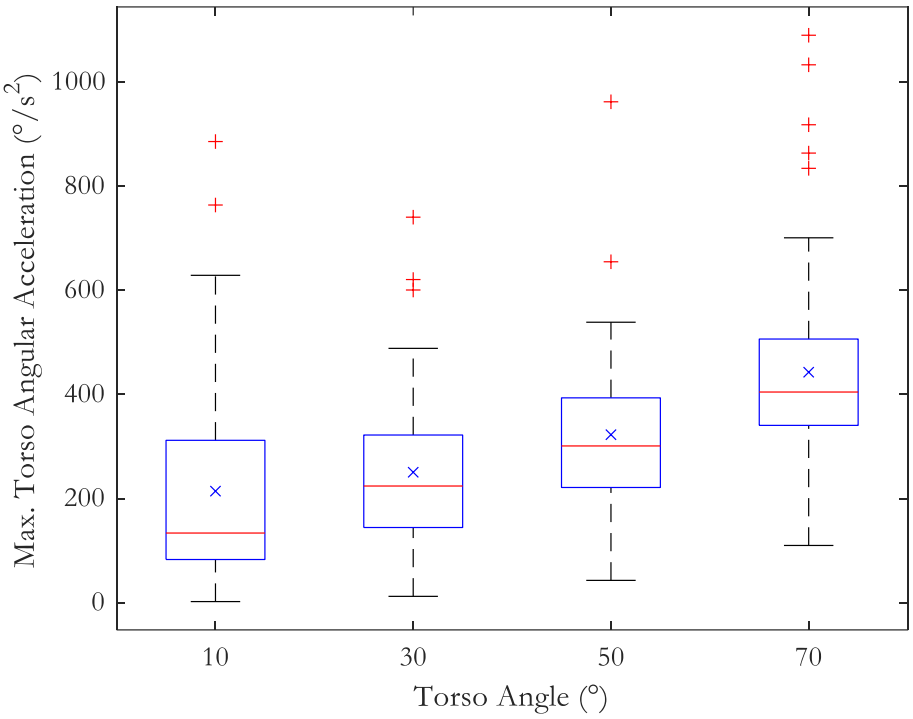

Figure 6-23 The maximum torso angular acceleration during the take-over process in different torso angle conditions

Figure 6-23 shows that the average of the maximum angular acceleration increases consistently from 214 °/s² to 443 °/s² as the initial torso angle increases (Table 6-4). The increasing medians (from 134 °/s² to 405 °/s²) illustrate an even clearer tendency without the influence of extreme values of outliers.

Table 6-4 Descriptive statistics of the maximum torso angular acceleration in different torso angle conditions

Descriptive Statistics

	Max. torso angle acceleration (°/s²)			
	Torso 10°	Torso 30°	Torso 50°	Torso 70°
Valid n	46	57	61	57
Mean	214.31	250.61	322.76	442.77
Median	133.82	224.15	301.11	404.71
Std. deviation	199.89	148.70	154.42	202.69
Minimum	2.15	12.20	42.88	109.96
Maximum	885.84	740.58	962.23	1090.09

Assuming that a human torso length is r = 0.45 m (from the hip to the breastbone), as an example, the medians of the maximum torso angular acceleration correspond to a breastbone acceleration of 1.05 m/s² (0.11 g) for torso condition 10°; 1.76 m/s² (0.18 g) for torso condition 30°; 2.36 m/s²

(0.24 g) for torso condition 50°; 3.18 m/s^2 (0.32 g) for torso condition 70°. The arc length formula $s = 2\,\pi\,r\,(\theta/360°)$ and the gravitational acceleration $1\,g = 9.8\,m/s^2$ are applied in this calculation.

6.3.3.3 Hand-on Torso Angular Speed

This section focuses on large torso angle conditions (50° and 70°) to investigate the forward-leaning speed at the hand-on moment. The hand-on torso angular speed is the torso angular speed at the time point when the driver's hand is just on the steering wheel and about to exercise the steering task, the boundary between the hand-on phase and the steering phase of the take-over process. Positive speed indicates that the driver's upper body is still approaching the steering wheel at the hand-on moment; a negative value means moving away from the steering wheel. Fourteen outliers are excluded (detail and reasoning in Table B-1 in Appendix B).

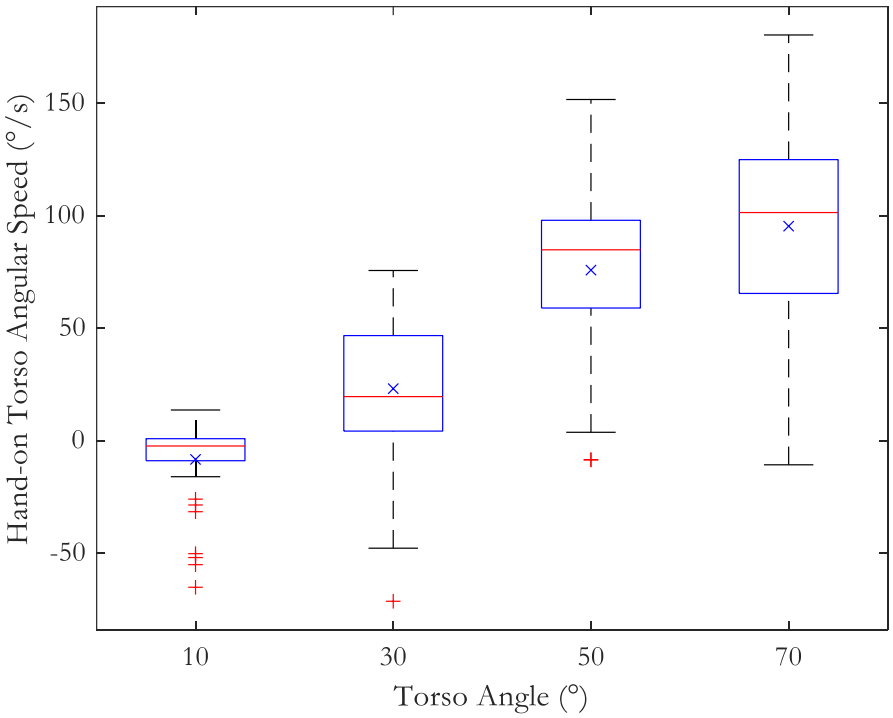

Figure 6-24 Torso angular speed when the driver's hand is on the steering wheel in different torso angle conditions

The distribution of the hand-on torso angular speed (n = 210) in different initial torso angle conditions is presented in Figure 6-24. The descriptive statistics are reported in Table 6-5. The breastbone speed is derived from the torso angular speed, assuming r = 0.45 m from the hip to the breastbone and applying the arc length formula $s = 2\,\pi\,r\,(\theta/360°)$.

The average hand-on torso angular speed increases consistently from -9.16 °/s to 95.29 °/s as the initial torso angle increases. Except for one outlier close to zero, all participants' upper bodies in the 50° and 70° conditions have positive speed approaching the steering wheel at the hand-on moment.

Table 6-5 Torso angular speed and an exemplary breastbone speed (r = 0.45m) when the driver's hand is on the steering wheel

Descriptive Statistics

	Hand-on Torso Speed			
	Torso 10°		Torso 30°	
	Torso Angular Speed (°/s)	Breastbone Speed (m/s)	Torso Angular Speed (°/s)	Breastbone Speed (m/s)
Valid n	39	39	55	55
Mean	-9.16	-0.07	23.53	0.18
Median	-3.05	-0.02	20.33	0.16
Std. deviation	18.28	0.14	31.97	0.25
Minimum	-65.22	-0.51	-71.44	-0.56
Maximum	13.58	0.11	79.09	0.62

	Torso 50°		Torso 70°	
	Torso Angular Speed (°/s)	Breastbone Speed (m/s)	Torso Angular Speed (°/s)	Breastbone Speed (m/s)
Valid n	59	59	57	57
Mean	76.10	0.60	95.29	0.75
Median	87.47	0.69	101.34	0.80
Std. deviation	36.07	0.28	41.22	0.32
Minimum	-8.63	-0.07	-10.78	-0.08
Maximum	151.60	1.19	180.28	1.42

6.3.3.4 Hand-on Torso Angular Acceleration

This section focuses on large torso angle conditions (50° and 70°) to investigate the forward-leaning acceleration at the hand-on moment. The hand-on torso angular acceleration is the torso angular acceleration at the time point when the driver's hand is just on the steering wheel and about to exercise the steering task, the boundary between the hand-on phase and the steering phase of the take-over process. Positive acceleration indicates that the driver's upper body is still accelerating toward the steering wheel at the hand-on moment; a negative value means deaccelerating (braking) against the steering wheel. Fourteen outliers are excluded (detail and reasoning in Table B-1 in Appendix B).

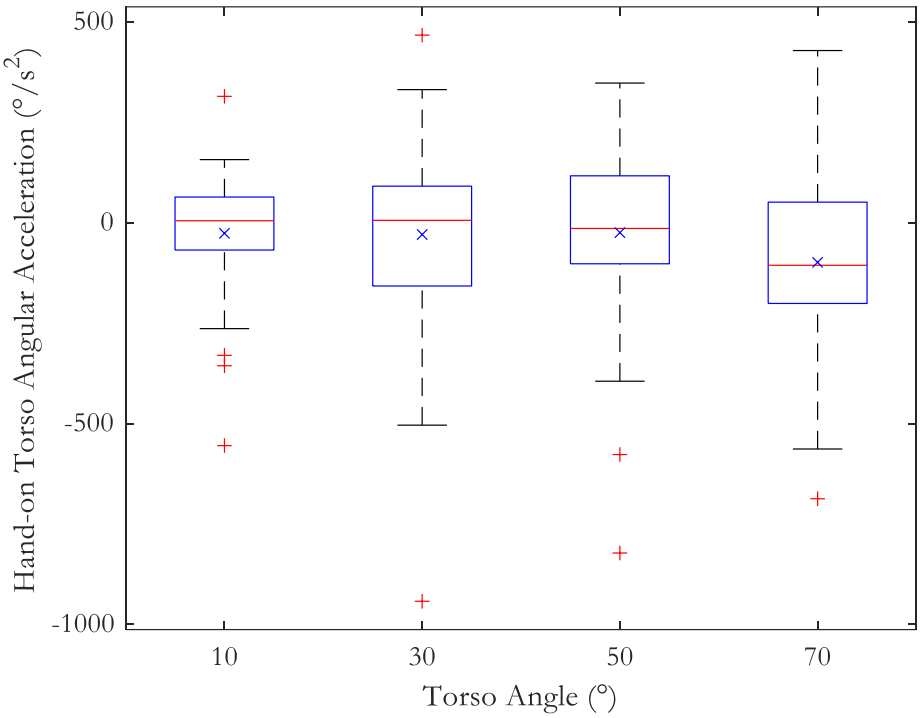

Figure 6-25 Torso angular acceleration when the driver's hand is on the steering wheel in different torso angle conditions

The distribution of the hand-on torso angular acceleration (n = 210) in different initial torso angle conditions is presented in Figure 6-25. The descriptive statistics are reported in Table 6-6. The breastbone acceleration is derived from the torso angular acceleration, assuming r = 0.45 m from the hip to the breastbone and applying the arc length formula $s = 2 \pi r (\theta/360°)$.

The average hand-on torso angular acceleration stays similar around 25 °/s^2 in the 10°, 30°, and 50° conditions. There are more negative values in the 70° condition, averaged about 100 °/s^2. The distributions of all conditions seem to be symmetric around 0, while the 50° and 70° conditions' distributions tend to shift in the negative direction slightly.

Table 6-6 Torso angular acceleration and an exemplary breastbone acceleration (r = 0.45m) when the driver's hand is on the steering wheel

Descriptive Statistics

	Hand-on Torso Acceleration			
	Torso 10°		Torso 30°	
	Torso Angular Speed (°/s²)	Breastbone Speed (m/s)	Torso Angular Speed (°/s²)	Breastbone Speed (m/s)
Valid n	39	39	55	55
Mean	-26.25	-0.21	-29.33	-0.23
Median	5.10	0.04	6.03	0.05
Std. deviation	159.64	1.25	220.65	1.73
Minimum	-554.81	-4.36	-942.41	-7.40
Maximum	314.76	2.47	467.15	3.67

	Torso 50°		Torso 70°	
	Torso Angular Speed (°/s²)	Breastbone Speed (m/s)	Torso Angular Speed (°/s²)	Breastbone Speed (m/s)
Valid n	59	59	57	57
Mean	-24.57	-0.19	-98.62	-0.77
Median	-14.14	-0.11	-105.78	-0.83
Std. deviation	218.54	1.72	203.21	1.60
Minimum	-822.21	-6.46	-687.15	-5.40
Maximum	347.82	2.73	428.81	3.37

6.3.4 Time Metrics of the Hand

The definition of the time metrics of the hand can be found in Section 6.2.3.

Figure 6-26 shows an overview of the average HoMT, HoT, ST, and TT in different torso angle conditions; the error bars represent the confident interval (significance level: 0.05). ST takes the shortest time, and their means range from 0.47 to 0.57 seconds. HoMT (0.57–0.68 seconds on average) has a similar increasing pattern. Both ST and HoMT remain at almost the same level in the 10° and 30° torso angles; they increase when the torso angle increases to more than 30°. HoT, consisting of the reaction time and HoMT, ranges from 0.69 to 0.95 seconds on average. HoT increases continuously as the torso angle increases. The TT equals HoT plus ST, ranging on average from 1.2 to 1.5 seconds. The exact distribution, descriptive statistics, and statistic tests of each time metric are presented in the following four sub-sections.

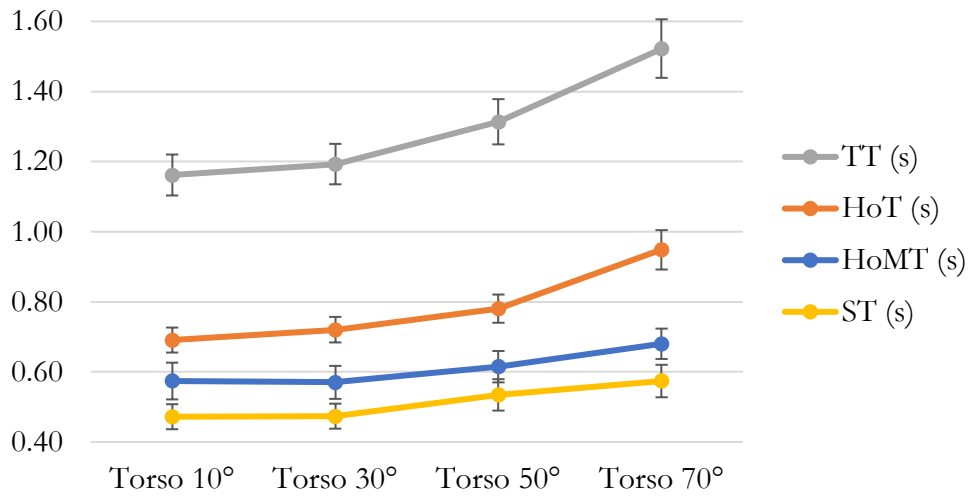

Figure 6-26 Overview of the averaged time metrics in different torso angle conditions

Table 6-7 shows the descriptive statistics of the HoMT, HoT, ST, and TT, including the number of the available datasets and their data sources.

Table 6-7 The descriptive statistics of the four take-over time metrics

Descriptive Statistics

	HoMT (s)	HoT (s)	TT (s)	ST (s)
Data Source	Vicon	GoPro	GoPro	GoPro
Valid n	213	298	298	298
Mean	0.61	0.78	1.29	0.51
Median	0.59	0.76	1.25	0.47
Std. deviation	0.18	0.21	0.32	0.18
Minimum	0.16	0.30	0.73	0.23
Maximum	1.24	1.63	2.54	1.20

Apart from the HoMT, which results from the motion-tracking Vicon data, the HoT, ST, and TT are video-based analyses with more datasets available. The smallest frame length in the video analysis was 0.03 seconds.

For the motion-tracking-based HoMT, the repeated measure ANOVA analysis is impossible due to a lack of complete datasets. Although there are still n = 213 postures available out of 27 * 12 = 324 postures, there was only one dataset with all 12 conditions available. Therefore, only the descriptive statistics in each torso angle condition are reported.

For the video-based HoT, ST, and TT, there are n = 298 postures available out of 27 * 12 = 324 postures. Among the 298 available records, 22 participants have the complete datasets of all 12 postures (22 * 12 = 264 postures). The repeated measure ANOVA (RMANOVA) for the normally distributed datasets was conducted to compare different torso angle conditions (10°, 30°, 50°, 70°) and knee angle conditions (105°, 133°, 90°). For the non-normally distributed datasets, the Durbin test combined with Connover's Post Hoc tests are conducted.

6.3.4.1 Hand-on motion time (HoMT)

HoMT is defined as starting from any tracked body parts' initial movement until the right hand reaches the steering wheel (Figure 6-4). This metric utilizes the Vicon motion data of the wrist. The Vicon data interval starts when any body segments start to move (three non-zero rows appear subsequently) until the speed of the right hand in the y-direction reaches its minimal. This specific ending criterion of the hand-on phase might only fit the dataset in this experiment. By exploring the local minimum and maximum in the trajectory, velocity, and acceleration data, it is found that, in most cases (except 11 outliers), the velocity of the right hand in the y-direction reaches a local minimum when it touches and grasps the steering wheel before steering. The right wrist is "braked" by the steering wheel transversely (y-direction). The details of the outliers can be found in Table B-1 in Appendix B. This ending cut point is also the separation point of the hand-on phase and the steering phase of the take-over process, indicated by the blue and green trajectories in Section 6.3.1.

In comparison, an exact cutting point that fits most datasets could not be found in the x- or the z-direction, where the wrist could move further and "smoothly" turning the steering wheel without much resistance after reaching the steering wheel. There are 11 outliers excluded under this data cutting criterion, in which the local minimum in the y-direction is reached on the way to the steering wheel.

Figure 6-27 shows the HoMT distribution in different torso angle conditions; the descriptive statistics are shown in Table 6-8. The HoMT stays at a similar level, around an average of 0.57 seconds in the torso angle of 10° and 30°. The HoMT increases consistently when drivers recline to 50° (average 0.61 seconds) and 70° (average 0.68 seconds).

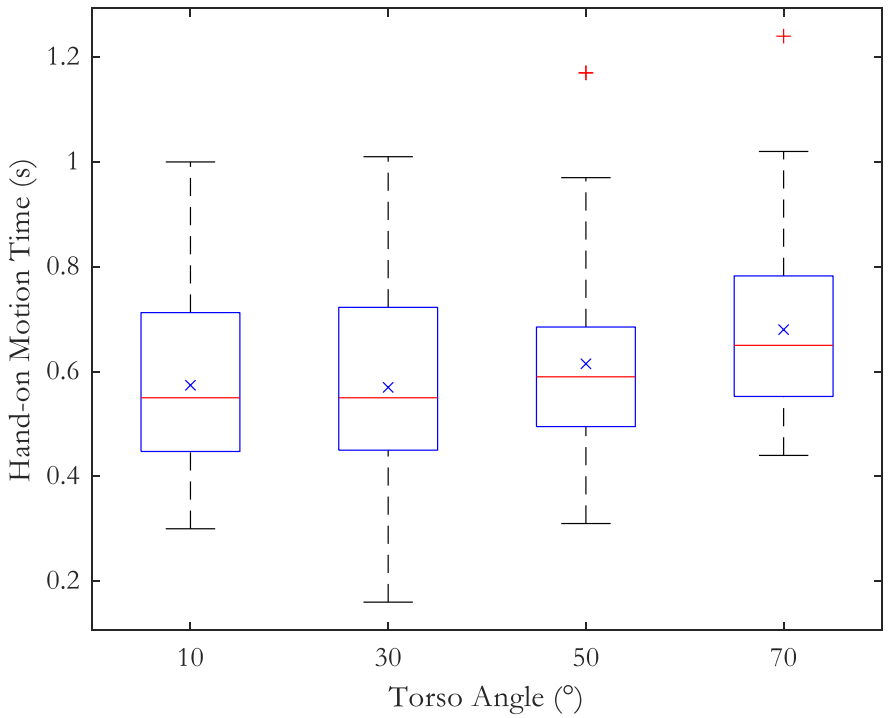

Figure 6-27 HoMT in different torso angle conditions

Table 6-8 The descriptive statistics of HoMT in different torso angle conditions

Descriptive Statistics

	HoMT (s)			
	Torso 10°	Torso 30°	Torso 50°	Torso 70°
Valid n	41	55	60	57
Mean	0.57	0.57	0.61	0.68
Median	0.55	0.55	0.59	0.65
Std. deviation	0.17	0.18	0.18	0.17
Minimum	0.30	0.16	0.31	0.44
Maximum	1.00	1.01	1.17	1.24

6.3.4.2 Hand-on Time (HoT)

Consisting of the reaction time and HoMT, HoT was defined as the period starting from the RtI signal until the right hand reaches the steering wheel (Figure 6-4). This matric utilizes video data. Figure 6-28 shows the HOT distribution in different torso angle conditions. The average HOT continuously increases when the torso angle is greater than 30° with statistical significance, ranging from 0.69 to 0.95 seconds. The SDs are around 0.2 seconds. Table 6-9 shows the descriptive statistics of the HoT in different torso angle conditions. The descriptive statistics of HoT in each torso-knee-angle combination are presented in Table I-4 in Appendix I.

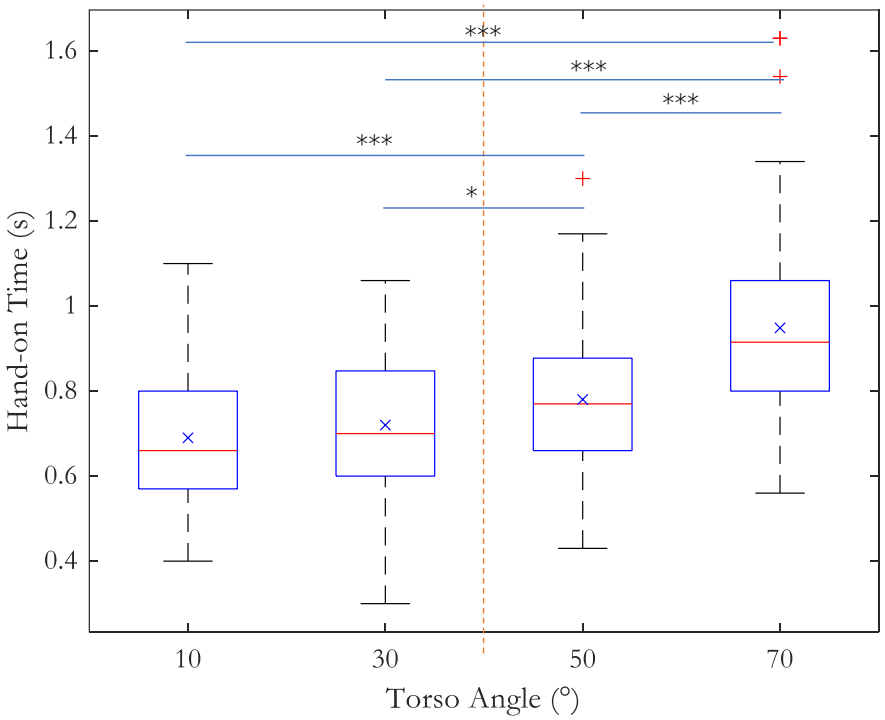

Figure 6-28 HoT in different torso angle conditions

Table 6-9 The descriptive statistics of HoT in different torso angle conditions

Descriptive Statistics

	HoT (s)			
	Torso 10°	Torso 30°	Torso 50°	Torso 70°
Valid n	78	77	73	70
Mean	0.69	0.72	0.78	0.95
Median	0.66	0.70	0.77	0.92
Std. eeviation	0.16	0.16	0.18	0.24
Minimum	0.40	0.30	0.43	0.56
Maximum	1.10	1.06	1.30	1.63

Among 298 measurements, twenty-two datasets are complete with all 12 postures and could be used for the statistical tests (n = 22 * 12 = 264). Mauchly's test of sphericity (Appendix Table I-1) is significant for the torso angle ($p < 0.001$). As the non-parametric alternative for RMANOVA, the Durbin test combined with Connover's post hoc tests were conducted. Appendix Table I-2 shows that the torso angle significantly influences HoT χ^2 (3) = 77.57, $p < 0.001$. The knee angle, however, has no significant effect on HoT.

Conover's post hoc test (Appendix Table I-3, labeled with "*" in Figure 6-28) with Bonferroni correction reveals that the HoT of the 70° torso angle is highly significantly longer than those of the 10°, the 30°, and the 50° torso angles ($p < 0.001$). The HoT of the 50° torso angle is significantly longer than those of the 10° ($p < 0.001$) and the 30° torso angles ($p < 0.05$). There is no significant difference between the 10° and the 30° torso angle conditions. The red dashed line in Figure 6-28 between the 30° and 50° schematically symbolizes a torso-angle threshold concerning HoT. HoT starts to increase more quickly when the torso angle is higher than the threshold, as discussed in Section 6.4.2.

6.3.4.3 Steering Time (ST)

Steering time (ST) is defined as the period starting when the right hand is on the steering wheel (Figure 6-4) until it reaches the left-most point of the left-steering task. The endpoints vary slightly around the 12 o'clock position of the steering wheel. This matric utilizes video data. Figure 6-29 shows the ST distribution in different torso angle conditions. The average ST continuously increases when the torso angle is greater than 30° with statistical significance, ranging from 0.47 to 0.57 seconds. The SDs are around 0.2 seconds. Table 6-10 shows the descriptive statistics of ST in different torso angle conditions. The descriptive statistics of ST in each torso-knee-angle combination are presented in Table I-8 in Appendix I.

Among 298 measurements, 22 datasets are complete with all 12 postures and could be used for the statistical tests (n = 22 * 12 = 264). Mauchly's test of sphericity (Appendix Table I-5) is significant for the torso angle ($p = 0.004$). As the non-parametric alternative for RMANOVA, the Durbin test combined with Connover's Post Hoc Tests were conducted. Appendix Table I-6 shows that the torso angle significantly influences ST χ^2 (3) = 23.491, $p < 0.001$. The knee angle has no significant effect on ST.

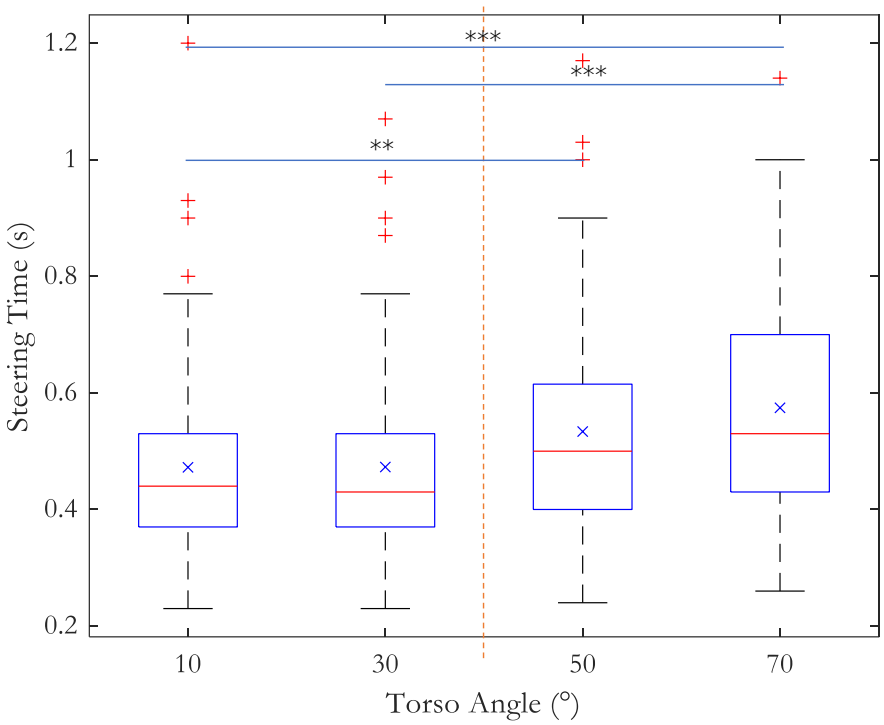

Figure 6-29 ST in different torso angle conditions

Conover's post hoc test (Appendix Table I-7, labeled with "*" in Figure 6-29) with Bonferroni correction reveals that the ST of the 70° torso angle is highly significantly longer than those of the 10° and 30° torso angle ($p < 0.001$). ST of the 50° torso angle is significantly longer than the 10° torso angle ($p < 0.01$). There is no significant difference between each adjacent group, meaning the ST might only have a significant difference if the torso angle changes to a large extent, e.g., 40°. The red dashed line in Figure 6-29 between the 30° and 50° schematically symbolizes a torso-angle threshold concerning ST. ST starts to increase more quickly when the torso angle is higher than the threshold, as discussed in Section 6.4.2.

Table 6-10 Descriptive statistics of ST in different torso angle conditions

Descriptive Statistics

	ST (s)			
	Torso 10°	Torso 30°	Torso 50°	Torso 70°
Valid n	78	77	73	70
Mean	0.47	0.47	0.53	0.57
Median	0.44	0.43	0.50	0.53
Std. deviation	0.16	0.16	0.20	0.20
Minimum	0.23	0.23	0.24	0.26
Maximum	1.20	1.07	1.17	1.14

6.3.4.4 Task Time (TT)

Starting from the RtI to the end of the steering task, the TT is a combination of the HoT and ST. The results are very similar to those of the HoT. Figure 6-30 shows the TT distribution in different torso angle conditions; statistical significance is labeled with "*." The average TT continuously

increases when the torso angle is greater than 30° with statistical significance, ranging from 1.16 to 1.52 seconds. The SDs are around 0.3 seconds. Table 6-11 shows the descriptive statistics of TT in different torso angle conditions. The descriptive statistics of TT in each torso-knee-angle combination are presented in Table I-12 in Appendix I. The knee angle has no significant effect on TT.

The torso angle is an influential factor to the TT; there are highly significant differences between all conditions except the 10° and 30° torso angle. The red dashed line in Figure 6-30 between the 30° and 50° schematically symbolizes a torso-angle threshold concerning TT. TT starts to increase more quickly when the torso angle is higher than the threshold, as discussed in Section 6.4.2.

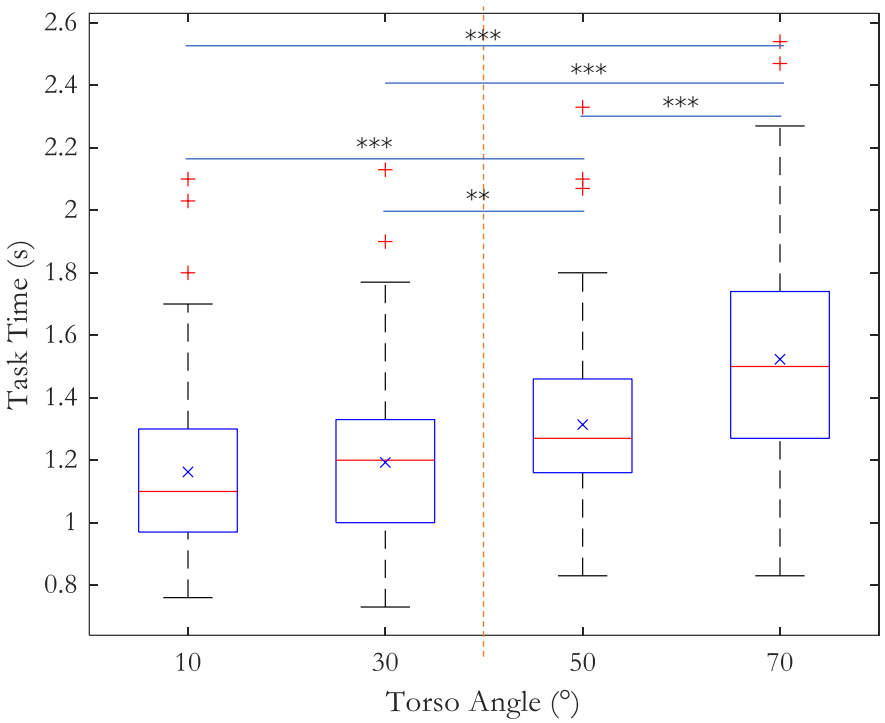

Figure 6-30 TT in different torso angle conditions

Table 6-11 The descriptive statistics of TT in different torso angle conditions

Descriptive Statistics

	TT (s)			
	Torso 10°	Torso 30°	Torso 50°	Torso 70°
Valid n	78	77	73	70
Mean	1.16	1.19	1.31	1.52
Median	1.10	1.20	1.27	1.50
Std. deviation	0.27	0.26	0.28	0.36
Minimum	0.76	0.73	0.83	0.83
Maximum	2.10	2.13	2.33	2.54

Among 298 measurements, 22 datasets are complete with all 12 postures and could be used for the statistical tests (n = 22 * 12 = 264). The statistical tests' details can be found in Table I-9, Table I-10, and Table I-11 in Appendix I.

6.3.5 Subjective Evaluation

The NASA TLX questionnaire was given to the participants after every three take-overs in one torso angle condition. Every data point of the questionnaire refers to the last three take-overs with the same torso angle but three different knee angles.

There are six categories in the NASA TLX questionnaire (Hart & Staveland, 1988): mental demand, physical demand, temporal demand, performance effort, frustration. Each item is scaled on 21 levels, representing a score from 0 (very low) to 100 (very high). The overall score in this study is the average of six items without weighing. In this section, the overall score is presented first, followed by the analysis of each item.

Figure 6-31 shows the general TLX score distribution in different torso angle conditions and visualizes the significant differences between the 70° torso angle and others.

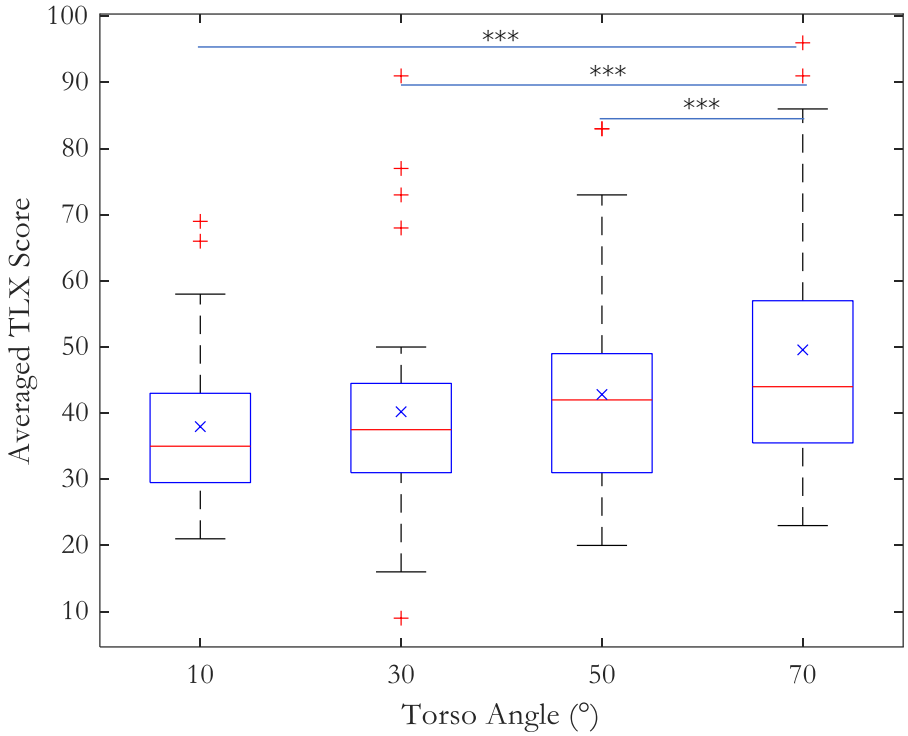

Figure 6-31 NASA TLX score

Table 6-12 shows that the average TLX score, representing workload, increases consistently from 38 to 50 as the torso angle increases, indicating an increasing demand for a general effort to take over.

Appendix Table J-1 results from the assumption checks for the repeated measures ANOVA without significance ($p = 0.058$). In this case of normally distributed data, the repeated measures ANOVA was conducted. Appendix Table J-2 shows the significant main effect ($p < 0.001$), indicating a significant difference between groups. In Appendix Table J-3, the posthoc pairwise tests with Bonferroni correction reveal that there are highly significant differences ($p < 0.001$) between the 70° torso angle and all the other ones (50°, 30°,10°), labeled with "*" in Figure 6-31.

Table 6-12 The Descriptive Statistics of the overall NASA TLX score in different torso conditions

Descriptive Statistics

	Torso 10°	Torso 30°	Torso 50°	Torso 70°
Valid n	28	28	28	28
Mean	37.83	40.09	42.71	49.58
Median	35.00	37.09	41.67	44.17
Std. deviation	12.94	18.13	16.26	19.46
Minimum	20.83	9.17	20.00	23.33
Maximum	69.17	90.83	83.33	95.83

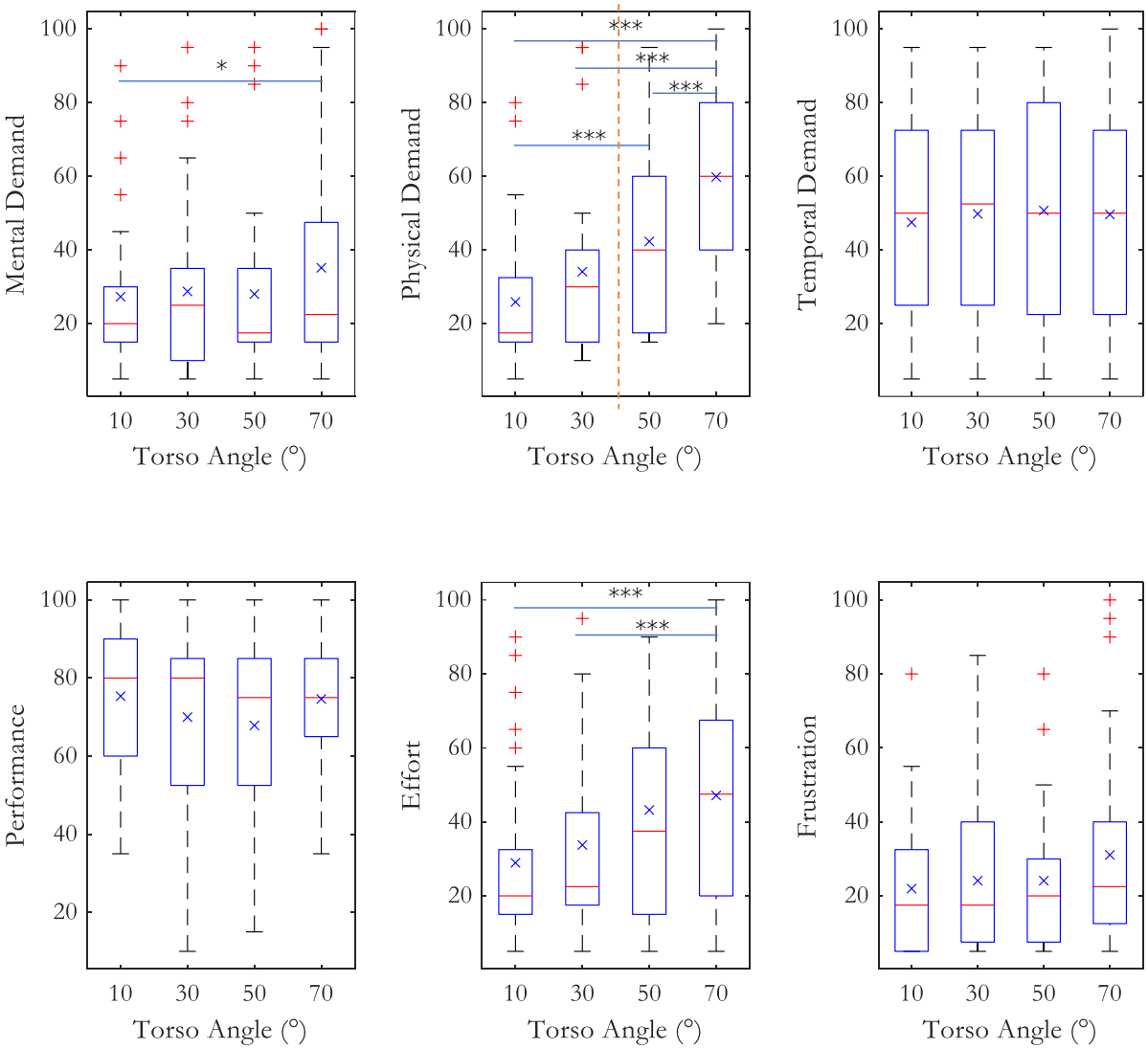

Figure 6-32 NASA TLX scores of each category

Regarding six categories individually, Figure 6-32 shows the distribution of the score in each NASA TLX category in four different torso angle conditions. Significant results (labeled with "*" in Figure 6-32) were found in the categories of "mental demand," "physical demand," and general "effort," among which there is no statistically significant difference between the 10° and 30° torso angle conditions. It demands significantly more mental resources to conduct a take-over with the 70° torso angle rather than the 10° torso angle. The "physical demand" continuously increased from

the 30° up to the 70° torso angle with statistical significance. A similar trend could be seen with the item "effort." A similar torso-angle threshold could be found concerning "physical demand," schematically symbolized by the red dash in Figure 6-32. The physical demand starts to be significantly higher when the torso angle increases higher than the threshold, as discussed in Section 6.4.6.

The statistical tests of each item in detail can be found in Appendix J: mental demand (Table J-4, Table J-5, Table J-6), physical demand (Table J-7, Table J-8, Table J-9), temporal demand (Table J-10, Table J-11, Table J-12), performance (Table J-13, Table J-14, Table J-15), effort (Table J-16, Table J-17, Table J-18), frustration (Table J-19, Table J-20, Table J-21).

6.4 Discussion

This section discusses the main findings of the motion tracking experiment. All results in Section 6.3 are interpreted and discussed, focusing on three focusing body parts: the hand, breastbone, and H-point.

The take-over trajectories presented in Section 4.3.1 have wide postural and anthropometric ranges. On the one hand, there are take-overs from the upright driving posture, which is well supported by the current interior concepts. On the other, there are also extremely reclined postures, which are not considered as a use case for the current seat concept but should be considered in the AVs.

Not only do the wide postural and anthropometric ranges introduce the systematic variance into the results, but the inter-and intra-individual variances of the human body movement (Arlt, 1999) also introduce the random variance, resulting in large SDs.

Compared to the torso angle, the knee angle shows a minor influence on either geometrical or temporal aspects during the take-over process. The "fixed-toe" method (Section 6.2.2) effectively controlled the leg and foot movement, independent of three knee angle variants.

6.4.1 Hand Motion and the Rotating Plane

Only the driver's hands can operate the lateral dynamic of the vehicle (steering) in normal cases. It is essential to avoid obstacles between the driver's hands and the steering wheel in critical take-over scenarios. The torso angle affects the movement range of the torso more significantly in the x-direction. Larger torso angles increase the distance between the upper body (including the shoulder and arm) and the steering wheel in the x-direction. Results show that the larger the torso angle is, the longer the distance the wrist moves in the x-direction. At the same time, the influences in the y-direction, z-direction are relatively minor. The large SD in the x-direction might be because of individual anthropometric characteristics (e.g., arm length) and individual gestures to grasp the steering wheel. Different knee angles directly affect the distance in the x-direction, also resulting in large SDs in the torso-grouped results. The knee angle geometrically influences the initial position of the hand due to the "toe-fixed" method. The larger the knee angle, the further the hand is away from the steering wheel (smaller x-value). Results in Appendix E show that the hand has a larger displacement in the x-direction when the knee angle increases from 105° to 130°.

Hand movement between two fixed points without obstacles (e.g., hand-on movement in this experiment) is mainly on one unique plane (Arlt, 1999). Results show that the hand movement, even including the steering movement, is primarily on one plane. The regressed plane covers 12 sitting positions and 27 anthropometric characteristics. The 7 cm RMSE of the fitted plane means for the interior development that the space about 7 cm above and underneath this plane should always be kept free without any obstacle during a Level 3 automated drive. Anything in this area (e.g., a small table for a laptop, a foldable cup holder) can block the take-over action of the right hand.

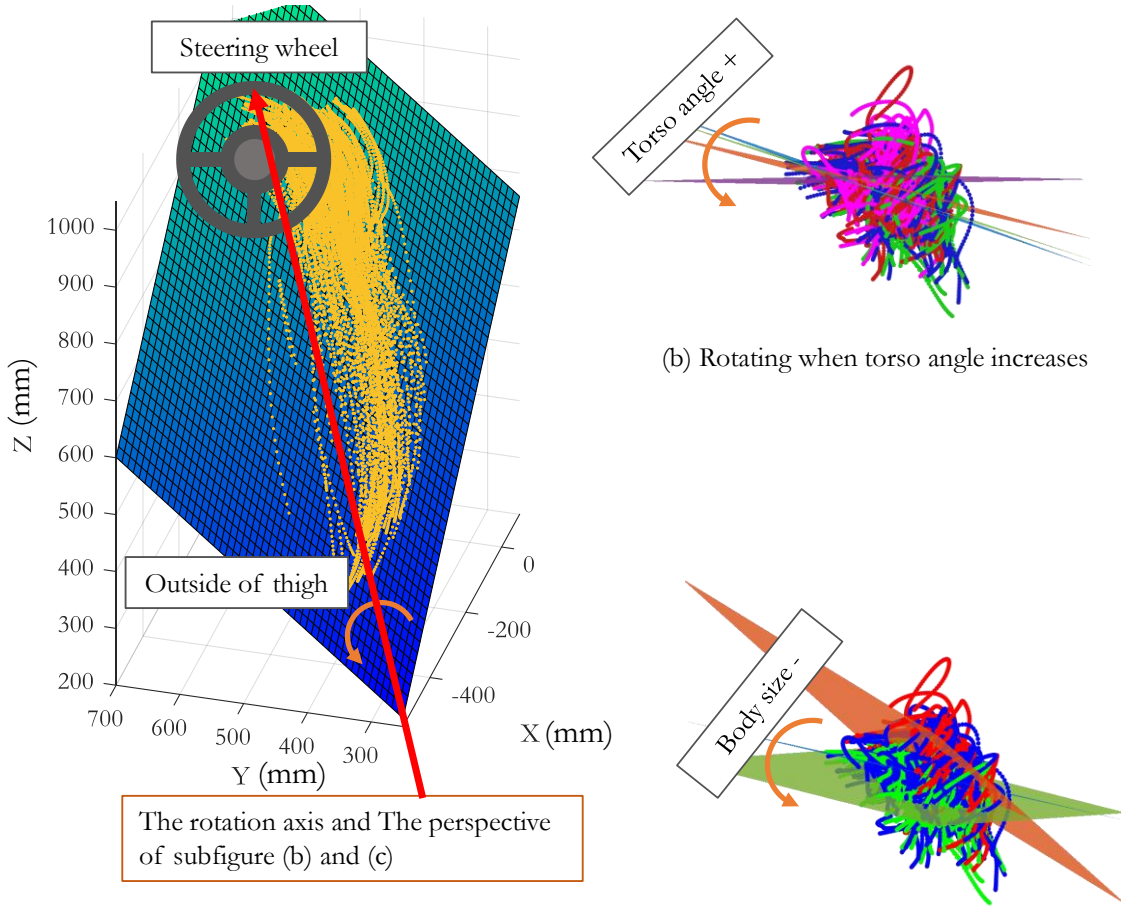

(a) The hand-on plane and the rotation axis

(b) Rotating when torso angle increases

(c) Rotating when body size decreases

Figure 6-33 The rotating pattern of hand-on fitted planes due to the varying torso angle and the body size

Different torso angles and body sizes lead to a slight rotation and minor shift of the hand-on movement plane. The red arrow in Figure 6-33 (a) schematically represents the rotation axis, a line through the initial point of the wrist and the top of the steering wheel. Figure 6-33 (b) and (c) are the subgroup fitted planes (Figure 6-19, a and b) from the perspective of the red arrow in Figure 6-33 (a). As the torso angle increases (Figure 6-33, b) or the body size decreases (Figure 6-33, c), the hand-on movement plane rotates counter-clockwise around the rotating axis in the same way. This rotating trend is shown as the same orange archy arrows in Figure 6-33 (a, b, and c). As an explanation, both the increasing torso angle and the decreasing body size share the effect of "shortening" the participants' arms, in other words, enlarging the distance between the hand and

the steering wheel. This effect results in more straight and point-to-point trajectories, namely less curvy trajectories in the x-z plane.

6.4.2 Hand Time Metrics and the Torso-Angle Threshold

Due to this strictly controlled experimental setting, the time metrics results can be interpreted as primarily the motoric time and a minimized reaction time. In reality, it should take the unprepared driver in the same posture longer due to extra cognitive loads and more complex situations.

Significant differences found in HoT confirm H_{11}: Torso angle affects hand-on time. A torso-angle threshold concerning HoT seems to lie between 30° and 50°. HoT starts to increase more significantly when the torso angle is greater than the threshold. H_{12} is rejected: the knee angle had no significant influence on HoT, which is in line with the findings in Chapter 5. Regarding ST, greatly reclined drivers need longer to steer, even though the steering task stays the same. This can be caused by the fact that reclined drivers are not entirely upright when they start to steer. Drivers without the support of the seatback also have to hold and pull the steering wheel tightly to keep their upper body upright and stable. These additional actions can cost reclined drivers more time to steer. A similar threshold with regard to ST between 30° and 50° also seems to exist as the torso angle increases from an upright position. As the sum of the HoT and ST, TT shows a similar pattern as in the HoT. There are significant differences between all groups except for 10° and 30°. The torso-angle threshold between 30° and 50° is more apparent here, where the TT starts to increase.

However, a shorter HoT does not always mean that the driver is able to take over control more quickly. The drivers might have their hands on the steering wheel, but still have unstable sitting positions which do not allow to operate the vehicle dynamic control appropriately. This might result from overreaction to the RtI, discussed at the end of the next Section 6.4.3.

From the curves of ST, HoMT, and HoT in Figure 6-26, it could be found that along with the increasing torso angle, the motion time (HoMT plus ST) and the reaction time (HoT minus HoMT) increase. These two kinds of increments result in the curve of HoT and TT. TT equals HoT plus ST, where the triple increasing effects (reaction time, HOMT, and ST) are also summed up together. The total increment of TT from the 10° to 70° torso angle is $\Delta \approx 0.36$ s which can be interpreted in three parts: increment of the HoMT ($\Delta \approx 0.1$ s); increment of the ST ($\Delta \approx 0.1$ s), and increment of the reaction time ($\Delta \approx 0.1$ s). The increment of the reaction time is larger between the 50° and 70° torso angles than any other intervals.

To sum up, large torso angles result in longer take-over time, even though participants tried to compensate by accelerating more, and even though it is primarily motion time. This finding also corresponds to the results of Lundström et al. (2006, 2008), which show that a reclined posture impairs the ability of stimulation detection (the RtI in this case) compared to an upright posture. The torso-angle threshold between 30° and 50° concerning time metrics exists in this experimental setting. A similar torso-angle threshold could be also found in the subjective perception of physical demand (Section 6.3.5). Longer take-over time and a lower torso-angle threshold should be

expected in the real-life scenario, where the situation is unexpected, dynamic, and complex. Furthermore, issues like fatigue must also be seriously considered with regard to reaction time and movement capability.

6.4.3 Breastbone Motion and Overreaction

In the 10° and 30° torso angle conditions, drivers could steer and brake without a large movement of their torsos. In the 50° and 70° torso angle conditions, the participant has to lean forward to reach the steering wheel. This motion consists of two kinds of movement; the first is the flexion of the spine; the second is the flexion of the entire torso rotating around the hip joint. Besides, the hand and foot movements also lead to variances and instability of the trajectories of the breatbone when the upper body lacks the support of the seatback.

The torso angle geometrically influences the length of the arciform trajectory of the breastbone and vice versa. Therefore the larger the torso angle is, the bigger are the x- and z-displacements. The large SD in each group indicates the inter- and intra-individual sitting position when conducting the take-over task. Different knee angles geometrically affect the distance between the breastbone and the steering wheel in the x-direction, therefore resulting in large SDs in the torso-grouped results. The larger the knee angle, the further the breastbone is away from the steering wheel (smaller x-value). Results in Appendix E show the hand has a larger displacement in the x-direction when the knee angle increases from 105° to 130°, and the torso gets more unstable in the y-direction as the knee angle increases.

The movement in the y-direction represents the flexibility of the hip joint and the instability of the upper body. This lateral displacement of the upper body in the take-over process can lead to an unintended crash between the upper body and the door panel or the central tunnel, which may deteriorate the take-over performance. Furthermore, the driver's head and chest may miss the centralized optimal contact point of the airbag, crash into the A-pillar or other hard interior parts in a front crash.

The maximum torso angular speed and acceleration represent the speed and acceleration of the breastbone. They both increase dramatically when the initial torso angle increases. Two reasons can explain this: trajectories are longer in the larger torso-angle conditions so that the torso has more space to accelerate and reach a higher maximum speed. Secondly, the torso is not the primary part of the take-over motion in the range of 10° to 30°, rather a shaking movement caused by the movement of the hand and foot. In contrast, in the 50° and 70° conditions, drivers seem to put in more effort leaning forward, compensating for sitting or "lying" away from the steering wheel.

However, extra effort to accelerate could result in negative overcompensating cases. Figure K-1, Figure K-2, and Figure K-3 in Appendix K show some examples of three kinds of hectic overreaction: first, missing to grasp the steering wheel, which led to a longer hand-on time; second, using the extra push-up movement to lean forward, which led to unstable sitting postures and a longer hand-on time; third, using too much force pulling the steering wheel, which led to a faulty steering operation. This effect also reflects the nervousness of reclined drivers before and during

the take-over process, leading to longer hand-on times and worse operational accuracy, deteriorating take-over performance. Overreaction might increase accident risk when taking over in critical situations (Roche, Thüring, & Trukenbrod, 2020).

The hand-on torso speed and acceleration indicate an unstable upper body in the 50° and 70° torso angle conditions during steering. Reclined drivers have to steer while their upper body moves toward (either accelerating or decelerating) the steering wheel, which might deteriorate the steering and braking quality. Drivers' upper bodies and heads might be too close to the front airbag. The wide distributions here might result from drivers' individual elbow angles. Some steered with almost straight arms, while some leaned very close to the steering wheel. Thus, the hand-on moment could be at any phase of the forward-leaning movement of the breastbone (accelerating and deaccelerating). Therefore, a shorter hand-on time of reclined drivers should not always indicate a proper driving posture or a quick take-over time. It can be simply because of the large elbow angle while the driver is still reclined or leaning forward, unable to take-over control yet. The risk of misoperation due to an unstable upper body should draw attention.

6.4.4 H-Point and the Unstable Posture

Theoretically, as the rotate point of a sit-up movement, the H-point does not have to move during the take-over process. The actual H-point movement reflects the instability of the posture through the take-over motion and the flexibility of the human hip joint.

The torso angle does not geometrically influence the position of the H-point. The knee angle geometrically influences the position of the H-point and vice versa, due to the "toe-fixed" method. The larger the knee angle, the further the H-point is away from the steering wheel (smaller x-value).

Results show that the H-point has larger x- and y-displacements when the torso angle increases. Especially when the torso angle is greater than 30°, the H-point starts to shift more during the take-over process, indicating unstable sitting positions. The critical torso-angle threshold between 30° and 50° concerning x-displacements is also partially determined by the x-position of the H-point, which is determined by the knee angle and the "toe-fix" method in this experiment. The threshold might thus be different in other settings. The H-point also has larger x-, y-, and z-displacements when the knee angle increases from 105° to 130° (Appendix E). H-point moving in the x-direction indicates that the driver is shifting his or her sitting position for- and backward, reaching out for the steering wheel and pedals. This displacement could deteriorate the steering or braking quality since the seat surfaces might not sufficiently support the shifted body. A tightened safety belt would prevent the shift of the H-point, but a buckled reclined driver might not be able to sit up and reach the steering wheel at all. The driver might not be able to exercise precise steering and adequate braking power with stretched arms and legs.

H-point shifting in y- and z-directions indicates the instability of the sitting position. The transverse shift has a similar risk as the transverse displacement of the torso, critical in a front crash. In addition, a shifting H-point also changes the orientation of the legs toward the knee airbag.

6.4.5 Knee & Ankle Motion

The "fixed-toe" method limited and controlled the movement of the legs. The knee and ankle motion were not the focus, presented in Appendix C, D, and E.

The averaged z-displacement of the ankle slightly increases when the torso angle increases, which might indicate reclined drivers' overreaction. Reclined drivers stretch their feet unnecessarily higher in the z-direction to press the brake pedal.

The averaged x-displacement of the knee continually increases with the increasing knee angle, indicating that the "toe-fix" condition could not prevent drivers from stretching their leg out, shifting forward to reach the pedal and brake. Drivers should sit closer to the control elements. For this purpose, the "heel-fix", as presentedin Chapter 5, might be a good compromise between having more space and a relaxed knee angle but still keeping the pedals well within reach.

In conclusion, no extra space is needed for reclined drivers' knees and feet during the take-over process. Drivers might stretch their legs a bit higher to brake if they are reclined. The "heel-fix" method could be more suitable as the reference to adjust SLA for a relaxed knee angle.

6.4.6 Subjective Workload

The unweighted NASA TLX workload score increases consistently with statistical significance when the torso angle increases, confirming H_{13}: drivers need make different levels of effort to take over in reclined postures, mainly because of the mental and physical demand, and the effort needed. The scores of all four torso angle conditions are within the interquartile range of the typical workload of driving a car (Grier, 2015). This indicates that the extremely reclined posture alone generates no more workload to the driver than the typical driving task. However, the combination of a reclined posture and the driving task might overload the driver, which could be partially proved in Chapter 5. The questionnaire was supplied for each torso angle group; an evaluation of the influence of the knee angle on the subjective perception is not possible.

Like the physical demand and the effort, participants rated the take-over with a large torso angle as more mentally demanding, in spite of the fact that the take-over task in this experiment is primarily motoric. Some explained that it was harder to look forward to the PC screen when the seat was extremely reclined. Drivers had to bend their cervical spines to a great extent. For this reason, they needed to be more focused and pay more attention. People typically would normally not remain in a reclined position, knowing that an emergency RtI was coming very soon; therefore, reclined drivers were more nervous and exhausted. This extra cognitive load can also be one reason drivers need longer to react to the RtI and take over with a larger torso angle since the high workload is associated with lower performance in reaction time tests (Arsintescu, Chachad, Gregory, Mulligan, & Flynn-Evans, 2020).

No significant difference was found between the subjective evaluations of the 10° and 30° torso angle. Like the time metrics results in Section 6.3.4, a threshold between 30° and 50° might also exist in the subjective evaluation, especially in terms of physical demand. Further research with

refined torso angles within the critical range 30° and 50° is needed to find the exact threshold, making a take-over objectively and subjectively critical.

6.5 Summary

This chapter presents a motion tracking experiment and reproduces the impact of an increasing torso angle on the take-over performance from a primarily motoric perspective. Trajectory, velocity, and acceleration of drivers' body segments were collected and modeled, quantifying the geometrical, temporal, and subjective consequences of reclined postures in the take-over process. Five main messages can be summized. First, drivers with larger torso angles need more space and time to take-over. Second, reclined drivers have to operate the vehicle dynamic control with a forward-leaning upper body. Third, passive safety risk increases when the torso and the H-point are less stable in the lateral direction. Fourth, the risk of overcompensation increases when reclined drivers overact to lean forward. Fifth, reclined postures might be relaxing during the automated driving cruise within the system limit. However, knowing a RtI is coming very soon, reclined drivers feel more mentally stressed.

In this experimental setting, a primarily motoric take-over process, the empirical evidence of take-over time, sitting stability, and subjective perception suggests a critical torso-angle threshold between 30° and 50°. A torso angle smaller than the threshold, e.g., 30°, is objectively a low risk and subjectively acceptable. A torso angle greater than the threshold, e.g., 50°, is objectively risky in take-over scenarios and mentally demanding, which is undoubtedly not recommended in Level 3 automation. This conclusion is solely based on the results and the scope of this experiment. In reality, the exact critical torso angle for Level 3 automation will probably be between 30° and 50° or even smaller than 30°. The threshold needs to be further researched and validated by extended take-over scenarios, all-round safety concepts of various vehicle types, and driver samples.

The motion data of the wrist, the breastbone, the H-point, the knee, and the ankle supplement the digital human modeling for AVs in take-over scenarios. Given sitting position and body size, the data can be used as empirical evidence to predict the take-over trajectories and motion time.

6.6 Limitation

Unstable markers attached to the surface of the cloth might pollute the motion data. Some high-frequency components could be filtered out. The remaining low-frequency data could still contain invalid values. Thus, the statistics of the data should draw more attention rather than single outlier cases. In a future motion-tracking study, markers should be attached to a particular suit or directly on the participants' skin. For practical reasons, this extra effort of the marker placement might lead to reducing the number of participants, given limited resources.

This strictly controlled experimental setting, e.g., the artificial take-over task, did not reflect reality. It was mainly a motoric take-over process, whereas other factors (e.g., cognitive state, situation) might play a dominant role in reality. Participants were instructed to perform the take-over as quickly as possible to ensure comparability. However, trajectories might be different depending on the urgency of the situation in reality. Other NDRTs, or other objects that are held by hand, e.g.,

a smartphone or a coffee cup, will result in different hand motions. The toe position was fixed right in front of the pedals when the RtI occurs. In reality, longer trajectories of the foot are expected due to individual foot positions during the automation. The steering wheel was fixed and could not be adjusted individually in this experiment, influencing participants' naturalistic behavior. A big Hawthorne effect (Merrett, 2006) is expected in this very "laboratory-like" setting: 21 sensors and markers attached to the driver's body; eight cameras were placed around them, which might constrain the participants' naturalistic movement. The critical torso-angle threshold between 30° and 50° needs to be further investigated, considering other influential factors of take-over performance, passive safety, and subjective acceptance in different vehicle types

7 Development and Implementation: Countermeasure

It takes the active seat assist 2.84 seconds on average to adjust the seatback from reclined 40° to upright 25°, which is comparable to the human reaction time and cognitive processing time before conducting the take-over action.

This chapter describes the fourth experiment of this thesis, developing and implementing the active seat assist to help reclined and backward-shifted drivers resume their sitting positions in the take-over process.

Two major points derived from the previous chapters were the guideline for the development of the active seat assist:

- Reclined and backward-shifted drivers want and need to be assisted in case of a RtI;
- The interior adjustment speed should be quick enough to be effective in the take-over scenario. Meanwhile, it should be gentle enough not to shock drivers.

As one pre-publication of this dissertation, Yang, Fleischer, et al. (2019) proposed four interior adjustment concepts (Figure 7-1) for reclined drivers to transit to a driving posture during the take-over process. First, the "do nothing" variant describes the interior of current conventional vehicles. The drivers have to sit upright by themselves without any assistance (the same condition as in the experiment of Chapter 5 and Chapter 6). Second, the "push me back" concept describes a seat that could adjust automatically and "push" the driver to sit upright and approach the operating elements. Third, the "come to me" concept, in which the seat stays static while the operating elements automatically move toward the driver. Fourth, the "both sides" concept is a combination of the "push me back" and "come to me" concept, where the driver seat and the operating elements adjust toward the driver simultaneously.

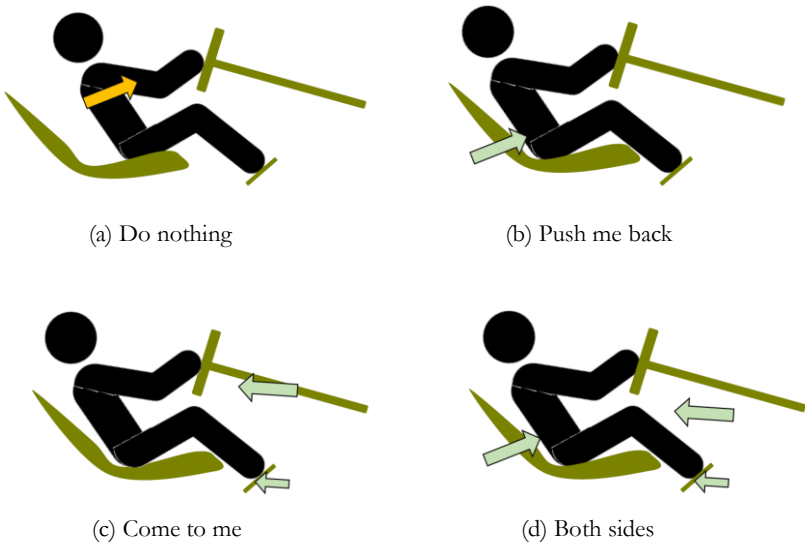

(a) Do nothing (b) Push me back

(c) Come to me (d) Both sides

Figure 7-1 Different interaction concepts during the transition between "Relaxing" and "Driving" (Yang et al., 2020)

The concept b "push me back" was implemented in this experiment, named the "active seat assist." The main goal was to develop signals for the seat adjustments that must assist reclined drivers (e.g., 40° torso angle) to take over the dynamic control of a Level 3 automated vehicle with a better level of effectiveness, efficiency, and satisfaction.

Moving operating elements in concept c and d in Figure 7-1 might lead to an imprecision of the driving operation, and it was also technically impossible to implement in the laboratories. Future research could investigate these two variants.

7.1 System Requirement and Structure

Four requirements of the active seat assist prototype were formed:

1. The active seat assist controls the seat for-/backward (SLA) and the seatback (SBA); other adjustments such as SIA and headrest adjustment are not the focus of this prototype.
2. The active seat assist must be able to save and adjust to at least two individual configurations: the upright setting, and the reclined and backward-shifted setting (effectiveness);
3. The active seat assist must adjust faster than the current series production and thus take less time to resume an upright setting (efficiency);
4. The adjustment movement must be acceptable for the user (satisfaction);
5. All active seat assist functions must be wirelessly controllable by a smartphone for the participants and accessible by the driving simulation software SILAB for the experimenter in further studies.

The seat was developed with Lukas Wolf's assistance as part of his semester thesis (Wolf, 2018). The connection to SILAB was developed with Matthias Gerlicher's assistance as part of his master's thesis (Gerlicher, 2019).

Figure 7-2 The system structure of the active seat assist prototype, modified from Wolf (2018)

Figure 7-2 shows the structure of the active seat assist, which consisted of eight parts. Only the blue area is relevant for the user: the adjustment UI and the seat itself. Other parts enable the power supply and the control of the electric motors, the communication to the UI, and the driving simulator.

1. Seat

   The driver seat of a Mercedes W221 S-class (Figure 3-12, c) was from the Modular Ergonomic Mockup (MEPS), of the Chair of Ergonomics, TUM, donated by Daimler AG in 2015 (Reiffert, 2015). All the original electronic control units (ECUs) and original cables were dismantled. The side airbag and the seat-belt emergency tensioning retractor were legally dismantled, neutralized, and disposed of by certified professionals from Autoverwertung Rottegger GmbH, Garching, Munich area, on June 21, 2018. The original parts of the seat applied in this experiment are the three DC motors, including three integrated Hall sensors. Three DC motors individually power three seat adjustments, Seat Inclination Adjustment (SIA), Seat Longitudinal Adjustment (SLA), and Seatback Adjustment (SBA). The seat adjustment ranges are shown in Table 7-1. SIA was implemented but not applied in further studies; the seat inclination was fixed to 10°. The electric motors were originally powered by the 12V on-board power supply in the vehicle. For the experimental purpose, the voltage was boosted to 16V to increase the adjustment speed without damaging the electric motors. The safety concept of the overvoltage seat was inspected by internal professionals of the mechanical and electrical workshops at the

Chair of Ergonomics, TUM. All the cable systems were redesigned and strengthened, and an emergency switch was built in.

Table 7-1 Ranges of the seat adjustments

	Min.	Max.
Seat longitudinal adjustment (SLA)	0 mm	291 mm
Seat inclination adjustment (SIA)	10°	18°
Seatback adjustment (SBA)	5°	50°

2. Motor driver BTS7960

The controller of the 16V-powered electric motors was powered by 5V. Thus, a motor driver was built in between each electric motor and the controller. The Pulse Width Modulation (PWM) signal was applied to vary the voltage. Table 7-2 shows the specification of the BTS7960 H-bridge motor driver.

Table 7-2 Relevant specifications of the BTS7960 H-bridge motor driver

	Min.	Max.
Control voltage	3.3V	5.3V
Power supply voltage	5.5V	27.5V

3. Emergency switch

This emergency switch was built in between the 16V power supply and the motor drivers. Once the red button was pressed, the power supply of the seat was cut off while the 5V power supply of the controller remained unaffected.

4. Electric power supply

This DC electric power supply could offer a maximum of 16V voltage and 40A current (Table 7-3).

Table 7-3 Electric power supply relevant specification

	Min.	Max.
Output voltage (DC)	1V	16V
Output current	0A	40A
Output power	0W	640W
Operating voltage (AC: 50/60Hz)	200V	240V

5. ESP8266 microcontroller

The microcontroller had the following functions: calibrating each electric motor for each adjustment; reading signals of hall sensors and processing them into seat adjustment percentage (0–100%); storing different seat adjustment configurations (using EEPROM); controlling motor drivers and sending the PWM signals to electric motors; storing the script of the HTML-based HMI; holding the HTTP and WebSocket servers for the control devices.

6. Router

   The router enabled the communication between the HMI devices (smartphone, tablet, or PC) and the microcontroller wirelessly.

7. HMI for drivers

   Users (e.g., participants of the experiment) could adjust the seat through an HTML browser-based smartphone application.

8. Interface to the driving simulator

   The interface between the active seat assist and the driving simulation SILAB from Würzburger Institut für Verkehrswissenschaften GmbH (WIVW) was implemented via a Data Processing Unit (DPU).

7.2 Implemented System Features

According to the requirements, the following features of the active seat assist are implemented: faster adjustment, programmable moving patterns, storage of different positions and adjustment of to those positions, control by means of a smartphone and the driving simulator.

7.2.1 Adjustment Speed

The adjustment speed is compared with four other seat adjustment systems in a Mercedes-Benz S-class (model W221), a Panamera 4 E-Hybrid Sport Turismo (model 2018), an Audi A8 (model 2018), and a Tesla Model X (model 2018). A spirit level, an angle ruler, and a lineal ruler were used to measure the range of the seats. The seatback angle is defined as the angle between the vertical and the inner surface of the seatback without pressing into the foam. All values are averaged from three measurements to compensate for the measurement error. There were two measuring conditions: one measurement with a driver of 75 kg on the seat (labeled as "with load") and another one without a driver (labeled as "without load"). The speed of electric motors varied in different adjustment phases due to the changing posture. Therefore, the average adjustment speeds in the whole adjustment ranges of SBA and SLA are reported in Table 7-4.

Table 7-4 Comparison of the adjustment range and speed

	Seatback adjustment (SBA)				Seat longitudinal adjustment (SLA)			
	Min. (°)	Max. (°)	Avg. speed (°/s)		Min. (mm)	Max. (mm)	Avg. speed (mm/s)	
			without load*	with load			without load*	with load
Porsche Panamera	5	46	3.52	2.83	0	224	14.22	13.01
Audi A8	3	55	2.80	2.25	0	242	15.67	14.37
Tesla Model X	4	59	4.31	3.59	0	250	21.20	19.39
Mercedes S-class	5	50	4.33	3.86	0	291	18.28	17.86
Modified seat	5	50	6.57	5.28	0	291	25.29	24.94

* Note: the load was a 75 kg driver seated with full contact to the seat surfaces.

Table 7-4 shows that the active seat assist is the fastest in both adjustments (SBA and SLA) and both conditions (with and without load). The average speed of the SLA with load is M = 24.94 mm/s (SD = 0.34 mm/s) or that without load is M = 25.29 mm/s (SD = 0.20 mm/s). The SBA of active seat assist is also the fastest in both conditions with load (M = 5.28 °/s, SD = 0.15°/s) or without load (M = 6.57°/s, SD = 0.13°/s).

7.2.2 Manual Adjustment

The seat could be manually adjusted utilizing the HTML-based web application stored in the microcontroller. The application could be visited via the IP address by a smartphone, a tablet, or a PC connected to the same router.

Drivers could use the application to adjust SBA and SLA, and save the seat adjustments as the "automated driving mode" and the "manual driving mode." The adjustments are saved in the EEPROM in the microcontroller, which could be rewritten by other drivers. Drivers could then toggle between both saved positions. The application could be visited by multiple devices simultaneously, meaning the experimenter could also control, save, and toggle the driver's seat adjustments.

For the developer and experimenter, the calibration program had to be started before every usage. Different adjustment patterns and signals could be configured, which are discussed in Section 7.2.4.

7.2.3 Automatic Adjustments

Once the "automated driving mode" and "manual driving mode" are saved for both SBA and SLA, the SILAB driving simulation could trigger the toggle function. For example, once the driver activated the automated driving function, the seat could be automatically adjusted to the reclined "automated driving mode"; once the RtI occured, the seat could automatically resume the upright "manual driving mode."

7.2.4 Seat Movement Pattern in Take-Over Scenarios

Two types of signals could be applied in take-over scenarios.

Firstly, the seat adjustment was able to execute an extra signal as a haptic RtI signal by "shaking" the seat before the adjustments started: the "take-over signal." This signal only has the warning function, but does not adjust the seat. Figure 7-3 (a, b, and c) are examples of the "take-over signals," lasting 200 ms after RtI.

Secondly, the "adjustment signal" has the main goal of adjusting the seat to reach the "manual driving mode" (effectiveness) as quickly as possible (efficiency) but not to shock users (acceptance). Figure 7-3 (d, e, and f) are examples of the "adjustment signals," starting after the"take-over signals" and lasting until the target position was reached. The gradual changes of the signal at the beginning and the end of the adjustment (position-based) are designed to offer users a smoother feeling to improve the acceptance.

In the evaluation study, every "take-over signal" (a, b, and c) could be matched to every "adjustment signal" (d, e, and f). The "take-over signal" (a, b, and c) could also be eliminated. The signals applied to the SBA and SLA are always the same.

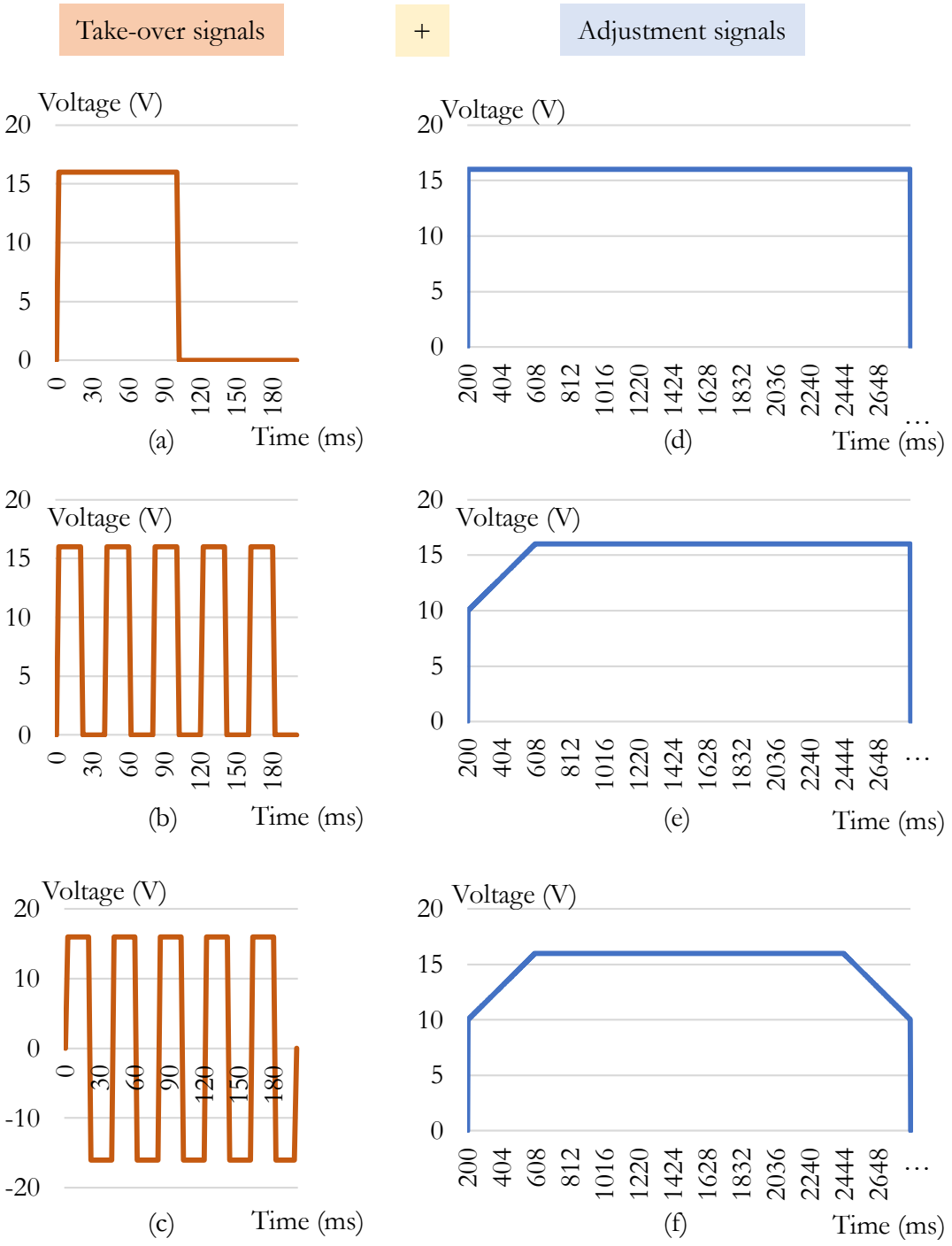

Figure 7-3 Take-over signals and adjustment signals of SBA and SLA, modified from Wolf (2018)

7.3 Expert Evaluation

The expert evaluation focuses on two issues: the general acceptance of the automatic adjustment and choices of the combination of the control signals for the simulator experiment.

Figure 7-4 shows a simple mock-up: a steering wheel, a gearbox, and three pedals fixed in front of the driver seat. The steering wheel, the gearbox, and the pedals had no additional function other than providing orientation for the seat adjustment. The seat was mounted at a typical seating height of an SUV (H30 around 300 mm). Two extended seat trails balanced the weight, preventing the driver from falling over when the seatback reclined extremely. The manual seat adjustment was enabled via the smartphone, mounted on the right-hand side of the seat.

Figure 7-4 A simple mock-up for the expert's evaluation

7.3.1 Method

The Thinking Aloud method (Nielsen, 1994) was applied throughout the expert evaluation. Spontaneous discussions were conducted, and feedback was given during the experiment.

After the seat was calibrated, the background of the project and the possible SAE Level 3 take-over scenarios were explained to the experts. All features of the active seat assist were introduced, except for the control signal combinations. After the demographic questionnaire was filled in, experts could try and get used to the system and the movement of seat elements, especially toggling between the "automated driving mode" and the "manual driving mode."

Experts were then asked to adjust the seat to an upright position: a conventional driving posture and save it as the "manual driving mode"; similarly, a reclined and relaxed sitting position as the "automated driving mode." Both positions were individually different.

Experts were given six auditory RtIs when they were in the reclined "automated driving mode." Each time, they performed an artificial take-over action by putting their hands back onto the

steering wheel, steering at least 90° to the left, and pressing the brake pedal hard, as if they had to avoid a frontal crash in an emergency.

The first three RtIs were triggered only by a beep tone, then three "adjustment signals" (Figure 7-3, d, e, or f) were applied respectively to resume the upright position. The remaining three RtI signals combined a beep tone with three "take-over signals" (Figure 7-3, a, b, or c), respectively. After 200ms, the first "adjustment signal" (Figure 7-3, d) was applied to resume the upright position.

The acceptance questionnaires according to the acceptance scale (Van Der Laan, Heino, & De Waard, 1997) regarding the "take-over signals" and the "adjustment signals" were filled out. This evaluation was not specific to one signal shown in Figure 7-3. Instead, it was about the general concept of "take-over signals" and "adjustment signals." In the end, the signal patterns in Figure 7-3 were shown to the experts, and they repeatedly tried different combinations for the discussion and feedback session.

7.3.2 Experts Sample

Four participants (n = 4) were research associates at the Chair of Ergonomics, TUM, experts in anthropometrics, automation, and robotics. They were aged between 25 and 30 years (M = 28 years, SD = 2.12 years). Their body height was between 174 and 189 cm (M = 182 cm, SD = 6.2 cm), and weight was between 65 and 100 kg (M = 80.8 kg, SD = 13.2 kg). They drove between 5,000 and 20,000 km every year (M = 10,000 km/year, SD = 6,124 km/year).

7.3.3 Results

Figure 7-5 shows that the acceptance level (Van Der Laan et al., 1997) of the "take-over signals" of the seat (Figure 7-3, a, b, and c) is rather negative for most items. The general rating was 0.05 for the "usefulness" and -0.63 for the "satisfaction."

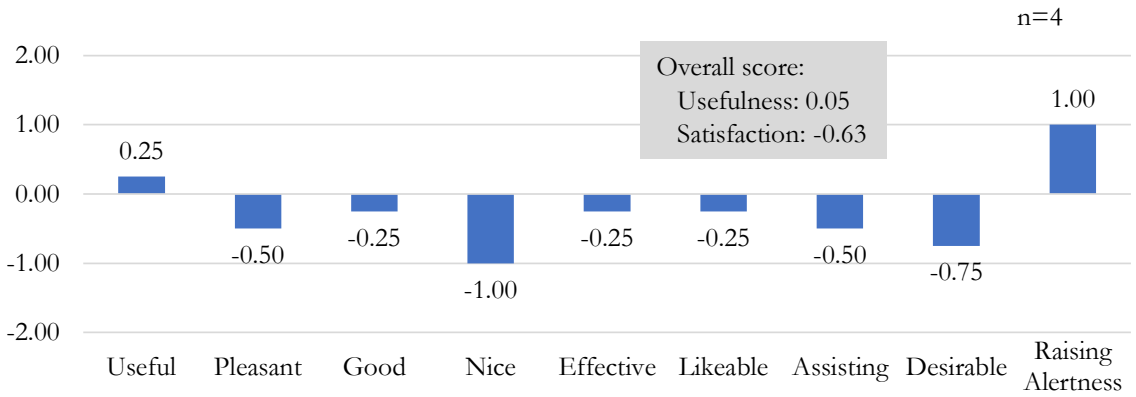

Figure 7-5 Acceptance level of take-over signals (a, b, and c in Figure 7-3)

The acceptance level (Van Der Laan et al., 1997) of the "adjustment signals" (Figure 7-3, d,e, and f) is shown in Figure 7-6. All items were in the positive range. The general rating was 0.85 for the "usefulness" and 1.11 for the "satisfaction." Regarding the 16 V boosted movement speed, the evaluation was positive: even though it is faster, it is still gentle enough so that the movements of the human body were not disturbed.

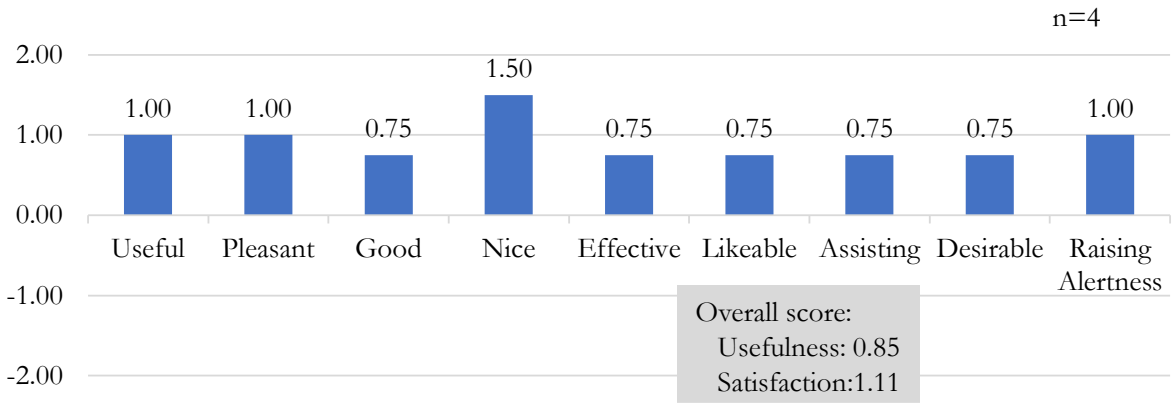

Figure 7-6 Acceptance level of adjustment signals (d, e, and f in Figure 7-3)

The "soft beginning/end" feature shown in Figure 7-3 (e and f) that are intended to ensure a smoother experience was rated neutral or rather negative with an average of -0.25 on a 5-point Likert scale (-2: very useless to +2: very useful). Experts expressed that the "soft beginning/end" concept was well-considered. However, the function in this prototype could not be accepted since the changing voltage of the power supply via the PWM signal caused the electric motors to make a strange noise. Only to a limited extent did the "soft beginning/end" feature make the movement of the seat feel more natural and user-friendly. Nevertheless, the minor change of the adjustment speed was harder to perceive than the dominating noise.

7.4 Discussion

Even though the adjustment speed of the active seat assist (≈ 6°/s) was already boosted and became faster, it was still much slower than the human body movement (Section 6.3.3.1). The active seat assist with the "push me back" concept (Yang et al., 2020) can probably only push the driver at the beginning of a take-over process in reality. When the driver starts to lean forward actively, the active seat assist can only follow the human torso. The effectiveness of this assistance system is questioned at first glance.

Assuming that the driver is taking the reclined sitting position described in Chapter 5 (Yang, Gerlicher, et al., 2018), the torso is ≈ 40°. There is ≈ 15° to adjust the seatback angle to reach an upright driving position (torso angle ≈ 25°). It would take the active seat assist 2.84 seconds (with load) to adjust, which is in the estimated ranges of the human take-over time and even close to the mean value (Gold, 2016). This means that drivers might need the first 2.84 seconds after the RtI anyway to react and cognitively process, within which the active seat assist might have already returned the seat to the driving position. In the study of Gold (2016), drivers were seated upright. Reclined drivers are expected to react even more slowly than upright ones (Lundström et al., 2006, 2008; Yang, Gerlicher, et al., 2018), which might take even longer than 2.84 seconds. It is highly possible that the active seat assist can resume an upright driving position within a period that a reclined driver might need to perceive the RtI, interpret, evaluate the situation, and work out a solution. By the time a driver starts to conduct the first steering, braking, or acceleration action, the active seat assist is already back in an upright setting, supporting the driver's body in a stable upright posture.

On the other hand, applying a higher voltage on the adjustment motors or replacing them with more powerful motors could increase the adjustment speed and further improve efficiency. However, more intensive seat movements might shock drivers, causing panic or crashes between the human body and the interior elements. Further investigation is needed.

Petermeijer (2017) applied haptic tactile vibration motors on the seat surfaces. In comparison, the "take-over signal" and "adjustment signal" in this work are applied to the SBA and SLA electric motors as haptic kinematic interfaces.

The take-over signals (Figure 7-3, a, b, and c) were not well accepted. Evaluations such as "unpleasant", "annoying", and "undesirable" indicate a bad user experience. The reason was that the back-and-forth (or start-and-stop) movement was very intensive, causing annoying mechanical noises. Generally, the quickly changing voltage of the electric motors led to a perception of an unstable, annoying, poorly built and even a broken seat adjustment system. Besides, the additional haptic take-over signals made the system less efficient, costing extra 200 ms. The take-over signal for the electric motors of the seat adjustment was thus discarded for the next experiment in Chapter 8. Nevertheless, other haptic tactile take-over signals, e.g., small and quiet vibrators on the surface of the seat, might be an alternative to combine with the seat adjustment signal. This new combination could be considered in the future, and it does not affect the adjustment efficiency and might further reduce the reaction time (Petermeijer, 2017).

The primary repositioning function, the adjustment signals (Figure 7-3, d, e, and f), are well accepted as rather useful and satisfying (Figure 7-6). The smoothing function in this setting was not accepted and thus also discarded for the next experiment in Chapter 8.

7.5 Summary

The 16 V boosted seat adjustment was faster than the mainstream products in the market. Although slower than the human torso movement, the seatback adjustment should be sufficient in the take-over process, considering the human reaction time and cognitive processing time before conducting the take-over action.

The adjustment pattern "take-over signal" was discarded for further study in the driving simulator due to its low acceptance and inefficiency.

The adjustment pattern "adjustment signal" was generally well accepted and considered useful and satisfying. However, the "soft beginning/end" feature was discarded since it reduces efficiency, and it is annoying and superfluous in an emergency

Concluding, based on the facts and the evaluation above, the control signal for the SBA and the SLA of the active seat assist is defined (Figure 7-7): no extra "take-over signal," no varied speed, the adjustment signal is at "full throttle" of 16 V for the entire time from the RtI until the target position is reached. This simple signal has three advantages:

- The sudden start of electric motors at time point zero could raise enough alertness with a directional (forward) indication.

- The constant power supply (16 V) provides better system predictability and transparency.
- This signal maximizes efficiency, essential in critical scenarios.

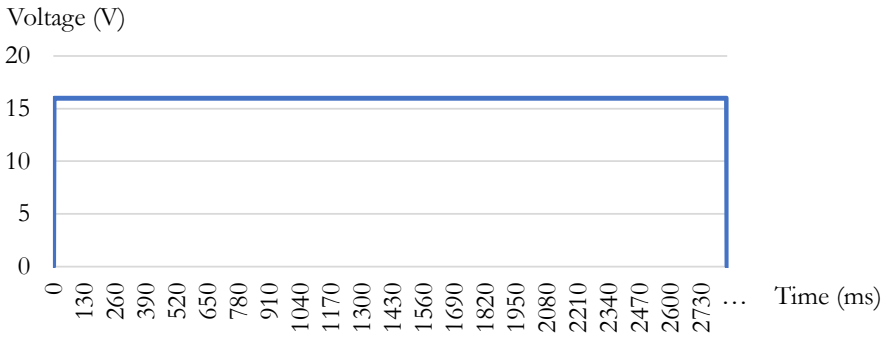

Figure 7-7 The simple, effective, and efficient variant of the seat adjustment signal

7.6 Limitation

The power supply of the seat was moderately boosted from 12 V to 16 V, resulting in a faster but still limited adjustment speed. Applying a higher voltage or replacing the electric motors with more powerful ones could extend the range of the adjustment speed, which should be investigated in the future and optimized with regard to comfort and efficiency. Due to the limited capability of prototyping it was not possible to build an acceptable "soft beginning/end" feature for the seat adjustments. The smoothing concept is worth further developing but calls for a better technical solution other than simply reducing the voltage of the electric motors. This modification of overvoltage was only for the experimental purpose with a low frequency of utilization. The active seat assist was limited to the SBA and the SLA. Other seat adjustments might also be useful as a haptic warning in the early phase of the take-over process. The steering wheel in the evaluation study was fixed and could not be adjusted individually, which might influence the judgment of the driving position.

8 Evaluation: Active Seat Assist

The active seat assist shifts the sequential take-over process so that it tends to be more parallel, and improves the take-over performance of reclined drivers with good acceptance.

This chapter describes the fifth experiment of this thesis, evaluating the active seat assist in the driving simulator in Level 3 automation.

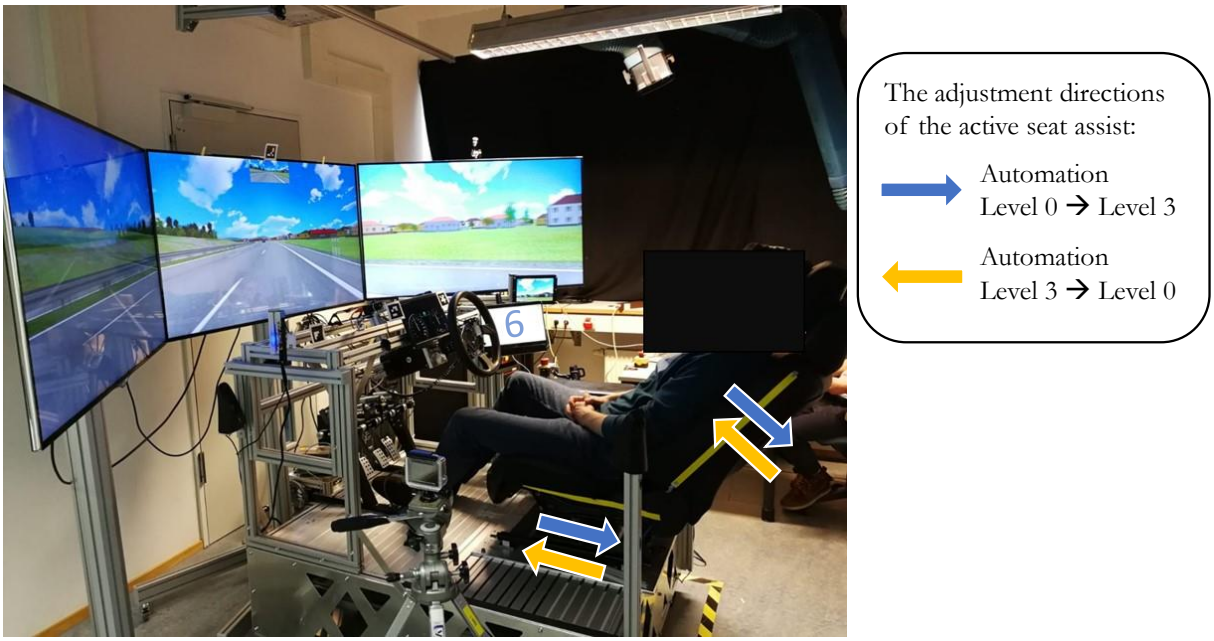

Figure 8-1 The dynamic driving simulator and functions of the active seat assist

The active seat assist prototype was integrated into the dynamic driving simulator of the Chair of Ergonomics, TUM (Figure 8-1). The seat applied was the one modified in Chapter 7 (Figure 3-12, c). There were three ultra-HD monitors, offering 120° of the driver's front field of view. The content of the driving scene in the displays was about 180°, which enabled the driver to see part of the vehicles in the adjacent lanes with less head movement. The interior rear mirror was simulated in the upper part of the middle screen. The left and right exterior side mirrors were simulated by two additional displays mounted on the aluminum frame. An additional display was mounted behind the steering wheel, simulating the instrument cluster display. The dynamic operation elements, i.e., the steering wheel and pedals, were mounted as in conventional vehicles. The clutch pedal had no function since an automatic transmission was simulated. There were no turning indicators and no safety belt in this driving simulator.

Figure 8-1 illustrates the two functions of the active seat assist in this experiment. When Level 3 automation is activated, SBA and SLA bring the driver to a reclined and backward-shifted sitting position; when the automation issues a RtI, SBA and SLA adjust the driver automatically to the previous upright sitting position. The previous Chapters 5 and 6 illustrated the limited influence of the knee angle on take-over performance when the feet position is controlled for SLA. Thus, the

focus in this chapter is on the torso angle and the SBA. Drivers in reclined and backward-shifted sitting positions are briefly reported to as reclined drivers or drivers with reclined posture in this part.

The interface between the active seat assist and the driving simulation SILAB was implemented through a DPU. The simulation software could log the driving data (e.g., steering wheel angle), the track data (e.g., track meter, timestamps), and the vehicle dynamics (e.g., velocity) in a frequency of 120 Hz. The seat adjustment duration could also be logged. An extra display for the NDRT was mounted to the right of the steering wheel to simulate the center information display (CID) (showing the number "6" in Figure 8-1). The side of the seat was marked with two yellow strips to emphasize the seat positions in the video, recorded by a GoPro camera. The experiment was conducted with Matthias Gerlicher's assistance as part of his master's thesis (Gerlicher, 2019). This experimental study was examined and approved by the Ethics Commission of the School of Medicine, TUM.

8.1 Objectives and Hypotheses

The development of the active seat assist was described in Chapter 7. This chapter aims to evaluate the effectiveness, efficiency of, and satisfaction with the active seat assist for distracted, reclined, and backward-shifted drivers in a Level 3 take-over scenario. The following four hypotheses were made:

- $H_{11:}$ The active seat assist affects take-over performance.
- $H_{12:}$ The active seat assist can be positively evaluated in the Van Der Laan acceptance scale.
- $H_{13:}$ Body height, sitting height, weight, and BMI affect the duration of repositioning the seatback.
- $H_{14:}$ Reclined drivers' torsos will not always have full contact with the seatback in the take-over process; the driver will reach the sitting posture more quickly than the seatback.

8.2 Method

A within-subject experimental design was chosen for the following reasons: One of the main goals of the study is to investigate the subjective acceptance of the active seat assist; it is essential to let all participants experience the take-over process both with and without the active seat assist. The relative comparison is as meaningful as the absolute values. Two measurements were taken to control the sequence effect. First, the within factor (with/without the active seat assist) was counterbalanced (Section 8.2.2); second, two take-over trials were conducted in the familiarization phase (Section 8.2.4). The experiment drive was no longer than 30 minutes, avoiding participants from getting too tired.

8.2.1 Sitting Positions

In this experiment, all participants were offered two posture variants, the reclined one for Level 3 automated driving (torso angle = 40°, knee angle = 133°) (Figure 8-2), the upright one for manual

driving (torso angle = 25°, knee angle = 115°). These two postures are based on the literature and the previous Chapter 5 (Bubb, 2015b; Mount et al., 2003; Yang, Gerlicher, et al., 2018). SBA and SLA were applied to realize these two postures (Figure 8-2). The SBA varied between two fixed values (25° or 40°) for all participants, assuming that the seatback angle equals the torso angle. When adjusting the SLA, the "fixed-heel" method was used, the same as in Chapter 5 (Yang, Gerlicher, et al., 2018). Individual SLAs should be applied to reach the same target knee angle (115° or 133°) due to the individual lengths of drivers' lower legs: longer legs needed longer adjustment distances, shorter legs needed shorter distances. The maximum SLA needed for the tallest participant in the study was 10 cm.

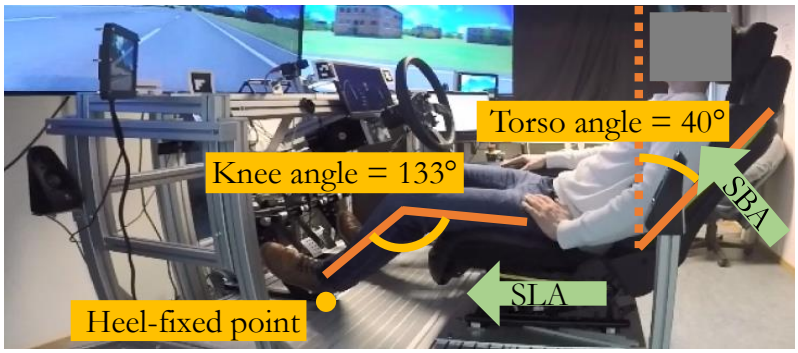

Figure 8-2 The reclined and backward-shifted sitting position; the seat adjustment directions in the take-over process

Adjustments between the upright and reclined settings were configured and stored individually for every participant before the experiment started.

In this experiment, the seat height was positioned at H30 = 30 cm, similar to a typical SUV. The SIA was fixed to 10°, with no adjustment made available.

8.2.2 Independent Variables and Dependent Variables

In this within-subject study, the only IV is the active seat assist with two variants (Table 8-1), on or off. In both conditions, drivers were in the reclined posture during Level 3 automated driving (Figure 8-2). Every reclined participant had to take over twice, once with the assistance and once without the assistance. The sequence was counterbalanced. The active seat assist adjusts the SLA and SBA simultaneously with the RtI, helping the reclined and backward-shifted driver to sit upright (torso angle from 40° to 25°) and closer to the steering wheel and pedals (knee angle from 133° to 115°).

Table 8-1 The independent variable and its variants

IV (within factor)	Variants
Active seat assist	on/off

DVs mainly have three aspects: time, take-over quality, seat adjustment, and subjective evaluation. They are measured by the camera systems (GoPro), the micro controller of the active seat assist,

the simulator environment (SILAB log files), and the questionnaires. Table 8-2 shows 14 DVs with detailed measurement ranges and their data sources.

The results of each DV are presented from Section 8.3.2 to Section 8.3.6.

Table 8-2 The measurement ranges and data source of the 14 dependent variables

Categories	DV	Measurement range	Data source
Reaction time	RT $_{\text{hand-on}}$ [s]: hand-on time	Starting from the RtI until the driver's left or right hand on the steering wheel.	Video
	RT $_{\text{foot-on}}$ [s]: foot-on time	Starting from the RtI until the driver's right foot on one of the pedals.	Video
	TOT [s]: take-over time	Starting from the RtI until the first conscious intervention begins: steering wheel angle > 2° or pedal pressed >10%	SILAB log data (60Hz)
	Time in the right lane [s]	Starting from the RtI until the ego-vehicle center has left the right lane	SILAB log data (60Hz)
Seat adjustment	Seat adjustment duration [s]	Starting from the RtI until SBA and SLA finish adjusting	Mirco controller log data
Take-over quality	Min a_{long} [m/s^2]: minimum longitudinal acceleration	Starting from the RtI until the ego-vehicle passes the broken-down vehicle	SILAB log data (60Hz)
	Max $\lvert a_{\text{lat}} \rvert$ [m/s^2]: maximum absolute lateral acceleration	Starting from the RtI until the ego-vehicle passes the broken-down vehicle	SILAB log data (60Hz)
	TTC [s]: time to collision	Starting from the RtI until the ego-vehicle center has left the right lane	SILAB log data (60Hz)
	SDLP [m]: standard deviation of lateral position	Starting when the ego-vehicle center reaches the middle lane and lasting for 4 seconds	SILAB log data (60Hz)
Subjective evaluation	Ease level	The take-over process with/without the active seat assist	Questionnaire
	Comfort level	The take-over process with/without the active seat assist	Questionnaire
	Acceptance: seat movement	Distance, speed, and acceleration of the adjustments	Questionnaire
	Acceptance: general	The active seat assist during the take-over process	Questionnaire
	Acceptance: sitting position	Two assigned sitting positions: torso angle = 25° vs. 40°, knee angle = 115° vs. 133°	Questionnaire

8.2.3 NDRT: 1-Back Task

The visual-oral 1-back task (Cools, 2010) was conducted to control participants' cognitive load at the moment of the RtI. The participant had to look at the 13-inch tablet to see a series of numbers in a large size (Calibri size: 422) shown one at a time. Each number was shown for 2 seconds. Participants had to orally repeat the previous number, only after the new number appeared. The display position simulated the CID in modern vehicles (Figure 8-1), which might generate visual distraction when the RtI occurs. By applying this visual-oral variant of the 1-back task, the participant's motoric state (posture and motion) stayed unaffected. One 1-back task session took 90 seconds, followed by pauses to reduce participants' cognitive load. It was ensured that the RtI only happened when the 1-back task was just being conducted to control participants' cognitive states. This would introduce an additional risk that participants might learn that once the 1-back task started, they should be prepared for the RtI. To minimize this association between the 1-back task and the RtI, two sessions of the 1-back task before the first RtI and three sessions before the second RtI were arranged which were not followed by a RtI.

8.2.4 Instruction and Familiarization

The goal was not to measure the first exposure of the active seat assist, but rather the effect after the driver became familiar with and was aware of the functions.

At the beginning of the experiment, the definitions of Level 3 automation, the RtI, the active seat assist, and the experimental procedure were explained to the participants. Relevant HMIs were presented: a blue steering wheel icon in the middle of the instrument cluster (Figure 8-3, a) represents the availability of the automation. The driver can then activate Level 3 automation by pressing a green button on the steering wheel. When the automation is activated, the steering wheel icon turns green and stays green as long as the automation works normally (Figure 8-3, b). The green blinker symbol in Figure 8-3 (b) is irrelevant for the automation status.

(a) Automation available (b) Automation activated

Figure 8-3 The HMI of the Level 3 automation system

The availability of the active seat assist was also displayed to the participants. The green seat icon (Figure 8-4, a) symbolizes an available system, while the grey seat icon (Figure 8-4, b) represents an unavailable system. Thus, participants knew exactly whether the seat would assist them in case of a take-over before the RtI occurs. In addition to the icons, a voice message was played when the participant activated the Level 3 automation: "the automation is now activated; the active seat assist is now activated (or deactivated).". The activated/deactivated status of the active seat assist only

affects the resumption function in the take-over process. In both cases, the seat adjusts to the reclined position once the automation is activated.

(a) Automation activated
Active seat assist activated

(b) Automation activated
Active seat assist deactivated

Figure 8-4 HMI of the automation system and the active seat assist

Instructions were also provided on the multimodal RtI signal (Figure 8-5): the steering wheel icon turned red with a hands-on symbol (visual) and a sharp double beep tone (auditory). In one experimental condition, the seat started to reposition itself (haptic kenimatic) simultaneously with the RtI.

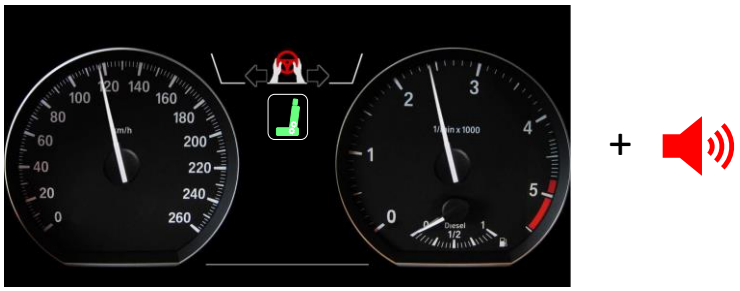

Figure 8-5 The multimodal RtI signal

The learning curve (regarding take-over time) became much flatter after the second take-over in the experiment of Chapter 5, and participants no longer experienced a shock effect with the third take-over. Gold (2016) offered empirical data and proved that the learning effect followed a logarithmic trend, indicating the learning curve should be relatively flat after two trials. In this experiment, the familiarization drive was an 8-kilometer (approx. 8 minutes) highway drive with two RtIs. The participants experienced the take-over process twice before this experimental drive began. The take-overs they encountered during the experimental drive were their third and fourth take-over. The dummy take-over scenarios of the familiarization drive were different from the experimental drive.

8.2.5 Experimental Drive

After the instruction and familiarization drive, the experimental drive started. It was a 30-minute Level 3 automation on a 53-km highway. There were two RtIs, one with the active seat assist and one without the active seat assist. In both conditions, drivers were in the reclined posture (Figure 8-2). The sequence of both conditions was counterbalanced.

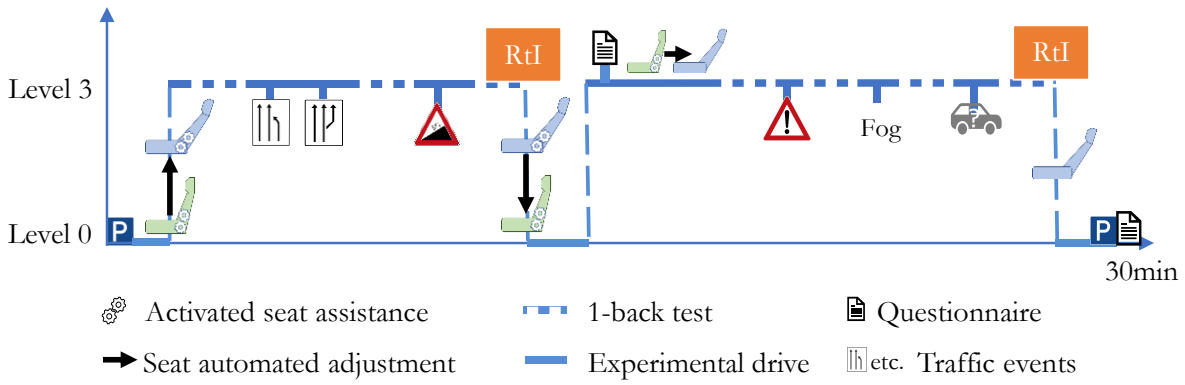

Figure 8-6 Schema of the experimental drive in an exemplary counterbalanced sequence

Figure 8-6 illustrates the experimental procedure. As an example, the first RtI was with the active seat assist, and the second RtI was without the active seat assist.

1. The experimenter helped the participant adjust the seat to fulfill two defined postures with an angle ruler. Two individual seat adjustments (upright and reclined) were stored in the program.
2. The participant started driving manually from a parking area onto a three-lane German highway (Autobahn), sitting upright.
3. The participant noticed that Level 3 automation was available.
4. The participant activated the automation. The seat adjusted automatically to the predefined reclined and backward-shifted position. In Level 3 automation, the participant can be out of the control loop.
5. The participant was asked to conduct two sessions of the 1-back task (with a pause in between). Meanwhile, several traffic events were happening, e.g., road narrowing, widening, and uphill. The automation could automatically drive all those scenarios; the ego-vehicle changed the velocity and/or lanes to be realistic and avoid being too monotonous.
6. The first RtI was triggered during the third session of the 1-back task after about 15 minutes of automated driving. The active seat assist was activated; the seat started to adjust simultaneously with the RtI to the stored upright position.
7. After the participants took over control, they drove manually for a short period until the automation was available again.
8. The participant activated the automation. The seat was not going to recline after the automation activation yet; this delay was only for allowing the participants to fill in the questionnaire in an upright sitting posture. This questionnaire was about the ease and comfort level of the previous take-over.
9. After the questionnaire was completed while the participant was being driven automatedly, the seat reclined and adjusted backward automatically. The participant again remained in

the reclined and backward-shifted position during the automation, as in the first half of the experiment. In this second half of the experiment, the active seat assist was deactivated.

10. There were three sessions of the 1-back task and three other traffic events during the next 15-minute automation.
11. The second RtI was triggered during the fourth session of the 1-back task. The active seat assist was deactivated, so the seat stayed reclined and backward-shifted.
12. After the participant managed to take over the dynamic control and stabilize the vehicle, The vehicle was to be manually driven to the highway exit, heading to the parking area.
13. When the vehicle was parked, the experimental drive was terminated. The participant was asked to fill in the last two questionnaires. This questionnaire was about the ease and comfort level of the previous take-over. Besides, additional questions about the comparison of the two take-overs and the seat adjustment acceptance were asked.

The difference in another counterbalanced sequence is the status of the active seat assist in steps 6 and 11. Participants experienced the deactivated seat first and then the activated seat.

8.2.6 Take-Over Scenario

The take-over scenario was designed to be clear and straightforward. Participants with different experiences and backgrounds should react more or less homogenously to ensure compatibility over all the take-over behaviors. Two take-over scenarios in the experiment drive were built with the same concept as in the study of Yang, Gerlicher, et al. (2018), while the infrastructural surroundings, the track, and the traffic events before the RtI were different in these two scenarios. Participants should not predict or recognize the situation quickly after the RtI. Instead, they had to react to the RtI. The participants knew from the instruction that two RtIs were coming, but it was impossible to predict when and where.

Figure 8-7 illustrates the take-over scenario. A truck ahead blocked the visibility to the broken-down car ahead of the truck; as soon as the truck changed lanes, the broken-down car was visible. At this moment, the RtI was triggered (TTC = 6 seconds, corresponding to a 200 m distance to the obstacle when the ego speed is 120 km/h). To access the driver's performance without interference, the automation functions were shut down entirely as soon as the RtI was triggered (a transition from Leve 3 to Level 0). The car was rolling straight forward. Any dynamic output except the constant deacceleration caused by the rolling resistance must result from the driver's take-over reaction.

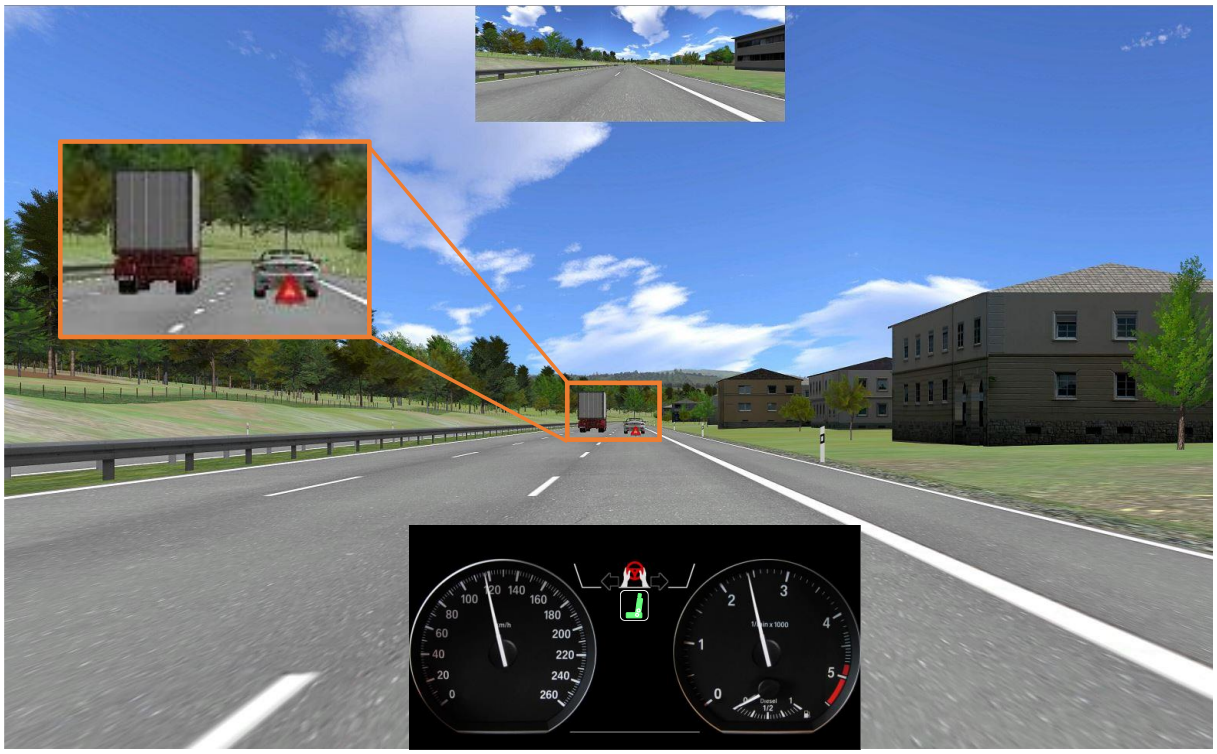

Figure 8-7 The take-over scenario and the HMI, modified from Gerlicher (2019)

8.2.7 Participants Sample

The first demographic questionnaire was handed out before the experiment. It mainly included demographic and anthropometric data, driving experience as well as ADAS experience. Forty-four participants (21 females and 23 males) in this study were distributed across wide ranges of age, body height, and driving experience. They were between 20 and 63 years old (M = 28.82 years, SD = 10.81 years). Their body height ranged between 158 and 194 cm (M = 177.5 cm, SD = 8.4 cm), their sitting height ranged between 82 and 104 cm (M = 92.7 cm, SD = 4.8 cm). Their proportion (the ratio of sitting height to body height) ranged from 0.51 to 0.56 (M = 0.52, SD = 0.01). The self-reported weight ranged from 50 to 104 kg (M = 72 kg, SD = 14 kg). Their BMI ranged from 16.5 to 32.1 (M = 22.7, SD = 3.2). Thirty two percent of the participants drive less than 1,000 km per year, 18% between 1,000 to 5,000 km, 36% between 5,000 to 10,000 km, 14% more than 10,000 km. Only 14% reported that they exercise little during the course of a month; 34% exercise several times a month, 45% several times a week, and 7% exercise every day. 41% of participants had never taken part in a driving simulator study, 41% had a one-time experience, and 18% two or more times. 80% knew little or nothing about automated driving, 68% never or only seldomly use the powered seat adjustment, and 86% have little practical experience with AV. To sum up, the participant collection is anthropometrically widely distributed, well gender-balanced, rather young, sporty, and inexperienced with driving, driving simulators, electric powered seat, and automated driving.

8.3 Results

In this section, the 14 DVs in both conditions (with/without the active seat assist) are compared pairwise to evaluate the effectiveness, efficiency, and acceptance of the active seat assist. The learning effect of this within-subject design study (Section 8.3.1) is evaluated.

For the pairwise comparison, preconditions of relevant statistical tests were checked. The Shapiro-Wilk normality test was conducted for the difference between the paired samples. The Student t-test was conducted for normal distributions, whose effect size is given by Cohen's d (J. Cohen, 1988). Cohen's d indicates a small (d = 0.2), medium (d = 0.5), or large (d = 0.8) effect based on benchmarks suggested by J. Cohen (1988). The Wilcoxon test was conducted for the abnormally distributed samples. The effect size is given by the matched rank biserial correlation (r_B), which is similarly interpreted as Pearson's r. The r_B indicates a small (r = 0.1), medium (r = 0.3), or large effect (r = 0.5) (J. Cohen, 1988).

Boxplots are used to demonstrate the distribution of the data. Outliers in all boxplots are values that are more than 1.5 times the interquartile range away from the bottom or top of the box, labeled with red '+' markers in the boxplots. These outliers are included in the statistics. Excluded outliers are mentioned explicitly for each specific case. Statistical significance is labeled with "*" in the boxplots, following the convention: * for $p < 0.05$, ** for $p < 0.01$, *** for $p < 0.001$.

One video file is lost, thus n = 43 available for video-based analysis of the hand-on and foot-on time (Sections 8.3.4.1 and 8.3.4.2). There are 44 datasets available for other analyses.

8.3.1 Learning Effect

To quantify the remaining learning effect, all the take-over performance measurements in the first take-over are compared with the second take-over, independent of the seat conditions.

In the experiment, 23 participants experienced the active seat assist in the first take-over, 21 participants experienced the active seat assist in the second take-over. Table 8-3 shows the results of the comparison. There is no significantly different take-over performance in the first and the second take-over, indicating that the learning/sequence effect in take-over time and quality was well counterbalanced.

Table 8-3 Take-over performance of the first and second take-over process

DV	Take-over sample	N	M	Mdn	SD	Min	Max	Shapiro-Wilk Test p	T-Test/ Wilcoxon p
$RT_{hands\text{-}on}$ [s]	1st	43	1.47	1.47	0.39	0.67	2.47	0.033	0.947
	2nd	43	1.50	1.41	0.50	0.59	2.77		
$RT_{Foot\text{-}on}$ [s]	1st	43	1.83	1.69	0.67	0.56	3.71	0.704	0.378
	2nd	43	1.73	1.73	0.56	0.77	3.11		
TOT [s]	1st	44	2.12	2.07	0.60	1.20	4.36	0.083	0.456
	2nd	44	2.07	2.03	0.58	0.80	3.13		
Min a_{long} [m/s²]	1st	44	-1.37	-0.64	1.88	-7.81	-0.64	< 0.001	0.576
	2nd	44	-1.31	-0.64	1.80	-8.10	-0.63		
Max a_{lat} [m/s²]	1st	44	2.84	2.57	1.49	0.71	6.22	0.558	0.559
	2nd	44	2.68	2.03	1.70	0.93	8.64		
Min TTC [s]	1st	44	2.46	2.43	0.59	0.78	3.86	0.53	0.915
	2nd	44	2.45	2.54	0.72	1.02	4.14		
SDLP [m]	1st	37	0.59	0.58	0.17	0.27	1.14	0.004	0.732
	2nd	37	0.56	0.58	0.12	0.30	0.81		

8.3.2 Seat Adjustment Duration and Speed

The seat adjustment duration was logged in every take-over process (n = 44), from the RtI until the SBA and SLA finished adjusting (Figure 8-2).

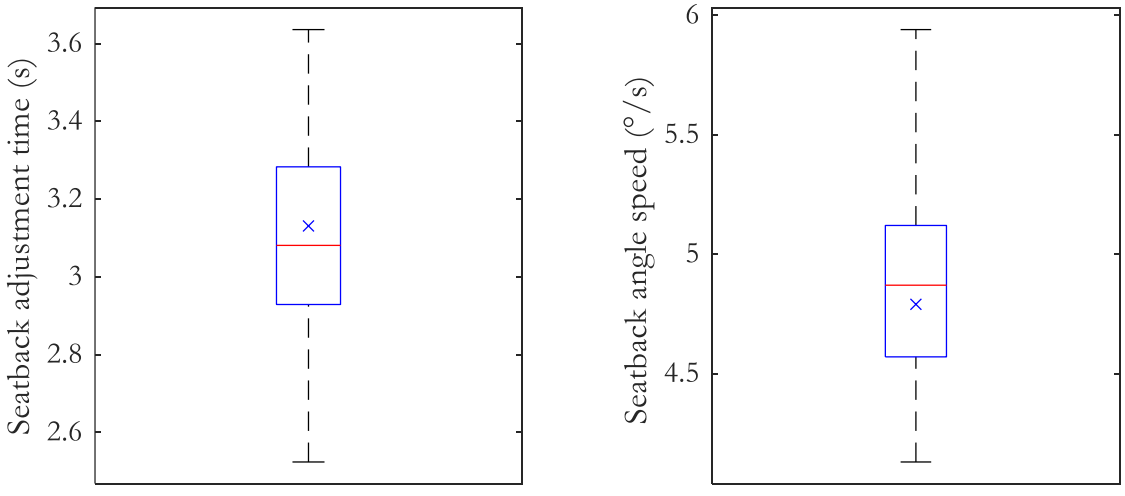

(a) Seatback adjustment time (b) Seatback angular speed

Figure 8-8 Seatback resumption time and its average angular speed from 40° to 25°

The SLA adjusted forward for individually different distances to reach the targeted 115° knee angle. The SBA adjusted upward from 40° to 25°. The SBA took longer than the SLA in all take-overs

of this experiment. Therefore, the logged seat adjustment duration also represents the SBA adjustment duration.

Figure 8-8 (a) shows the duration distribution that the seatback (SBA) needed to return from 40° to 25°. The average duration was M = 3.10 s, SD = 0.27 s. The shortest was 2.52 seconds, and the longest was 3.64 seconds. Figure 8-8 (b) illustrates the average seatback angular speed (M = 4.87 °/s, SD = 0.43 °/s). The fastest average angular speed was 4.13 °/s, while the slowest was 3.64 °/s.

Table 8-4 shows that the seatback angular speed correlated significantly to the body height (r = -0.341, p = 0.023) and sitting height (r = -0.307, p = 0.043). The longer the driver's upper body is, the longer the seatback needs to adjust. The proportion is defined as the ratio of the sitting height to the body height.

Table 8-4 Bayesian Pearson Correlations

Pearson Correlations

		Height	Sitting height	Weight	BMI	Proportion
Seatback angular speed	Pearson's r	-0.341*	-0.307*	-0.256	-0.090	0.007
	p-value	0.023	0.043	0.094	0.561	0.963

* p < 0.05, ** p < 0.01, *** p < 0.001

The video analysis shows that 29 participants out of 44 (65.91%) actively leaned forward to take over after the RtI occured. There are significantly (Chi-Square = 4.455, p = 0.035) fewer reclined drivers (34.09%) staying in full contact with the seatback and being pushed upward and forward in the take-over process. The driver's torso angular speed (Section 6.3.3.1) can be much higher than the SBA angular speed if the driver actively leans forward, which results in a gap between the torso and the seatback. This gap is gradually reduced as the seatback catches up with the torso. After an average of 3.10 seconds (the average SBA duration), the torso has full contact with the seatback again.

8.3.3 Time in the Right Lane

The simple take-over scenario (Section 8.2.6) results in a homogeneous take-over strategy. All participants chose to change to the middle lane, and no one crashed into the broken-down vehicle in the right lane. Table 8-5 shows that drivers without assistance on average spent slightly more time (3.97 seconds) in the right lane (n = 44) after the RtI than drivers with assistance (3.89 seconds) before changing to the middle lane.

Table 8-5 Time in the right lane after RtI

	Sample	N	M	Mdn	SD	Min	Max	Shapiro-Wilk Test p	T-Test/ Wilcoxon p
Time in the right lane after RtI	Without assistance	44	3.97	3.99	0.66	2.69	5.36	0.038	0.16
	With assistance	44	3.89	3.75	0.73	2.04	5.96		

8.3.4 Reaction Time

Three time-relevant DVs are defined in Section 8.2.2: hand-on time (Section 8.3.4.1), foot-on time (Section 8.3.4.2), and take-over time (Section 8.3.4.3). Table 8-6 summarizes their descriptive statistics and statistical tests. Statistically significant results are found in hand-on time and foot-on time.

Table 8-6 Descriptive statistics and statistical tests of the take-over time

DV	Sample	N	M	Mdn	SD	Min	Max	Shapiro-Wilk Test p	T-Test/ Wilcoxon p	Effect size
$RT_{hand\text{-}on}$ [s]	Without assistance	43	1.53	1.47	0.41	0.73	2.77	0.035	0.039 *	r_B = 0.363
	With assistance	43	1.43	1.38	0.48	0.59	2.64			
$RT_{Foot\text{-}on}$ [s]	Without assistance	43	1.89	1.92	0.62	0.77	3.71	0.660	0.039 *	d = 0.324
	With assistance	43	1.67	1.68	0.60	0.56	3.11			
TOT [s]	Without assistance	44	2.12	2.11	0.51	1.2	3.13	0.006	0.115	
	With assistance	44	2.06	2.01	0.66	0.8	4.36			

Note. * $p < 0.05$; for the Student t-test, the effect size is given by Cohen's d ; for the Wilcoxon test, the effect size is given by the matched rank biserial correlation.

8.3.4.1 Hand-on Time

One video record is missing for the hand-on time analysis (n = 43). The differences of the paired samples are not normally distributed (Shapiro-Wilk p = 0.035), a Wilcoxon test was conducted, indicating that the average hand-on time without assistance (M = 1.53 s, Mdn = 1.47 s) was significantly (Z = 301.5, p = 0.039) longer than that with assistance (M = 1.43 s, Mdn = 1.38 s). The effect size r_B was 0.363, indicating a medium effect (J. Cohen, 1988). Figure 8-9 shows the

distribution of the hand-on time with a statistically significant difference. The descriptive statistics can be found in Table 8-6.

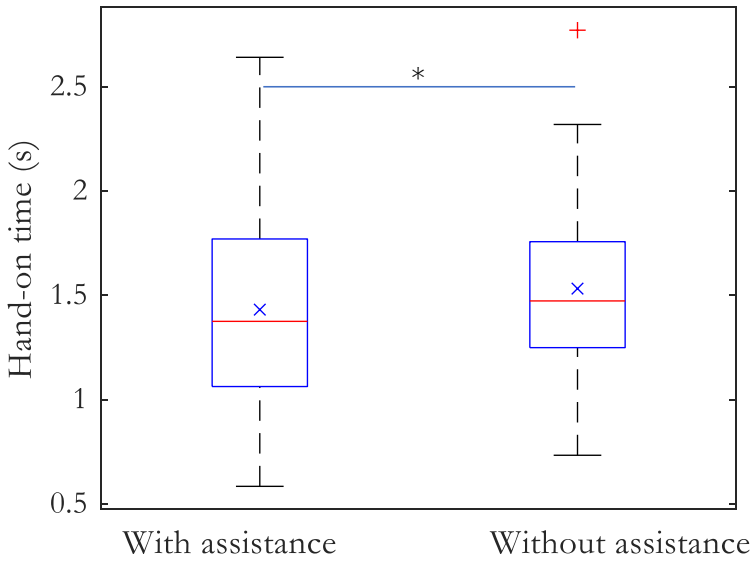

Figure 8-9 Distribution of the hand-on time with/without the active seat assist

Every individual pair of the hand-on time measurements with/without assistance was compared; the active seat assist improved 66% of the participants' hand-on time.

Nevertheless, the hand-on time strongly depends on individual performance. Among those who rank better than the 22nd place (50 percentile) with assistance, most (62%, 13 participants) still rank in the first half without assistance. Meaning, more than half of the quick participants stay quick in another condition without assist.

8.3.4.2 Foot-on Time

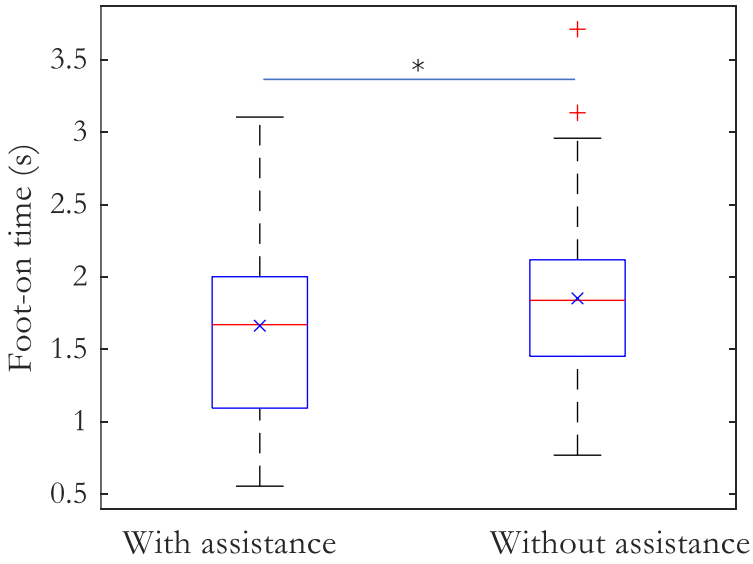

Figure 8-10 Distribution of the foot-on time with/without the active seat assist

One video record is missing for the foot-on time analysis (n = 43). In this case of a normal distribution (Shapiro-Wilk p = 0.660), the paired-samples t-test indicated that the foot-on time without assistance (M = 1.89 s, SD = 0.62 s) was statistically significantly (t(42) = -2.13, p = 0.039) longer than that with assistance (M = 1.67 s, SD = 0.60 s). The effect size d = 0.324 indicates a small to medium effect (J. Cohen, 1988). Figure 8-10 shows the distribution of the foot-on time with a statistically significant difference. The descriptive statistics can be found in Table 8-6.

Every individual pair of the hand-on time measurements with/without assistance is compared; the active seat assist improves 61% of the participants' foot-on time.

Like the hand-on time, the foot-on time also strongly depends on individual performance. Among those who rank better than the 22nd place (50 percentile) with assistance, 62% of them (13 participants) still rank in the first half without assistance. Meaning, more than half of the quick participants stay quick in another condition without assist.

8.3.4.3 Take-over Time

The differences of the paired TOT samples (n = 44) are not normally distributed (Shapiro-Wilk p = 0.006). A Wilcoxon Signed-Ranks Test shows there is no significant difference (Z = 630.5, p = 0.115) between the TOT without assistance (Mdn = 2.11 s) and the TOT with assistance (Mdn = 2.01 s). The average TOT with assistance (M = 2.06 s) is lower than that without assistance (M = 2.12 s). Figure 8-11 shows the TOT distribution. The descriptive statistics can be found in Table 8-6.

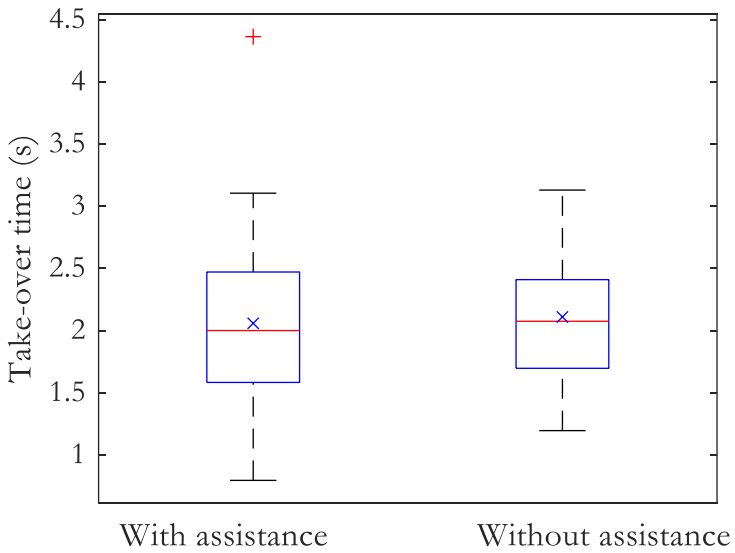

Figure 8-11 Distribution of the take-over time with/without the active seat assist

8.3.5 Take-Over Quality

Results show that all participants took over without an accident. The majority could calmly redirect their attention and resume the upright posture after the RtI was triggered. Their take-over strategies were homogenous: braking (or not) and changing to the middle lane.

Besides the DVs quantifying the take-over quality, a video analysis was conducted to compare the forward-leaning movements with/without assistance in the take-over process. Six participants without assistance pulled the steering wheel first to shift the H-point forward as the first reaction to the RtI (an example in Appendix L Figure L-1), and no one with assistance did that. One participant was startled by the RtI without assistance, and two with assistance were startled. The drivers' active forward-leaning movement was quicker than the seat adjustment, reported in Section 8.3.2.

Four DVs regarding the take-over quality are defined in Section 8.2.2: the minimum longitudinal acceleration (Section 8.3.5.1) for the braking behavior, maximum lateral acceleration (Section 8.3.5.2) for the steering behavior, minimum time to collision (Section 8.3.5.3), and the standard deviation of lateral position (Section 8.3.5.4). Table 8-7 summarizes their descriptive statistics and statistical tests, among which statistically significant results are found in minimum time to collision (Min. TTC).

Table 8-7 Descriptive statistics and significant test of the take-over quality

DV	Sample	N	M	Mdn	SD	Min	Max	Shapiro-Wilk Test p	T-Test/ Wilcoxon p	Effect size
Min a_{long} [m/s^2] (All data)	Without assistance	44	-0.58	0.00	1.66	-6.82	0.00	< 0.001	0.108	
	With assistance	44	-0.82	0.00	1.99	-7.47	0.00			
Min a_{long} [m/s^2] (Non-zero data)	Without assistance	7	-3.66	-3.66	2.59	-6.82	0.00	0.247	0.508	
	With assistance	13	-2.79	-2.79	2.87	-7.47	0.00			
Max a_{lat} [m/s^2]	Without assistance	44	2.82	2.40	1.63	0.71	8.64	0.095	0.641	
	With assistance	44	2.70	2.19	1.57	0.73	6.65			
Min TTC [s]	Without assistance	44	2.35	2.29	0.58	1.02	3.53	0.753	0.043 *	d = 0.315
	With assistance	44	2.56	2.53	0.71	0.78	4.14			
SDLP [m]	Without assistance	37	0.55	0.56	0.13	0.30	0.85	0.010	0.309	
	With assistance	37	0.59	0.60	0.16	0.27	1.14			

Note. * $p < 0.05$; for the Student t-test, effect size is given by Cohen's d

8.3.5.1 Minimum Longitudinal Acceleration

The minimum longitudinal acceleration is the maximum longitudinal deacceleration (braking). The measurement interval starts from the RtI until the ego-vehicle passes the broken-down vehicle. Among the total 88 take-overs (n = 44, each participant twice), there are 68 cases in which participants could master the emergency by only steering without braking. Considering all data, drivers brake slightly harder with the active seat assist (M = -0.82 m/s^2) than without (M = -0.58 m/s^2). Both average values are very low due to many zeros (non-brakers). Participants braked in 20 cases, among which 13 are with assistance, which is almost twice as many as those without assistance. Among those braking cases (non-zero data), assisted ones brake less hard (M = -2.79 m/s^2) than unassisted ones (M = -3.66 m/s^2) (Figure 8-12). The descriptive statistics can be found in Table 8-7. Four out of 13 (31%) with assistance, and 3 out of 7 (43%) without assistance are < -4.41 m/s^2, defined as hard brakes (Simons-Morton et al., 2009).

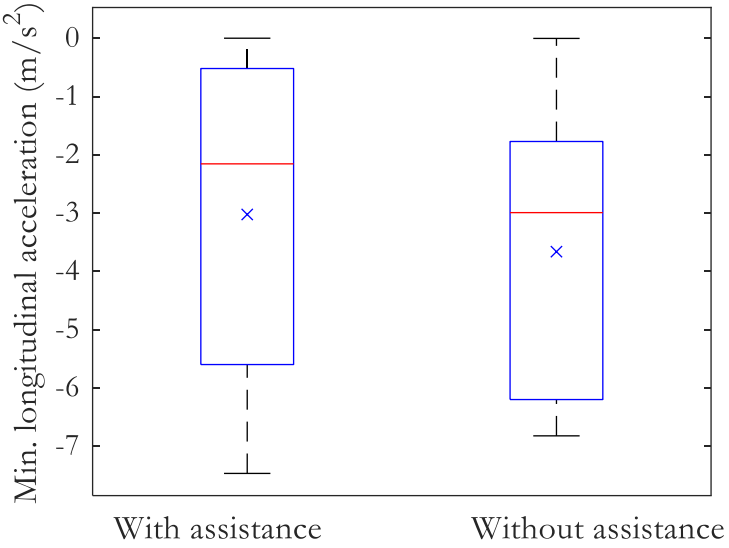

Figure 8-12 Distribution of Min a_{long} with/without the active seat assist (only non-zero data)

8.3.5.2 Maximum Absolute Lateral Acceleration

The maximum absolute lateral acceleration (n = 44) reflects the smoothness of the steering behavior during the take-over process. The measurement starts from the RtI until the ego-vehicle passes the broken-down vehicle. Figure 8-13 shows the distributions of Max $|a_{lat}|$ in two conditions. Assisted participants steered slightly more smoothly (M = 2.70 m/s^2) than unassisted ones (M = 2.82 m/s^2) without statistical significance. The descriptive statistics can be found in Table 8-7.

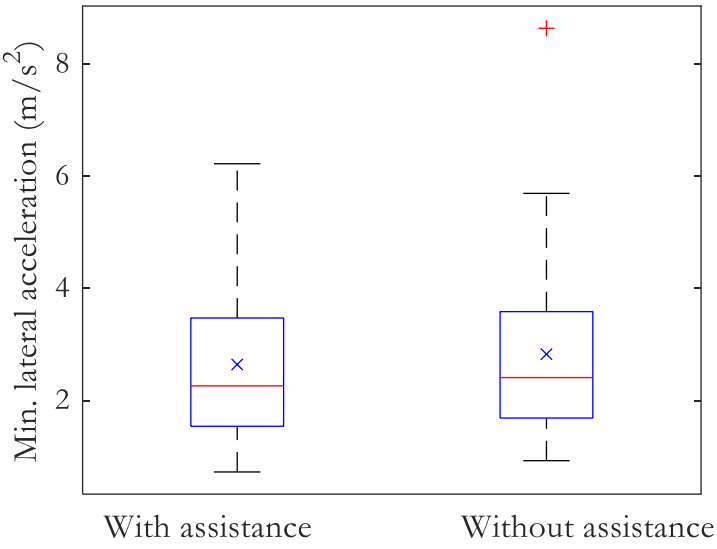

Figure 8-13 Distribution of Max $|a_{lat}|$ with/without the active seat assist

8.3.5.3 Minimum Time to Collision

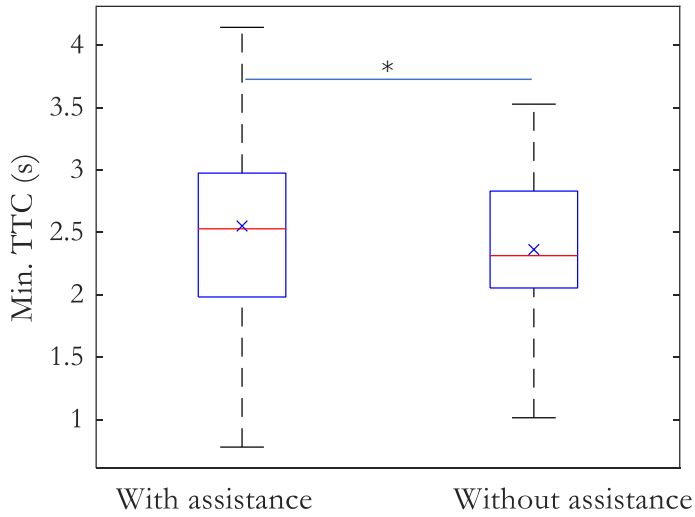

Figure 8-14 Distribution of min. time to collision with/without the active seat assist

TTC (n = 44) is a safety indicator for rear-end crashes; it is a predicted time that one object needs to crash into the object ahead, assuming constant speeds of both objects during the whole course of the accident. A longer TTC indicates a safer state with a smaller likelihood of a crash than with a short TTC. In this experiment, TTC to the broken-down car ahead is measured from the RtI until the ego-vehicle center has left the right lane. The minimum TTC represents the TTC of the most dangerous moment (regarding rear-end crashes) in the take-over process.

Table 8-7 shows that in this case of normally distributed samples (Shapiro-Wilk p = 0.753), a paired-samples t-test indicates that the minimum TTC without assistance (M = 2.35 s, SD = 0.58 s) was statistically significantly (t(43) = -2.09, p = 0.043) lower than that with assistance (M = 2.56 s, SD = 0.71 s). The effect size d = 0.315 corresponds to a small to medium effect (J. Cohen, 1988). Figure 8-14 shows the distribution of the minimum TTC of both conditions with a statistically significant difference.

8.3.5.4 Standard Deviation of Lateral Position

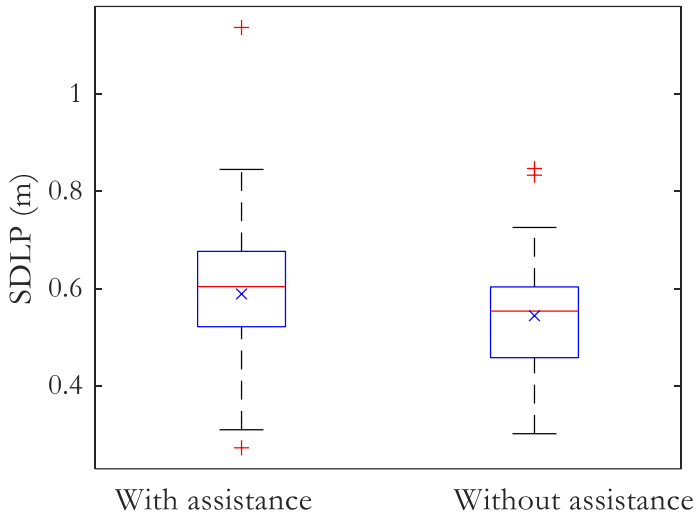

Figure 8-15 Distribution of standard deviation of lateral position with/without the active seat assist

SDLP reflects the lateral stability of the vehicle, which should be measured after the lane change. Even though drivers have a similar take-over strategy of changing to the middle lane, the time that the vehicle stays in the middle lane varies individually. Some drivers in the middle lane drive back to the right lane very soon after overtaking, while others stay in the middle lane longer. The measurement interval of SDLP should have the same length for all cases. The longer the time interval, the more data points each dataset has, but the fewer datasets would be available. Compromising between the length of measurement and the number of available datasets, the measurement interval is defined as four seconds long, starting when the ego-vehicle center has reached the middle lane. Seven participants out of 44 must be excluded (n = 37) when applying this four-second measurement interval. Figure 8-15 shows that assisted participants are slightly less stable (M = 0.59 m) than unassisted ones (M = 0.55 m) without statistical significance. The descriptive statistics can be found in in Table 8-7.

8.3.6 Subjective Evaluation

Five subjective DVs are defined in Section 8.2.2 comparing take-overs with/without the active seat assist. Questionnaires were given to the participants after the first take-over and at the end of the experiment (as described in Section 8.2.5).

Figure 8-16 shows the distribution of the answers to the question "how easy was the take-over?" and the question "how comfortable was the take-over?" after each take-over process (n = 44). Table 8-8 shows the corresponding descriptive statistics.

8.3.6.1 Ease and Comfort Level

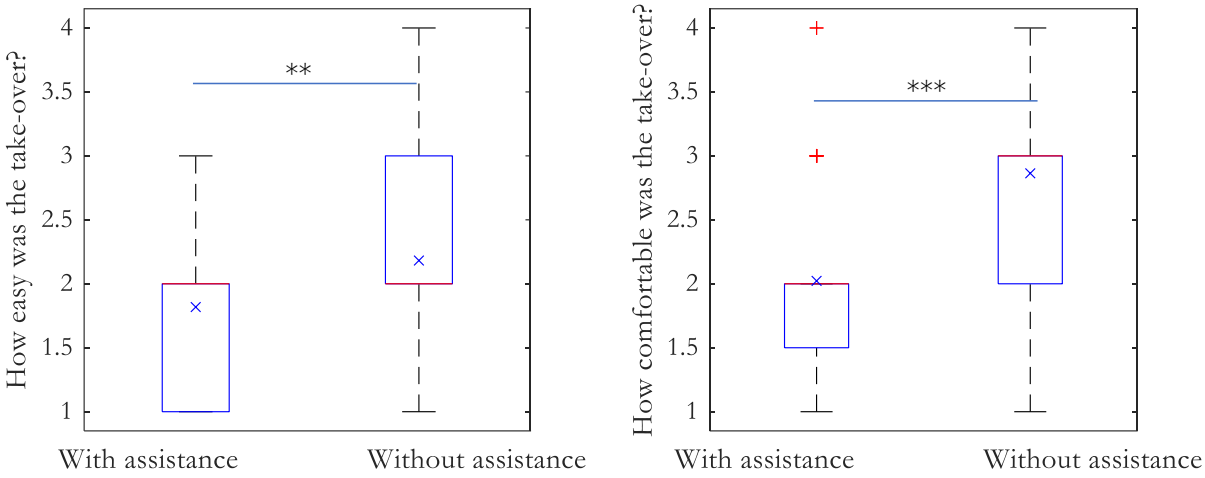

(a) "How easy was the take-over?" (1 = very easy, 2 = rather easy, 3 = rather hard, 4 = very hard)

(b) "How comfortable was the take-over?" (1 = very comfortable, 2 = rather comfortable, 3 = rather uncomfortable, 4 = very uncomfortable)

Figure 8-16 The comparison of the ease and comfort level of take-over with/without the active seat assist

Table 8-8 Descriptive statistics of the results of the ease and comfort level

Descriptive Statistics

		Valid n	Mean	Median	SD	Min.	Max.
Ease level (four-point Likert 1 = very easy)	With assistance	44	1.8	2	0.6	1	3
	Without assistance	44	2.2	2	0.9	1	4
Comfort level (four-point Likert 1 = very comfortable)	With assistance	44	2.0	2	0.8	1	4
	Without assistance	44	2.9	3	0.7	1	4

To compare the coded ordinal categorical data, Wilcoxon tests were conducted (Table 8-9). Participants found take-overs with the active seat assist were significantly easier ($p = 0.006$) and more comfortable ($p < 0.001$) than those without the active seat assist.

Table 8-9 Significant tests of the results of ease and comfort level

Wilcoxon Test for the Ordinal data

			Statistic	p	Effect Size
Ease level with	-	Ease level without	69.00	0.006	-0.575
Comfort level with	-	Comfort level without	10.50	< 0.001	-0.952

The direct comparison of the two take-over processes confirms the results above. Thirty participants (68.18%) reported that it was easier to take over with assistance, which is significantly

more than those who regarded it as less easy (13.64%) or no different (18.18%) (Chi-Squared = 24.182, $p < 0.001$). Thirty-seven participants (84.09%) reported that it was more comfortable to take-over with assistance, which is significantly more than those who regarded it as less comfortable (4.55%) or no different (11.36%) (Chi-Squared = 51.318, $p < 0.001$) (Figure 8-17).

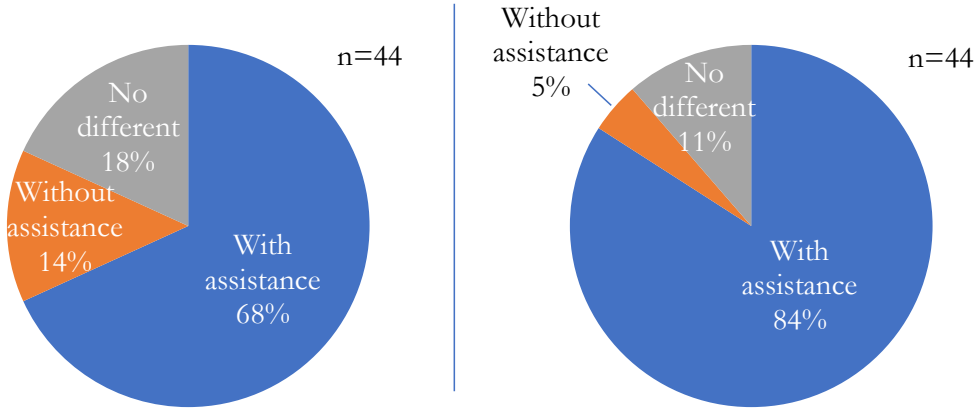

(a) Which take-over was easier? (b) Which take-over was more comfortable?

Figure 8-17 Direct comparisons of two take-overs

The reasons mentioned for choosing the blue parts in Figure 8-17 are summarized as follows: it was easier to reach the steering wheel and pedals; the participant forgot the reclined and backward-shifted status and could not reach the steering wheel and pedals quickly without assistance; it was due to the sequence effect; the seat offered a better driving position for delicate operations; the motion of the seat generated a quicker reaction; the seat gave an additional indication of the situation and directed the attention to the front; the participant could concentrate more on the environment without thinking about the sitting posture; the seat helped the participant to "wake up"; the seat made the participant feel more relaxed in the take-over situation.

Several reasons for choosing the orange parts in Figure 8-17 are mentioned: it was due to the sequence effect; taking-over without a moving seat was more routine-like and predictable; the active seat was distracting, alarming, superfluous for uncritical situations.

8.3.6.2 Movement Range and Speed

Six participants (14%) reported that they did not perceive the movement of the seat in the experiment (Figure 8-18, pie diagram on the left). Without noticing the seat had moved, 3 of 6 (50%) chose the easier take-overs, which turned out to be those with the active seat assist. Five of 6 (83%) chose those take-overs with more comfort, which were those with the active seat assist. This means the active seat assist could also help improving users' comfort even "secretly" without their awareness of its existence. Among the remaining 38 participants who noticed the seat movement, twenty-two participants (57.89%) mentioned that the movement of the seat influenced their steering behavior, and 23 participants (60.53%) mentioned it influenced their braking

behavior. Both numbers are not significantly higher than the numbers of those who thought there was no influence.

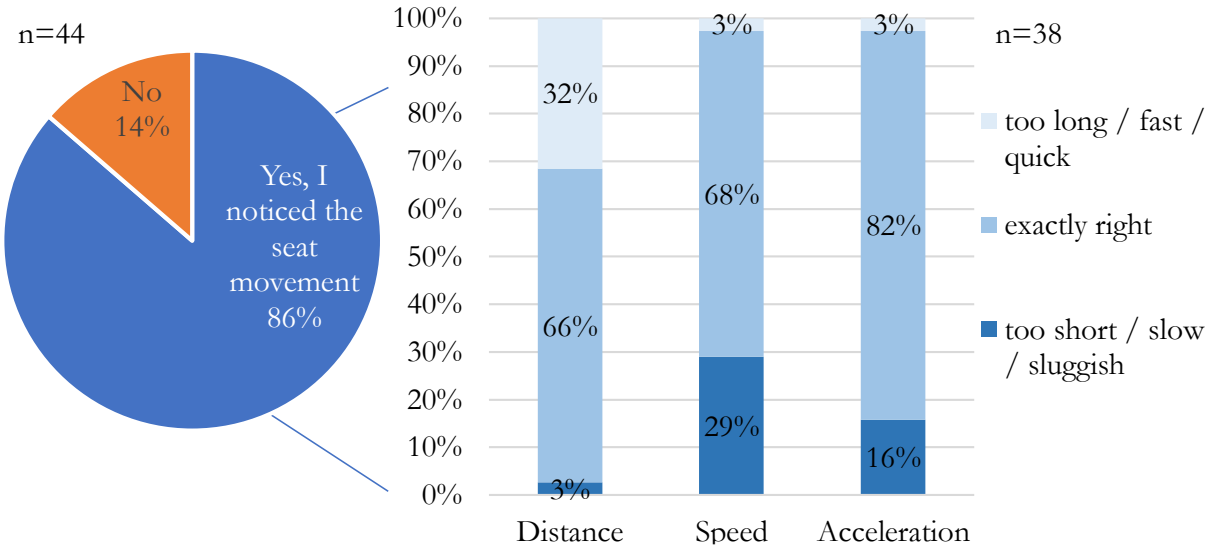

Figure 8-18 Evaluation of the seat movement among those who did notice it

The diagram on the right side in Figure 8-18 shows the evaluation of the seat movement given by the participants who perceived it (n = 38). The majority found the seat moved a proper distance (66%), at a proper speed (68%), and with proper acceleration (82%).

8.3.6.3 Acceptance of the Active Seat Assist

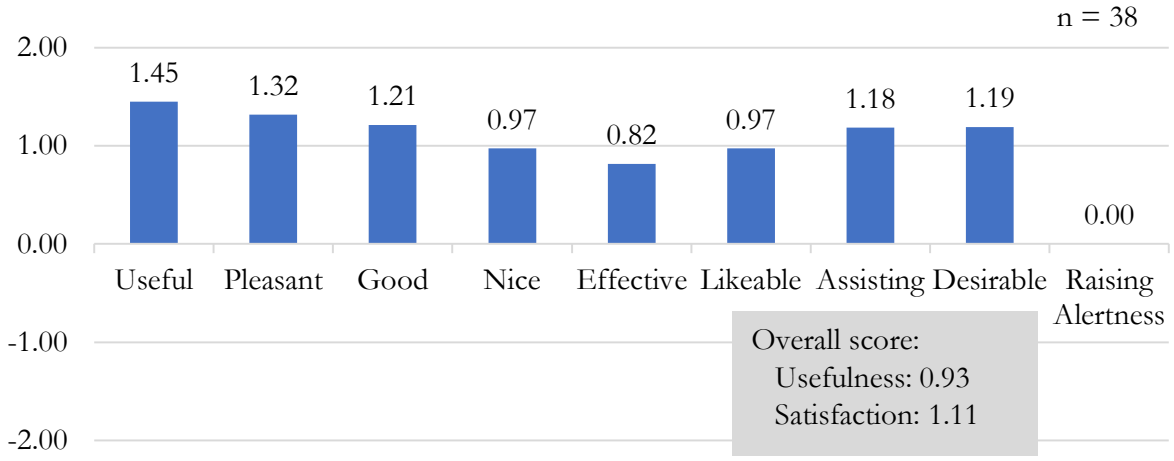

Note: for the item "Desirable", one datapoint is lost, thus n=37.

Figure 8-19 General acceptance of the active seat assist

Participants who noticed the movement of the seat (n = 38) evaluated the acceptance level of the active seat assist according to Van Der Laan et al. (1997). Figure 8-19 shows the averaged acceptance level in nine categories. For every item (e.g., "Useful"), there was a 5-point Likert scale (-2 to 2). The automated seat was generally considered useful, pleasant, good, nice, effective, likable, assisting, and desirable. Results of every item show a positive acceptance level, except "raising

alertness." In general, the "Usefulness score" of 0.93 and a "Satisfaction score" of 1.11 indicate a well-accepted system.

8.3.6.4 Acceptance of Sitting Postures

During the automated drive, 21 participants (47.73%) wished to reduce the seatback angle to sit more upright; 13 participants (29.55%) also wanted to reduce the longitudinal distance from pedals and steering wheels. Only 13 participants (29.55%) wished to stay in the defined reclined and backward-shifted position when being driven in automated mode. Multiple choice was possible for this question.

8.4 Discussion

The discussion concerns four aspects: Section 8.4.1 discusses the seat adjustment movement with the human movement, referring to the Results Sections 8.3.2 and 8.3.3; Section 8.4.2 interprets the take-over performance results in Sections 8.3.4 and 8.3.5; The overall take-over process and strategies were discussed in Section 8.4.3 and Section 8.4.4; Section 8.4.5 interprets the subjective results in Section 8.3.6.

8.4.1 Seat Adjustments Speed

The seat adjustment is slower than the movement of the human torso once the driver starts to lean forward actively (Section 8.3.2 versus Section 6.3.3). Significantly more participants sat up actively to react to the RtI and moved faster than the seat adjustments, which confirmed hypothesis $H_{14:}$ Reclined drivers' torsos will not always have full contact with the seatback during the take-over process, they will move more quickly than the seatback. Due to the fixation of the human torso during the forward-leaning movement, the lower part of the torso and the hip were in contact with the lower part of the seatback most of the time, which played an essential role in stabilizing the driver's upper body. Thus, SLA adjusting longitudinally forward is also important for reclined drivers to provide support to the hip and lower part of the torso.

Results show that the average time that the ego-vehicle spends in the right lane (Section 8.3.3) is longer than the time the seat takes on average to resume the driving position. Although the seat is slower than the human body movement, it is quick enough to finish the adjustment before the driver changes lanes. While the seat is adjusting, the driver reacts, re-configures the driver state, evaluates the situation, works out the driving strategy, and prepares to change the lane. Before the ego-vehicle enters the middle lane, which can cause a crash with upcoming traffic, the active seat assist can already be in a proper upright driving position offering adequate support for the driver's body. In the meantime, the driver without the active seat assist is still sitting on a reclined and backward-shifted seat.

The correlation analysis indicates that the body height and the torso length are more relevant to the seatback adjustment speed than the weight, BMI, and proportion. The taller the driver (or longer the torso) is, the longer it takes for the seat to resume its position, i.e., the slower the seatback angular speed. This refutes the third hypothesis, $H_{13:}$ Body height, sitting height, weight, and BMI

affect the duration of repositioning the seat. The hypothesis is partially correct for body height and sitting height. The physical explanation is that the longer the torso is, the longer the distance between the center of gravity of the upper body and the rotating axis of the seatback, resulting in a bigger resistance when the seatback starts to rotate. In reality, electric motors should be validated with the various loads if used in emergency cases to ensure their effectiveness.

8.4.2 Improvement of Take-Over Performance

The statistically significant results of a shorter hand-on time (Section 8.3.4.1) and foot-on time (Section 8.3.4.2) show that the active seat assist helps drivers react more quickly. No significant difference was found for TOT (Section 8.3.4.3). Drivers who spent less time putting their hands on the steering wheel and the right foot on the pedal did not operate more quickly. This corresponds to Chapter 5, and it was also explained in Section 6.4.3 of Chapter 6 that a shorter hand-on time does not always mean that the driver is ready to take over, especially for those who are reclined and who might still be in the forward-leaning process. However, a shorter hand-on time and foot-on time could indicate a quicker posture-resuming time, giving drivers more time to rebuild their situation awareness before any operational decision is made. TOT is measured automatically by the steering wheel angle and pedal pressing percentage (Table 8-2), which could also result from non-operational and unintended movements despite the thresholds set. For example, there are six participants without assistance who pulled the steering wheel to shift the H-point forward while starting to steer and brake (Figure L-1 in Appendix L).

A significantly longer TTC (Section 8.3.5.3) in this specific scenario means that assisted participants were able to keep a safer distance from the obstacle ahead than unassisted ones. A TTC of below 2.6 seconds should be regarded as a higher safety risk (Minderhoud & Bovy, 2001). The hypothesis $H_{11:}$ "The active seat assist affects the take-over performance" is confirmed, and it is a positive effect. No significant result is found in Min a_{long}, Max $|a_{lat}|$, and SDLP.

Overall, the hand-on time has been measured in three experiments (Chapters 5, 6, and 8); Table O-1 in Appendix O lists the hand-on time in the different conditions of these three within-subject experiments, visualized in Figure O-1. In the motion tracking study in Chapter 6, the take-over motion is primarily a motoric reaction without much cognitive load. Every 20° torso angle increment until 50° results in 0.03 seconds to 0.06 seconds of hand-on time increment. The experiments described in Chapter 5 and Chapter 8 (with the active seat assist) were conducted in the same driving simulator. In Chapter 5, a 15° torso angle increment results in an averaged 0.15 seconds of hand-on time increment, which is about three times as much as in Chapter 6. The additional driving task and the NDRT in Chapter 5 seem to have more significant influence than the postural factors (here: the torso angle) on the hand-on time. This corresponds to Arsintescu et al. (2019), who found that a high workload is associated with lower performance in the reaction time test. Thus, reclined drivers' disadvantages could be more significant when more workload (e.g., complex traffic, distraction) is added. One could hypothesize that the consequences of being reclined might not only directly result from the physical postural factors per se; rather, they might be mainly caused by the reclined drivers' cognitive and sensory states. For example, reclined drivers

might be more likely to fall asleep (Cole, 1989; Johns, 2000). Some other studies also suggested that postures affect cognitive performance. Specific cognitive functions are deteriorated in a supine position compared to the upright position, such as problem-solving (Lipnicki & Byrne, 2005; Schulman & Shontz, 1971) or perception (Lundström et al., 2006, 2008). Quality of sleep prior to the experiment can be more influential in a supine posture, affecting reaction times (Muehlhan et al., 2014). Reclined drivers might thus need more time to perceive, react, and perform under a higher workload. Larger SDs of the hand-on time in Chapters 5 and 8 indicate that drivers' performance varies significantly with the higher workload generated by the driving and NDRTs.

8.4.3 Sequential Take-Over Process Without the Active Seat Assist

Participants without the active seat assist tend to have a sequential take-over process. A typical sequential process (an example is given in Figure M-1 in Appendix M) begins when the participants perceive the visual-auditory RtI signal and redirect their attention to the driving scene. Up until this moment, the participants do not change their postures. They look ahead and realize that the driving task has to be taken over and start to lean forward, putting their hands onto the steering wheel and their right feet onto the pedals. Meanwhile, they start to interpret and understand the situation. They then check the left mirror, preparing to change the lane. The participants brake, change lanes, stabilize the car, and pass the broken-down car.

In this take-over process, the participants must hold their postures without the support of the seatback and might have to slide their hips forward to press the pedal. The participants operate the critical dynamic driving task (lane change) in unstable sitting postures. Their arms must help to stabilize the torsos while steering. These unstable sitting postures could reduce the accuracy of steering and pressing the pedals.

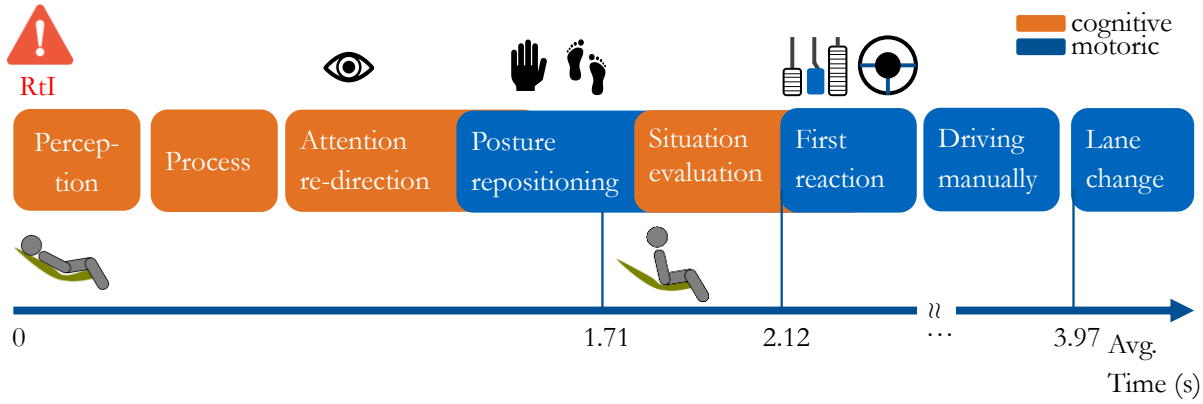

Figure 8-20 Sequential take-over process and sitting postures without the active seat assist

Figure 8-20 schematically illustrates the rather sequential take-over process with different cognitive and motoric activities. The orange blocks represent the cognitive activities; the blue blocks represent the motoric activities. The overlaps of the text boxes symbolize that even though these activities occurred sequentially for the most part, they do overlap. A clear separation is not possible via video analysis. The manikin in Figure 8-20 shows the changing posture with the unchanged reclined and backward-shifted seat. The four numbers on the x-axis are the time point 0 (RtI), the

average of the hand-on time (Section 8.3.4.1) and the foot-on time (Section 8.3.4.2) as the posture repositioning time, TOT (Section 8.3.4.3), and the average time of participants in the right lane (Section 8.3.3). The mean values are taken from the condition "without the active seat assist." These values can vary due to situational, postural, and other individual differences. Without the active seat assist, participants react and operate the critical dynamic controls in an unstable sitting posture lacking the proper support of the seat.

8.4.4 Parallel Take-Over Process With the Active Seat Assist

Participants with the active seat assist tend to have a parallel take-over process. A typical parallel process (an example is given in Figure N-1 in Appendix N) begins when the participants perceive the visual-auditory-haptic RtI signal and redirect their attention to the driving scene. In the meantime, their sitting positions are already passively pushed upright and forward by the seat adjustment without requiring a human reaction. In addition to this physical assist, this movement also gives the drivers a cognitive impulse to sit straight and lean forward. The participants then lean forward actively, losing some contact with the seatback, putting their hands onto the steering wheel and their feet on the pedals. Meanwhile, they start to interpret and understand the situation, check the left mirror, and prepare to change lanes. In parallel to this, the seat keeps returning to the upright position and finishes the adjustment. The participants regain full contact and the support of the upright seat, then they brake, change the lane, stabilize the car, and pass the broken-down car.

In this take-over process with the active seat assist, the participants' upper bodies could be mostly supported by the seatback. There are gaps between the upper parts of the torsos and the seatback after the participants have actively leaned forward. However, the lower parts of the torsos continuously benefit from the increasing support of the seatback. The seatback catches up with the torsos, finishes the adjustment, and provides full support before the critical dynamic operation is conducted.

Figure 8-21 schematically illustrates the effect of the active seat assist on the take-over process. The orange blocks represent the cognitive activities; the blue blocks represent the motoric activities. Like the sequential take-over process (Section 8.4.3), most activities run sequentially with some overlaps. However, the active seat assist affects the "posture repositioning" motoric activity in a fundamental way. The active seat assist shifts the "posture repositioning" task parallel to the cognitive perception and process right at the beginning of the take-over process, thus shortening the whole take-over process duration. The participants do not have to "realize" that they have to sit upright immediately; instead, they are passively pushed up to sit upright by the seat without knowing what is happening. Though the participants then lean actively forward after realizing the take-over situation, they are still able to spare the time and the cognitive resource to observe and evaluate the situation to react more appropriately.

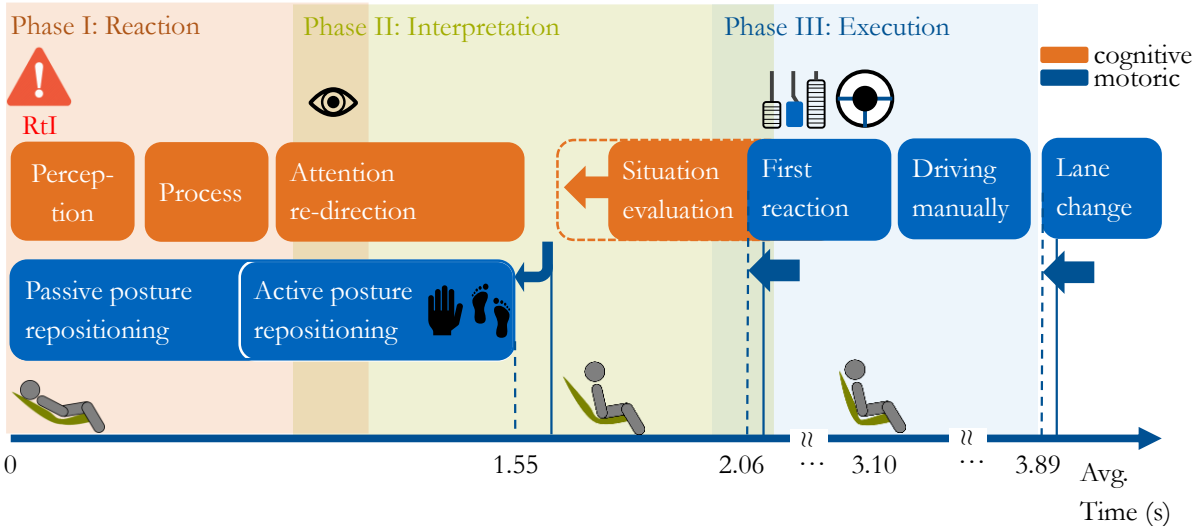

Figure 8-21 Benefits of the active seat assist: shifting posture repositioning parallel to other activities

The manikin in Figure 8-21 shows the changing posture with the changing seat adjustments. The five numbers on the x-axis are the time point 0 (RtI), the average of the hand-on time (Section 8.3.4.1) and the foot-on time (Section 8.3.4.2) as the posture repositioning time, TOT (Section 8.3.4.3), the seat adjustment time (Section 8.3.2), and the average time of participants in the right lane (Section 8.3.3). The mean values are taken from the condition "with the active seat assist." These values can vary in other cases due to situational, postural, or other individual differences. After the time point of about 3.1 seconds, the SBA and the SLA finished adjusting to the upright driving setup, offering the driver's body better physical support and better reachability of the pedals and the steering wheel. The driver could thus operate the critical dynamic controls in a more stable and upright posture.

To summarize the take-over process of reclined drivers with the active seat assist: there are three phases: the reaction phase, the interpretation phase, and the execution phase. Three overlays in orange, green, and blue symbolize the three phases in Figure 8-21. The boundaries between the phases are not strictly defined since they are not absolutely sequential, and they could overlap.

Phase I, the reaction phase, begins with the RtI until the drivers look at the road for the first time. This could take around 1 second. In this phase, the drivers with the active seat assist have been pushed up and forward, repositioning their postures passively while reacting to the visual-auditory-haptic RtI. Their torsos have full contact with the seatback in this phase. By the end of this phase, the seat can adjust ≈ 5° upright (SBA) and ≈ 2.5 cm forward (SLA). This 5° SBA is about one-third of the necessary adjustment range (40° - 25° = 15° in total). It shortens the gap to the steering wheel and pedals; the seatback continuously offers full support to the driver's back until the next phase begins.

Phase II, the interpretation phase, begins with the resumption of the drivers' cognitive status: observation, interpretation, and evaluation of the situation parallel to the motoric resumption. Because of the strong directional impulse of the seat adjustment, the drivers actively lean forward more quickly, which might be one reason for the shorter hand-on time and foot-on time in Section 8.3.5 (average ≈ 1.55 seconds after RtI). The upper parts of the torsos might partially lose contact

with the seatback in this phase. It depends a lot on the drivers' experience and individual performance with regard to interpreting scenarios and developing a strategy to resolve the critical situation quickly. The drivers might also already start to steer, brake, or accelerate without a correct situation assessment and an appropriate decision (Gold, Körber, Lechner, & Bengler, 2016), which might be one reason why there is no significant difference in TOT. By the end of this phase, the drivers begin to steer, brake, or accelerate (average ≈ 2.06 seconds after RtI). In the meantime, the seat has been adjusted another ≈ 5° upright and another ≈ 2.5 cm forward. At the end of this phase, the drivers' postures are much closer to a driving posture; the gap between the driver's back and the seatback becomes smaller, and the contact area increases.

Phase III, the execution phase, begins when the drivers start to consciously operate the dynamic control of the vehicle (average TOT = 2.06 seconds, with the active seat assist). The last third of the seat adjustment is finished in the middle of this phase at the time point of 3.10 seconds on average (Section 8.3.1). This one-second (from 2.06 to 3.10 seconds) driving-while-seat-adjusting situation might be critical if the scenario becomes more complicated and precise control of steering and pedals is required. Nevertheless, in this experiment, this has not been observed as critical in the simple take-over scenario for three reasons. First, two-thirds of the adjustment had already taken place in the two previous phases, when the drivers were still reacting before any action was carried out. Second, the drivers stayed in their own lane, and no critical dynamic control was conducted until the first lane change at 3.89 seconds. Third, the gentle and constant seat adjustment movement was well predictable and accordant with the drivers' intention.

This simple take-over scenario only requires a small motoric maneuver, i.e., mild steering and braking. More sophisticated actions are necessary for more complicated scenarios, e.g., higher traffic density in the middle and the left lane approaching from behind. Drivers sitting on a reclined and backward-shifted seat without the support of the seatback (as in Figure M-1 in Appendix M, c, d, e, f) and away from the steering wheel and pedals might impair operational accuracy. In a real car, a more dynamic movement is expected compared to the simulator, making it even harder to keep sitting upright without support. The drivers might pull and seize the steering wheel more tightly (examples in Figure L-1 in Appendix L), impairing the steering and braking quality. Besides, sitting upright on a reclined seat like in Figure N-1 c, d, e, f in Appendix N was not considered in the current passive safety concepts and tests, which could lead to serious injuries in the event of a crash.

8.4.5 Acceptance

The subjective evaluation (Section 8.3.6) confirms H_{12}: The active seat assist can be positively evaluated as useful and satisfying with the help of the Van Der Laan acceptance scale. Results show that most items averaged in a very positive area (> 1.00), indicating good acceptance. The item regarding alertness is evaluated as neutral, neither "raising alertness" nor "sleep-inducing." This might be the average of the two extreme statuses of this function, either "hibernated" in normal automated driving or active in take-over cases. Generally, the movement of the seat is perceived rather as gentle despite the 16V-power boost. Compared with the take-over without the active seat

assist, drivers feel that they are warned in the critical situation, and more importantly, that they are assisted by the vehicle; the upright sitting position is more suitable for the manual driving in the later phases of the take-over process; it makes the take-over process easier and more comfortable. More instructions on and experience with the seat functions can make the active seat assist more predictable and improve the acceptance.

The predefined reclined posture (torso angle 40°, knee angle 130°) was not well accepted. This corresponds to the finding in Chapter 6 that the combination of a reclined posture and the take-over process can subjectively stress drivers. Thus, they want to sit more upright and closer to the steering wheel, knowing that an RtI is coming and inevitable. Predefined sitting positions might generally not be well accepted due to the highly individual preferences with regard to the sitting position (S. Lorenz, 2011; Yang, Orlinskiy, Bubb, & Bengler, 2016).

8.5 Summary

In conclusion, the active seat assist system improves the take-over performance of reclined and backward-shifted drivers in Level 3 automation. Drivers can reach the control elements within a significantly shorter time and have a safer TTC towards the obstacle ahead. The active seat assist system also subjectively increases the ease and comfort level of the take-over and is therefore well accepted as useful and satisfying.

As the primary effect, the seat automatically pushes the reclined and backward-shifted driver upward and forward simultaneously with the RtI, which helpes the driver start to resume the posture without any human reactive delay and reach the upright posture before the critical dynamic control is conducted. This effect shows the outer compatibility (Bubb, Bengler, Breuninger, Gold, & Helmbrecht, 2015; Flemisch, Schieben, Kelsch, & Löper, 2008) between the driver and the active seat assist, whose outer borders physically fit each other (reclined or upright). Dynamically, the human driver and the seat move concordantly during the take-over process.

As the secondary effect, the active seat assist offers the RtI signal an additional haptic modality. The initial movement of electric motors has a warning characteristic. Multimodal RtI signals could result in faster steer-touch times and have good subjective acceptance (Petermeijer et al., 2017). The continuous upward-and-forward adjustment during the take-over process extends the RtI signal. This directional haptic signal takes about 3.1 seconds, giving the driver an intuitive and continuous impulse to actively redirect the attention toward the front driving scene and lean forward toward the operating elements. This effect shows the inner compatibility (Bubb, Bengler, et al., 2015; Flemisch, Schieben, et al., 2008) between the driver and the active seat assist, where the predictable and assistive behavior of the seat matches the driver's intention in the take-over process. Following the guidance of Coll & Coll (1989), the active seat assist "operates and interacts with the user in a manner which parallels the flow of the user's own thought processes," leaning forward in the take-over process. This cognitive match and the compatible trajectory of the driver and seat contribute to the cooperativeness of control (Flemisch, Bengler, Bubb, Winner, & Bruder, 2014), potentially improving usability of the active seat assist.

Figure 8-22 illustrates the take-over process schematically with regard to the human performance model, according to Embrey (2005), Rasmussen (1983), and Reason (1990). Different skill-, rule-, knowledge-based actions could be conducted in each of the take-over phases. Phase I is a series of relatively automatic reactions, including perceiving and recognizing (skill-based). In phase II, the driver is rebuilding his or her situation awareness and acting increasingly on a conscious level. The driver interprets the signal, evaluates the scenario, assesses the reclined and backward-shifted state with the take-over task, and searches for the stored rules to react (skill-based or rule-based). Phase III and further driving behaviors are mainly conscious behaviors (rule-based or knowledge-based). The boundaries between phases and proportion of skill-, rule-, and knowledge-based behavior are not precisely defined and vary according to individual capability and experience. Activities could move toward "automatic reaction" to the left through, e.g., training, getting more experience (Rasmussen, 1983) to spare more cognitive resources, thus be more efficient and effective.

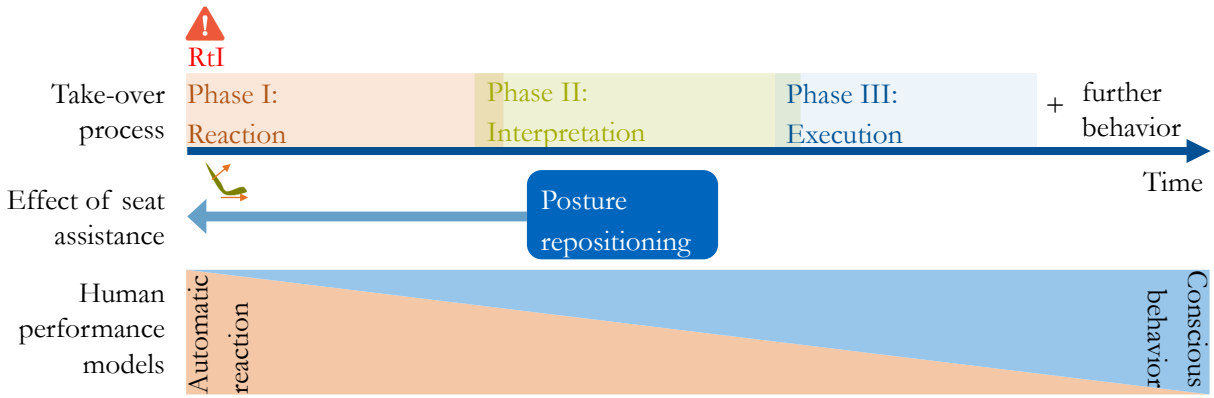

Figure 8-22 Take-over process with the active seat assist concerning the human performance model according to (Embrey, 2005; Rasmussen, 1983; Reason, 1990)

Without any human reaction time, the active seat assist starts to reposition the driver's posture instantly and simultaneously with the RtI. The instant start of the seat adjustment is quicker than any driver's skill-based reaction. The active seat assist is not only useful for inexperienced drivers, whose reaction is not at a skill-based level yet, but it also makes use of the response time of every human driver, including the skilled ones. Having assistance systems like the active seat assist has a similar effect of shifting the task into a lower skill-based level and also into the reaction phase, making the take-over process more effective, efficient, and ultimately safer (Figure 8-22).

8.6 Limitation

Participants were informed about the availability of the active seat assist to avoid a shock effect. However, this might introduce the bias that participants might take the take-over with the active seat assist less seriously. In reality, the functionality of a car should be known to its owner or the driver, who might rely on the movement of the seat to reposition passively and thus react more slowly in an emergency. During the experiment, the experimenter's intervention with requests for the 1-back tests and questionnaires might intensify the Hawthorne effect (Merrett, 2006), resulting in unnaturalistic behavior. The dynamic of the driving simulator only represented a limited range of possible dynamics. Reclined drivers had an unrealistically better visibility of the front/side

driving scene on the displays. Interior panels in real vehicles can limit the reclined driver's visibility. Two given postures do not correspond to the individual preferences in most cases; this mismatch could deteriorate take-over performance. The simple take-over scenario was on the highway with a moderate time budget; the different complexity and urgency of the take-over situation can lead to different results. To avoid participants developing an automatic reaction because of too many take-overs in one experiment, two take-overs were two essential variants to test for the research question. There is no take-over from the upright sitting posture as a reference. Thus, the direct evidence for the question whether reclined and backward-shifted drivers with the active assist seat could take over as well as upright seated ones is not provided. The case that the driver is operating while the seat is moving should be more precisely investigated in the future, in order to find out to what extent the active seat assist influences the steering, braking, and accelerating behavior.

9 Overarching Discussion: The Chicken-Egg Dilemma

The results of each study are discussed in the "Discussion" sections of each Chapter: Chapters 4, 5, Sections 6.4, 7.4, and 8.4, respectively. This chapter discusses an overarching topic: a chicken-egg dilemma from the perspective of the development process. This topic is illustrated in the pre-publication "Chicken or Egg Problem? New Challenges and Proposals of Digital Human Modelling and Interior Development of Automated Vehicles" (Yang et al., 2020) in the Proceedings of the Human Factors and Ergonomics Society Annual Meeting 2019. This section presents a brief summary.

Different NDPs are evaluated in four studies in Chapters 4, 5, 6, and 8, even though this was not always the central research question in each study. The acceptance toward reclined postures varies in different experimental mock-ups. Results show significant individual differences in preferences of NDPs. Participants tend to have a higher acceptance of reclined postures with an interior mock-up of a lower fidelity (e.g., without the driving scenario). More realistic vehicle dynamics, more interactive and contextual experience with the automation, and especially encountering the system limits lead to a lower acceptance of reclined postures. This is closely related to the mental models of manual driving, trust in automation, and the extra effort necessary to take over safely in a reclined posture. The reclined posture seems to be favored during the Level 3 automated driving but is not preferred during the take-over process. However, the take-over process is, by definition, an inevitable part of Level 3 automation. Besides, different use cases of Level 3 automation will generate more diverse opinions on reclined postures.

The quickly changing opinions towards the reclined posture signify a general problem overarching all Chapters: the identified user behavior (Chapter 4), the risks of reclined postures (Chapter 5), the take-over motion (Chapter 6), and the user interaction with the active seat assist (Chapters 7 and 8) are all based on the consumers' current expectations of automated driving and the established mental models of manual driving. Users' subjective opinions and behavior change rapidly parallel to the automation technology development. How can developers keep updated and ensure that the functional development is not based on an invalid "outdated version" of the user's need? The requirement acquisition is based on and adapts to customer behavior and needs; on the other hand, real customers' behavior appears only after the product is available. The observed customer behavior without a real product can be misleading, whereas disruptive concepts could lead to new customer behavior but risk not fulfilling the customer's needs. This problem is not a new issue in automotive development. However, it is especially challenging in human behavior modeling in AVs due to the conflict between the established complex automotive development process and the unclear requirements of AVs, which could not refer to previous products and require much more agility to deal with.

The influence of the interior (symbolized by the orange arrow in Figure 9-1) on the driver's behavior are much smaller in a conventional manually driven vehicle due to the restricted and predictable driving task. After all, drivers have to operate the vehicle dynamic control at all times, no matter what interior is available. Automation "releases" drivers from the constant driving task

and opens opportunities for them to conduct NDRTs, e.g., reading or relaxing. This expanded range of inter- and intra-individual human behaviors are relatively unpredictable and hard to identify. On the other hand, AV products are not yet available on the market.

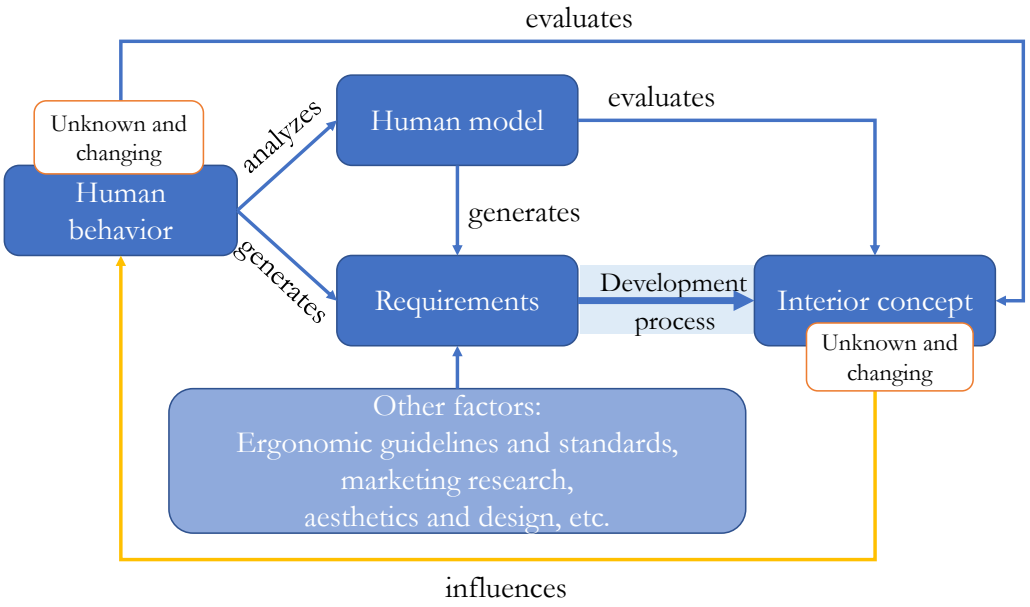

Figure 9-1 Challenges to the traditional interior development process, modified from Yang, Fleischer, et al. (2019)

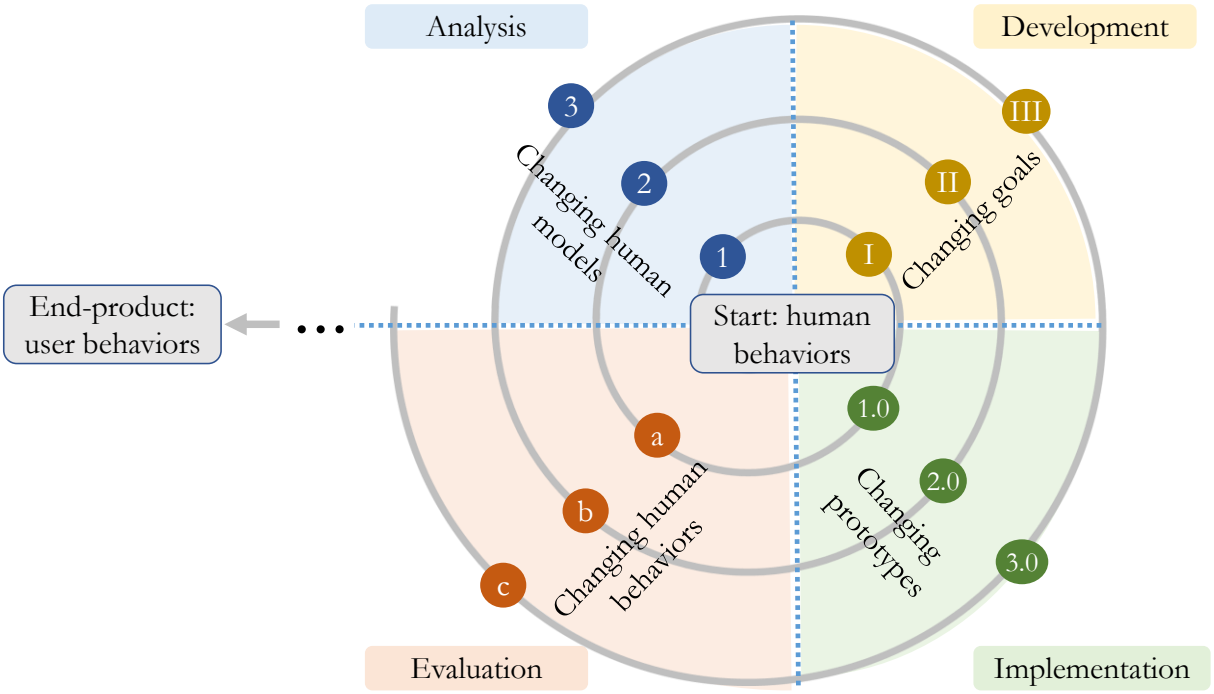

Figure 9-2 A user-centered, iterative development framework for the development of AV interior functions (Yang et al., 2020)

It is not essential for the developers to argue from which side to start: whether the observed or predicted user behavior defines the product or a disruptive interior concept creates new user needs

and behaviors. It is rather important in this situation to be iterative and agile in order to be in pace with the highly dynamic evolution of user-automation interaction.

Yang, Fleischer, et al. (2019) proposed an iterative working framework (Figure 9-2) for the development of AV interior functions. It is based on the user-centered development (ISO 9241-210, 2010), the spiral model (Boehm, 1986), the star lifecycle interaction design model (Hartson & Hix, 1989), and the interaction prototyping model (Conti et al., 2020).

The framework focuses on changes: it starts with human behavior as an example (could also start from a prototype). The changing models, changing goals, and changing prototypes are built to serve the changing behaviors, which are all only tentative. As the iterative process proceeds, if the differences are small enough between two iterations, the prototype might be valid enough to be an end-product. User behavior might then stay relatively stable. The user might interact with the product in a relatively known, predictable, and intended way (Yang et al., 2020).

Like other agile working processes, this framework emphasizes the process to be adaptive rather than predictive (Boehm & Turner, 2004); agile and light (Collier, 2012) rather than cumbersome and heavy; iterative (Vijayasarathy & Butler, 2016) rather than a sequential waterfall (Royce, 1970).

It is also essential to involve the real representative user in the early development phase, not only experts or developers, thus reducing the risk of usability mistakes and avoiding high costs in the long term (Yang et al., 2020).

For example, the scope of this dissertation can be positioned in this model as the first two iterations, starting from the NDRT and NDP identification. The following notations correspond to Figure 9-2.

1. The first iteration:

   1 – A static posture model of NDPs (Chapter 4)

   I – Setting the scope of reclined postures (Chapters 4 and 5)

   1.0 – Reclined drivers taking over without assistance (Chapter 5)

   a – The evaluation of the take-over behavior and performance of reclined drivers (Chapter 5)

2. The second iteration:

   2 – A dynamic take-over motion model for reclined postures (Chapter 6)

   II – Setting the goal of improving the reclined drivers' take-over performance (Chapters 6 and 7)

   2.0 – The development of the active seat assist and its application in the automation simulation (Chapter 7)

   b – The evaluation of reclined drivers' take-over behavior and performance with the active seat assist (Chapters 7 and 8)

10 General Summary

Five experiments are summarized in detail in the "Summary" section of each Chapter: Chapters 4, 5, Sections 6.5, 7.5, and 8.5, respectively. This section summarizes the key messages, from which the answer to the research question (Chapter 2) is derived.

Research on take-over performance in Level 3 automation has set a valuable methodological foundation for this work. Beyond the factors investigated in the literature (Chapter 3), this work focuses on the effects of driver postures on take-over performance. Furthermore, this work develops an application, the active seat assist, as a possible countermeasure to compensate for the reclined and backward-shifted drivers' disadvantages in take-over situations.

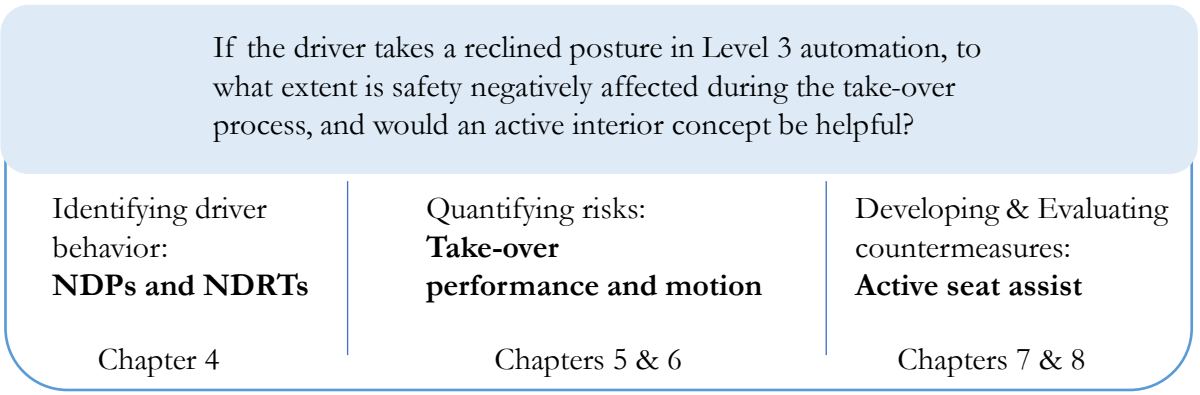

Figure 10-1 Recap of the main question and the structure of its answers

Figure 10-1 shows the main research question defined at the beginning of the work (Chapter 2). The answer consists of five empirical studies in three steps: first, identifying driver behavior: the NDPs and NDRTs in Chapter 4; second, quantifying risks: modeling the reclined drivers' take-over performance and motion in Chapters 5 and 6; third, developing and evaluating countermeasures: the active seat assist in Chapters 7 and 8.

Chapter 4 provides a catalog of NDRTs which can be conducted with significantly higher probability in an AV than a conventional vehicle; NDPs with measured joint angles and seat adjustments quantify the individual preferences concerning postures. Results indicate that drivers intend to conduct a wider variety of NRDTs and sit differently (NDP) in AVs. Apart from the conventional upright sitting posture, which is still the favorite in most activities, the reclined posture with a large torso angle is shown as one potential NDP in future AVs. This chapter provides empirical evidence to place the focus of this thesis on the reclined posture.

Chapter 5 focuses on the take-over performance of reclined and backward-shifted drivers. Results show that reclining to the 38° torso angle via SBA deteriorates the take-over performance in Level 3 automated driving, while a relaxed knee angle of 133° via SLA shows no significant influence. Reclined drivers with a 38° torso angle might still manage to control the vehicle back to a safe state in simple take-over scenarios. However, it can be critical in complex and emergency situations. The take-over motion is investigated in further detail separately in Chapter 6.

Chapter 6 has collected a dataset of the take-over motion from 12 different reclined postures (torso angle: 10°–70°, knee angle: 90°–130°). The take-over motion data, including the trajectory, the speed, and the acceleration, can be used as empirical evidence to predict the take-over trajectories, time, and the driver's motoric state. The objective and subjective disadvantages of reclined drivers in the take-over process are illustrated. From a primarily motoric perspective, this chapter supplements the evaluation of reclined drivers' take-over performance in Chapter 5. The torso angle has a major influence on the take-over motion and time compared to the knee angle. Reclined drivers have unstable sitting positions during the take-over process, need more time to take over, and sustain subjectively more workload during the take-over process. Evidence supports a critical torso-angle threshold between 30° and 50° concerning the take-over time, sitting stability, and subjective perception. A reclined torso angle greater than the critical threshold is certainly not recommended for Level 3 automation. The presented geometrical and temporal differences between the upright and reclined drivers' take-overs are the empirical evidence to set new interior requirements for AVs.

Chapter 7 describes the development of the active seat assist to help the reclined and backward-shifted drivers resume an upright driving position in take-over situations. The active seat assist can be adjusted manually using a smartphone wirelessly or triggered automatically by the driving simulation. The boosted seat adjustment was faster than the mainstream products on the market. It takes about 2.8 seconds to adjust the seatback angle from 40° to 25°. Different adjustment signals are tested regarding effectiveness, efficiency, and acceptance. This chapter offers one technical solution assisting reclined and backward-shifted drivers in the take-over process.

Chapter 8 evaluates the active seat assist in a simulated Level 3 automated drive. The take-over scenario is similar to Chapter 5. The active seat assist improves the reclined driver's take-over performance by shifting the relatively sequential process to be more parallel, making use of the human reaction time to resume the sitting posture. This system compatibly corresponds to both of the driver's take-over intention and movement, thus improving the ease and comfort of take-overs. The system was subjectively well accepted as useful and satisfying. This chapter illustrates a possible countermeasure that compensates for the disadvantages of reclined and backward-shifted drivers during the take-over process.

To provide the answer to the main research question, drivers intend to conduct NDRTs (e.g., relaxing) and take NDPs (e.g., sitting reclined and backward-shifted) in AVs. Even though the simple take-over situation seems controllable for ≈40° reclined drivers, the large torso angles (e.g., 40°) impair take-over performance. The reason is probably a combination of the reclined state and the workload of the driver (introduced by the driving/non-driving task), rather than the pure postural and motoric factors. However, active interior elements such as the active seat assist can effectively compensate for the reclined and backward-shifted drivers' disadvantages, improving the take-over performance and the acceptance of Level 3 automated driving.

11 Limitations and Recommendations

The limitations of the specific experiments are discussed in the "Limitation" section in each corresponding chapter: Chapter 4, Chapter 5, Section 6.6, 7.6, and 8.6. In this section, common limitations across the experiments and the general research scope are summarized. Recommendations for future work focusing on reclined postures and improving the user experience of reclined drivers in Level 3 automation are provided.

This work began with a broad scope by exploring the possible NDPs in AVs with as few restrictions as possible in Chapter 4. In the questionnaires and the experiment participants were not instructed with regard to a specific level of automation. Only the generic term "automated driving" was mentioned to avoid any restrictions stopping participants from demonstrating their preferred activities and postures. The mixed results undoubtedly contain many mental models, especially regarding the definition of the AV. This generic and broad scope resulted in large variances of the results.

Based on Chapter 4, the scopes of Chapters 5, 6, and 8 are narrowed down, focusing on reclined drivers' take-over performance in Level 3 automation. In both Chapter 5 and Chapter 8, the focus reclined posture is the relaxed NASA neutral posture with a torso angle of ≈ 40° and a knee angle of ≈ 133°. The take-over scenarios in both experiments follow the same principle: being simple and straightforward in order to generate a homogeneous and comparable take-over strategy.

The motion tracking experiment in Chapter 6 focuses on the influence of the reclined postures on the take-over motion regarding space and time. The artificial take-over task is independent of automation level and traffic. The strictly controlled experimental conditions were to generate comparable take-over motions, which vary from reality.

In Chapters 5, 6, and 8, driver states (e.g., cognitive, drowsiness) other than the motoric state were possibly either minimized or controlled, but their reciprocal influences could not be excluded. Controlling and stimulating methods like the 1-back task could not prevent participants from having different cognitive workload and fatigue levels. Similarly, the active seat assist also influences drivers' cognitive processes during the take-over process as a secondary effect. As such cognitive factors are not the focus of this thesis, no relevant metrics and measurements were applied; thus, none of the relevant influences mentioned could be quantified. The relevant discussions are based on inductive analyses.

The seats (Figure 3-12), the steering wheel, and the pedals used were from current conventional vehicles optimized for an upright driving position. Research on reclined postures or other NDPs in conventional seat setups might result in low acceptance of NDPs, unnaturalistic user behavior, and misleading results.

This chicken-egg dilemma, a general limitation of the interior development of AVs in research and industry, is discussed in Chapter 9. The key message is that it is impossible to access real users' behavior within one iteration due to the unclear requirements and a lack of the Level 3 automated vehicle for real users. The results gained in labs and simulators might not be transferable to reality.

When AVs are technically and legally available, users' individual postural preferences can vary in different scenarios, with different user goals and different vehicle types. In addition, inter- and intra-individual changes should be considered. The active seat assist in Chapter 7 might thus only be a transitional concept until a systematic interior concept for reclined postures in AVs is developed in the future.

There are further common limitations of these five experiments: The participants are mostly young technical students who live in Germany. Results should be interpreted with the consideration of demographic, anthropometric, cultural limits. In the laboratory experiments, the participants were aware that they were being observed and measured by cameras and other devices. Thus, their behavior might not be naturalistic due to the Hawthorne effect (Merrett, 2006). The participants' numbers were very limited in most cases. It is generally impossible to validate the truthfulness of the questionnaires. The mock-ups in the laboratory and the driving simulators are very basic. There is no door panel, middle console, and front interior panels in the simulators, which might block reclined drivers' visibility in an actual vehicle. The forward sight conditions influence the choice of the sitting position (D. Lorenz, 2015). Thus, the acceptance of reclined postures and the take-over performance should be investigated in each specific type of vehicle. This work only focuses on a very short phase of Level 3 automated driving, the take-over process. Other SAE automation levels (e.g., Level 2 or Level 4); other driver states (e.g., drowsiness); other NDPs (e.g., rotated sitting positions); other complex scenarios (e.g., high traffic flow, critical time budget); other NDRTs (e.g., playing on a smartphone); other interior components (e.g., safety belt, armrest); other safety aspects (e.g., passive safety, functional safety); other comfort aspects (e.g., motion sickness, long-term effect) and other legal and product liability issues are out of the scope of this work. However, they must be addressed in future research and development before the reclined posture is offered in Level 3 automated driving products.

Following the research scope of the reclined postures in Level 3 automation, further research could go in three different directions:

1. Uncritical phases of Level 3 automated drive

   The goal is to evaluate the reclined experiences within the Level 3 system limit and access the added value for the customer of being able to lean back as a driver. There are many other uncritical phases of the human-automation interaction, the availability of the automation, the activation of the automation, the ride with different dynamics, traffic and lighting conditions, and uncritical take-over scenarios, e.g., 5 km before the highway exit. In all these phases, aspects such as acceptance, comfort, motion sickness, visibility, and situation awareness of reclined drivers can be investigated. It is highly recommended to conduct field studies using real Level 3 or high-fidelity Wizard-of-Oz vehicles for those topics. Mock-ups in laboratories might generate misleading results concerning user experiences. A wide range of demographies should be included.

2. Take-over performance modeling

The many-to-many relationship between NDRTs and NDPs (Chapter 4) indicates that reclined drivers' take-over performance should also be investigated with extended ranges of other realistic NDRTs. For example, being reclined while playing on a smartphone might be a very probable and critical use case. Motoric states and cognitive states are inseparable due to the reciprocal influence; they should be addressed together or controlled with great caution. The goal here is to identify and further specify the critical reclined torso angle (probably between 30° and 50°). This threshold should not only come from a primarily motoric perspective, which is probably less influential than factors like traffic, NDRTs, and driver's cognitive state. An all-round consideration of the critical torso angle is expected.

A monitoring system for the driver's postures might help to predict the reclined drivers' availability to take over. Sensors can be interior cameras, seat adjustments, and the seat pressure mat.

3. Interior development for reclined drivers

   New seats and HMI concepts for reclined drivers should be developed iteratively, based on specific use cases, since the general requirements are unclear and NDRTs/NDPs are very situation-dependent. New concepts can only be validated by a long-term observation. The driver's sight to the front and the all-round visibility should be validated and modeled with different anthropometric characteristics and vehicle setups.

   Passive safety for new interior concepts should be addressed: the submarine effect and the extra load on the pelvis in case of a front crash; positioning of the seat belt; a seat belt pre-tensioner allowing a forward-leaning take-over movement; side crash test focusing on the head position of reclined drivers.

   Regarding the adaptive interior like the active seat assist, further research with extended ranges of vehicle dynamic, take-over scenarios, postures, and situationally varied seat adjustment speeds could provide a more comprehensive reference for the concept design. Human factors, functional safety, and cybersecurity issues should be addressed for this safety-critical electric/electronic system.

   The goal here is to develop a new interior concept for reclined postures and access real user behavior to validate the concept.

Assuming the customer added value of the driver's reclined posture is verified, there are five recommendations to improve the user experience for reclined drivers in Level 3 automated driving:

1. Regarding the seat adjustment, an SBA of more than 40° reclined should be prohibited for the driver during Level 3 automated driving. As long as the reachability of the pedals is ensured, SLA could enable a maximum relaxed knee angle of 133°. This recommendation is simply from the perspective of the drivers' take-over performance. The exact permitted SBA and SLA value must be addressed under a broader scope and other restrictions.
2. A new reclined seat concept should offer better support for the neck, the lumbar, and the thigh.

3. The HMI displays and operation elements should be applicable for reclined postures. HMI in the periphery field, such as the ambient light, might help convey abstract information for reclined drivers while not annoying and distracting them from NDRTs.
4. Reducing the dynamic performance of the automation system (e.g., maximum 80 km/h without changing lanes) and limited applicable areas (e.g., only applicable on the highway) could increase the ride comfort and reduce the probability and criticality of a potential take-over. Urgent take-over experiences can damage the trust in automation, and reduce comfort and acceptance of reclined postures.
5. System transparency is essential. Only displaying the current system status, such as a lack of lane marks or missing the target object, costs the driver extra cognitive resources to recognize, interpret, and react. This extra workload is critical especially for reclined drivers in an urgent take-over situation. Warning for critical cases should be combined with explicit or implicit instructions to the driver about the current to-dos from the driver's perspective. For example, a hand-on animation or an acoustic instruction tells the driver explicitly to "steer", and the active seat assist indicates the forward-leaning direction. In comparison, a beep tone or a vibrating seat only says, "something is happening."

   Adaptive interior elements such as the active seat assist during the take-over can be considered a haptic kinematic interface. The continuous adjustment of the active seat assist implicitly sends a directional impulse to the driver, "something is happening in the front, lean forward." This kind of kinematic adjustment/signal does not only help reconfigure the driver's motoric state. It also leads the driver's attention in its moving direction, helping to reconfigure the driver's sensory and cognitive state more quickly. As a result, it could improve performance, raise the comfort level, and improve the acceptance of the inevitable system limit. It is noteworthy that the sudden movement of interior elements in critical situations may potentially surprise, distract, and even shock the driver to overreact. Thus, the kinematic movement should be accordant with the driver's intention and movement. Both inner and outer compatibilities between the driver and the interior elements are essential in urgent take-over situations. Furthermore, consistent and predictable system behavior is expected.

References

AAM. (2003). Statement of Principles, Criteria and Verification Procedures on Driver Interactions with Advanced In- Vehicle Information and Communication Systems. *Alliance of Automobile Manufacturers*, 23. Retrieved from http://www.umich.edu/~driving/publications/DF-T 3.0 rev3.pdf

Ahn, H. Il, Teeters, A., Wang, A., Breazeal, C., & Picard, R. (2007). Stoop to conquer: Posture and affect interact to influence computer users' persistence. *Lecture Notes in Computer Science (Including Subseries Lecture Notes in Artificial Intelligence and Lecture Notes in Bioinformatics)*, *4738 LNCS*, 582–593. https://doi.org/10.1007/978-3-540-74889-2_51

Allport, A., Styles, E., & Hsieh, S. (1994). Shifting intentional set: Exploring the dynamic control of tasks. In C. Umilta & M. Moscovitch (Eds.), *Attention and performance series. Attention and performance 15: Conscious and nonconscious information processing* (pp. 421–452). The MIT Press.

Andersson, B. J. G., & Ortengren, R. (1974). Lumbar disc pressure and myoelectric back muscle activity during sitting. II. Studies on an office chair. *Scandinavian Journal of Rehabilitation Medicine*, *6*(3), 115–121. https://doi.org/10.1016/0003-6870(76)90024-7

Arlt, F. (1999). *Untersuchung zielgerichteter Bewegungen zur Simulation mit einem CAD-Menschmodell (Dissertation)*. Chair of Ergonomics, Department of Mechanical Engineering, Technical University of Munich, Munich, Germany.

Arsintescu, L., Chachad, R., Gregory, K. B., Mulligan, J. B., & Flynn-Evans, E. E. (2020). The relationship between workload, performance and fatigue in a short-haul airline. *Chronobiology International*, *37*(9–10), 1492–1494. https://doi.org/10.1080/07420528.2020.1804924

Bazilinskyy, P., Petermeijer, S., Petrovych, V., Dodou, D., & de Winter, J. C. F. (2018). Take-over requests in highly automated driving: A crowdsourcing survey on auditory, vibrotactile, and visual displays. *Transportation Research Part F: Traffic Psychology and Behaviour*, *56*, 82–98. https://doi.org/10.1016/j.trf.2018.04.001

Beggiato, M., Hartwich, F., Schleinitz, K., Krems, J. F., Othersen, I., & Petermann-Stock, I. (2015). What would drivers like to know during automated driving? Information needs at different levels of automation. *7th Conference on Driver Assistance*. https://doi.org/10.13140/RG.2.1.2462.6007

Bengler, K., Dietmayer, K., Farber, B., Maurer, M., Stiller, C., & Winner, H. (2014, December 1). Three decades of driver assistance systems: Review and future perspectives. *IEEE Intelligent Transportation Systems Magazine*, Vol. 6, pp. 6–22. https://doi.org/10.1109/MITS.2014.2336271

Bengler, K., Drüke, J., Hoffmann, S., Manstetten, D., & Neukum, A. (2018). UR:BAN Human Factors in Traffic. In *UR:BAN Human Factors in Traffic*. https://doi.org/10.1007/978-3-658-15418-9

Benjamin, K. (1921). *Patent No. US1471168A*.

Berton, R. J. (1968). Whiplash: Tests of the influential variables. *SAE Technical Papers*. https://doi.org/10.4271/680080

Bhise, V. D. (2016). *Ergonomics in the Automotive Design Process*. https://doi.org/10.1201/b11237

BMW Group. (2020a). BMW M4 Design Study by KITH and Ronnie Fiegs E30 [Image]. Retrieved December 4, 2020, from https://www.press.bmwgroup.com/global/photo/detail/P90403307/bmw-m4-design-study-by-kith-and-ronnie-fiegs-e30-10/2020

BMW Group. (2020b). MINI Vision Urbanaut [Image]. Retrieved December 4, 2020, from https:/

/www.press.bmwgroup.com/global/photo/compilation/T0320384EN/mini-vision-urbanaut-make-it-your-space

BMW Group. (2020c). The BMW Group at the Consumer Electronics Show (CES) 2020 in Las Vegas. Retrieved March 29, 2020, from BMW Group PressClub website: https://www.press.bmwgroup.com/global/article/detail/T0304187EN/the-bmw-group-at-the-consumer-electronics-show-ces-2020-in-las-vegas

Boehm, B. (1986). A spiral model of software development and enhancement. *ACM SIGSOFT Software Engineering Notes*, *11*(4), 22–42. https://doi.org/10.1145/12944.12948

Boehm, B., & Turner, R. (2004). *Balancing agility and discipline : a guide for the perplexed*. Boston: Addison-Wesley.

Bohlin, N. I. (1967). A statistical analysis of 28,000 accident cases with emphasis on occupant restraint value. *SAE Technical Papers*. https://doi.org/10.4271/670925

Bohrmann, D., & Bengler, K. (2020). Reclined Posture for Enabling Autonomous Driving. *Advances in Intelligent Systems and Computing*, *1026*, 169–175. https://doi.org/10.1007/978-3-030-27928-8_26

Bolhin, N. (1959). *Patent No. US3043625A*. US.

Brose. (2019). IAA 2019 : Enter the interior of the future with Brose. Retrieved December 4, 2020, from https://www.brose.com/de-en/press/2019/iaa-2019-enter-the-interior-of-the-future-with-brose.html

Bubb, H. (2015a). Gestaltung der Konditionssicherheit. In *Automobilergonomie* (pp. 471–523). https://doi.org/10.1007/978-3-8348-2297-0_8

Bubb, H. (2015b). Menschmodelle. In *Automobilergonomie* (pp. 221–258). https://doi.org/10.1007/978-3-8348-2297-0_5

Bubb, H., Bengler, K., Breuninger, J., Gold, C., & Helmbrecht, M. (2015). Systemergonomie des Fahrzeugs. In *Automobilergonomie* (pp. 259–344). https://doi.org/10.1007/978-3-8348-2297-0_6

Bubb, H., Grünen, R. E., & Remlinger, W. (2015). Anthropometrische Fahrzeuggestaltung. In *Automobilergonomie* (pp. 345–470). https://doi.org/10.1007/978-3-8348-2297-0_7

Bullinger-Hoffmann, A. C., & Mühlstedt, J. (2016). *Homo Sapiens Digitalis - Virtuelle Ergonomie und digitale Menschmodelle*. https://doi.org/10.1007/978-3-662-50459-8

Cao, S., Tang, P., & Sun, X. (2020). Driver Take-Over Reaction in Autonomous Vehicles with Rotatable Seats. *Safety*, *6*(3), 34. https://doi.org/10.3390/safety6030034

Capaldo, F. S. (2012). Road Sight Design and Driver Eye Height: Experimental Measures. *Procedia - Social and Behavioral Sciences*, *53*, 731–740. https://doi.org/10.1016/j.sbspro.2012.09.923

Cohen, A., & Einav, L. (2003). The effects of mandatory seat belt laws on driving behavior and traffic fatalities. *Review of Economics and Statistics*, *85*(4), 828–843. https://doi.org/10.1162/003465303772815754

Cohen, J. (1988). *Statistical Power Analysis for the Behavioral Sciences*. https://doi.org/10.4324/9780203771587

Cole, R. J. (1989). Postural baroreflex stimuli may affect EEG arousal and sleep in humans. *Journal of Applied Physiology*, *67*(6), 2369–2375. https://doi.org/10.1152/jappl.1989.67.6.2369

Coll, R., & Coll, J. H. (1989). Cognitive match interface design, a base concept for guiding the development of user friendly computer application packages. *Journal of Medical Systems*, *13*(4), 227–235. https://doi.org/10.1007/BF00996646

Collier, K. (2012). *Agile analytics : a value-driven approach to business intelligence and data warehousing*. Amsterdam: Addison-Wesley.

Conti, A., Prasch, L., Danner, S., Gleissl, B., Petermeijer, B., Zimmermann, M., … Scotto, M. (2020). Interaction Prototyping. Retrieved March 14, 2021, from The practical course Interaction Prototyping at the Chair of Ergonomics, Technical University of Munich website: https://interactionprototyping.github.io/exercises_2.0/index.html

Cools, R. (2010). N-Back Test. In I. P. Stolerman (Ed.), *Encyclopedia of Psychopharmacology* (p. 822). https://doi.org/10.1007/978-3-540-68706-1_1625

Daimler AG. (2002). The PRE-SAFE® occupant protection system. Retrieved March 6, 2021, from https://media.daimler.com/marsMediaSite/de/instance/ko/PRE-SAFE-Praeventiver-Insassenschutz-verringert-die-Unfallbelastungen-um-bis-zu-40-Prozent.xhtml?oid=9361558#prevId=7432319

Daimler AG. (2006). Airbag and belt tensioner – world premiere in 1981. Retrieved December 5, 2020, from https://media.daimler.com/marsMediaSite/ko/en/9913288

Daimler AG. (2020a). Benz Patent Motor Car: The first automobile [Image]. Retrieved December 4, 2020, from https://www.daimler.com/company/tradition/company-history/1885-1886.html

Daimler AG. (2020b). First-class, even in the second row. Retrieved November 22, 2020, from https://media.daimler.com/marsMediaSite/ko/en/48160625

Daimler AG. (2020c). Mercedes-Benz 600 and 600 Pullman (W100) [Image]. Retrieved December 6, 2020, from https://mercedes-benz-publicarchive.com/marsClassic/en/instance/ko/600-and-600-Pullman-W-100-1963---1981.xhtml?oid=5048

Damböck, D. (2013). *Automationseffekte im Fahrzeug – von der Reaktion zur Übernahme (Dissertation)*. Chair of Ergonomics, Department of Mechanical Engineering, Technical University of Munich, Munich, Germany.

Damon, A., Stoudt, H. W., & McFarland, R. A. (1966). *The human body in equipment design*. Retrieved from http://www.hup.harvard.edu/catalog.php?isbn=9780674491892

de Winter, J., Happee, R., Martens, M., & Stanton, N. (2014). Effects of adaptive cruise control and highly automated driving on workload and situation awareness: A review of the empirical evidence. *Transportation Research Part F: Traffic Psychology and Behaviour*, *27*, 196–217. https://doi.org/10.1016/j.trf.2014.06.016

Diels, C., & Bos, J. E. (2016). Self-driving carsickness. *Applied Ergonomics*, *53*, 374–382. https://doi.org/10.1016/j.apergo.2015.09.009

Dozza, M. (2013). What factors influence drivers' response time for evasive maneuvers in real traffic? *Accident Analysis & Prevention*, *58*, 299–308. https://doi.org/10.1016/j.aap.2012.06.003

Embrey, D. (2005). Human Error Understanding Human Behaviour and Error. *Human Reliability Associates*, *1*.

Endsley, M. R. (1988). Design and Evaluation of System Awareness Enhancement. *Human Factors and Ergonomics Society Annual Meeting*, (August), 97–101. https://doi.org/10.1177/154193128803200221

Endsley, M. R. (1997). Supporting situation awareness in aviation systems. *IEEE International Conference on Systems, Man, and Cybernetics. Computational Cybernetics and Simulation*, *5*, 4177–4181. https://doi.org/10.1109/ICSMC.1997.637352

Eriksson, A., Banks, V. A., & Stanton, N. A. (2017). Transition to manual: Comparing simulator with on-road control transitions. *Accident Analysis and Prevention*, *102*, 227–234. https://

doi.org/10.1016/j.aap.2017.03.011

Eriksson, Alexander, & Stanton, N. A. (2017). Takeover Time in Highly Automated Vehicles: Noncritical Transitions to and from Manual Control. *Human Factors*, *59*(4), 689–705. https://doi.org/10.1177/0018720816685832

Feldhütter, A., Gold, C., Hüger, A., & Bengler, K. (2016). Trust in Automation as a Matter of Media Influence and Experi-ence of Automated Vehicles. *Proceedings of the Human Factors and Ergonomics Society Annual Meeting*, *60*(1), 2024–2028. https://doi.org/10.1177/1541931213601460

Feldhütter, A., Kroll, D., & Bengler, K. (2018). Wake Up and Take Over! the Effect of Fatigue on the Take-over Performance in Conditionally Automated Driving. *IEEE Conference on Intelligent Transportation Systems, Proceedings, ITSC*, 2080–2085. https://doi.org/10.1109/ITSC.2018.8569545

Feldhütter, A., Ruhl, A., Feierle, A., & Bengler, K. (2019). The Effect of Fatigue on Take-over Performance in Urgent Situations in Conditionally Automated Driving. *IEEE Conference on Intelligent Transportation Systems, Proceedings, ITSC*, 1889–1894. https://doi.org/10.1109/ITSC.2019.8917183

Ferdinand, A. O., & Menachemi, N. (2014). Associations Between Driving Performance and Engaging in Secondary Tasks: A Systematic Review. *American Journal of Public Health*, *104*(3), e39–e48. https://doi.org/10.2105/AJPH.2013.301750

Fitzen, F., Amereller, M., & Paetzold, K. (2018). Approximation of the User Behaviour in a Fully Automated Vehicle Referring To a Stationary Prototype-Based Research Study. *DS 92: Proceedings of the DESIGN 2018 15th International Design Conference*, 2187–2196. https://doi.org/10.21278/idc.2018.0130

Flemisch, F., Bengler, K., Bubb, H., Winner, H., & Bruder, R. (2014). Towards cooperative guidance and control of highly automated vehicles: H-Mode and Conduct-by-Wire. *Ergonomics*, *57*(3), 343–360. https://doi.org/10.1080/00140139.2013.869355

Flemisch, F., Heesen, M., Hesse, T., Kelsch, J., Schieben, A., & Beller, J. (2012). Towards a dynamic balance between humans and automation: Authority, ability, responsibility and control in shared and cooperative control situations. *Cognition, Technology and Work*, *14*(1), 3–18. https://doi.org/10.1007/s10111-011-0191-6

Flemisch, F., Kelsch, J., Löper, C., Schieben, A., Schindler, J., & Heesen, M. (2008). Cooperative Control and Active Interfaces for Vehicle Assitsance and Automation. *FISITA World Automotive Congress 2008*. Retrieved from https://elib.dlr.de/57618/

Flemisch, F., Kelsch, J., Schieben, A., & Schindler, J. (2006). Stücke des Puzzles hochautomatisiertes Fahren: H-Metapher und H-Mode, Zwischenbericht 2006. In C. Stiller & M. Maurer (Eds.), *Workshop Fahrerassistenz* (pp. 60–69). Retrieved from https://elib.dlr.de/45248/

Flemisch, F., Schieben, A., Kelsch, J., & Löper, C. (2008). Automation spectrum, inner / outer compatibility and other potentially useful human factors concepts for assistance and automation. *Annual Meeting Human Factors & Ergonomics Society, European Chapter*. Braunschweig: Shaker Publishing.

Flemisch, F., Schieben, A., Schoemig, N., Strauss, M., Lueke, S., & Heyden, A. (2011). Design of human computer interfaces for highly automated vehicles in the EU-project HAVEit. *Lecture Notes in Computer Science (Including Subseries Lecture Notes in Artificial Intelligence and Lecture Notes in Bioinformatics)*, *6767 LNCS*(PART 3), 270–279. https://doi.org/10.1007/978-3-642-21666-4_30

Foley, J., Young, R., Angell, L., & Domeyer, J. (2013). Towards Operationalizing Driver Distraction. *Driving Assessment Conference*. https://doi.org/10.17077/drivingassessment.1467

Ford Motor Company. (2020). The Model T [Image]. Retrieved December 4, 2020, from https://corporate.ford.com/articles/history/the-model-t.html

Forster, Y., Naujoks, F., Neukum, A., & Huestegge, L. (2017). *Driver compliance to take-over requests with different auditory outputs in conditional automation*. https://doi.org/10.1016/j.aap.2017.09.019

Gasser, T. M., Arzt, C., Ayoubi, M., Bartels, A., Bürkle, L., Eier, J., … Vogt, W. (2012). Rechtsfolgen zunehmender Fahrzeugautomatisierung. In *Wirtschaftsverlag N. W. Verlag für neue Wissenschaft*. Retrieved from https://bast.opus.hbz-nrw.de/opus45-bast/frontdoor/deliver/index/docId/541/file/F83.pdf

Gasser, T. M., & Westhoff, D. (2012). *BASt-study: Definitions of Automation and Legal Issues in Germany Legal Issues in Germany*. Retrieved from http://onlinepubs.trb.org/onlinepubs/conferences/2012/Automation/presentations/Gasser.pdf

Gaylor, L., Junge, M., & Abanteriba, S. (2017). Efficacy of seat-mounted thoracic side airbags in the German vehicle fleet. *Traffic Injury Prevention*, *18*(8), 852–858. https://doi.org/10.1080/15389588.2017.1316843

Geiser, G. (1985). Mensch-Maschine-Kommunikation im Kraftfahrzeug. *Automobiltechnische Zeitschrift : ATZ*, *87*(Nr.2), 77–84.

Geisler, C., Schöneburg, R., Feese, J., Gärtner, E., Öztürk, A., Richert, D. J., & Warwel, J. (2019). New driver safety concept for automated and manual driving mode. *The Proceeding of 26th Enhanced Safety of Vehicles Conference*, 463–466. https://doi.org/978-1-5108-8887-6

General Motors. (2012). Front Bench Takes a Back Seat [Image]. Retrieved December 4, 2020, from https://media.gm.com/media/us/en/gm/news.detail.html/content/Pages/news/us/en/2012/Sep/0928_bench_seat.html

Gerlicher, M. (2017). *Study about the influence of the driver's seat adjustment and the body posture on the take-over of the driving task in highly automated driving (unpublished semester thesis)*. Chair of Ergonomics, Department of Mechanical Engineering, Technical University of Munich, Munich, Germany.

Gerlicher, M. (2019). *Study about the influence of an automatically moving seat on the take-over of the driving task during highly automated driving (unpublished Master's thesis)*. Chair of Ergonomics, Department of Mechanical Engineering, Technical University of Munich, Munich, Germany.

Gold, C. (2016). *Modeling of Take-Over Situations in Highly Automated Vehicle Guidance (Dissertation)*. Chair of Ergonomics, Department of Mechanical Engineering, Technical University of Munich, Munich, Germany.

Gold, C., Damböck, D., Bengler, K., & Lorenz, L. (2013). Partially Automated Driving as a Fallback Level of High Automation. *6. Tagung Fahrerassistenz*. Munich: TÜV SÜD Akademie GmbH.

Gold, C., Damböck, D., Lorenz, L., & Bengler, K. (2013). "Take over!" How long does it take to get the driver back into the loop? *Proceedings of the Human Factors and Ergonomics Society Annual Meeting*, *57*(1), 1938–1942. https://doi.org/10.1177/1541931213571433

Gold, C., Körber, M., Lechner, D., & Bengler, K. (2016). Taking Over Control From Highly Automated Vehicles in Complex Traffic Situations: The Role of Traffic Density. *Human Factors: The Journal of the Human Factors and Ergonomics Society*, *58*(4), 642–652. https://doi.org/10.1177/0018720816634226

Gonçalves, J., Happee, R., & Bengler, K. (2016). Drowsiness in conditional automation: Proneness, diagnosis and driving performance effects. *IEEE Conference on Intelligent Transportation Systems,*

Proceedings, ITSC, 873–878. https://doi.org/10.1109/ITSC.2016.7795658

Grabner, J., & Nothhaft, R. (2002). Konstruieren von Pkw-Karosserien. In *Konstruieren von Pkw-Karosserien*. https://doi.org/10.1007/978-3-662-08158-7

Grandjean, E., & Hünting, W. (1977). Ergonomics of posture-Review of various problems of standing and sitting posture. *Applied Ergonomics*, *8*(3), 135–140. https://doi.org/10.1016/0003-6870(77)90002-3

Green, P. (1999). Estimating Compliance with the 15-Second Rule for Driver-Interface Usability and Safety. *Proceedings of the Human Factors and Ergonomics Society Annual Meeting*, *43*(18), 987–991. https://doi.org/10.1177/154193129904301809

Grey, P. (2016). *A History of Travel in 50 Vehicles* (1st editio; P. Hoose, Ed.). Tilbury House Publishers.

Grier, R. A. (2015). How High is High? A Meta-Analysis of NASA-TLX Global Workload Scores. *Proceedings of the Human Factors and Ergonomics Society Annual Meeting*, *59*(1), 1727–1731. https://doi.org/10.1177/1541931215591373

Grünen, R. E., Günzkofer, F., & Bubb, H. (2015). Anatomische und anthropometrische Eigenschaften des Fahrers. In H. Bubb, K. Bengler, R. E. Grünen, & M. Vollrath (Eds.), *Automobilergonomie* (pp. 163–219). https://doi.org/10.1007/978-3-8348-2297-0_4

Guo, J. (2019). *Tobeedited: Study about the influence of an automatically moving seat on the take-over of the driving task during highly automated driving (unpublished Master's thesis)*. Chair of Ergonomics, Department of Mechanical Engineering, Technical University of Munich, Munich, Germany.

Hale, K. S., & Stanney, K. M. (2004). Deriving haptic design guidelines from human physiological, psychophysical, and neurological foundations. *IEEE Computer Graphics and Applications*, *24*(2), 33–39. https://doi.org/10.1109/MCG.2004.1274059

Happee, R., Gold, C., Radlmayr, J., Hergeth, S., & Bengler, K. (2017). Take-over performance in evasive manoeuvres. *Accident Analysis and Prevention*, *106*, 211–222. https://doi.org/10.1016/j.aap.2017.04.017

Hart, S. G. (2006). Nasa-Task Load Index (NASA-TLX); 20 Years Later. *Proceedings of the Human Factors and Ergonomics Society Annual Meeting*, *50*(9), 904–908. https://doi.org/10.1177/154193120605000909

Hart, S. G., & Staveland, L. E. (1988). Development of NASA-TLX (Task Load Index): Results of Empirical and Theoretical Research. *Advances in Psychology*, *52*(C), 139–183. https://doi.org/10.1016/S0166-4115(08)62386-9

Hartson, H. R., & Hix, D. (1989). Human-computer interface development: concepts and systems for its management. *ACM Computing Surveys*. https://doi.org/10.1145/62029.62031

Hecht, T., Darlagiannis, E., & Bengler, K. (2020). Non-driving Related Activities in Automated Driving – An Online Survey Investigating User Needs. *Advances in Intelligent Systems and Computing*, *1026*, 182–188. https://doi.org/10.1007/978-3-030-27928-8_28

Hecht, T., Feldhütter, A., Draeger, K., & Bengler, K. (2020). What do you do? An analysis of non-driving related activities during a 60 minutes conditionally automated highway drive. *Advances in Intelligent Systems and Computing*, *1018*, 28–34. https://doi.org/10.1007/978-3-030-25629-6_5

Heckler, B., Wohlpart, M., & Bengler, K. (2019). Anthropometric factors in seat comfort evaluation: Identification and quantification of body dimensions affecting seating comfort. *Advances in Intelligent Systems and Computing*, *826*, 612–622. https://doi.org/10.1007/978-3-319-96065-4_65

Helldin, T., Falkman, G., Riveiro, M., & Davidsson, S. (2013). Presenting system uncertainty in automotive UIs for supporting trust calibration in autonomous driving. *Proceedings of the 5th International Conference on Automotive User Interfaces and Interactive Vehicular Applications - AutomotiveUI '13*, 210–217. https://doi.org/10.1145/2516540.2516554

Hergeth, S., Lorenz, L., & Krems, J. F. (2017). Prior Familiarization With Takeover Requests Affects Drivers' Takeover Performance and Automation Trust. *Human Factors*, *59*(3), 457–470. https://doi.org/10.1177/0018720816678714

Hirao, A., Kato, K., Kitazaki, S., & Yamazaki, N. (2007). Evaluations of physical fatigue during long-term driving with a new driving posture. *SAE Technical Papers*. https://doi.org/10.4271/2007-01-0348

Hirao, A., Kitazaki, S., & Yamazaki, N. (2006). Development of a new driving posture focused on biomechanical loads. *SAE Technical Papers*. https://doi.org/10.4271/2006-01-1302

Hoffmann, J., & Gayko, J. E. (2012). Fahrerwarnelemente. In *Handbuch Fahrerassistenzsysteme* (pp. 343–354). https://doi.org/10.1007/978-3-8348-8619-4_25

Huemer, A. K., & Vollrath, M. (2012). Ablenkung durch fahrfremde Tätigkeiten - Machbarkeitsstudie. *BASt-Bericht M 225*. Retrieved from https://www.bast.de/BASt_2017/DE/Publikationen/Berichte/unterreihe-m/2013-2012/m225.html

ISO 9241-210. (2010). *Ergonomics of human-system interaction -- Part 210: Human-centred design for interactive systems* (p. 32). p. 32. Retrieved from https://www.iso.org/standard/52075.html

Jamson, A. H., Merat, N., Carsten, O. M. J., & Lai, F. C. H. (2013). Behavioural changes in drivers experiencing highly-automated vehicle control in varying traffic conditions. *Transportation Research Part C: Emerging Technologies*, *30*, 116–125. https://doi.org/10.1016/j.trc.2013.02.008

Jarosch, O., Kuhnt, M., Paradies, S., & Bengler, K. (2017). *It's Out of Our Hands Now! Effects of Non-Driving Related Tasks During Highly Automated Driving on Drivers' Fatigue*. 319–325. https://doi.org/10.17077/drivingassessment.1653

Johns, M. W. (2000). A sleep physiologist's view of the drowsy driver. *Transportation Research Part F: Traffic Psychology and Behaviour*, *3*(4), 241–249. https://doi.org/10.1016/S1369-8478(01)00008-0

Jonsson, B., Stenlund, H., Svensson, M. Y., & Björnstig, U. (2008). Seat adjustment - Capacity and repeatability among occupants in a modern car. *Ergonomics*, *51*(2), 232–241. https://doi.org/10.1080/00140130701561793

Jorlöv, S., Bohman, K., & Larsson, A. (2017). Seating positions and activities in highly automated cars - A qualitative study of future automated driving scenarios. *Conference Proceedings International Research Council on the Biomechanics of Injury, IRCOBI*, *2017-Septe*, 13–22.

Kaber, D. B., & Endsley, M. R. (1997). Out-of-the-loop performance problems and the use of intermediate levels of automation for improved control system functioning and safety. *Process Safety Progress*, *16*(3), 126–131. https://doi.org/10.1002/prs.680160304

Kamp, I., Kilincsoy, Ü., & Vink, P. (2011). Chosen postures during specific sitting activities. *Ergonomics*, *54*(11), 1029–1042. https://doi.org/10.1080/00140139.2011.618230

Kang, S. J., & Chun, B. K. (2000). Effective approach to prediction of the collapse mode in automotive seat structure. *Thin-Walled Structures*, *37*(2), 113–125. https://doi.org/10.1016/S0263-8231(00)00014-8

Kerschbaum, P. (2018). *Design for Automation : The Steering Wheel in Highly Automated Cars (Dissertation)*. Chair of Ergonomics, Department of Mechanical Engineering, Technical University of Munich, Munich, Germany.

Kerschbaum, P., Lorenz, L., & Bengler, K. (2015). A transforming steering wheel for highly automated cars. *IEEE Intelligent Vehicles Symposium, Proceedings*, *2015-Augus*, 1287–1292. https://doi.org/10.1109/IVS.2015.7225893

Kiesel, A., Steinhauser, M., Wendt, M., Falkenstein, M., Jost, K., Philipp, A. M., & Koch, I. (2010). Control and interference in task switching-a review. *Psychological Bulletin*, *136*(5), 849–874. https://doi.org/10.1037/a0019842

Kilincsoy, Ü., Wagner, A.-S., Bengler, K., Bubb, H., & Vink, P. (2014). *Comfortable Rear Seat Postures Preferred by Car Passengers*. (July), 823–831.

Klinkner, J. N. (2017). *Conception of an experimental set-up for researches on postures of drivers performing non-driving related activities during a highly automated drive (unpublished semester thesis)*. Chair of Ergonomics, Department of Mechanical Engineering, Technical University of Munich, Munich, Germany.

Köhler, A.-L., Pelzer, J., Seidel, K., & Ladwig, S. (2019). Sitting Postures and Activities in Autonomous Vehicles – New Requirements towards Occupant Safety. *Proceedings of the Human Factors and Ergonomics Society Annual Meeting*, *63*(1), 1874–1878. https://doi.org/10.1177/1071181319631327

Kolich, M. (2010). Occupant Preferred Back Angle Relative to Head Restraint Regulations. *SAE Int. J. Passeng. Cars – Mech. Syst.*, *3*, 626–632. https://doi.org/10.4271/2010-01-0779

Kolich, M., & Taboun, S. (2004). Ergonomics modelling and evaluation of automobile seat comfort. *Ergonomics*, *47*(8), 841–863. https://doi.org/10.1080/00140130420001932 73

König, M., & Neumayr, L. (2017). Users' resistance towards radical innovations: The case of the self-driving car. *Transportation Research Part F: Traffic Psychology and Behaviour*, *44*, 42–52. https://doi.org/10.1016/j.trf.2016.10.013

Körber, M., Gold, C., Lechner, D., & Bengler, K. (2016). The influence of age on the take-over of vehicle control in highly automated driving. *Transportation Research Part F: Traffic Psychology and Behaviour*, *39*, 19–32. https://doi.org/10.1016/j.trf.2016.03.002

Körber, M., Prasch, L., & Bengler, K. (2017). Why Do I Have to Drive Now? Post Hoc Explanations of Takeover Requests. *Human Factors*. https://doi.org/10.1177/0018720817747730

Kremser, F., Lorenz, D., Remlinger, W., & Bengler, K. (2012). Nutzerzentrierte Fahrerplatzauslegung des Elektrofahrzeugs MUTE mit dem digitalen Menschmodell RAMSIS. *Zeitschrift Für Arbeitswissenschaft*, *66*(2–3), 104–114. https://doi.org/10.1007/BF03373867

Kreuzmair, C., Gold, C., & Meyer, M.-L. (2017). The Influence of Driver Fatigue on Take-Over Performance in Highly Automated Vehicles. *25th International Technical Conference on the Enhanced Safety of Vehicles (ESV)*, 17–0199. Detroit Michigan, United States.

Kyriakidis, M., Happee, R., & De Winter, J. C. F. (2015). Public opinion on automated driving: Results of an international questionnaire among 5000 respondents. *Transportation Research Part F: Traffic Psychology and Behaviour*, *32*, 127–140. https://doi.org/10.1016/j.trf.2015.04.014

Large, D. R., Burnett, G., Morris, A., Muthumani, A., & Matthias, R. (2018). A longitudinal simulator study to explore drivers' behaviour during highly-automated driving. *Advances in Intelligent Systems and Computing*, *597*, 583–594. https://doi.org/10.1007/978-3-319-60441-1_57

Latka, J. (2020). *Nutzerzentrierte Entwicklung von Ein- und Ausstiegskonzepten im Nutzfahrzeugbereich unter der Betrachtung von Bewegungsstrategien (Dissertation)*. Chair of Ergonomics, Department of Mechanical Engineering, Technical University of Munich, Munich, Germany.

Lewis, D. (1972). *Patent No. US3841654A*.

Lipnicki, D. M., & Byrne, D. G. (2005). Thinking on your back: Solving anagrams faster when supine than when standing. *Cognitive Brain Research*, *24*(3), 719–722. https://doi.org/10.1016/j.cogbrainres.2005.03.003

Loehmann, S., & Hausen, D. (2014). Automated Driving: Shifting the Primary Task from the Center to the Periphery of Attention. *Workshop Peripheral Interaction: Shaping the Research and Design Space in 32nd SIGCHI Conference on Human Factors in Computing Systems*. Retrieved from https://www.medien.ifi.lmu.de/pubdb/publications/pub/loehmann2014chipiws/loehmann2014chipiws.pdf

Lorenz, D. (2015). *Äußere Einfl uss- parameter auf Sitzpositionen im Fahrzeug (Dissertation)*. Chair of Ergonomics, Department of Mechanical Engineering, Technical University of Munich, Munich, Germany.

Lorenz, L., Kerschbaum, P., Hergeth, S., Gold, C., & Radlmayr, J. (2015). Der Fahrer im Hochautomatisierten Fahrzeug. Vom Dual-Task zum Sequential-Task Paradigma: Ein Rückblick über Fahrsimulatorstudien. *7. Tagung Fahrerassistez*, 7. Munich, Germany.

Lorenz, L., Kerschbaum, P., & Schumann, J. (2014). Designing take over scenarios for automated driving. *Proceedings of the Human Factors and Ergonomics Society Annual Meeting*, *58*(1), 1681–1685. https://doi.org/10.1177/1541931214581351

Lorenz, S. (2011). *Assistenzsystem zur Optimierung des Sitzkomforts im Fahrzeug (Dissertation)*. Chair of Ergonomics, Department of Mechanical Engineering, Technical University of Munich, Munich, Germany.

Louw, T., Markkula, G., Boer, E., Madigan, R., Carsten, O., & Merat, N. (2017). Coming back into the loop: Drivers' perceptual-motor performance in critical events after automated driving. *Accident Analysis and Prevention*, *108*, 9–18. https://doi.org/10.1016/j.aap.2017.08.011

Lundström, J. N., Boyle, J. A., & Jones-Gotman, M. (2006). Sit up and smell the roses better: olfactory sensitivity to phenyl ethyl alcohol is dependent on body position. *Chemical Senses*, *31*(3), 249–252. https://doi.org/10.1093/chemse/bjj025

Lundström, J. N., Boyle, J. A., & Jones-Gotman, M. (2008). Body position-dependent shift in odor percept present only for perithreshold odors. *Chemical Senses*, *33*(1), 23–33. https://doi.org/10.1093/chemse/bjm059

Lutz, L., Tang, T., & Lienkamp, M. (2012). Analyse der rechtlichen Situation von teleoperierten (und autonomen) Fahrzeugen. *5. Tagung Fahrerassistenz*, 57–63. Retrieved from https://mediatum.ub.tum.de/1142084

Marberger, C., Mielenz, H., Naujoks, F., Radlmayr, J., Bengler, K., & Wandtner, B. (2017). *Understanding and Applying the Concept of "Driver Availability" in Automated Driving*. https://doi.org/10.1007/978-3-319-60441-1_58

Maurer, M., & Stiller, C. (2005). *Fahrerassistenzsysteme mit maschineller Wahrnehmung* (M. Maurer & C. Stiller, Eds.). https://doi.org/10.1007/b138667

McMurry, T. L., Poplin, G. S., Shaw, G., & Panzer, M. B. (2018). Crash safety concerns for out-of-position occupant postures: A look toward safety in highly automated vehicles. *Traffic Injury Prevention*, *19*(6), 582–587. https://doi.org/10.1080/15389588.2018.1458306

Melcher, V., Rauh, S., Diederichs, F., Widlroither, H., & Bauer, W. (2015). Take-Over Requests for Automated Driving. *Procedia Manufacturing*, *3*, 2867–2873. https://doi.org/10.1016/j.promfg.2015.07.788

Menache, A. (2011). *Understanding motion capture for computer animation* (Second Edi). https://doi.org/

https://doi.org/10.1016/C2009-0-62989-5

Merat, N., Jamson, A. H., Lai, F. C. H., Daly, M., & Carsten, O. M. J. (2014). Transition to manual: Driver behaviour when resuming control from a highly automated vehicle. *Transportation Research Part F: Traffic Psychology and Behaviour*, *27*(PB), 274–282. https://doi.org/10.1016/j.trf.2014.09.005

Merrett, F. (2006). Reflections on the Hawthorne Effect. *Educational Psychology*, *26*(1), 143–146. https://doi.org/10.1080/01443410500341080

Minderhoud, M. M., & Bovy, P. H. L. (2001). Extended time-to-collision measures for road traffic safety assessment. *Accident Analysis & Prevention*, *33*(1), 89–97. https://doi.org/10.1016/S0001-4575(00)00019-1

Mount, F. E., Whitmore, M., & Stealey, S. L. (2003). Evaluation of Neutral Body Posture on Shuttle Mission STS-57 (SPACEHAB-1). *NASA TM−2003-104805*. Retrieved from https://ston.jsc.nasa.gov/collections/TRS/_techrep/TM-2003-104805revA.pdf

Mroz, K., Pipkorn, B., Cecilia Sunnevång, Eggers, A., & Bråse, D. (2018). Evaluation of Adaptive Belt Restraint Systems for the Protection of Elderly Occupants in Frontal Impacts. *IRCOBI Conference 2018*, 470–479. Athena, Greece.

Muehlhan, M., Marxen, M., Landsiedel, J., Malberg, H., & Zaunseder, S. (2014). The effect of body posture on cognitive performance: a question of sleep quality. *Frontiers in Human Neuroscience*, *8*(MAR), 171. https://doi.org/10.3389/fnhum.2014.00171

Mueller, M. (1999). *Thunderbird Milestones* (First Edit; C. Batio, Ed.). MBI Publishing Company.

Mulgund, S., Stokes, J. F., Turieo, M. J., & Devine, M. A. (2002). *Human/Machine Interface Modalities for Soldier Systems Technologies (Report No. 71950-00)*. Retrieved from https://apps.dtic.mil/dtic/tr/fulltext/u2/a414918.pdf

Naujoks, F., Befelein, D., Wiedemann, K., & Neukum, A. (2018). A review of non-driving-related tasks used in studies on automated driving. *Advances in Intelligent Systems and Computing*, *597*, 525–537. https://doi.org/10.1007/978-3-319-60441-1_52

Naujoks, F., Purucker, C., & Neukum, A. (2016). Secondary task engagement and vehicle automation - Comparing the effects of different automation levels in an on-road experiment. *Transportation Research Part F: Traffic Psychology and Behaviour*, *38*, 67–82. https://doi.org/10.1016/j.trf.2016.01.011

Naujoks, F., Purucker, C., Neukum, A., Wolter, S., & Steiger, R. (2015). Controllability of Partially Automated Driving functions – Does it matter whether drivers are allowed to take their hands off the steering wheel? *Transportation Research Part F: Traffic Psychology and Behaviour*, *35*, 185–198. https://doi.org/10.1016/J.TRF.2015.10.022

NHTSA. (2004). *Federal Motor Vehicle Safety Standards Final rule-Head Restraints (Docket No. NHTSA-2004-19807)*. National Highway Traffic Safety Administration, United States Department of Transportation.

NHTSA. (2011a). *Head Restraints - Dimensional and Static Testing (TP-202aS-01)*. National Highway Traffic Safety Administration, United States Department of Transportation.

NHTSA. (2011b). *Quick Reference Guide to Federal Motor Vehicle Safety Standards and Regulations (DOT HS 811 439)*. National Highway Traffic Safety Administration, United States Department of Transportation.

NHTSA. (2014). *Visual-Manual NHTSA Driver Distraction Guidelines for In-Vehicle Electronic Devices (Docket No. NHTSA-2010-0053)*. National Highway Traffic Safety Administration, United States Department of Transportation.

NHTSA. (2016). *Visual-Manual NHTSA Driver Distraction Guidelines for Portable and Aftermarket Devices (Docket No. NHTSA-2013-0137)*. National Highway Traffic Safety Administration, United States Department of Transportation.

Nielsen, J. (1994). Guerrilla HCI: Using Discount Usability Engineering to Penetrate the Intimidation Barrier. Retrieved March 14, 2021, from Nielsen Norman Group website: https://www.nngroup.com/articles/guerrilla-hci/

Ohmori, N., & Harata, N. (2008). How different are activities while commuting by train? A case in Tokyo. *Tijdschrift Voor Economische En Sociale Geografie*, *99*(5), 547–561. https://doi.org/10.1111/j.1467-9663.2008.00491.x

Östling, M. (2017). Potential Benefit of a 3+2 Criss Cross Seat Belt System in Frontal and Oblique Crashes. *Proceedings of IRCOBI Conference*. Retrieved from http://www.ircobi.org/wordpress/downloads/irc17/pdf-files/57.pdf

Östling, M., & Larsson, A. (2019). Occupant Activities and Sitting Positions in Automated Vehicles in China and Sweden. *The 26th International Technical Conference on the Enhanced Safety of Vehicles (ESV) At: Eindhoven, Netherlands*, (June), Paper No. 19-0083. Retrieved from http://indexsmart.mirasmart.com/26esv/PDFfiles/26ESV-000083.pdf

Östling, M., & Sunnevång, C. (2017). Potential future seating positions and the impact on injury risks in a Learning Intelligent Vehicle (LIV). *11. VDI-Tagung Fahrzeugsicherheit*. Berlin.

Otat, O. V., Otat, V., Tutunea, D., Geonea, I., & Marinescu, G. (2019). *The Monitoring of the Submarine Effect in Frontal Collisions, at Different Impact Speeds and for the Driver's Out of Position Instances*. https://doi.org/10.1007/978-3-319-94409-8_93

Park, S. J., Kim, C. B., Kim, C. J., & Lee, J. W. (1998). Comfortable driving postures for Koreans. *International Journal of Industrial Ergonomics*, *26*(4), 489–497. https://doi.org/10.1016/S0169-8141(00)00020-2

Payre, W., Cestac, J., & Delhomme, P. (2016). Fully Automated Driving: Impact of Trust and Practice on Manual Control Recovery. *Human Factors*, *58*(2), 229–241. https://doi.org/10.1177/0018720815612319

Petermeijer, S. (2017). *A vibrotactile interface to support the driver during the take-over process (Dissertation)*. Chair of Ergonomics, Department of Mechanical Engineering, Technical University of Munich, Munich, Germany.

Petermeijer, S., Bazilinskyy, P., Bengler, K., & de Winter, J. (2017). Take-over again: Investigating multimodal and directional TORs to get the driver back into the loop. *Applied Ergonomics*, *62*, 204–215. https://doi.org/10.1016/j.apergo.2017.02.023

Petermeijer, S., De Winter, J. C. F., & Bengler, K. J. (2016, April 1). Vibrotactile Displays: A Survey with a View on Highly Automated Driving. *IEEE Transactions on Intelligent Transportation Systems*, Vol. 17, pp. 897–907. https://doi.org/10.1109/TITS.2015.2494873

Pettersson, I., & Karlsson, I. C. M. (2015). Setting the stage for autonomous cars: A pilot study of future autonomous driving experiences. *IET Intelligent Transport Systems*, *9*(7), 694–701. https://doi.org/10.1049/iet-its.2014.0168

Pfleging, B., Rang, M., & Broy, N. (2016). Investigating user needs for non-driving-related activities during automated driving. *Proceedings of the 15th International Conference on Mobile and Ubiquitous Multimedia*, 91–99. https://doi.org/10.1145/3012709.3012735

Pischinger, S., & Seiffert, U. (2016). Vieweg Handbuch Kraftfahrzeugtechnik. In *Vieweg Handbuch Kraftfahrzeugtechnik*. https://doi.org/10.1007/978-3-658-09528-4

Pschenitza, M., & Unger, T. (2015). Field of vision of modern cars – a study to improve the

evaluation of car geometries based on real world accident scenarios documented in the ADAC Accident Research. *Berichte Der Bundesanstalt Fuer Strassenwesen. Unterreihe Fahrzeugtechnik*, (102), 14p. Retrieved from http://bast.opus.hbz-nrw.de/volltexte/2015/1348/pdf/F102_ESAR_komplett_CD.pdf%5Cnhttps://trid.trb.org/view/1359582

Radlmayr, J. (2020). *Take-over Performance in Conditionally Automated Driving: Effects of the Driver State and the Human-Machine-Interface (Dissertation)*. Chair of Ergonomics, Department of Mechanical Engineering, Technical University of Munich, Munich, Germany.

Radlmayr, J., & Bengler, K. (2015). Literaturanalyse und Methodenauswahl zur Gestaltung von Systemen zum hochautomatisierten Fahren. *FAT-Schriftenreihe*, *276*, 1–57. https://doi.org/10.13140/RG.2.1.2222.4401

Radlmayr, J., Gold, C., Lorenz, L., Farid, M., & Bengler, K. (2014). How Traffic Situations and Non-Driving Related Tasks Affect the Take-Over Quality in Highly Automated Driving. *Proceedings of the Human Factors and Ergonomics Society Annual Meeting*, *58*(1), 2063–2067. https://doi.org/10.1177/1541931214581434

Radlmayr, J., Ratter, M., Feldhütter, A., Körber, M., Prasch, L., Schmidtler, J., … Bengler, K. (2019). Take-Overs in Level 3 Automated Driving – Proposal of the Take-Over Performance Score (TOPS). In *20th Congress International Ergonomics Association* (pp. 436–446). https://doi.org/10.1007/978-3-319-96074-6_46

Rang, M. (2018). *Modeling body movement in the take over situation in highly automated driving based on Motion Capture Data (unpublished Master's thesis)*. Chair of Ergonomics, Department of Mechanical Engineering, Technical University of Munich, Munich, Germany.

Rasmussen, J. (1983). Skills, Rules, and Knowledge; Signals, Signs, and Symbols, and Other Distinctions in Human Performance Models. *IEEE Transactions on Systems, Man and Cybernetics*, *SMC-13*(3), 257–266. https://doi.org/10.1109/TSMC.1983.6313160

Reason, J. (1990). *Human Error*. https://doi.org/10.1017/CBO9781139062367

RECARO Automotive. (2020). RECARO Race overall program [Image]. Retrieved December 4, 2020, from https://www.recaro-automotive.com/fileadmin/00-corporate-website/pdf/en/downloads/recaro-hotsheet-p1300-gt-lw-en.pdf

Reed, M. P., Manary, M. A., Flannagan, C. A. C., & Schneider, L. W. (2000). Effects of Vehicle Interior Geometry and Anthropometric Variables on Automobile Driving Posture. *Human Factors: The Journal of the Human Factors and Ergonomics Society*, *42*(4), 541–552. https://doi.org/10.1518/001872000779698006

Reiffert, S. (2015). Daimler AG spendet Modularen Ergonomie-Prüfstand: Von der Limousine zum Lkw in wenigen Stunden. Retrieved April 13, 2019, from TUM Press statement website: https://www.tum.de/nc/die-tum/aktuelles/pressemitteilungen/detail/article/32526/

Roche, F., Thüring, M., & Trukenbrod, A. K. (2020). What happens when drivers of automated vehicles take over control in critical brake situations? *Accident Analysis and Prevention*, *144*, 105588. https://doi.org/10.1016/j.aap.2020.105588

Rogers, M., Zhang, Y., Kaber, D., Liang, Y., & Gangakhedkar, S. (2011). *The Effects of Visual and Cognitive Distraction on Driver Situation Awareness*. https://doi.org/10.1007/978-3-642-21741-8_21

Royce, D. W. W. (1970). Managing the Development of large Software Systems. *Proceedings, IEEE Wescon*. https://doi.org/10.1016/0378-4754(91)90107-E

Russell, M., Price, R., Signal, L., Stanley, J., Gerring, Z., & Cumming, J. (2011). What Do Passengers Do During Travel Time? Structured Observations on Buses and Trains. *Journal of Public Transportation*, *14*(3), 123–146. https://doi.org/10.5038/2375-0901.14.3.7

SAE J1100. (2009). SAE J1100: Motor Vehicle Dimensions. *SAE International*. Retrieved from https://www.sae.org/standards/content/j1100_200911/

SAE J3016. (2018). SAE J3016: Taxonomy and Definitions for Terms Related to Driving Automation Systems for On-Road Motor Vehicles. *SAE International*. https://doi.org/10.4271/2012-01-0107.

SAE J826. (2008). SAE J826: Devices for Use in Defining and Measuring Vehicle Seating Accommodation - SAE International. *SAE International*. Retrieved from http://standards.sae.org/wip/j826/

SAE J941. (2010). SAE J941: Motor Vehicle Drivers' Eye Locations - SAE International. *SAE International*. Retrieved from https://www.sae.org/standards/content/j941_201003/

Salter, S., Diels, C., Herriotts, P., Kanarachos, S., & Thake, D. (2019). Motion sickness in automated vehicles with forward and rearward facing seating orientations. *Applied Ergonomics*, *78*, 54–61. https://doi.org/10.1016/j.apergo.2019.02.001

Schaller, T., Schiehlen, J., & Gradenegger, B. (2008). Stauassistenz - Unterstützung des Fahrers in der Quer- und Längsführung: Systementwicklung und Kundenakzeptanz. *3. Tagung Aktive Sicherheit Durch Fahrerassistenz*.

Schenk, J., & Rigoll, G. (2010). *Mensch-Maschine-Kommunikation: Grundlagen von sprach- und bildbasierten Benutzerschnittstellen*. https://doi.org/10.1007/978-3-642-05457-0

Schmidt, S., Seiberl, W., & Schwirtz, A. (2015). Influence of different shoulder-elbow configurations on steering precision and steering velocity in automotive context. *Applied Ergonomics*, *46*(Part A), 176–183. https://doi.org/10.1016/j.apergo.2014.07.017

Schulman, D., & Shontz, F. C. (1971). Body Posture and Thinking. *Perceptual and Motor Skills*, *32*(1), 27–33. https://doi.org/10.2466/pms.1971.32.1.27

Severy, D. M., Brink, H. M., & Baird, J. D. (1967). Study of seat and head-support performance during full-scale rear-end collisions. *SAE Technical Papers*. https://doi.org/10.4271/670921

Severy, D. M., Brink, H. M., & Baird, J. D. (1968). Vehicle design for passenger protection from high-speed rear-end collisions. *SAE Technical Papers*. https://doi.org/10.4271/680774

Shah, D., Falco, P., Saveriano, M., & Lee, D. (2016). Encoding human actions with a frequency domain approach. *IEEE International Conference on Intelligent Robots and Systems*, *2016-Novem*, 5304–5311. https://doi.org/10.1109/IROS.2016.7759780

Shalev-Shwartz, S., Shammah, S., & Shashua, A. (2017). *On a Formal Model of Safe and Scalable Self-driving Cars*. Retrieved from http://arxiv.org/abs/1708.06374

Shladover, S. E., Nowakowski, C., Lu, X.-Y., & Ferlis, R. (2015). Cooperative Adaptive Cruise Control. *Transportation Research Record: Journal of the Transportation Research Board*, *2489*(1), 145–152. https://doi.org/10.3141/2489-17

Simons-Morton, B. G., Ouimet, M. C., Wang, J., Klauer, S. G., Lee, S. E., & Dingus, T. A. (2009). Hard Braking Events Among Novice Teenage Drivers By Passenger Characteristics. *Proceedings of the 5th International Driving Symposium on Human Factors in Driver Assessment, Training, and Vehicle Design : Driving Assessment 2009*, *2009*, 236–242. https://doi.org/10.17077/drivingassessment.1327

Stanley, L. M. (2006). Haptic and Auditory Cues for Lane Departure Warnings. *Proceedings of the Human Factors and Ergonomics Society Annual Meeting*, *50*(22), 2405–2408. https://doi.org/10.1177/154193120605002212

Sugioka, I. (2015). *Patent No. US9783206B2*.

Sugioka, I., Downs, J., Zinn, A., & Frasher, D. (2014). *Patent No. EP3000651B1*.

Sugioka, I., Frasher, D., & Norberg, S. (2016). *Patent No. US9908440B2*.

Surya Sengottu Velavan. (2018). Development of Occupant Restraint Systems for Future Seating Positions in Fully or Semi Autonomous Vehicles. *FISITA World Automotive Congress 2018*. Chennai, India.

Susilo, Y. O., Lyons, G., Jain, J., & Atkins, S. (2012). Rail Passengers' Time Use and Utility Assessment. *Transportation Research Record: Journal of the Transportation Research Board*, *2323*(1), 99–109. https://doi.org/10.3141/2323-12

Teoh, E. R. (2020). What's in a name? Drivers' perceptions of the use of five SAE Level 2 driving automation systems. *Journal of Safety Research*, *72*, 145–151. https://doi.org/10.1016/j.jsr.2019.11.005

Tran, C., & Trivedi, M. M. (2010). Towards a vision-based system exploring 3D driver posture dynamics for driver assistance: Issues and possibilities. *IEEE Intelligent Vehicles Symposium, Proceedings*, (ii), 179–184. https://doi.org/10.1109/IVS.2010.5547957

Tzivanopoulos, T., Watschke, H., Krasteva, P., & Vietor, T. (2015). Neue Denkansätze in der Fahrzeugkonzeption. *ATZ - Automobiltechnische Zeitschrift*, *117*(9), 16–21. https://doi.org/10.1007/s35148-015-0101-y

Ulherr, A. (2019). *Bewertung des aktuellen Vorgehens bei Diskomfortuntersuchungen im Sitzen (Dissertation)*. Chair of Ergonomics, Department of Mechanical Engineering, Technical University of Munich, Munich, Germany.

Van Der Laan, J. D., Heino, A., & De Waard, D. (1997). A simple procedure for the assessment of acceptance of advanced transport telematics. *Transportation Research Part C: Emerging Technologies*, *5*(1), 1–10. https://doi.org/10.1016/S0968-090X(96)00025-3

Viano, D. C., & Gargan, M. F. (1996). Headrest position during normal driving: Implication to neck injury risk in rear crashes. *Accident Analysis & Prevention*, *28*(6), 665–674. https://doi.org/10.1016/S0001-4575(96)00011-5

Vijayasarathy, L. R., & Butler, C. W. (2016). Choice of Software Development Methodologies: Do Organizational, Project, and Team Characteristics Matter? *IEEE Software*, *33*(5), 86–94. https://doi.org/10.1109/MS.2015.26

Vogelpohl, T., Kühn, M., Hummel, T., Gehlert, T., & Vollrath, M. (2018). Transitioning to manual driving requires additional time after automation deactivation. *Transportation Research Part F: Traffic Psychology and Behaviour*, *55*, 464–482. https://doi.org/10.1016/j.trf.2018.03.019

Volvo Car. (2009). Volvo's three-point safety belt turns 50. Retrieved December 4, 2020, from https://www.media.volvocars.com/us/en-us/media/pressreleases/20115

Waltz, G. H., & Luckett, H. (1950, July). Making the death seat safer. *Popular Science*, 83–89.

Weinbeer, V., Baur, C., Radlmayr, J., Bill, J.-S., Muhr, T., & Bengler, K. (2017). Highly automated driving: How to get the driver drowsy and how does drowsiness influence various take-over-aspects? *8. Tagung Fahrerassistenz*. München.

White, H., Large, D. R., Salanitri, D., Burnett, G. E., Lawson, A., & Box, E. (2019). Rebuilding Drivers' Situation Awareness During Take-Over Requests in Level 3 Automated Cars. In R. Charles & D. Golightly (Eds.), *Contemporary Ergonomics and Human Factors*. Retrieved from https://publications.ergonomics.org.uk/uploads/Rebuilding-drivers'-situation-awareness-during-take-over-requests-in-level-3-automated-cars.pdf

Winner, H., Hakuli, S., Lotz, F., & Singer, C. (2015). *Handbuch Fahrerassistenzsysteme* (H. Winner, S. Hakuli, F. Lotz, & C. Singer, Eds.). https://doi.org/10.1007/978-3-658-05734-3

Winner, H., & Wachenfeld, W. (2015). Auswirkungen des autonomen Fahrens auf das Fahrzeugkonzept. In *Autonomes Fahren* (pp. 265–285). https://doi.org/10.1007/978-3-662-45854-9_13

Wolf, L. (2018). *Conception and Construction of an Adjustable Seat for Take-Over Experiments of Highly Automated Driving (unpublished semester thesis)*. Chair of Ergonomics, Department of Mechanical Engineering, Technical University of Munich, Munich, Germany.

Wysocky, K. (2016). In luxury cars, the seat becomes a "seating experience." Retrieved December 5, 2020, from The British Broadcasting Corporation website: http://www.bbc.com/autos/story/20160525-building-the-perfect-drivers-seat

Yang, Y., Fleischer, M., & Bengler, K. (2020). Chicken or Egg Problem? New Challenges and Proposals of Digital Human Modeling and Interior Development of Automated Vehicles. In *10th International Conference on Applied Human Factors and Ergonomics* (pp. 453–463). https://doi.org/10.1007/978-3-030-20216-3_42

Yang, Y., Gerlicher, M., & Bengler, K. (2018). How does relaxing posture influence take-over performance in an automated vehicle? *Proceedings of the Human Factors and Ergonomics Society Annual Meeting*, *62*(1), 696–700. https://doi.org/10.1177/1541931218621157

Yang, Y., Götze, M., Laqua, A., Caccia Dominioni, G., Kawabe, K., & Bengler, K. (2017). A method to improve driver's situation awareness in automated driving. *Proceedings of the Human Factors and Ergonomics Society Europe Chapter 2017 Annual Conference*, 29–47. Rome.

Yang, Y., Karakaya, B., Dominioni, G. C., Kawabe, K., & Bengler, K. (2018). An HMI Concept to Improve Driver's Visual Behavior and Situation Awareness in Automated Vehicle. *IEEE Conference on Intelligent Transportation Systems, Proceedings, ITSC*, 650–655. https://doi.org/10.1109/ITSC.2018.8569986

Yang, Y., Klinkner, J. N., & Bengler, K. (2019). How Will the Driver Sit in an Automated Vehicle? – The Qualitative and Quantitative Descriptions of Non-Driving Postures (NDPs) When Non-Driving-Related-Tasks (NDRTs) Are Conducted. In S. Bagnara, R. Tartaglia, S. Albolino, T. Alexander, & Y. Fujita (Eds.), *Proceedings of the 20th Congress of the International Ergonomics Association* (pp. 409–420). https://doi.org/10.1007/978-3-319-96074-6_44

Yang, Y., Orlinskiy, V., Bubb, I., & Bengler, K. (2016). Development and evaluation of a method for an intuitive driver's workplace adjustment in a motor vehicle. *Proceedings of the Human Factors and Ergonomics Society Europe Chapter 2016 Annual Conference*, 107–122. Prague.

Young, K. L., Salmon, P. M., & Cornelissen, M. (2013). Missing links? The effects of distraction on driver situation awareness. *Safety Science*, *56*, 36–43. https://doi.org/10.1016/j.ssci.2012.11.004

Zeeb, K., Buchner, A., & Schrauf, M. (2015). What determines the take-over time? An integrated model approach of driver take-over after automated driving. *Accident Analysis and Prevention*, *78*, 212–221. https://doi.org/10.1016/j.aap.2015.02.023

Zeeb, K., Buchner, A., & Schrauf, M. (2016). Is take-over time all that matters? the impact of visual-cognitive load on driver take-over quality after conditionally automated driving. *Accident Analysis and Prevention*, *92*, 230–239. https://doi.org/10.1016/j.aap.2016.04.002

Zenk, R. (2008). *Objektivierung des Sitzkomforts und seine automatische Anpassung (Dissertation)*. Chair of Ergonomics, Department of Mechanical Engineering, Technical University of Munich, Munich, Germany.

Zhou, H., Zhan, J., Wang, W., & Zhang, J. (2017). Dynamic simulation of train driver under secondary impact. *Advances in Mechanical Engineering*, *9*(12), 1–10. https://doi.org/10.1177/1687814017743111

Appendix of Chapter 6 "Modeling: Take-Over Motion"

A. Captiv Motion Data (Section 6.2.7)

The applied Captiv system version was based on the IMU sensors and had no reference to the environment. The manikin's absolute position was unknown.

There were 140 measurements in the experiment, 43% of the total 324 measurements, either missing or containing obvious errors during the take-over process. These errors were, for instance, the broken torso (Figure A-1, a), displacements of body parts (Figure A-1, a and c), the collapsed avatar (Figure A-1, b), or the unrealistic body posture (Figure A-1, d).

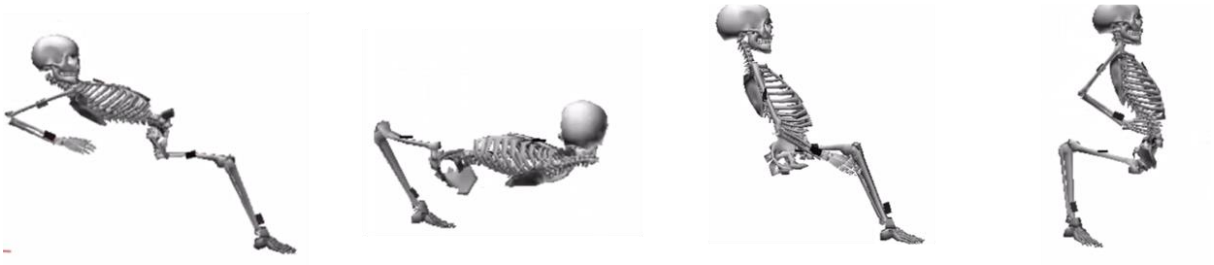

(a) (b) (c) (d)

Figure A-1 Examples of collapsed avatars

In addition to the postural errors, unrealistic and unfiltered acceleration values, e.g., over 1000 m/s^2 (converted from $°/s^2$), polluted the movement data.

Two reasons might cause the low tracking quality in this experiment: the unpredictable electromagnetic interference (EMI) in the Motion Laboratory. There were many metal parts, wireless antenna, and electronics in the laboratory. It was even difficult to get the sensors successfully calibrated at the beginning of each measurement. Another reason might be the participant's abrupt movement pattern in the take-over experiment. The participant was in a relatively stationary state for a long time before taking over: adjusting the posture, sitting still, and waiting for the RtI. The IMU sensors drifted in this phase. This stationary state was followed by a sudden, strong, and short take-over motion of the whole body, which also shook the sensors locally, causing a local displacement of the IMU sensors. The Captiv software could neither filter the signals nor export the raw data for another program. Only the distorted statistics over a certain period could be exported. Unfortunately, no proper way was found to repair and filter the corrupted data after the measurement. As a result, the Captiv data were not used for the analysis.

This should not be interpreted as a general criticism on the Captiv system, which had a wide application in other ergonomic studies, in which gentle and continuous body movement over a long time is excised. The Captiv system's main advantage against Vicon is that it has no problem with covered markers which are not seen by the camera. Captiv could be carried around and especially suitable for studies in which participants change places, e.g., ingress and egress motion (Latka, 2020). Concluding, Captiv is not recommended for the combination of the stationary state and the abrupt body motion in further take-over studies.

B. Data Pre-Processing (Section 6.2.7 and 6.3)

a) Excluded Trajectory Data

Table B-1 shows 15 excluded datasets of different setups for different analyses. The first four cases directly affect trajectory, speed, acceleration analysis. The last 11 cases are due to the criterion to separate the steering phase and the steering phase, which only affects the calculation related to the hand-on time point in the motion data: HoMT and Hand-on torso speed/acceleration.

Table B-1 Overview of the excluded data

Participant	Posture	Torso angle (°)	Knee angle (°)	Relevant analysis	Reason
3	7	50	105	Knee	Massive sensor drift
5	2	10	130	1. Hip 2. Torso speed/acceleration	Partial loss of the hip x-, y-, z-positions
	3	10	90	1. Breastbone 2. Torso speed/acceleration	Wrong calibration of the breastbone marker calibration
21	9	50	90	1. Hip 2. Torso speed/acceleration	Massive sensor drift
3	6	30	90	1. HoMT 2. Hand-on torso speed/acceleration	The cutting criterion between the hand-on phase and the steering phase: the local minimum of the right hand's y-velocity does not fit those 11 cases, where the minimums are reached in the middle of the hand-on movement.
	7	50	105		
8	2	10	130		
17	1	10	105		
	2	10	130		
	3	10	90		
25	2	10	130		
	7	50	105		
26	1	10	105		
	3	10	90		
	4	30	105		

b) Data Frequency Spectrum

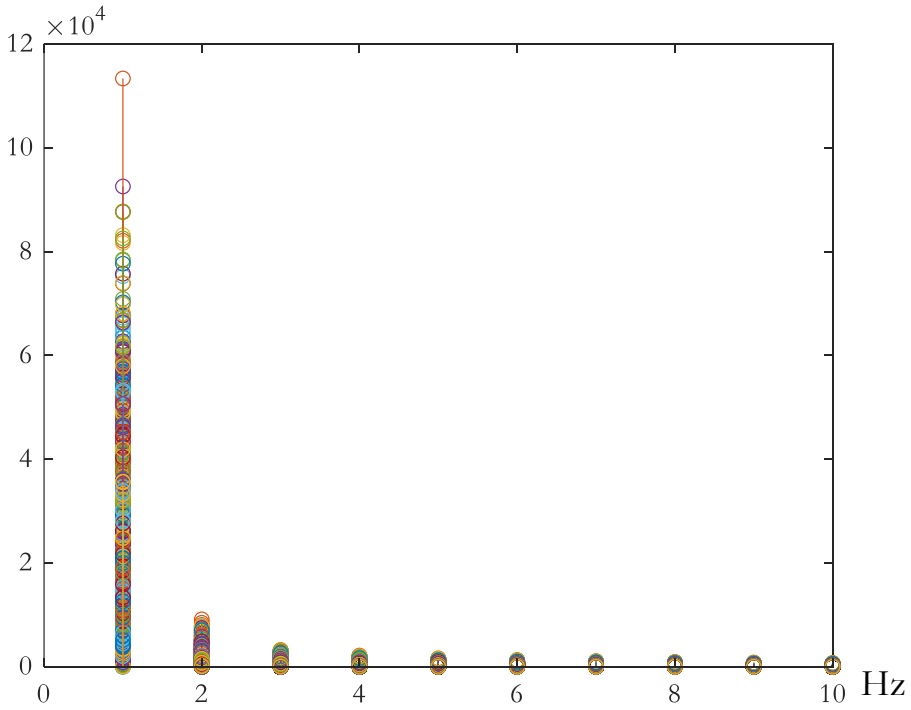

Figure B-1FFT spectrum of all filtered Vicon motion data

C. All Trajectories of the Torso, Hip, Wrist, Knee, and Ankle in the Take-Over Process (Section 6.3.1)

a) An Example in x-z, x-y, and y-z Planes

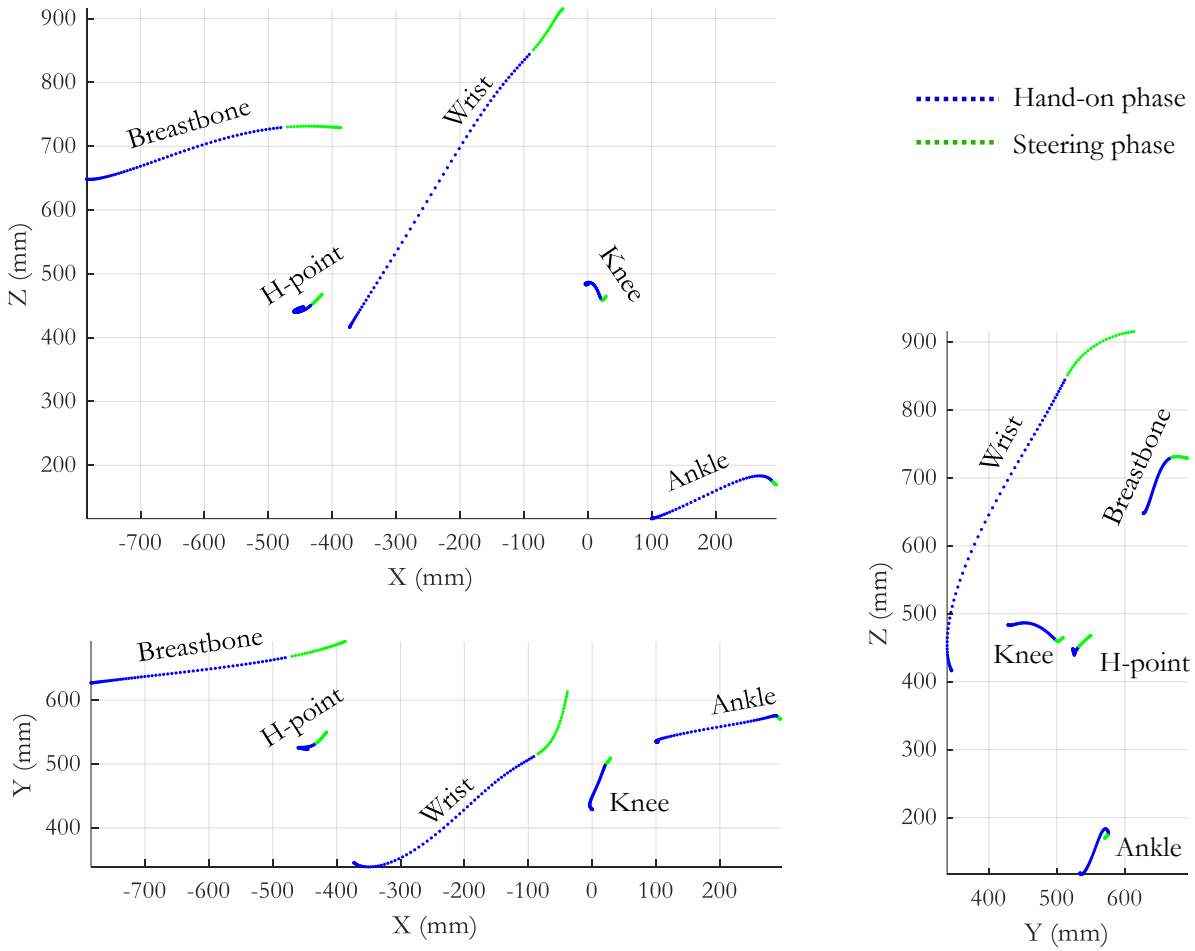

Figure C-1 An example of one participant's trajectories in Figure 6-10 in 2D: x-z, x-y, and y-z planes

b) All Trajectories in x-z, x-y, and y-z Planes

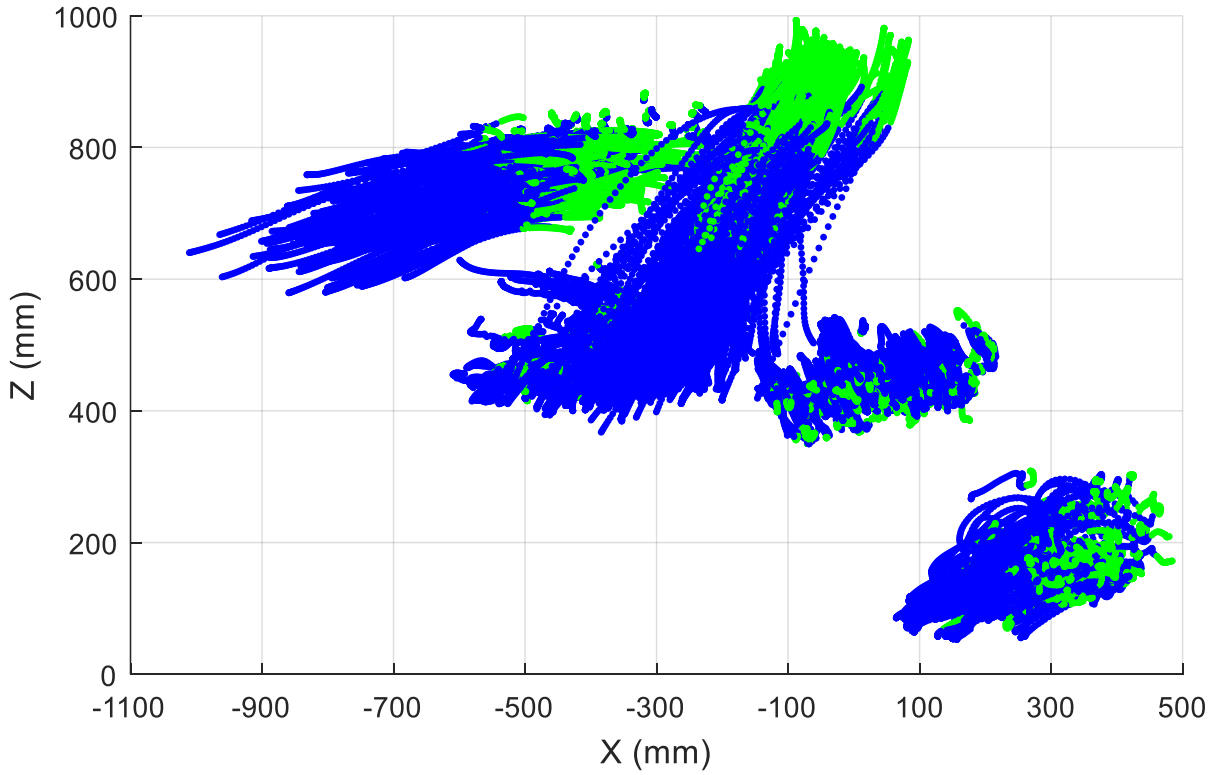

Figure C-2 All take-over trajectories of the torso, hip, wrist, knee, and ankle in the x-z plane

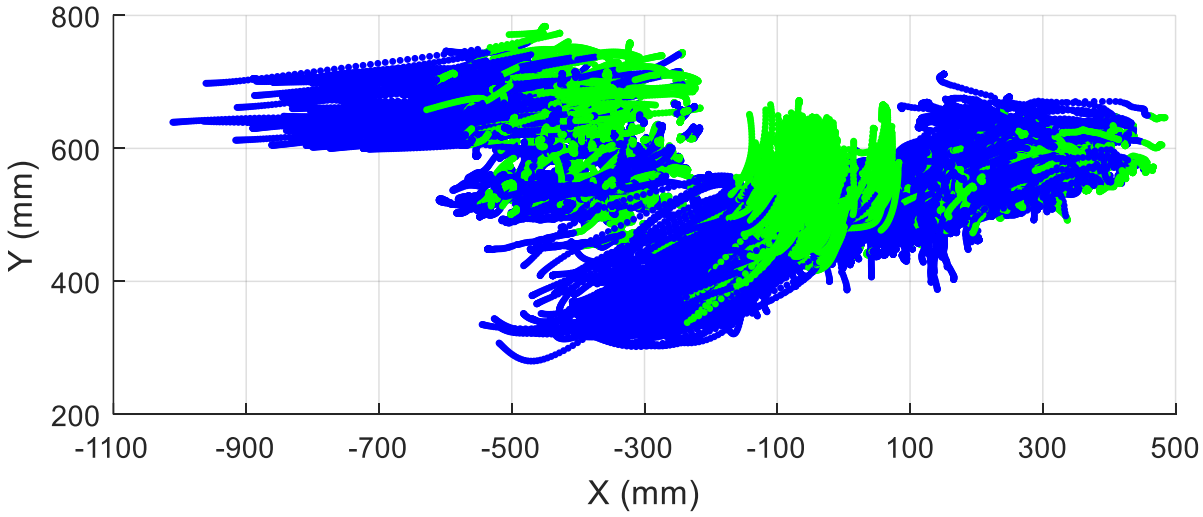

Figure C-3 All take-over trajectories of the torso, hip, wrist, knee, and ankle in the x-y plane

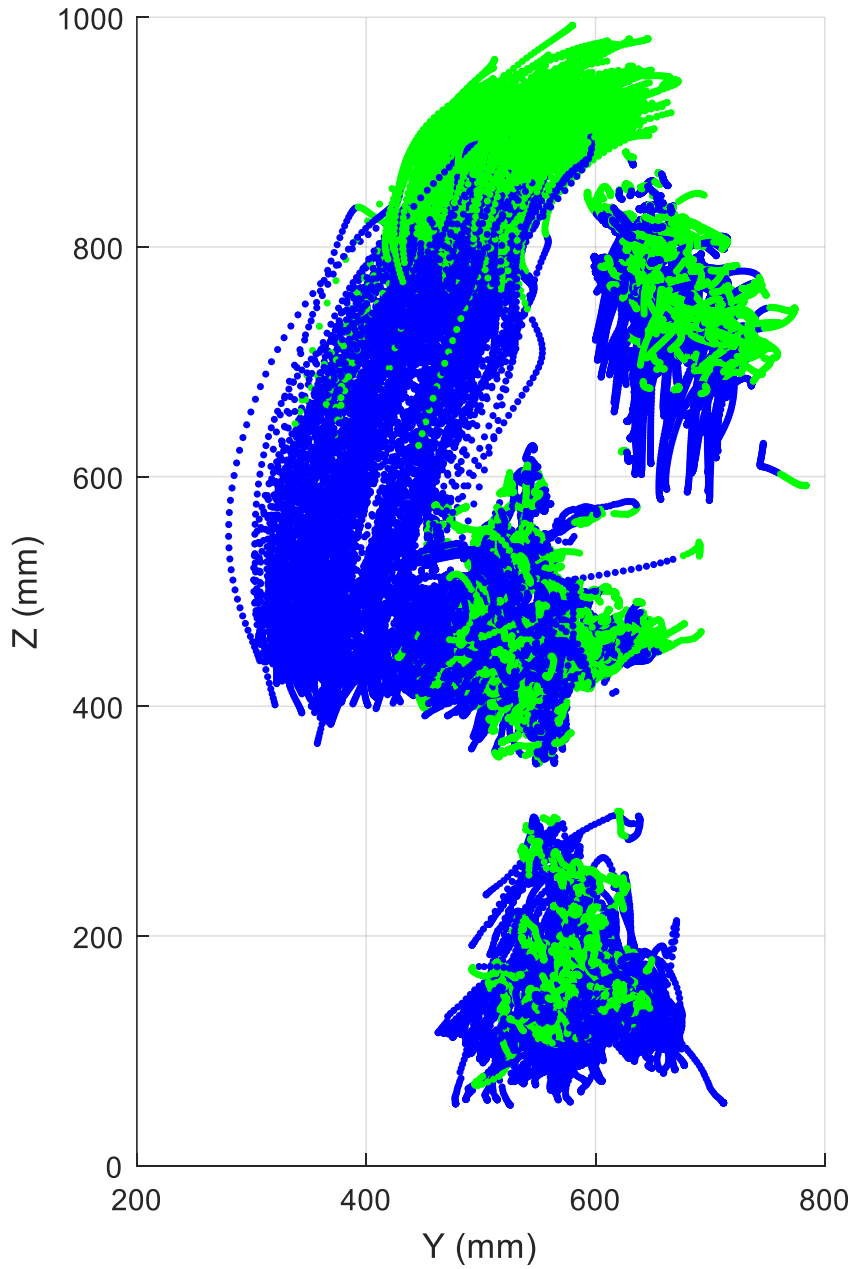

Figure C-4 All take-over trajectories of the torso, hip, wrist, knee, and ankle in the y-z plane

c) All Knee and Ankle Trajectories in 3D

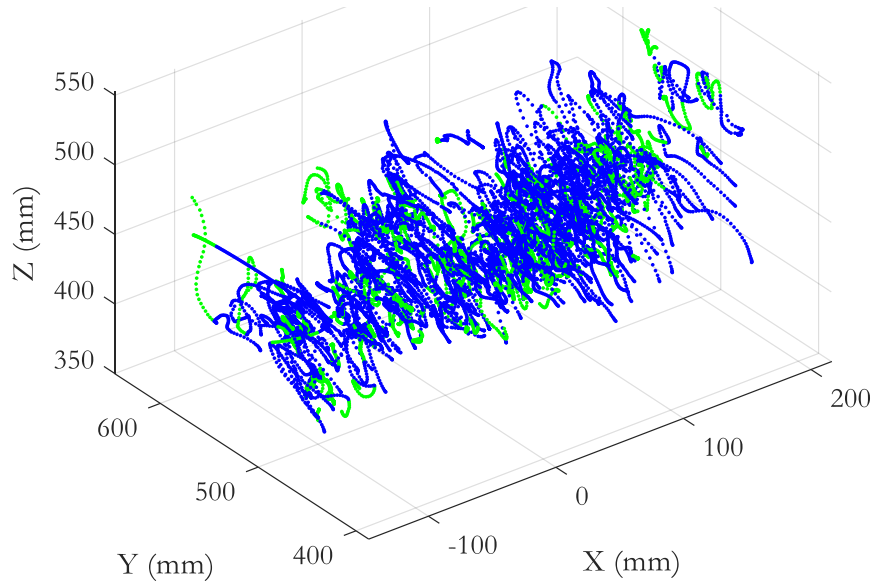

Figure C-5 All trajectories of the knee in take-over processes (n = 223)

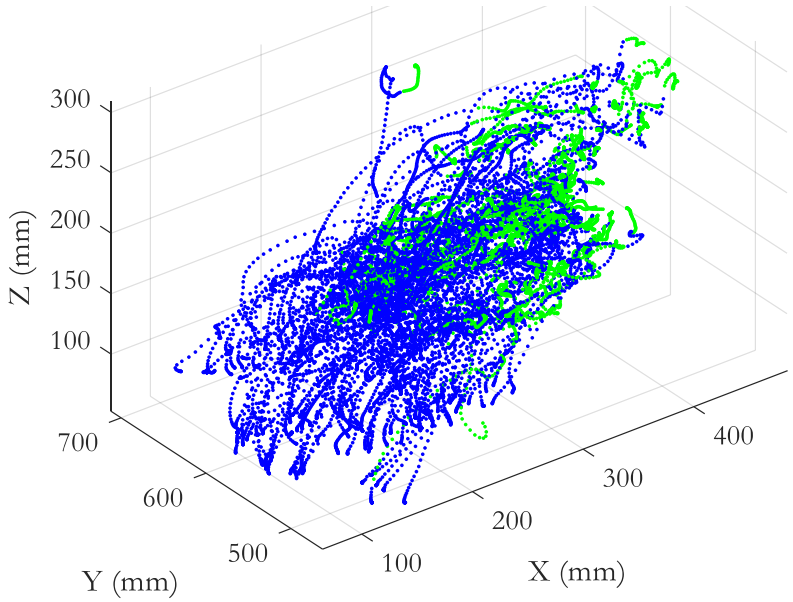

Figure C-6 All trajectories of the ankle in take-over processes (n = 224)

D. The x-, y- and z-Displacements: Descriptive Statistics of Different Torso Conditions (Section 6.3.1)

a) Wrist

Table D-1 Descriptive statistics of the wrist's x-displacement in different torso angle conditions

Descriptive Statistics

	X-displacement (mm)			
	Torso 10°	Torso 30°	Torso 50°	Torso 70°
Valid n	48	57	62	57
Mean	225	243	283	318
Std. deviation	75	78	71	78
Minimum	68	61	135	154
Maximum	373	451	434	501

Table D-2 Descriptive statistics of the wrist's y-displacement in different torso angle conditions

Descriptive Statistics

	Y-displacement (mm)			
	Torso 10°	Torso 30°	Torso 50°	Torso 70°
Valid n	48	57	62	57
Mean	235	242	229	211
Std. deviation	48	48	51	52
Minimum	133	115	118	105
Maximum	323	348	334	303

Table D-3 Descriptive statistics of the wrist's z-displacement in different torso angle conditions

Descriptive Statistics

	Z-displacement (mm)			
	Torso 10°	Torso 30°	Torso 50°	Torso 70°
Valid n	48	57	62	57
Mean	479	487	492	492
Std. deviation	30	37	32	33
Minimum	407	395	430	389
Maximum	557	572	568	542

b) Breastbone

Table D-4 Descriptive statistics of the breastbone's x-displacement in different torso angle conditions

Descriptive Statistics

	X-displacement (mm)			
	Torso 10°	Torso 30°	Torso 50°	Torso 70°
Valid n	47	57	62	57
Mean	11	109	298	415
Std. deviation	7	94	107	106
Minimum	1	4	6	97
Maximum	29	369	471	611

Table D-5 Descriptive statistics of the breastbone's y-displacement in different torso angle conditions

Descriptive Statistics

	Y-displacement (mm)			
	Torso 10°	Torso 30°	Torso 50°	Torso 70°
Valid n	47	57	62	57
Mean	14	28	37	42
Std. deviation	7	25	26	26
Minimum	3	2	3	8
Maximum	37	99	121	110

Table D-6 Descriptive statistics of the breastbone's z-displacement in different torso angle conditions

Descriptive Statistics

	Z-displacement (mm)			
	Torso 10°	Torso 30°	Torso 50°	Torso 70°
Valid n	47	57	62	57
Mean	11	16	48	105
Std. deviation	7	11	32	36
Minimum	2	1	5	9
Maximum	33	44	121	183

c) H-point

Table D-7 Descriptive statistics of the H-point's x-displacement in different torso angle conditions

Descriptive Statistics

	X-displacement (mm)			
	Torso 10°	Torso 30°	Torso 50°	Torso 70°
Valid n	47	57	61	57
Mean	20	26	54	81
Std. deviation	16	25	39	48
Minimum	2	4	10	11
Maximum	71	123	183	206

Table D-8 Descriptive statistics of the H-point's y-displacement in different torso angle conditions

Descriptive Statistics

	Y-displacement (mm)			
	Torso 10°	Torso 30°	Torso 50°	Torso 70°
Valid n	47	57	61	57
Mean	13	22	26	33
Std. deviation	7	27	18	19
Minimum	3	4	6	5
Maximum	34	169	72	79

Table D-9 Descriptive statistics of the H-point's z-displacement in different torso angle conditions

Descriptive Statistics

	Z-displacement (mm)			
	Torso 10°	Torso 30°	Torso 50°	Torso 70°
Valid n	47	57	61	57
Mean	29	25	27	31
Std. deviation	15	16	16	18
Minimum	6	6	8	6
Maximum	60	82	75	74

d) Knee

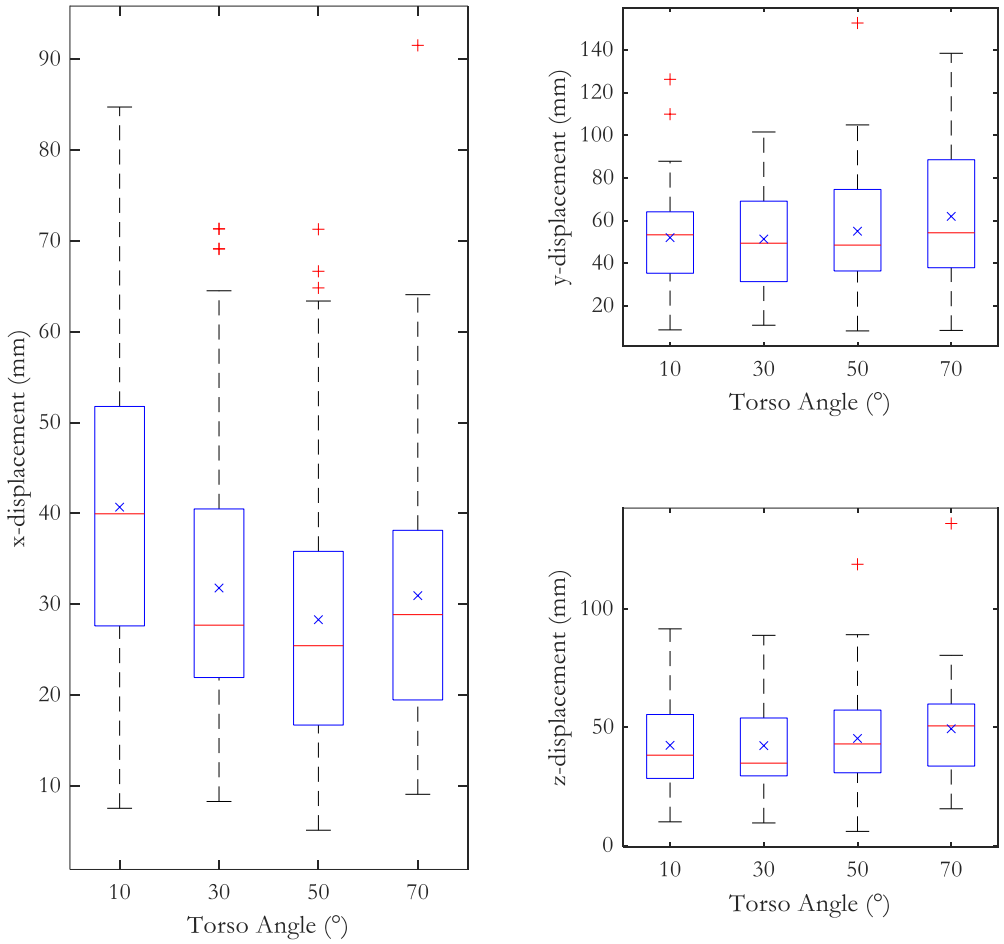

Figure D-1 The knee's x-, y-, and z-displacement in different torso angle conditions

Table D-10 Descriptive statistics of the knee's x-displacement in different torso angle conditions

Descriptive Statistics

	X-displacement (mm)			
	Torso 10°	Torso 30°	Torso 50°	Torso 70°
Valid n	48	57	61	57
Mean	41	32	28	31
Std. deviation	18	16	15	16
Minimum	8	8	5	9
Maximum	85	71	71	92

Table D-11 Descriptive statistics of the knee's y-displacement in different torso angle conditions

Descriptive Statistics

	Y-displacement (mm)			
	Torso 10°	Torso 30°	Torso 50°	Torso 70°
Valid n	48	57	61	57
Mean	52	51	55	62
Std. deviation	24	24	27	32
Minimum	9	11	8	8
Maximum	126	102	153	138

Table D-12 Descriptive statistics of the knee's z-displacement in different torso angle conditions

Descriptive Statistics

	Z-displacement (mm)			
	Torso 10°	Torso 30°	Torso 50°	Torso 70°
Valid n	48	57	61	57
Mean	42	42	45	49
Std. deviation	19	20	20	20
Minimum	10	10	6	16
Maximum	92	89	119	136

e)Ankle

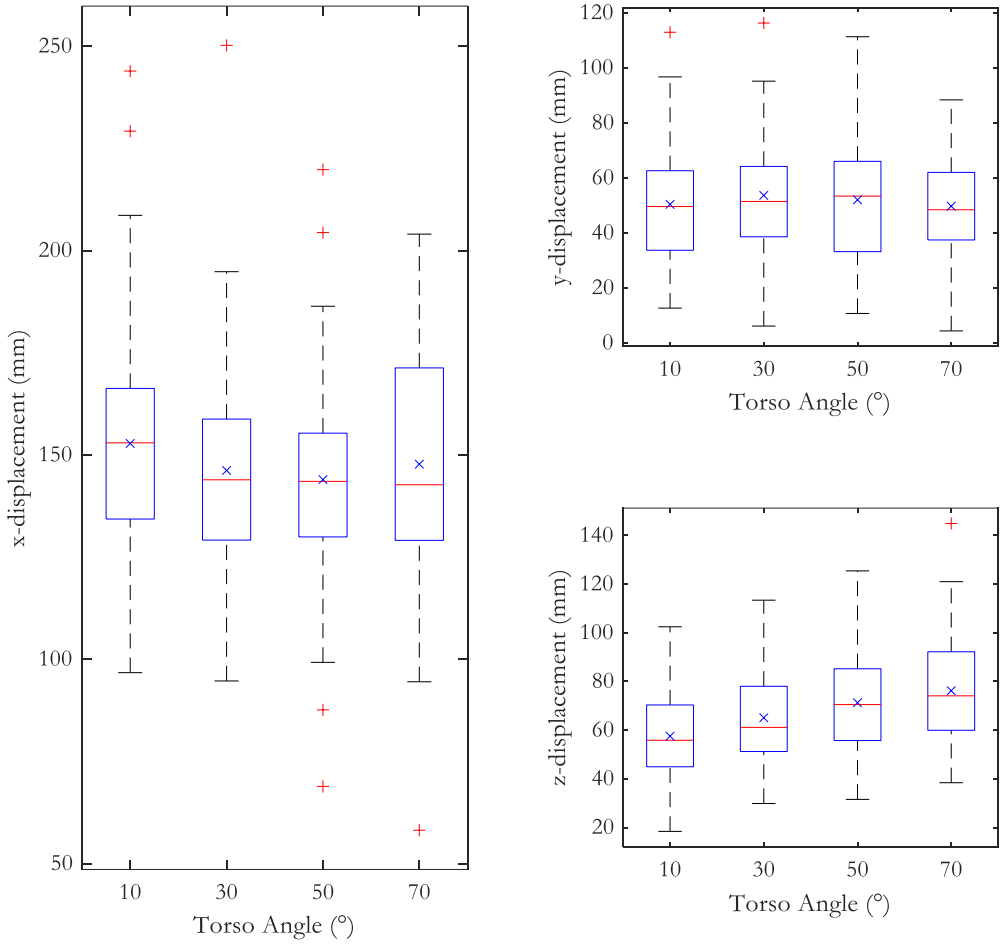

Figure D-2 The ankle's x-, y-, and z-displacement in different torso angle conditions

Table D-13 Descriptive statistics of the ankle's x-displacement in different torso angle conditions

Descriptive Statistics

	X-displacement (mm)			
	Torso 10°	Torso 30°	Torso 50°	Torso 70°
Valid n	48	57	62	57
Mean	153	146	144	148
Std. deviation	29	26	27	30
Minimum	97	95	69	58
Maximum	244	250	220	204

Table D-14 Descriptive statistics of the ankle's y-displacement in different torso angle conditions

Descriptive Statistics

	Y-displacement (mm)			
	Torso 10°	Torso 30°	Torso 50°	Torso 70°
Valid n	48	57	62	57
Mean	50	54	52	50
Std. deviation	24	22	22	18
Minimum	13	6	11	4
Maximum	113	116	111	88

Table D-15 Descriptive statistics of the ankle's z-displacement in different torso angle conditions

Descriptive Statistics

	Z-displacement (mm)			
	Torso 10°	Torso 30°	Torso 50°	Torso 70°
Valid n	48	57	62	57
Mean	58	65	71	76
Std. deviation	17	19	20	22
Minimum	18	30	32	38
Maximum	103	113	126	145

E. The x-, y- and z-Displacements: Different Knee Angles Conditions (Section 6.3.1)

a) Wrist

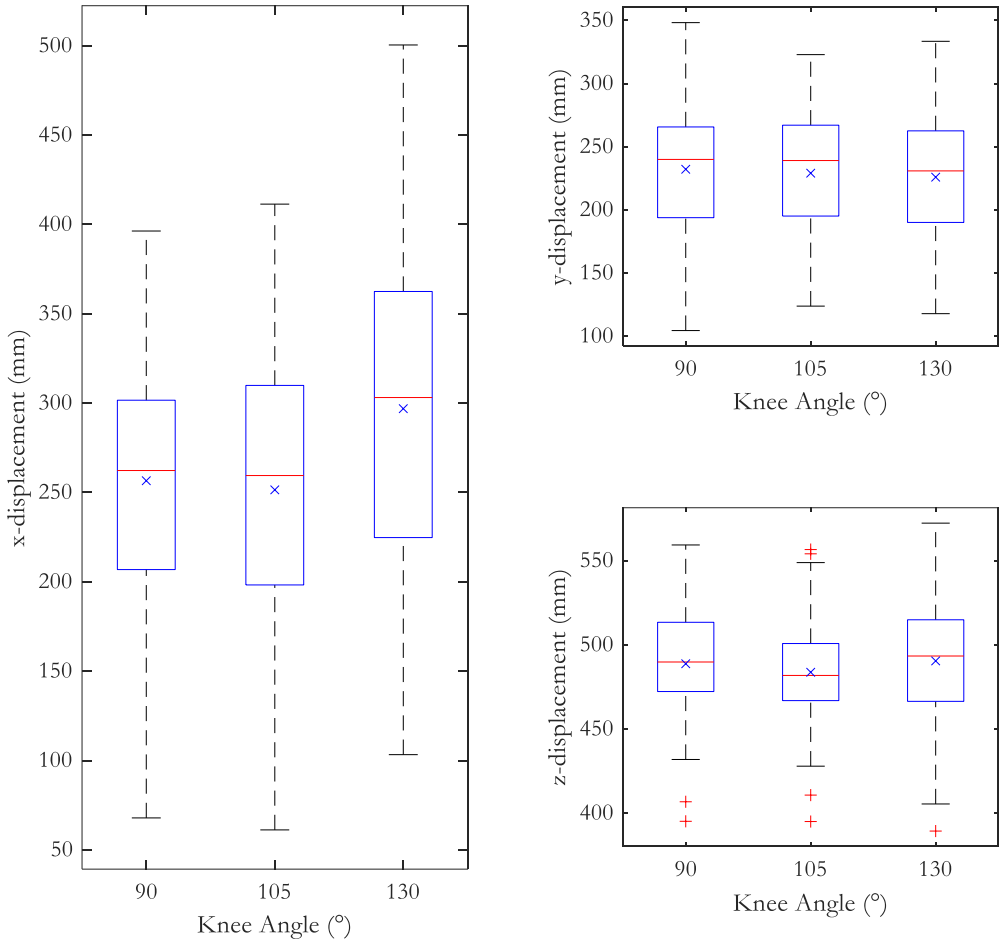

Figure E-1 The wrist's x-, y-, and z-displacement in different knee angle conditions

Table E-1 Descriptive statistics of the wrist's x-, y-, and z-displacements in different knee angle conditions

Descriptive Statistics

	x-displacement (mm)		
	Knee 90° crossed leg	Knee 105°	Knee 130°
Valid n	73	71	80
Mean	257	251	297
Median	262	259	303
Std. deviation	70	74	95
Minimum	68	61	103
Maximum	396	411	500

	y-displacement (mm)		
	Knee 90° crossed leg	Knee 105°	Knee 130°
Valid n	73	71	80
Mean	232	229	226
Median	240	239	231
Std. deviation	52	49	52
Minimum	104	124	118
Maximum	348	323	333

	z-displacement (mm)		
	Knee 90° crossed leg	Knee 105°	Knee 130°
Valid n	73	71	80
Mean	489	484	490
Median	490	482	493
Std. deviation	31	31	37
Minimum	395	395	389
Maximum	559	557	572

b) Breastbone

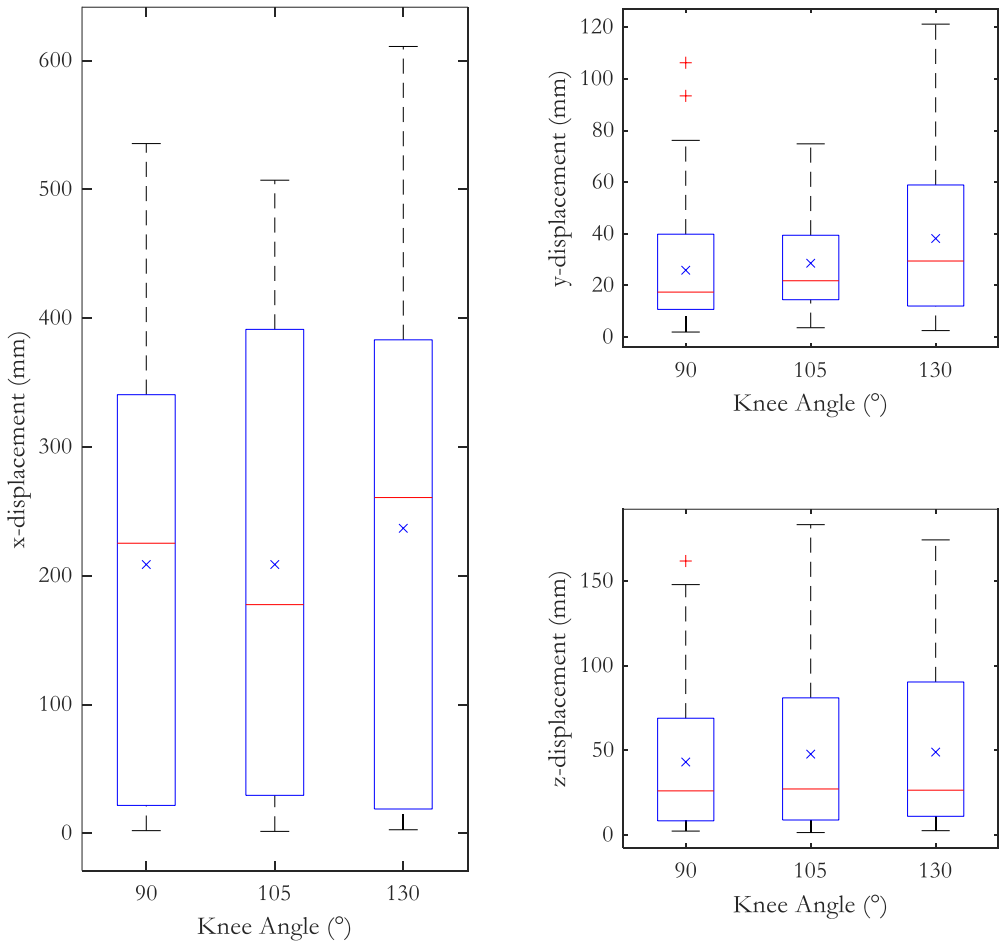

Figure E-2 The breastbone's x-, y-, and z-displacement in different knee angle conditions

Table E-2 Descriptive statistics of the breastbone's x-, y-, and z-displacements in different knee angle conditions

Descriptive Statistics

	x-displacement (mm)		
	Knee 90° crossed leg	Knee 105°	Knee 130°
Valid n	72	71	80
Mean	209	209	237
Median	225	178	261
Std. deviation	168	175	192
Minimum	2	1	3
Maximum	536	507	611

	y-displacement (mm)		
	Knee 90° crossed leg	Knee 105°	Knee 130°
Valid n	72	71	80
Mean	26	29	38
Median	17	22	29
Std. deviation	21	20	30
Minimum	2	4	3
Maximum	106	75	121

	z-displacement (mm)		
	Knee 90° crossed leg	Knee 105°	Knee 130°
Valid n	72	71	80
Mean	43	48	49
Median	26	27	27
Std. deviation	42	47	46
Minimum	2	1	3
Maximum	162	183	174

c) H-point

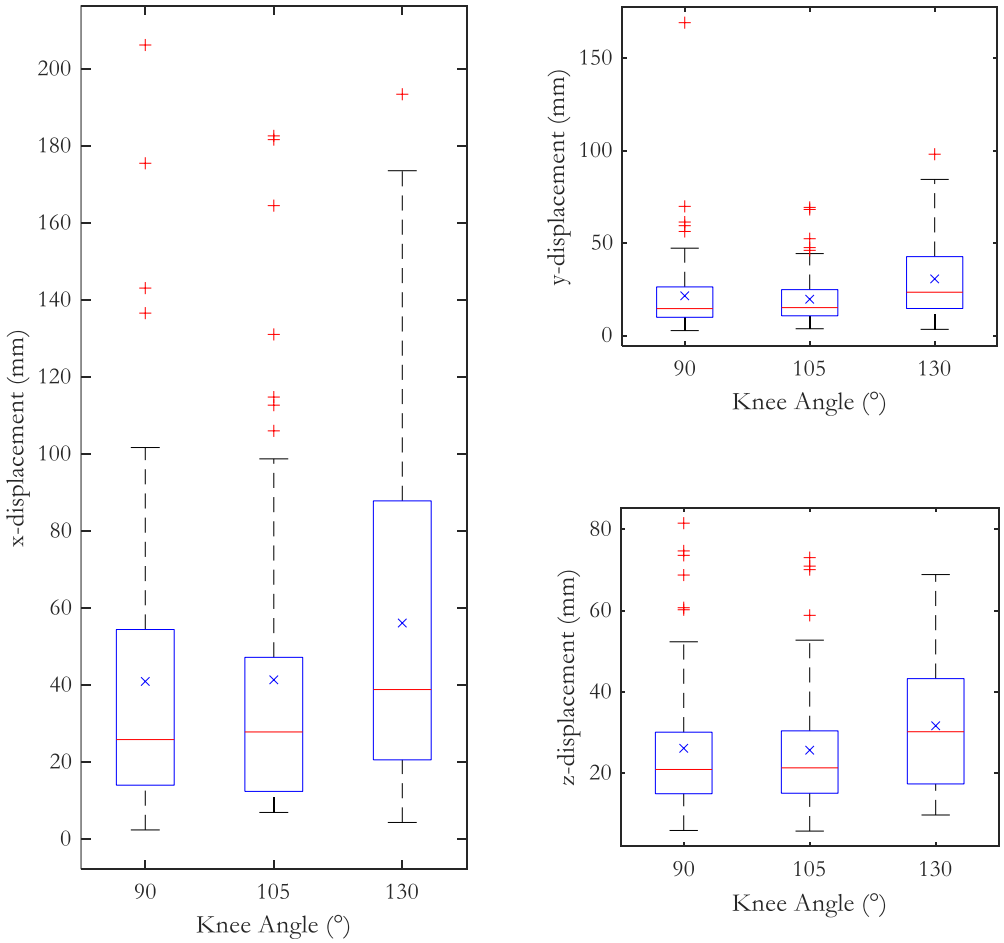

Figure E-3 The H-point's x-, y-, and z-displacement in different knee angle conditions

Table E-3 Descriptive statistics of the H-point's x-, y-, and z-displacements in different knee angle conditions

Descriptive Statistics

	x-displacement (mm)		
	Knee 90° crossed leg	Knee 105°	Knee 130°
Valid n	72	71	79
Mean	41	41	56
Median	26	28	39
Std. deviation	40	41	45
Minimum	2	7	4
Maximum	206	183	193

	y-displacement (mm)		
	Knee 90° crossed leg	Knee 105°	Knee 130°
Valid n	72	71	79
Mean	22	20	31
Median	15	15	23
Std. deviation	23	14	22
Minimum	3	4	3
Maximum	169	69	98

	z-displacement (mm)		
	Knee 90° crossed leg	Knee 105°	Knee 130°
Valid n	72	71	79
Mean	26	26	32
Median	21	21	30
Std. deviation	17	15	16
Minimum	6	6	10
Maximum	82	73	69

d) Knee

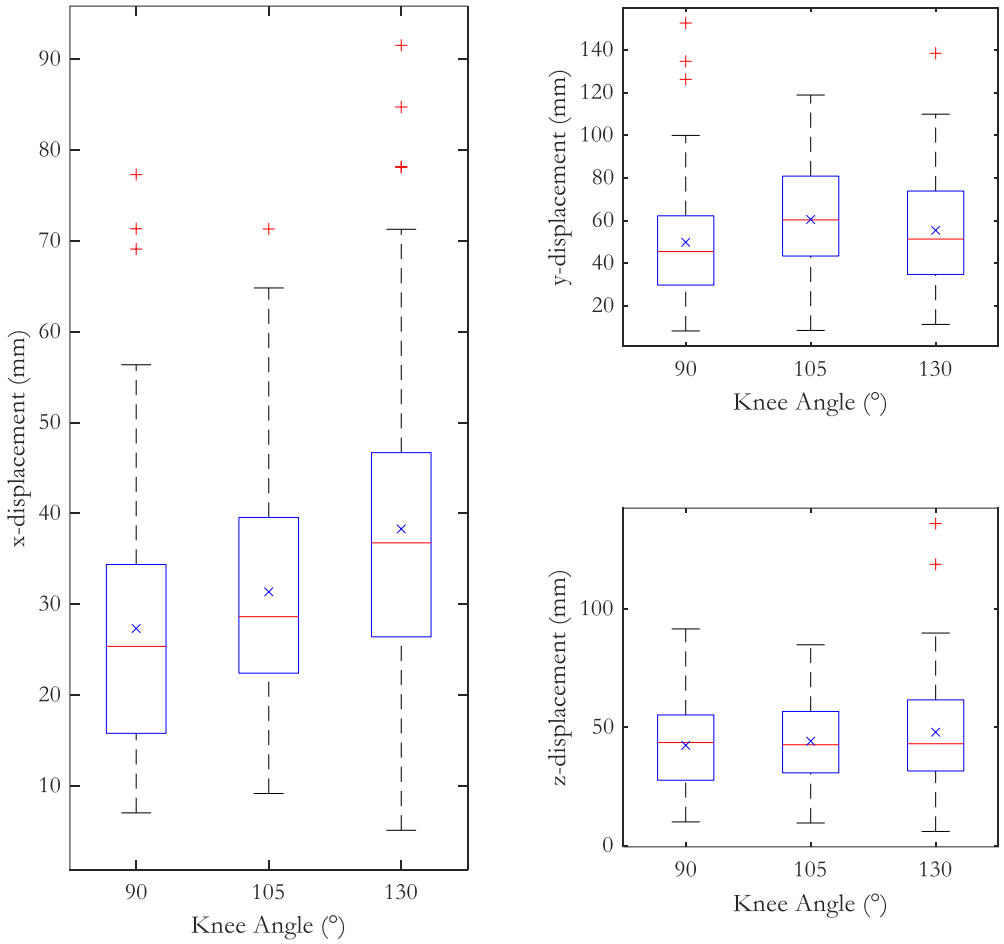

Figure E-4 The knee's x-, y-, and z-displacement in different knee angle conditions

Table E-4 Descriptive statistics of the knee's x-, y-, and z-displacements in different knee angle conditions

Descriptive Statistics

	x-displacement (mm)		
	Knee 90° crossed leg	Knee 105°	Knee 130°
Valid n	73	70	80
Mean	27	31	38
Median	25	29	37
Std. deviation	15	14	18
Minimum	7	9	5
Maximum	77	71	92

	y-displacement (mm)		
	Knee 90° crossed leg	Knee 105°	Knee 130°
Valid n	73	70	80
Mean	50	61	55
Median	45	60	51
Std. deviation	29	26	27
Minimum	8	8	11
Maximum	153	119	138

	z-displacement (mm)		
	Knee 90° crossed leg	Knee 105°	Knee 130°
Valid n	73	70	80
Mean	42	44	48
Median	44	43	43
Std. deviation	19	18	22
Minimum	10	10	6
Maximum	92	85	136

e)Ankle

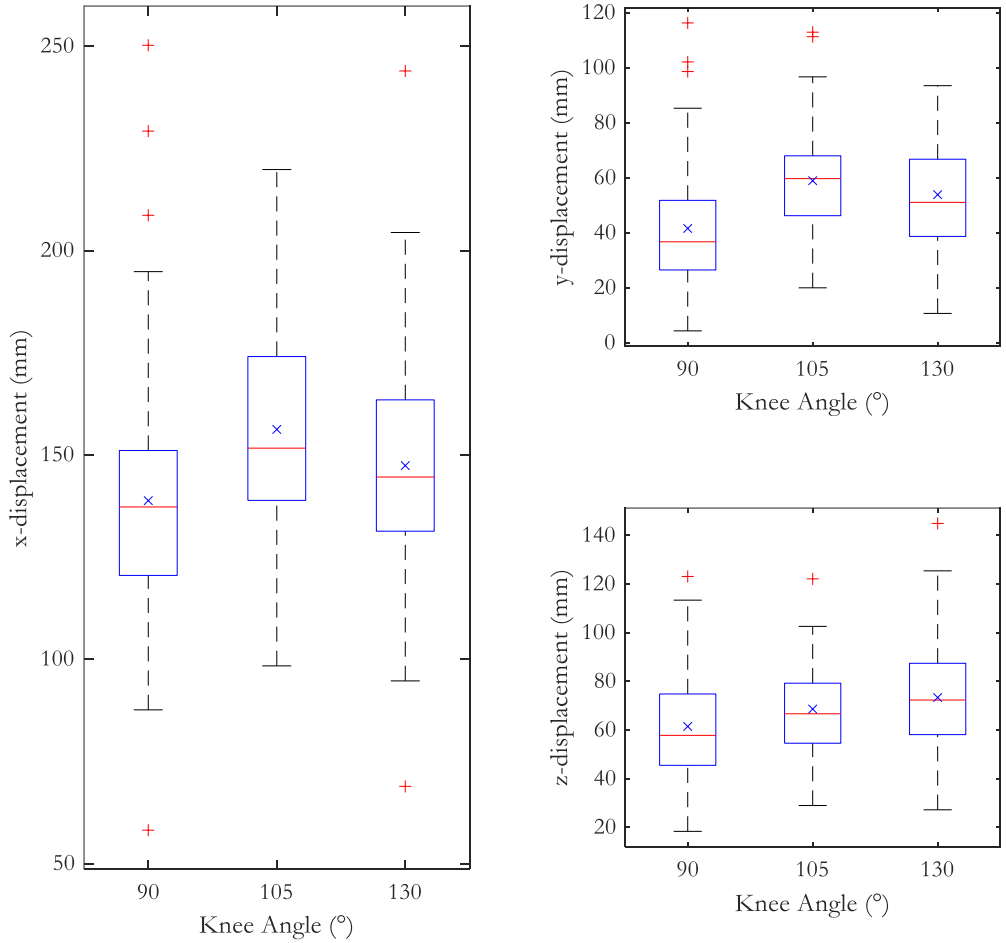

Figure E-5 The ankle's x-, y-, and z-displacement in different knee angle conditions

Table E-5 Descriptive statistics of the ankle's x-, y-, and z-displacements in different knee angle conditions

Descriptive Statistics

	x-displacement (mm)		
	Knee 90° crossed leg	Knee 105°	Knee 130°
Valid n	73	71	80
Mean	139	156	147
Median	137	152	145
Std. deviation	30	23	27
Minimum	58	98	69
Maximum	250	220	244

	y-displacement (mm)		
	Knee 90° crossed leg	Knee 105°	Knee 130°
Valid n	73	71	80
Mean	42	59	54
Median	37	60	51
Std. deviation	23	19	20
Minimum	4	20	11
Maximum	116	113	94

	z-displacement (mm)		
	Knee 90° crossed leg	Knee 105°	Knee 130°
Valid n	73	71	80
Mean	62	69	73
Median	58	67	72
Std. deviation	21	17	22
Minimum	18	29	27
Maximum	123	122	145

F. The Fitted Planes of Hand's Movement (3D) (Section 6.3.2.1)

a) Body-Size Subgroups

Table F-1 Parameters and the fitting quality of planes grouped by the body size

Fitted surfaces				
	Group S		Group M	
	$z = p_{00} + p_{10}*x + p_{01}*y$		$z = p_{00} + p_{10}*x + p_{01}*y$	
Coefficients (with 95% confidence bounds)	p_{00}	475.7 (460.8, 490.6)	p_{00}	488.8 (475.6, 502)
	p_{10}	1.067 (1.049, 1.085)	p_{10}	0.8593 (0.8418, 0.8767)
	p_{01}	0.8605 (0.8335, 0.8876)	p_{01}	0.8162 (0.7934, 0.8389)
Quality	R^2 adj.	0.89	R^2 adj.	0.88
	RMSE	55.80	RMSE	60.30

	Group L	
	$z = p_{00} + p_{10}*x + p_{01}*y$	
Coefficients (with 95% confidence bounds)	p_{00}	203.1 (176.3, 229.9)
	p_{10}	0.4039 (0.3742, 0.4335)
	p_{01}	1.346 (1.294, 1.398)
Quality	R^2 adj.	0.81
	RMSE	76.70

b) Torso-Angle Subgroups

Table F-2 Parameters and the fitting quality of planes grouped by the initial torso angle

Fitted surfaces				
	Group 10° Torso		Group 30° Torso	
	$z = p_{00} + p_{10}*x + p_{01}*y$		$z = p_{00} + p_{10}*x + p_{01}*y$	
Coefficients (with 95% confidence bounds)	p_{00}	391.6 (370.5, 412.7)	p_{00}	367.2 (348.4, 385.9)
	p_{10}	0.8065 (0.7741, 0.8389)	p_{10}	0.7889 (0.763, 0.8148)
	p_{01}	0.9752 (0.9377, 1.013)	p_{01}	1.018 (0.9855, 1.051)
Quality	R^2 adj.	0.83	R^2 adj.	0.86
	RMSE	67.97	RMSE	64.60
	Group 50° Torso		Group 70° Torso	
	$z = p_{00} + p_{10}*x + p_{01}*y$		$z = p_{00} + p_{10}*x + p_{01}*y$	
Coefficients (with 95% confidence bounds)	p_{00}	474.8 (456.2, 493.3)	p_{00}	680.2 (661.8, 698.5)
	p_{10}	0.8413 (0.8186, 0.8641)	p_{10}	1.009 (0.9896, 1.029)
	p_{01}	0.8226 (0.7892, 0.856)	p_{01}	0.4894 (0.456, 0.5228)
Quality	R^2 adj.	0.85	R^2 adj.	0.87
	RMSE	67.20	RMSE	63.21

c) Knee-Angle Subgroups

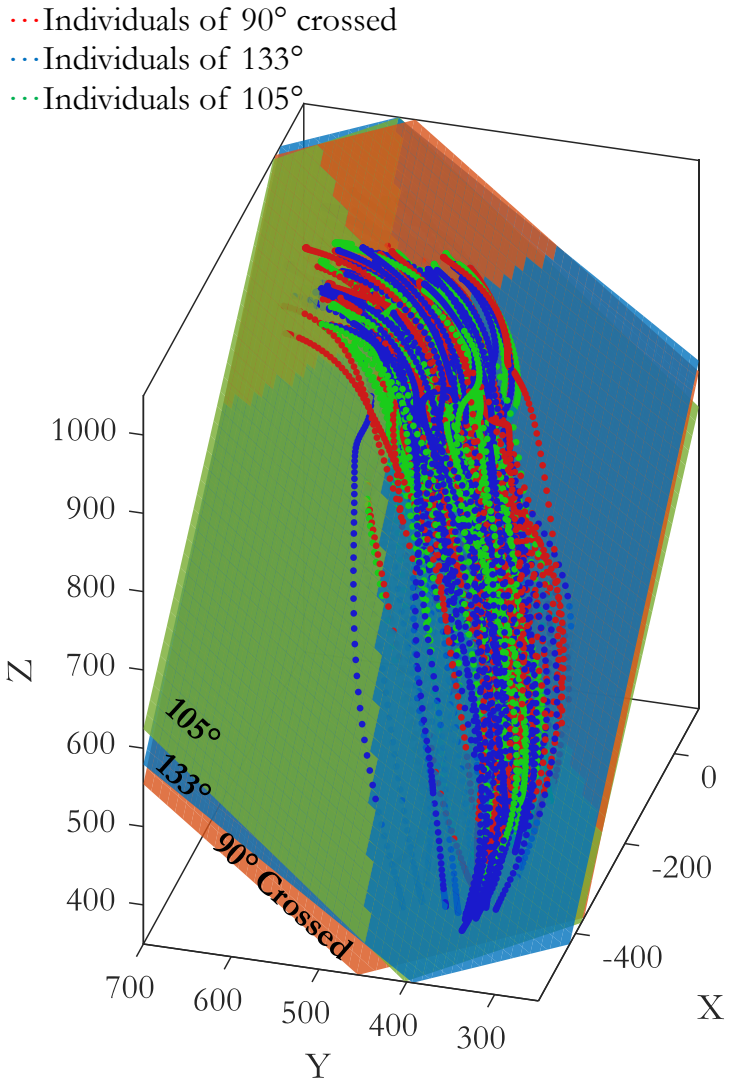

Figure F-1 Fitted planes grouped by the initial knee angle

Table F-3 Parameters and the fitting quality of planes grouped by the initial knee angle

Fitted surfaces				
	Group 105° Knee		Group 133° Knee	
	$z = p_{00} + p_{10}*x + p_{01}*y$		$z = p_{00} + p_{10}*x + p_{01}*y$	
Coefficients (with 95% confidence bounds)	p_{00}	423.7 (406.9, 440.5)	p_{00}	522.6 (505.5, 539.7)
	p_{10}	0.8093 (0.7872, 0.8315)	p_{10}	0.8482 (0.8287, 0.8678)
	p_{01}	0.9229 (0.8926, 0.9532)	p_{01}	0.7473 (0.7168, 0.7779)
Quality	R^2 adj.	0.85	R^2 adj.	0.84
	RMSE	67.33	RMSE	69.64

	Group 90° Crossed	
	$z = p_{00} + p_{10}*x + p_{01}*y$	
Coefficients (with 95% confidence bounds)	p_{00}	479.2 (463, 495.3)
	p_{10}	0.9264 (0.9046, 0.9481)
	p_{01}	0.8349 (0.8061, 0.8637)
Quality	R^2 adj.	0.86
	RMSE	63.77

G. The Fitted Curve of Hand-On Movement (2D) (Section 6.3.2.2)

a) Overall

Table G-1 Parameters and the fitting quality of curves in each 2D plane for all the data

Fitted curves

		x-y plane		x-z plane
		$y = p_1*x + p_2$		$z = p_1*x + p_2$
Coefficients (with 95% confidence bounds)	p_1	0.54 (0.5342, 0.5459)	p_1	1.301 (1.292, 1.31)
	p_2	549.7 (548.5, 550.9)	p_2	932.6 (930.8, 934.5)
Quality	R^2 adj.	0.60	R^2 adj.	0.78
	RMSE	51.92	RMSE	81.05

		y-z plane
		$z = p_1*y + p_2$
Coefficients (with 95% confidence bounds)	p_1	1.785 (1.77, 1.799)
	p_2	-102.7 (-109.7, -95.72)
Quality	R^2 adj.	0.72
	RMSE	91.98

b) Body-Size Subgroups

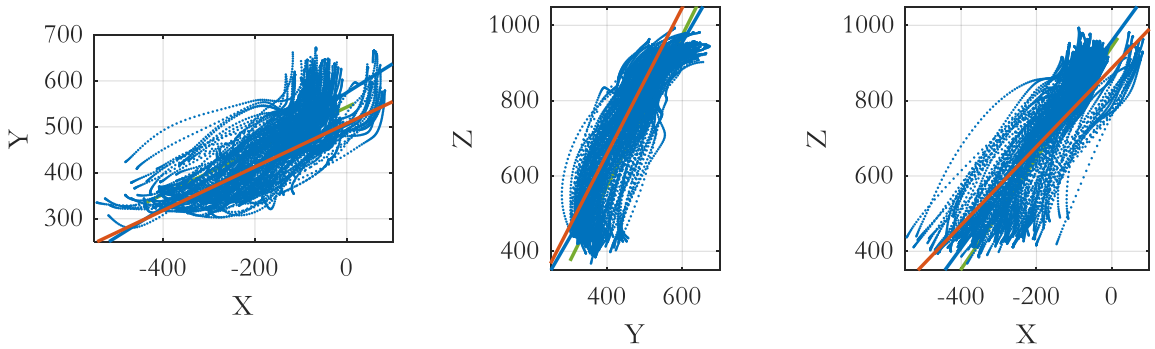

(a) All trajectories with fitted curves of each subgroup (green: S; blue: M; red: L) in xy-, yz-, xz-view

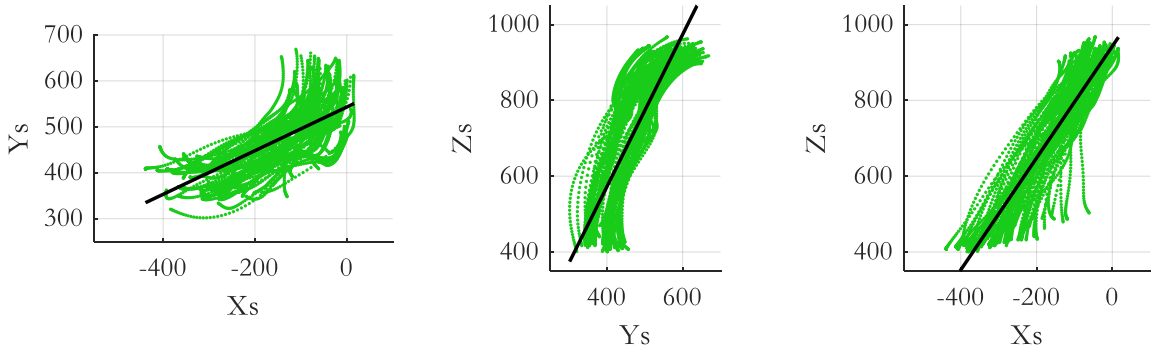

(b) Trajectories of subgroup body size S with the fitted curves in xy-, yz-, xz-view

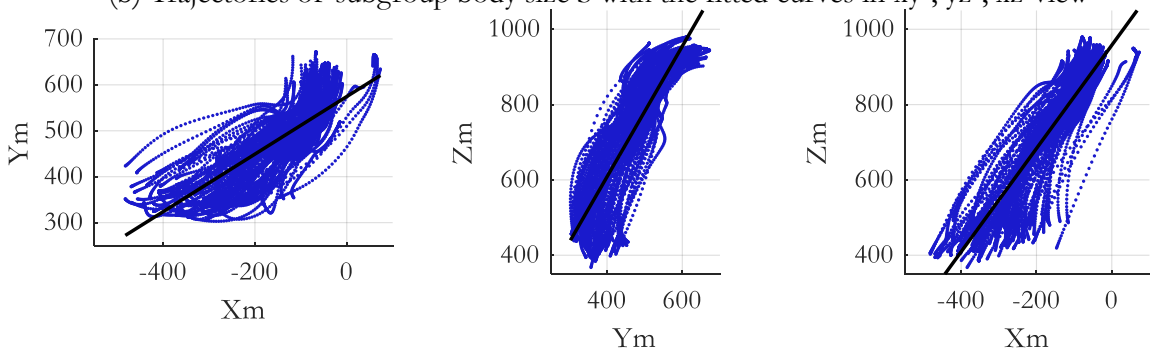

(c) Trajectories of subgroup body size M with the fitted curves in xy-, yz-, xz-view

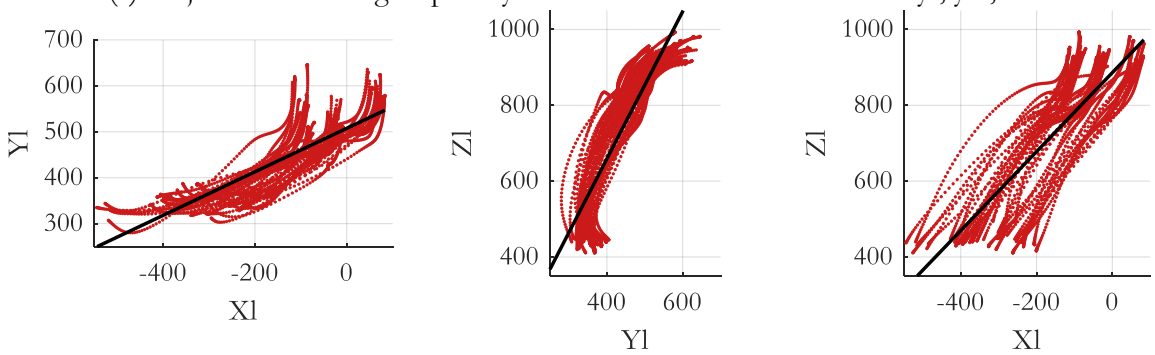

(d) Trajectories of subgroup body size L with the fitted curves in xy-, yz-, xz-view

Figure G-1 Hand-on trajectories of body-size subgroups (S, M, L) and fitted curves: overviews and separate views of each subgroup

Table G-2 Parameters and the fitting quality of body size subgroups in the x-y plane

Fitted curves (x-y plane)				
	S		M	
	$y = p_1*x + p_2$		$y = p_1*x + p_2$	
Coefficients (with 95% confidence bounds)	p_1	0.4749 (0.4638, 0.4861)	p_1	0.6269 (0.6186, 0.6352)
	p_2	543 (540.8, 545.1)	p_2	574.5 (572.9, 576.2)
Quality	R^2 adj.	0.51	R^2 adj.	0.67
	RMSE	49.46	RMSE	49.77

	L	
	$y = p_1*x + p_2$	
Coefficients (with 95% confidence bounds)	p_1	0.4737 (0.4645, 0.483)
	p_2	507.5 (505.6, 509.4)
Quality	R^2 adj.	0.70
	RMSE	43.60

Table G-3 Parameters and the fitting quality of body size subgroups in the x-z plane

Fitted curves (x-z plane)				
	S		M	
	$z = p_1*x + p_2$		$z = p_1*x + p_2$	
Coefficients (with 95% confidence bounds)	p_1	1.475 (1.46, 1.491)	p_1	1.371 (1.359, 1.383)
	p_2	942.9 (939.9, 946)	p_2	957.7 (955.3, 960.1)
Quality	R^2 adj.	0.83	R^2 adj.	0.82
	RMSE	70.17	RMSE	72.70

	L	
	$z = p_1*x + p_2$	
Coefficients (with 95% confidence bounds)	p_1	1.042 (1.021, 1.062)
	p_2	886.2 (881.9, 890.4)
Quality	R^2 adj.	0.70
	RMSE	96.57

Table G-4 Parameters and the fitting quality of body size subgroups in the y-z plane

Fitted curves (y-z plane)

		S		M
		$z = p_1*y + p_2$		$z = p_1*y + p_2$
Coefficients (with 95% confidence bounds)	p_1	2.009 (1.976, 2.042)	p_1	1.734 (1.716, 1.752)
	p_2	-231.6 (-247.2, -216.1)	p_2	-85.26 (-93.8, -76.72)
Quality	R^2 adj.	0.68	R^2 adj.	0.77
	RMSE	97.07	RMSE	82.17

		L
		$z = p_1*y + p_2$
Coefficients (with 95% confidence bounds)	p_1	1.942 (1.911, 1.973)
	p_2	-117.8 (-131.5, -104.1)
Quality	R^2 adj.	0.78
	RMSE	82.75

c) Torso-Angle Subgroups

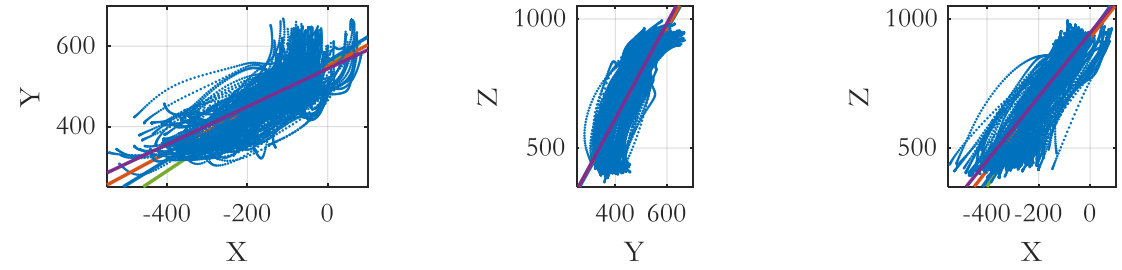

a) All trajectories with fitted curves of each subgroup (green: 10°; blue: 30°; red: 50°; magenta: 70°)

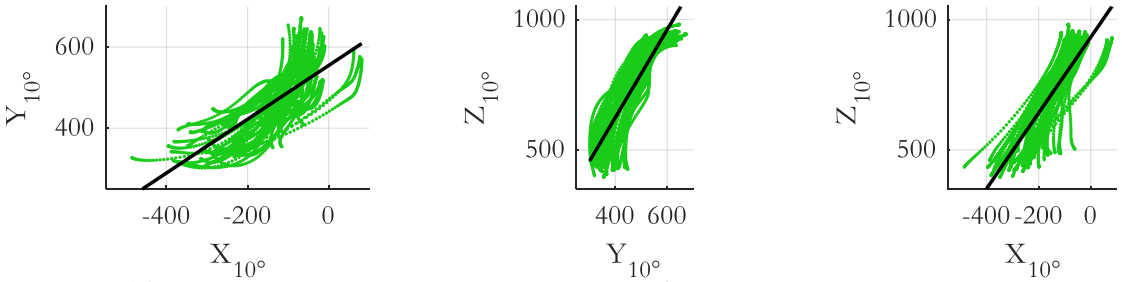

(b) Trajectories of the subgroup torso angle 10° with the fitted curves in xy-, yz-, xz-view

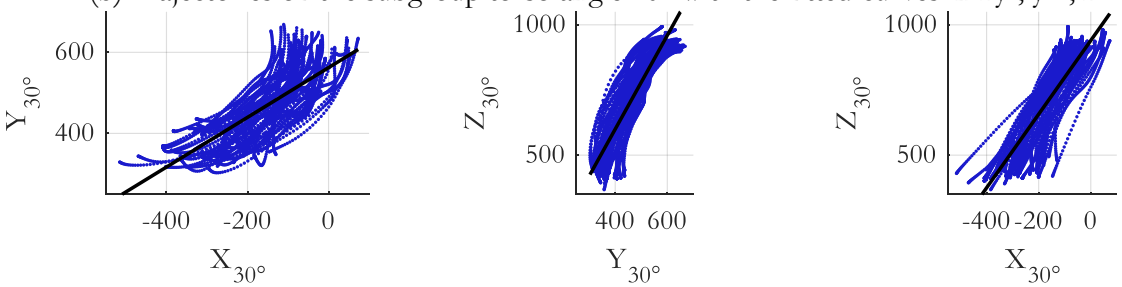

(c) Trajectories of the subgroup torso angle 30° with the fitted curves in xy-, yz-, xz-view

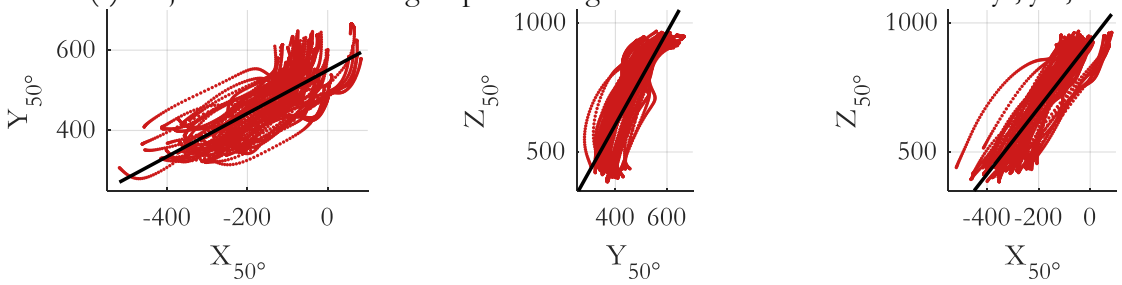

(d) Trajectories of the subgroup torso angle 50° with the fitted curves in xy-, yz-, xz-view

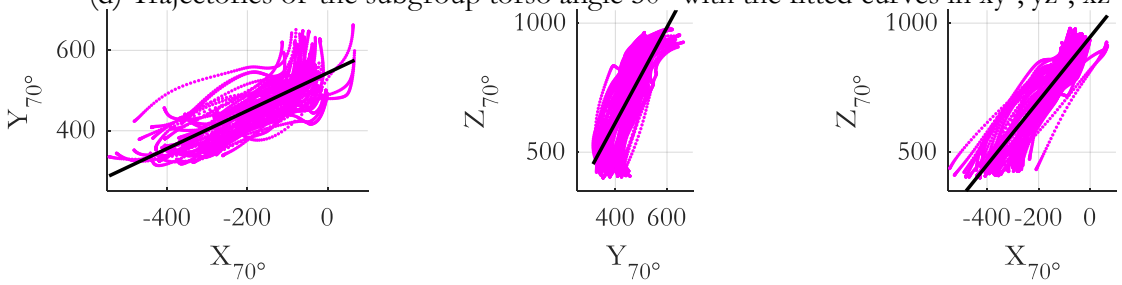

(e) Trajectories of the subgroup torso angle 70° with the fitted curves in xy-, yz-, xz-view

Figure G-2 Hand-on trajectories of torso-angle subgroups (10°, 30°, 50°, 70°) and fitted curves: overviews and separate views of each subgroup

Table G-5 Parameters and the fitting quality of torso angle subgroups in the x-y plane

Fitted curves (x-y plane)

		Group 10° Torso		Group 30° Torso
		$y = p_1*x + p_2$		$y = p_1*x + p_2$
Coefficients (with 95% confidence bounds)	p_1	0.6625 (0.6458, 0.6792)	p_1	0.6128 (0.5994, 0.6263)
	p_2	554.5 (551.6, 557.4)	p_2	562.2 (559.7, 564.8)
Quality	R^2 adj.	0.59	R^2 adj.	0.61
	RMSE	54.59	RMSE	53.47

		Group 50° Torso		Group 70° Torso
		$y = p_1*x + p_2$		$y = p_1*x + p_2$
Coefficients (with 95% confidence bounds)	p_1	0.5368 (0.5261, 0.5474)	p_1	0.471 (0.4623, 0.4796)
	p_2	549.8 (547.7, 552)	p_2	543.9 (542, 545.8)
Quality	R^2 adj.	0.62	R^2 adj.	0.63
	RMSE	50.93	RMSE	45.95

Table G-6 Parameters and the fitting quality of torso angle subgroups in the x-z plane

Fitted curves (x-z plane)

		Group 10° Torso		Group 30° Torso
		$z = p_1*x + p_2$		$z = p_1*x + p_2$
Coefficients (with 95% confidence bounds)	p_1	1.453 (1.426, 1.479)	p_1	1.413 (1.392, 1.434)
	p_2	932.4 (927.8, 936.9)	p_2	939.7 (935.7, 943.8)
Quality	R^2 adj.	0.73	R^2 adj.	0.77
	RMSE	86.33	RMSE	84.48

		Group 50° Torso		Group 70° Torso
		$z = p_1*x + p_2$		$z = p_1*x + p_2$
Coefficients (with 95% confidence bounds)	p_1	1.283 (1.266, 1.299)	p_1	1.24 (1.227, 1.252)
	p_2	927.1 (923.7, 930.4)	p_2	946.4 (943.6, 949.1)
Quality	R^2 adj.	0.79	R^2 adj.	0.85
	RMSE	79.19	RMSE	67.08

Table G-7 Parameters and the fitting quality of torso angle subgroups in the y-z plane

Fitted curves (y-z plane)

		Group 10° Torso		Group 30° Torso
		$z = p_1*y + p_2$		$z = p_1*y + p_2$
Coefficients (with 95% confidence bounds)	p_1	1.692 (1.662, 1.722)	p_1	1.799 (1.772, 1.826)
	p_2	-52.79 (-66.89, -38.68)	p_2	-119.5 (-132.3, -106.8)
Quality	R^2 adj.	0.74	R^2 adj.	0.77
	RMSE	84.95	RMSE	83.93

		Group 50° Torso		Group 70° Torso
		$z = p_1*y + p_2$		$z = p_1*y + p_2$
Coefficients (with 95% confidence bounds)	p_1	1.792 (1.764, 1.821)	p_1	1.849 (1.817, 1.881)
	p_2	-110.5 (-123.8, -97.23)	p_2	-125.2 (-140.2, -110.2)
Quality	R^2 adj.	0.72	R^2 adj.	0.66
	RMSE	91.97	RMSE	100.73

d) Knee-Angle Subgroups

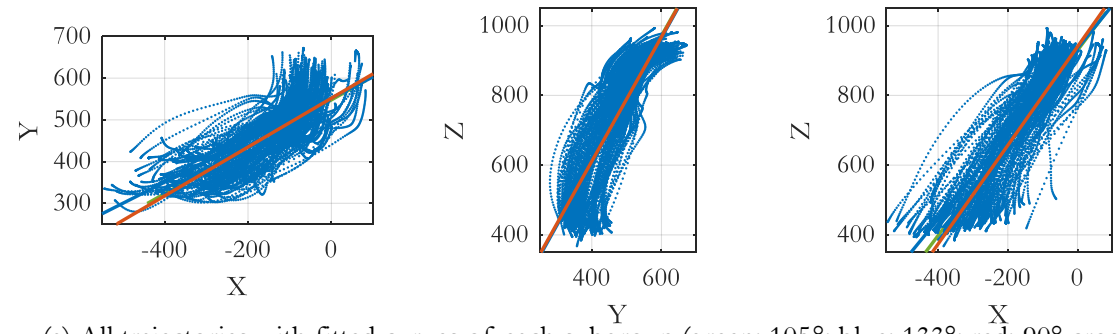

(a) All trajectories with fitted curves of each subgroup (green: 105°; blue: 133°; red: 90° crossed)

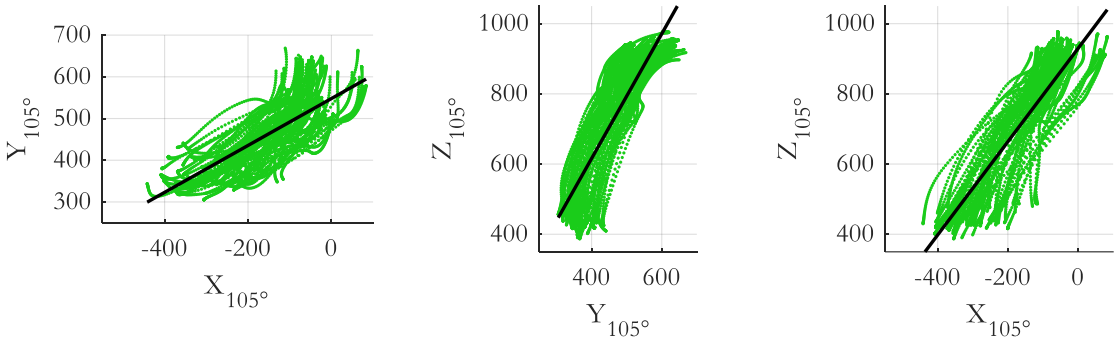

(b) Trajectories of the subgroup knee angle 105° with the fitted curves in xy-, yz-, xz-view

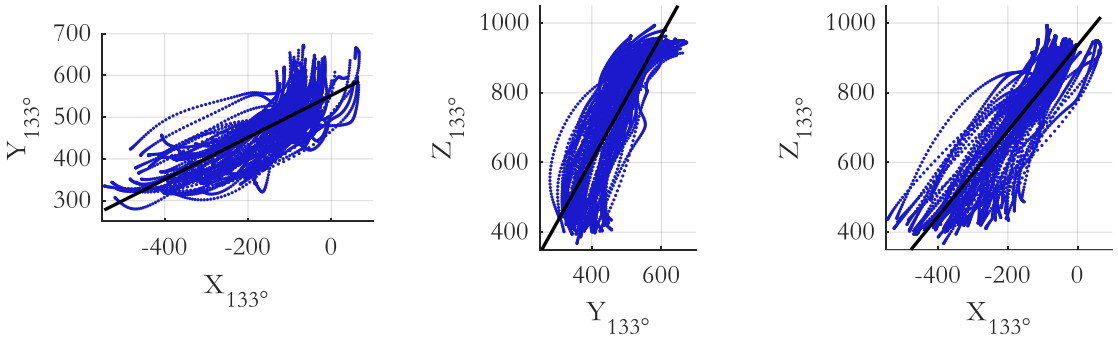

(c) Trajectories of the subgroup knee angle 133° with the fitted curves in xy-, yz-, xz-view

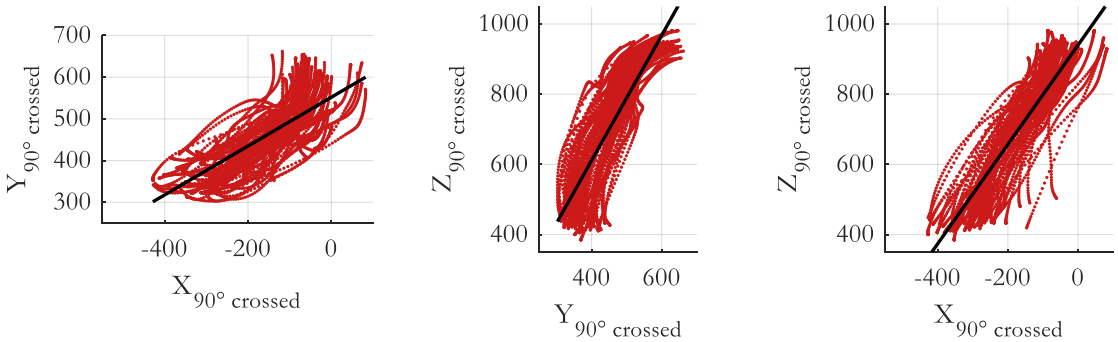

(d) Trajectories of subgroup the knee angle 90° crossed leg with the fitted curves in xy-, yz-, xz-view

Figure G-3 Hand-on trajectories of knee-angle subgroups (105°, 133°, 90° with legs crossed) and fitted curves: overviews and separate views of each subgroup

Table G-8 Parameters and the fitting quality of knee angle subgroups in the x-y plane

Fitted curves (x-y plane)

		Group 105° Knee		Group 133° Knee
		$y = p_1*x + p_2$		$y = p_1*x + p_2$
Coefficients (with 95% confidence bounds)	p_1	0.5622 (0.5512, 0.5732)	p_1	0.505 (0.4963, 0.5137)
	p_2	547.9 (545.8, 550)	p_2	552.6 (550.7, 554.4)
Quality	R^2 adj.	0.59	R^2 adj.	0.62
	RMSE	52.51	RMSE	50.11

		Group 90° Knee with crossed legs
		$y = p_1*x + p_2$
Coefficients (with 95% confidence bounds)	p_1	0.5857 (0.5746, 0.5968)
	p_2	552 (549.9, 554.1)
Quality	R^2 adj.	0.60
	RMSE	51.52

Table G-9 Parameters and the fitting quality of knee angle subgroups in the x-z plane

Fitted curves (x-z plane)

		Group 105° Knee		Group 133° Knee
		$z = p_1*x + p_2$		$z = p_1*x + p_2$
Coefficients (with 95% confidence bounds)	p_1	1.328 (1.311, 1.346)	p_1	1.226 (1.212, 1.239)
	p_2	929.4 (926.1, 932.7)	p_2	935.5 (932.6, 938.4)
Quality	R^2 adj.	0.77	R^2 adj.	0.80
	RMSE	82.96	RMSE	79.07

		Group 90° Knee with crossed legs
		$z = p_1*x + p_2$
Coefficients (with 95% confidence bounds)	p_1	1.415 (1.399, 1.432)
	p_2	940 (936.8, 943.1)
Quality	R^2 adj.	0.80
	RMSE	76.92

Table G-10 Parameters and the fitting quality of knee angle subgroups in the y-z plane

Fitted curves (y-z plane)

		Group 105° Knee		Group 133° Knee
		$z = p_1*y + p_2$		$z = p_1*y + p_2$
Coefficients (with 95% confidence bounds)	p_1	1.777 (1.751, 1.802)	p_1	1.793 (1.767, 1.818)
	p_2	-94.75 (-106.7, -82.78)	p_2	-110.1 (-122.4, -97.84)
Quality	R^2 adj.	0.73	R^2 adj.	0.70
	RMSE	89.01	RMSE	96.22

		Group 90° Knee with crossed legs
		$z = p_1*y + p_2$
Coefficients (with 95% confidence bounds)	p_1	1.786 (1.761, 1.812)
	p_2	-103.5 (-115.5, -91.51)
Quality	R^2 adj.	0.72
	RMSE	89.78

H. Torso Angular Speed and Acceleration in Different Knee Angle Conditions (Section 6.3.3)

a) Torso Angular Speed

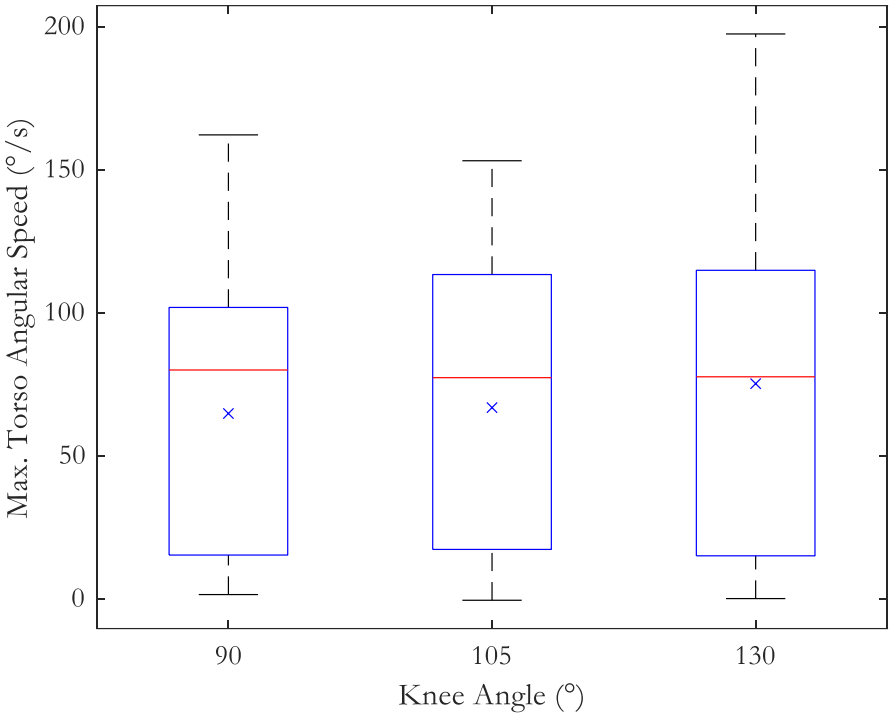

Figure H-1 The maximum torso angular speed during the take-over process in different knee angle conditions

Table H-1 Descriptive statistics of the maximum torso angular speed in different knee angle conditions

Descriptive Statistics

	Max torso angle speed (°/s)		
	Knee 90° leg crossed	Torso 30°	Torso 50°
Valid	71	71	79
Mean	65	67	75
Std. deviation	48	48	53
Minimum	2	0	0
Maximum	162	153	197

b) Torso Angular Acceleration

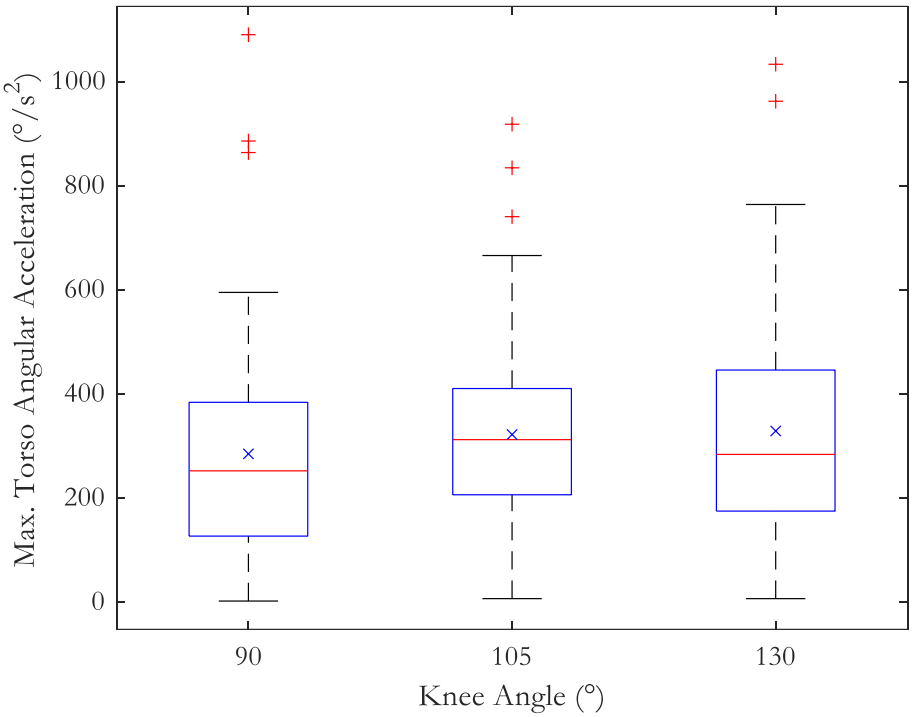

Figure H-2 The maximum torso angular acceleration during the take-over process in different knee angle conditions

Table H-2 Descriptive statistics of the maximum torso angular acceleration in different knee angle conditions

Descriptive Statistics

	Max. torso angle acceleration (°/s²)		
	Knee 90° leg crossed	Knee 105°	Knee 130°
Valid n	71	71	79
Mean	285	322	329
Std. deviation	205	183	197
Minimum	2	7	7
Maximum	1090	918	1033

I. Statistics of Time Metrics (Section 6.3.4)

a)Hand-on Time (HoT)

Table I-1 Assumption checks of HoT for RMANOVA

Test of Sphericity

	Mauchly's W	p	Greenhouse-Geisser ε	Huynh-Feldt ε
Torso Angle	0.254	< .001	0.548	0.589
Knee Angle	0.824	0.145	0.851	0.918
Torso Angle ✻ Knee Angle	0.195	0.062	0.677	0.860

Table I-2 Non-parametric Durbin test of HoT

Durbin Test

	Chi-Squared	df	p	Kendall's W	F	df num	df den	p_F
Torso Angle	77.570	3	< .001	-169.700	37.583	11	239	< .001
Knee Angle	1.117	2	0.572	-659.100	0.556	11	240	0.863

Table I-3 Conover's Post Hoc test of the torso angle to HoT

Connover's Post Hoc Comparisons - Torso Angle

		T-Stat	df	W_i	W_j	p	p_{bonf}	p_{holm}
Torso 10°	Torso 30°	1.921	239	279.500	345.000	0.056	0.336	0.056
	Torso 50°	4.634	239	279.500	437.500	< .001	< .001	< .001
	Torso 70°	10.983	239	279.500	654.000	< .001	< .001	< .001
Torso 30°	Torso 50°	2.713	239	345.000	437.500	0.007	0.043	0.014
	Torso 70°	9.062	239	345.000	654.000	< .001	< .001	< .001
Torso 50°	Torso 70°	6.350	239	437.500	654.000	< .001	< .001	< .001

Table I-4 Descriptive statistics of the HoT in each condition

Descriptives

		Mean	SD	n
Torso 10°	Knee 105°	0.674	0.177	22
	Knee 130°	0.665	0.166	22
	Knee 90°	0.695	0.149	22
Torso 30°	Knee 105°	0.700	0.168	22
	Knee 130°	0.705	0.166	22
	Knee 90°	0.722	0.168	22
Torso 50°	Knee 105°	0.747	0.161	22
	Knee 130°	0.790	0.169	22
	Knee 90°	0.755	0.198	22
Torso 70°	Knee 105°	0.915	0.219	22
	Knee 130°	0.981	0.241	22
	Knee 90°	0.939	0.276	22

b) Steering Time (ST)

Table I-5 Assumption checks of ST for RMANOVA

Test of Sphericity

	Mauchly's W	p	Greenhouse-Geisser ε	Huynh-Feldt ε
Torso Angle	0.411	0.004	0.622	0.680
Knee Angle	0.909	0.387	0.917	1.000
Torso Angle ✻ Knee Angle	0.265	0.209	0.722	0.933

Table I-6 Non-parametric Durbin test of ST

Durbin Test

	Chi-Squared	df	p	Kendall's W	F	df num	df den	p_F
Torso Angle	23.491	3	< .001	-175.500	8.565	11	239	< .001
Knee Angle	0.129	2	0.938	-706.800	0.064	11	240	1.000

Table I-7 Conover's Post Hoc test of torso angle to ST

Connover's Post Hoc Comparisons - Torso Angle

		T-Stat	df	W_i	W_j	p	p_{bonf}	p_{holm}
Torso 10°	Torso 30°	0.981	239	338.500	377.000	0.328	1.000	0.328
	Torso 50°	3.107	239	338.500	460.500	0.002	0.013	0.008
	Torso 70°	5.132	239	338.500	540.000	< .001	< .001	< .001
Torso 30°	Torso 50°	2.127	239	377.000	460.500	0.034	0.207	0.103
	Torso 70°	4.151	239	377.000	540.000	< .001	< .001	< .001
Torso 50°	Torso 70°	2.025	239	460.500	540.000	0.044	0.264	0.103

Table I-8 Descriptive Statistics of the ST in each condition

Descriptives

		Mean	SD	n
Torso 10°	Knee 105°	0.501	0.147	22
	Knee 130°	0.469	0.205	22
	Knee 90°	0.461	0.171	22
Torso 30°	Knee 105°	0.497	0.214	22
	Knee 130°	0.480	0.144	22
	Knee 90°	0.497	0.132	22
Torso 50°	Knee 105°	0.554	0.175	22
	Knee 130°	0.525	0.205	22
	Knee 90°	0.553	0.232	22
Torso 70°	Knee 105°	0.550	0.195	22
	Knee 130°	0.627	0.208	22
	Knee 90°	0.554	0.187	22

c) Task Time (TT)

Table I-9 Assumption checks of TT for RMANOVA

Test of Sphericity

	Mauchly's W	p	Greenhouse-Geisser ε	Huynh-Feldt ε
Torso Angle	0.153	< .001	0.485	0.512
Knee Angle	0.876	0.266	0.890	0.966
Torso Angle ✻ Knee Angle	0.429	0.727	0.790	1.000

Table I-10 Non-parametric Durbin test of TT

Durbin Test

	Chi-Squared	df	p	Kendall's W	F	df num	df den	p_F
Torso Angle	67.750	3	< .001	-157.200	30.975	11	239	< .001
Knee Angle	0.305	2	0.859	-576.500	0.151	11	240	0.999

Table I-11 Conover's Post Hoc test of torso angle to TT

Connover's Post Hoc Comparisons - Torso Angle

		T-Stat	df	W_i	W_j	p	p_{bonf}	p_{holm}
Torso 10°	Torso 30°	2.272	239	274.000	354.000	0.024	0.144	0.024
	Torso 50°	5.269	239	274.000	459.500	< .001	< .001	< .001
	Torso 70°	10.070	239	274.000	628.500	< .001	< .001	< .001
Torso 30°	Torso 50°	2.997	239	354.000	459.500	0.003	0.018	0.006
	Torso 70°	7.797	239	354.000	628.500	< .001	< .001	< .001
Torso 50°	Torso 70°	4.800	239	459.500	628.500	< .001	< .001	< .001

Table I-12 Descriptive Statistics of the TT in each condition

Descriptive Statistics

		Mean	SD	n
Torso 10°	Knee 105°	1.175	0.264	22
	Knee 130°	1.134	0.320	22
	Knee 90°	1.155	0.265	22
Torso 30°	Knee 105°	1.197	0.326	22
	Knee 130°	1.185	0.256	22
	Knee 90°	1.219	0.244	22
Torso 50°	Knee 105°	1.301	0.265	22
	Knee 130°	1.315	0.290	22
	Knee 90°	1.309	0.333	22
Torso 70°	Knee 105°	1.465	0.350	22
	Knee 130°	1.609	0.338	22
	Knee 90°	1.493	0.402	22

J. Statistical Tests of NASA TLX Scores of Each Category (Section 6.3.5)

a) General TLX Score

Table J-1 Assumption checks for Repeated Measures ANOVA

Test of Sphericity				
	Mauchly's W	p	Greenhouse-Geisser ε	Huynh-Feldt ε
Torso angle	0.660	0.058	0.797	0.880

Table J-2 Results of Repeated Measures ANOVA

Within Subjects Effects					
	Sum of Squares	df	Mean Square	F	p
Torso angle	2180	3	726.520	16.590	< .001
Residual	3548	81	43.800		

Table J-3 Post Hoc test of torso angles

Post Hoc Comparisons - Torso angle					
		Mean Difference	SE	t	p_{bonf}
Torso 10°	Torso 30°	-2.262	1.573	-1.438	0.972
	Torso 50°	-4.881	1.790	-2.727	0.067
	Torso 70°	-11.755	2.134	-5.508	< .001
Torso 30°	Torso 50°	-2.619	1.830	-1.431	0.983
	Torso 70°	-9.493	1.827	-5.196	< .001
Torso 50°	Torso 70°	-6.874	1.359	-5.058	< .001

b) Mental Demand

Table J-4 Assumption checks for Repeated Measures ANOVA

Test of Sphericity				
	Mauchly's W	p	Greenhouse-Geisser ε	Huynh-Feldt ε
Torso angle	0.309	< .001	0.633	0.680

Table J-5 Non-parametric statistical Friedman Test

Friedman Test				
	Chi-Squared	df	p	Kendall's W
Torso angle	9.297	3	0.026	0.866

Table J-6 Post Hoc Comparisons

Connover's Post Hoc Comparisons - Torso angle

		T-Stat	df	W_i	W_j	p	p_{bonf}	p_{holm}
Torso 10°	Torso 30°	0.130	81	63.000	64.000	0.897	1.000	1.000
	Torso 50°	0.716	81	63.000	68.500	0.476	1.000	1.000
	Torso 70°	2.798	81	63.000	84.500	0.006	0.038	0.038
Torso 30°	Torso 50°	0.586	81	64.000	68.500	0.560	1.000	1.000
	Torso 70°	2.668	81	64.000	84.500	0.009	0.055	0.046
Torso 50°	Torso 70°	2.083	81	68.500	84.500	0.040	0.243	0.162

c) Physical Demand

Table J-7 Assumption checks for Repeated Measures ANOVA

Test of Sphericity

	Mauchly's W	p	Greenhouse-Geisser ε	Huynh-Feldt ε
Torso angle	0.560	0.011	0.757	0.830

Table J-8 Non-parametric statistical Friedman Test

Friedman Test

	Chi-Squared	df	p	Kendall's W
Torso angle	50.060	3	< .001	0.705

Table J-9 Post Hoc Comparisons

Connover's Post Hoc Comparisons - Torso angle

		T-Stat	df	W_i	W_j	p	p_{bonf}	p_{holm}
Torso 10°	Torso 30°	2.660	81	42.500	58.500	0.009	0.056	0.019
	Torso 50°	5.154	81	42.500	73.500	< .001	< .001	< .001
	Torso 70°	10.475	81	42.500	105.500	< .001	< .001	< .001
Torso 30°	Torso 50°	2.494	81	58.500	73.500	0.015	0.088	0.019
	Torso 70°	7.815	81	58.500	105.500	< .001	< .001	< .001
Torso 50°	Torso 70°	5.321	81	73.500	105.500	< .001	< .001	< .001

d) Temporal Demand

Table J-10 Assumption checks for Repeated Measures ANOVA

Test of Sphericity

	Mauchly's W	p	Greenhouse-Geisser ε	Huynh-Feldt ε
Torso angle	0.433	< .001	0.704	0.765

Table J-11 Non-parametric statistical Friedman Test

Friedman Test				
	Chi-Squared	df	p	Kendall's W
Torso angle	0.258	3	0.968	0.795

Table J-12 Post Hoc Comparisons

Connover's Post Hoc Comparisons - Torso angle								
		T-Stat	df	W_i	W_j	p	p_{bonf}	p_{holm}
Torso 10°	Torso 30°	0.182	81	69.500	68.000	0.856	1.000	1.000
	Torso 50°	0.121	81	69.500	70.500	0.904	1.000	1.000
	Torso 70°	0.303	81	69.500	72.000	0.763	1.000	1.000
Torso 30°	Torso 50°	0.303	81	68.000	70.500	0.763	1.000	1.000
	Torso 70°	0.484	81	68.000	72.000	0.630	1.000	1.000
Torso 50°	Torso 70°	0.182	81	70.500	72.000	0.856	1.000	1.000

e)Performance

Table J-13 Assumption checks for Repeated Measures ANOVA

Test of Sphericity				
	Mauchly's W	p	Greenhouse-Geisser ε	Huynh-Feldt ε
Torso angle	0.652	0.051	0.791	0.872

Table J-14 Results of Repeated Measures ANOVA

Within Subjects Effects					
	Sum of Squares	df	Mean Square	F	p
Torso angle	1104	3	367.900	1.775	0.158

Table J-15 Post Hoc Comparisons

Post Hoc Comparisons - Torso angle					
		Mean Difference	SE	t	p_{bonf}
Torso 10°	Torso 30°	5.357	3.779	1.418	1.000
	Torso 50°	7.500	3.947	1.900	0.409
	Torso 70°	0.714	2.860	0.250	1.000
Torso 30°	Torso 50°	2.143	4.828	0.444	1.000
	Torso 70°	-4.643	4.202	-1.105	1.000
Torso 50°	Torso 70°	-6.786	3.131	-2.167	0.235

f) Effort

Table J-16 Assumption checks for Repeated Measures ANOVA

Test of Sphericity				
	Mauchly's W	p	Greenhouse-Geisser ε	Huynh-Feldt ε
Torso angle	0.212	< .001	0.504	0.528

Table J-17 Non-parametric statistical Friedman Test

Friedman Test				
	Chi-Squared	df	p	Kendall's W
Torso angle	19.880	3	< .001	0.778

Table J-18 Post Hoc Comparisons

Connover's Post Hoc Comparisons - Torso angle								
		T-Stat	df	W_i	W_j	p	p_{bonf}	p_{holm}
Torso 10°	Torso 30°	0.507	81	55.000	59.000	0.614	1.000	0.614
	Torso 50°	2.661	81	55.000	76.000	0.009	0.056	0.038
	Torso 70°	4.435	81	55.000	90.000	< .001	< .001	< .001
Torso 30°	Torso 50°	2.154	81	59.000	76.000	0.034	0.205	0.103
	Torso 70°	3.928	81	59.000	90.000	< .001	0.001	< .001
Torso 50°	Torso 70°	1.774	81	76.000	90.000	0.080	0.479	0.160

g) Frustration

Table J-19 Assumption checks for Repeated Measures ANOVA

Test of Sphericity				
	Mauchly's W	p	Greenhouse-Geisser ε	Huynh-Feldt ε
Torso angle	0.785	0.286	0.878	0.982

Table J-20 Results of Repeated Measures ANOVA

Within Subjects Effects					
	Sum of Squares	df	Mean Square	F	p
Torso angle	1324	3	441.300	3.545	0.018

Table J-21 Post Hoc Comparisons

Post Hoc Comparisons - Torso angle				
	Mean Difference	SE	t	p_{bonf}

Torso 10°	Torso 30°	-2.143	2.499	-0.857	1.000
	Torso 50°	-2.143	3.026	-0.708	1.000
	Torso 70°	-9.107	3.441	-2.646	0.080
Torso 30°	Torso 50°	0.000	NaN	0.000	1.000
	Torso 70°	-6.964	2.714	-2.566	0.097
Torso 50°	Torso 70°	-6.964	3.454	-2.017	0.323

K. Overcompensation Examples (Section 6.4.3)

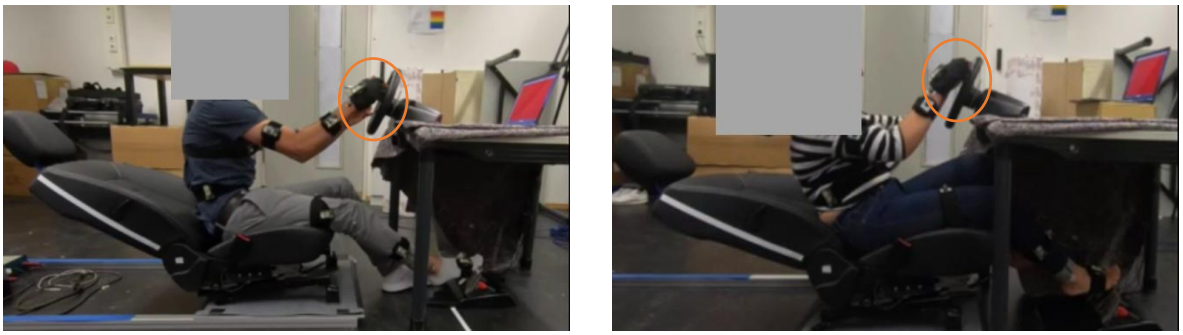

(a) (b)

Figure K-1 Examples of overcompensating: missing to grasp the steering wheel

Figure K-1 shows that participants harried up to lean forward, but failed to estimate the distance to the steering wheel and missed the steering wheel by grasping "in the air" shortly before reaching the steering wheel. Their hands stopped in the x-direction shortly before realizing not reaching the steering wheel yet. They stretched out further for the second try and finally reached the steering wheel. This cost longer take-over time and could derogate the steering accuracy.

(a) (b)

Figure K-2 Examples of overcompensating: using the extra push-up movement

Figure K-2 shows examples, where participants held the seat's edges and pushed against them to lift the torso upright, instead of directly leaning forward and putting the hands on the steering wheel. They might feel nervous and unusual to be greatly reclined, wanted to compensate accelerating more quickly. It might also simply because it was too physically demanding to lean forward from strongly reclined positions without the hands' support. This pushing-up movement might result in unstable H-points and longer hand-on time.

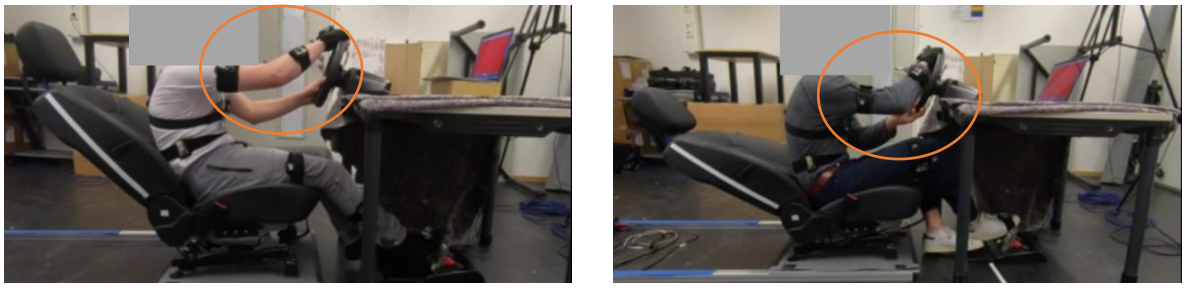

(a) (b)

Figure K-3 Examples of overcompensating: using too much force

Figure K-3 shows examples of participants using too much force. They tried to compensate for the disadvantage of being reclined by applying too much force on the steering wheel to keep the upper body upright and stable. They even pulled the whole heavy table toward themselves, which destroyed the experimental setup. They were asked to restart again in this case. These cases also indicate the upper bodies' instability without the seatback's support. The drivers had to hold the steering wheel to keep sitting upright. These might derogate the steering quality and braking force.

Appendix of Chapter 8 “Evaluation: Active Seat Assist”

L. An Example of Pulling the Steering Wheel to Shift the H-Point (Section 8.3.5)

(a) Hands on the steering wheel (b) Pulling and shifting forward

Figure L-1 An example of the driver pulling the steering wheel to shift the H-point as the first take-over reaction without the active seat assist

M. An Example of a Sequential Take-Over Process Without the Active Seat Assist (Section 8.4.3)

(a) RtI (0 s)

(b) Processing + attention re-direction (1 s)
Noticeable event: eyes on road

(c) Posture repositioning (2.5 s)
Noticeable event: hand on the steering wheel

(d) Situation evaluation (check mirrors) (3 s)
Noticeable event: start to steer

(e) Driving manually and changing lane (5 s)
Noticeable event: left the right lane

(f) Passing the broken car (6 s)
Noticeable event: parallel to the broken car

Figure M-1 An example of a sequential take-over process without the active seat assist, starting with the RtI (time point 0). The "noticeable events" mean the cutting criteria of each step. The time point refers to the RtI.

N. An Example of a Parallel Take-Over Process With the Active Seat Assist (Section 8.4.4)

(a) RtI (0 s)

(b) Process + attention re-direction + posture repositioning (passively) (0.7 s)
Noticeable event: eyes on road

(c) Posture repositioning (actively & passively) + situation evaluation (check the left mirror) (2.8 s)
Noticeable event: start to steer

(d) Driving manually and changing lane (4.5 s)
Noticeable event: left the right lane

(e) Passing the broken car (5.7 s)
Noticeable event: parallel to the broken car

Figure N-1 An example of a parallel take-over process with the active seat assist, starting with the RtI (time point 0). The "noticeable events" mean the cutting criteria of each step. The time point refers to the RtI.

General Appendix

O. Overarching Comparison of the Hand-On Time (Section 8.4.2)

Table O-1 Comparison of the hand-on time across three experiments with different setups

Experiment	Driving simulation	Torso angle	Assist system	NDRT	Average hand-on time (sec)	SD (sec)
Chapter 6	No	Torso 10°	No	No	0.69	0.16
	No	Torso 30°	No	No	0.72	0.16
	No	Torso 50°	No	No	0.78	0.18
	No	Torso 70°	No	No	0.95	0.24
Chapter 5	Yes, static	Torso 24°	No	1-back task	1.53	0.56
	Yes, static	Torso 38°	No	1-back task	1.68	0.55
Chapter 8	Yes, dynamic	Torso 40°	No	1-back task	1.47	0.41
	Yes, dynamic	Torso 40°	Yes	1-back task	1.38	0.48

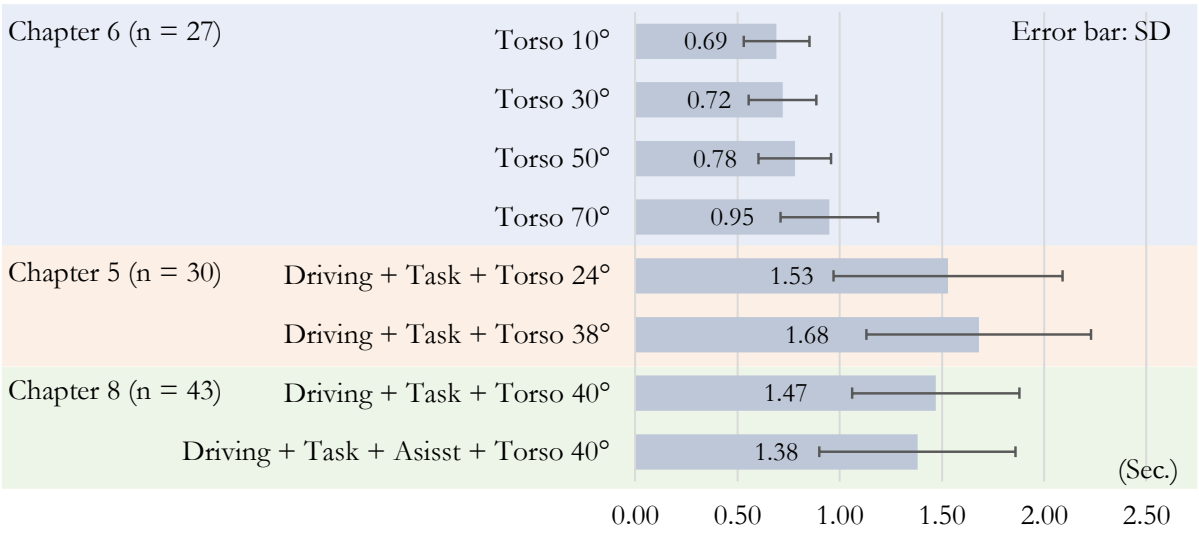

Figure O-1 Comparison of the hand-on time across three experiments with different setups, corresponding to Table O-1